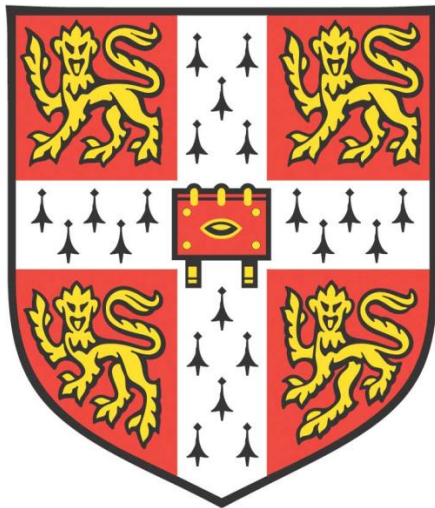


*A NOVEL TECHNIQUE FOR THE SEPARATION OF
DILUTE BUTANOL FROM AQUEOUS
FERMENTATION BROTHS*



Paul J. Hodgson

**Department of Chemical Engineering and Biotechnology
University of Cambridge**

**A dissertation submitted for the degree of
*Doctor of Philosophy***

November 2018

Trinity College

A NOVEL TECHNIQUE FOR THE SEPARATION OF DILUTE BUTANOL FROM AQUEOUS FERMENTATION BROTHS

PAUL J. HODGSON

SUMMARY

Butanol is a promising biofuel which can be manufactured by fermentation. Irrespective of whether *n*-butanol or *iso*-butanol is produced, the alcohol is generally expressed at low concentrations (~1 wt%) in these fermentations. It also inhibits the organisms, and so removal of the butanol from the fermentation vessel as it is produced can improve the productivity of the fermentation. However, separation of dilute butanol from aqueous fermentation broths requires substantial amounts of energy. In this dissertation, a novel separation technique has been devised, employing the solvent extraction of butanol from aqueous broths by volatile hydrocarbons. This separation technique performs the separation of butanol selectively and efficiently. It is investigated theoretically in this dissertation.

The use of volatile hydrocarbons allows the extracted butanol and the hydrocarbon to be separated by distillation, employing waste heat from the fermenter or other similar low-grade heat sources. Such heat is often abundant on fermentation plants. Therefore, minimal high-grade heat (heat at temperatures higher than the fermenter) would be required for the process. The equilibria of butanol and side-products with C₄ – C₅ hydrocarbons were investigated using vapour-liquid equilibria and excess enthalpy measurements from the literature. Models of the extraction and distillation processes were then built using these analyses. A flowsheet simulation predicted that under 2 MJ/kg butanol of high-grade heat (mostly at only ~50°C) was required by the separation scheme provided that sufficient low-grade waste heat was available (~40 – 20 MJ/kg butanol for extraction of 1 – 2 wt% broths). This high-grade heat requirement is around 5% of the heat required for distillation of butanol from aqueous broths at 1 wt%

Various configurations of flowsheet and solvent were investigated to improve the process. Distribution coefficients of butanol in C₄ – C₆ hydrocarbons were found to triple between 37°C and 100°C, and therefore extraction performed at elevated temperatures was found to significantly reduce the low-grade heat requirements of the system. The formation of butanol-gasoline blends *via* extraction of butanol into volatile hydrocarbons could also eliminate high-grade heat requirements.

DECLARATION

This dissertation is the result of my own work and includes nothing, which is the outcome of work done in collaboration except where specifically indicated in the text. It has not been previously submitted, in part or whole, to any university or institution for any degree, diploma, or other qualification.

In accordance with the Department of Engineering guidelines, this thesis does not exceed 65,000 words, and it contains less than 150 figures.

Signed: _____

Date: _____

Paul J. Hodgson

Department of Chemical Engineering and Biotechnology

University of Cambridge

November 2018

Dedicated to my wife, Rachel, for our ‘Paper Anniversary’ Year

ACKNOWLEDGEMENTS

Whilst writing this Dissertation, I have realised that I am greatly indebted to a long list of people for their help over the course of this research.

First and foremost, I would like to thank my supervisor, Prof. John Dennis for his help in both the research and financial aspects throughout the duration of my PhD, and for allowing me the creative freedom to pursue any avenue of inquiry whilst patiently listening to a variety of ideas from the poorly conceived to the near-deranged. I have also greatly appreciated the support and guidance of my advisor, Dr. Bart Hallmark, who has never hesitated in giving up his time to enthusiastically discuss my research.

Thanks must also go to my colleagues in the Combustion Group. In particular, I am indebted to Matthias Schnellmann and Martin Chan for keeping me on the straight and narrow, and to Zach Bond for creating a left-wing, tea-based system of government in which I can eat as many biscuits as I please. I am also indebted to Iain Morrison for ensuring that I have had access to any software I've needed, wherever I am, and access to as many monitors as I please.

I am grateful to Cambridge Enterprise for diligently working with me on the butanol separation patent. In particular, I am indebted to Dr. Jennie Flint and Dr. Gillian Davis for their infinite patience with my shenanigans and endless drivelling on about butanol.

The financial support from this research was generously funded by an EPSRC Doctoral Training Grant from the Department of Chemical Engineering and Biotechnology, for which I am grateful.

I would like to thank my family for their support throughout my Ph.D. Most of all, I am indebted to my wife, Rachel, for her unwavering support and countless hours of reading this dissertation, despite no formal training in engineering aside from patiently listening to me ramble on about ‘acetogens’, ‘butanol’ and ‘hydrocarbons’.

CONTENTS

1. BUTANOL PRODUCTION BY FERMENTATION: AN INTRODUCTION.....	1
1.1 BACKGROUND.....	1
1.2 GASOLINE REPLACEMENTS: ETHANOL VERSUS BUTANOL	2
1.3 PRODUCTION ROUTES FOR BIO-BUTANOL AND OTHER REPLACEMENTS FOR GASOLINE	4
1.3.1 <i>Biochemical Routes</i>	4
1.3.2 <i>Thermochemical Routes</i>	6
1.3.3 <i>Fermentation of Synthesis Gas</i>	6
1.4 CHALLENGES IN THE PRODUCTION OF BUTANOL VIA FERMENTATION.....	7
1.5 EXISTING METHODS FOR THE SEPARATION OF BUTANOL FROM AQUEOUS BROTHS.....	9
1.6 OBJECTIVES AND STRUCTURE OF WORK	17
2. DEVELOPMENT OF A NOVEL BUTANOL SEPARATION METHOD USING SHORT HYDROCARBONS AS EXTRACTANTS.....	19
2.1 INTRODUCTION	19
2.1.1 <i>Distribution Coefficient and Selectivity</i>	19
2.1.2 <i>Previous Research to Identify Suitable Extractants</i>	21
2.2 EMPLOYING VOLATILE HYDROCARBONS AS EXTRACTANTS	25
2.3 PROCESS DESIGN	30
2.3.1 <i>Multicomponent Broths</i>	33
2.3.2 <i>Extraction at Elevated Temperature</i>	35
2.3.3 <i>Other Design Modifications</i>	37
2.4 THE MUTUAL SOLUBILITY OF SHORT HYDROCARBONS AND WATER	40
2.4.1 <i>The Solubility of Volatile Hydrocarbons in Water</i>	40
2.4.2 <i>The Solubility of Water in Volatile Hydrocarbons</i>	48
2.5 ESTIMATING THE PERFORMANCE OF THE DISTILLATION SYSTEM FOR THE SEPARATION OF BUTANOL FROM VOLATILE HYDROCARBONS	50
2.5.1 <i>Assumptions</i>	50
2.5.2 <i>Methodology</i>	51
2.5.3 <i>Results</i>	54
2.5.4 <i>Discussion</i>	56

2.6 ESTIMATING THE DISTRIBUTION COEFFICIENT OF BUTANOL AT INFINITE DILUTION BETWEEN WATER AND SELECTED HYDROCARBONS	58
2.6.1 <i>Theory</i>	58
2.6.2 <i>Estimates of \mathcal{M} and Methodology</i>	63
2.6.3 <i>Results</i>	64
2.6.4 <i>Discussion</i>	67
2.7 CONCLUSION.....	68
3. ANALYSIS OF BINARY THERMODYNAMIC DATA OF SHORT HYDROCARBONS WITH FERMENTATION PRODUCTS.....	71
3.1 INTRODUCTION.....	71
3.2 BINARY THERMODYNAMIC MEASUREMENTS AVAILABLE IN THE LITERATURE	72
3.3 REGRESSION OF VLE AND EXCESS ENTHALPY MEASUREMENTS	73
3.3.1 <i>Types of VLE Datasets and Correction of Liquid Phase Compositions</i>	73
3.3.2 <i>Correction of Temperature Variation in Isothermal Datasets</i>	75
3.3.3 <i>Regression Methodologies</i>	75
3.3.4 <i>The 'Barker Method'</i>	76
3.3.5 <i>The 'Mixon Method'</i>	78
3.3.6 <i>Direct Measurement of Vapour-Liquid Equilibrium (Pxy Measurements)</i> 79	79
3.4 METHODOLOGY FOR THE REGRESSION OF VLE AND EXCESS ENTHALPY	79
3.4.1 <i>Development of the Legendre Activity Coefficient Model</i>	80
3.4.2 <i>Vapour Phase Equation of State</i>	83
3.4.3 <i>Physical Properties of Pure Fermentation Products and Hydrocarbon Solvents</i>	83
3.4.4 <i>Objective Function</i>	83
3.4.5 <i>Regression Procedure</i>	84
3.5 ACTIVITY MODEL REGRESSION RESULTS	86
3.5.1 <i>Model Predictions of Activity Coefficients</i>	86
3.5.2 <i>Deviation of Model Predictions from Literature Datasets</i>	93
3.5.3 <i>Model Predictions of Vapour-Liquid Equilibria and Excess Enthalpy</i>	97
3.6 DISCUSSION	106
3.7 CONCLUSIONS	113
4. MODELLING THE EXTRACTION OF FERMENTATION PRODUCTS USING VOLATILE HYDROCARBONS	115
4.1 INTRODUCTION.....	115

4.1.1	<i>Models for the Prediction of Ternary LLE from Binary Activity Coefficients</i>	116
4.1.2	<i>Approximating Ternary LLE of Dilute Mixtures using Binary Activity Coefficients</i>	117
4.2	CALCULATION OF ACTIVITY COEFFICIENTS OF AQUEOUS BUTANOL	118
4.2.1	<i>Development of an Activity Coefficient Model</i>	119
4.2.2	<i>Correlations of Limiting Activity Coefficients at Infinite Dilution and Correlations of Mutual Solubilities for Butanol and Water</i>	120
4.2.3	<i>Model Validation</i>	121
4.2.4	<i>Model Results</i>	122
4.3	CALCULATION OF THE ACTIVITY COEFFICIENT OF AQUEOUS ETHANOL	126
4.3.1	<i>Methodology</i>	126
4.3.2	<i>Results</i>	127
4.4	CALCULATION OF THE ACTIVITY COEFFICIENT OF AQUEOUS ACETONE	130
4.5	PREDICTIONS OF DISTRIBUTION COEFFICIENTS FOR DILUTE FERMENTATION PRODUCTS.....	131
4.5.1	<i>Predicted Distribution Coefficients</i>	133
4.5.2	<i>Predicted Selectivity of Butanol over Side-Products</i>	138
4.5.3	<i>Comparison with Experimental Measurements</i>	140
4.5.4	<i>Discussion</i>	143
4.5.5	<i>Conclusion</i>	144
4.6	DESIGN AND EFFICIENCY OF THE LIQUID-LIQUID EXTRACTION UNIT	145
4.6.1	<i>Direct Extraction in the Fermenter, in situ</i>	145
4.6.2	<i>Counter-Current Extraction, ‘in stream’</i>	147
4.6.3	<i>Conclusion</i>	153
5.	A FLOWSHEET MODEL OF LIQUID-LIQUID EXTRACTION	
	USING VOLATILE HYDROCARBONS	155
5.1	INTRODUCTION	155
5.2	ASSUMPTIONS AND METHODOLOGY	156
5.2.1	<i>Assumptions</i>	156
5.2.2	<i>Model of a Simple Distillation Column</i>	157
5.2.3	<i>Operating Conditions of the Flowsheet Distillation Columns</i>	160
5.2.4	<i>Model of the Extraction</i>	164
5.2.5	<i>Heating Requirements for the Aqueous Phase</i>	166
5.2.6	<i>Heating Requirements for the Organic Phase</i>	167

5.2.7	<i>Total Heating Requirements</i>	170
5.2.8	<i>Pumping Requirements</i>	170
5.2.9	<i>Simulation in Matlab</i>	172
5.3	RESULTS OF THE SIMPLE FLOWSHEET MODEL FOR EXTRACTIONS PERFORMED AT FERMENTATION TEMPERATURES.....	173
5.3.1	<i>Accounting for the Supply of Low-Grade Heat</i>	182
5.3.2	<i>Optimising the Temperature Gradient of DC1</i>	185
5.3.3	<i>Optimisation of Extraction Efficiency</i>	188
5.3.4	<i>Effect of the Composition of Aqueous Butanol</i>	190
5.4	DISCUSSION: EXTRACTION AT FERMENTATION TEMPERATURES	190
5.5	RESULTS OF THE SIMPLE FLOWSHEET MODEL FOR EXTRACTIONS PERFORMED AT ELEVATED TEMPERATURES.....	193
5.5.1	<i>Optimisation of the Extraction Efficiency</i>	197
5.5.2	<i>Comparison of Extraction at Fermentation Temperatures with Extraction at Elevated Temperatures</i>	199
5.6	DISCUSSION: EXTRACTION AT ELEVATED TEMPERATURES	201
5.7	CONCLUSION.....	201
6.	CONCLUSIONS	203
7.	FUTURE WORK	209
APPENDIX A. MODELLING THE DISTILLATION OF AQUEOUS BUTANOL FROM FERMENTATION BROTHS		213
A.1	INTRODUCTION.....	213
A.2	ASSUMPTIONS	213
A.3	FEED COMPOSITION	221
A.4	SIMULATION IN UNISIM	222
A.5	RESULTS OF THE DISTILLATION SIMULATIONS.....	223
A.6	DISCUSSION OF THE DISTILLATION SIMULATIONS	224
APPENDIX B. DERIVATION OF THE CO-EXISTENCE EQUATION AT CONSTANT TEMPERATURE, AND ESTIMATING DISTRIBUTION COEFFICIENTS FOR BUTANOL		229
B.1	DERIVATION OF THE Co-EXISTENCE EQUATION AT CONSTANT TEMPERATURE	
	229	
B.2	APPLYING THE VIRIAL EQUATION TO THE Co-EXISTENCE EQUATION	230
B.3	VIRIAL Co-EXISTENCE EQUATION AT $x_1 \rightarrow 0$	231

B.4 DERIVATIONS OF THE LIMITING ACTIVITY CO-EFFICIENT FROM THE VIRIAL CO-EXISTENCE EQUATION.....	232
B.5 THE LIMITING DISTRIBUTION COEFFICIENT FOR DILUTE BUTANOL IN HYDROCARBONS VS. WATER.....	234
APPENDIX C. MASS BALANCE OF THE EQUILIBRIUM CELL.....	235
APPENDIX D. VAPOUR PHASE EQUATIONS OF STATE	236
D.1 IDEAL GAS LAW.....	236
D.2 SOAVE-REDLICH-KWONG EQUATION OF STATE	236
D.3 VIRIAL EQUATION OF STATE.....	237
D.4 TSONOPOULOS' METHOD FOR CALCULATION OF SECOND VIRIAL COEFFICIENTS	
238	
D.5 COMPARISON OF SECOND VIRIAL COEFFICIENTS OF PURE PENTANE AND BUTANOL CALCULATED BY DIFFERENT METHODS	240
APPENDIX E. VARIATION OF ACTIVITY COEFFICIENTS WITH TEMPERATURE AND PRESSURE.....	242
E.1 THEORETICAL DEPENDENCE OF ACTIVITY COEFFICIENT ON TEMPERATURE AND PRESSURE	242
E.2 PRACTICAL VARIATION OF ACTIVITY COEFFICIENT WITH PRESSURE	243
APPENDIX F. LIMITING ACTIVITY COEFFICIENTS OF WATER AND ALCOHOLS AT INFINITE DILUTION	245
F.1 THE LIMITING ACTIVITY COEFFICIENT OF ALCOHOLS AT INFINITE DILUTION IN WATER.....	245
F.2 THE LIMITING ACTIVITY COEFFICIENT OF WATER AT INFINITE DILUTION IN BUTANOL ISOMERS	246
APPENDIX G. LOW-GRADE HEAT PRODUCED BY FERMENTATION.....	250
G.1 FERMENTATION OF SYNTHESIS GASES	250
G.2 ISO-BUTANOL FERMENTATION.....	252
G.3 ABE FERMENTATION.....	253
NOMENCLATURE: SYMBOLS, ABBREVIATIONS AND ACRONYMS	255
REFERENCES.....	261

1. Butanol Production by Fermentation: An Introduction

1.1 Background

Biofuels are seen as a promising, sustainable alternative to fossil fuels amidst concerns over CO₂-driven climate change, rising demand for transport fuels and dwindling reserves of oil and gas (Stern, 2007). Due to conflict in oil-producing nations in the Middle East, nations increasingly seek greater energy security. Biofuels offer a potential route to source liquid fuels from locally-produced biomass.

‘First generation’ biofuels (*e.g.* bioethanol, biodiesel), *viz.* those derived from food crops (*e.g.* sugarcane, corn), are a well-developed technology, with substantial volumes of production in places such as Brazil and the USA (bioethanol) and Europe (biodiesel). However, the consequent necessity of displacing productive agricultural land, and the increased use of fertilisers (which lead to increased NO_x emissions), have prevented first generation biofuels from becoming sustainable or secure fuel sources. Indeed, the use of food crops for fuels might even lead to a rise in food prices, thereby directly conflicting with the desire of most countries to improve food security; a problem dubbed the ‘food-fuel debate’. With both the EU and the USA setting ambitious targets and mandates for the production of biofuels (110th United States Congress, 2007; The European Union, 2009), much interest and research has been directed towards producing biofuels from crops that do not compete with food production in order to overcome the limitations of first generation biofuels.

‘Second generation’ biofuels are derived from non-food crops, such as woody biomass. Lignocellulosic biomass has the advantage that it can be produced from indigenous, non-food crops grown on marginal, low-grade land (*e.g.* switchgrass). There are also vast quantities of waste biomass of this type available, in the form of corn stover and other agricultural by-products, forestry residues and municipal waste. Because the supply of waste biomass is abundant, second-generation biofuels have received much research and commercial interest.

In summary, biofuels are a direct replacement for transport fuels derived from fossil resources, and present at least a partial solution to issues surrounding the use of fossil

resources (CO_2 emissions, fuel security, *etc.*). However, due to the use of feedstocks derived from crops, the environmental benefits of current biofuels are debatable, and so much research has been focused on utilising lignocellulosic feedstocks.

1.2 Gasoline Replacements: Ethanol *versus* Butanol

Ethanol is a biofuel produced extensively in Brazil and USA as a gasoline replacement. However, butanol can be used as a drop-in gasoline replacement, possessing fuel properties clearly superior to those of ethanol, as well as being a valuable chemical feedstock.

Bioethanol, a gasoline replacement normally produced by the fermentation of substrates prepared from food crops, has been extremely successful: the annual global production of fuel ethanol exceeded 10^5 m^3 in 2017, with the USA and Brazil accounting for 58% and 26% of production respectively (Renewable Fuel Association, 2018). Ethanol can be blended with gasoline at moderate concentrations (typically 10-20 vol% ethanol) and utilised in unmodified vehicles. Indeed, at high concentrations (or even pure) it can be used in modified vehicles (common in Brazilian ‘flex-fuel’ cars).

Butanol is currently an important bulk chemical, mainly produced from petroleum-derived propene *via* the oxo process (Hahn *et al.*, 2013). The global capacity of *n*-butanol (butan-1-ol) was over 3.5 million tonnes in 2010, whilst the that of *iso*-butanol (2-methylpropan-1-ol) exceeded 0.5 million tonnes in 2010 (Hahn *et al.*, 2013). The major use for *n*-butanol is for surface coating: it can be used directly as a solvent for varnishes, or converted into derivatives such as butyl acrylate and butyl acetate (Hahn *et al.*, 2013). *Iso*-butanol is sometimes used as a substitute for *n*-butanol. The global market for *n*-butanol was estimated to be over \$4 billion USD in 2017, and is projected to grow substantially in the future (Rohan, 2018).

Table 1-1 compares the fuel properties of ethanol and gasoline with those of butanol, both for *n*-butanol (butan-1-ol) and *iso*-butanol (2-methylpropan-1-ol). Much recent research has been directed towards butanol production in order to overcome the limitations of ethanol as a gasoline replacement. The fuel properties of butanol – such as RON and MON – and its calorific value per unit volume (‘energy density’), which affects the vehicle’s range, more closely resemble those of gasoline than ethanol does. The relatively low vapour pressure of butanol improves the safety of using the fuel, and its low heat of evaporation reduces cold start issues in engines as compared with ethanol. Since ethanol is fully miscible with water, ethanol cannot be piped in existing gasoline infrastructure as

a gasoline-ethanol blend would separate between a gasoline phase and, favourably, an aqueous phase where there is any water present in the distribution system. Therefore, it must be blended at the pump, requiring extra infrastructure and cost in transporting ethanol to fuel stations separately. Potentially, the limited aqueous miscibility of butanol might be low enough to allow it to be piped in the existing gasoline infrastructure (Tao *et al.*, 2013b). The hydroxyl group in ethanol also causes corrosive action on some rubber seals and some metals in unmodified engines. The additional stability of the longer-chained butanol and reduced number of alcohol groups per carbon reduces this problem. The presence of oxygen in the hydroxyl group can also have an impact on the emissions of the blended mixture.

Table 1-1 – Comparative fuel characteristics (Tao *et al.*, 2013b)

Property	N-Butanol	Iso-Butanol	Ethanol	Gasoline (C ₄ – C ₁₂)
Energy density (MJ/l)	26.9	26.6	21.4	30 – 33
Research Octane Number (RON)	96	106	110	88 – 98
Motor Octane Number (MON)	84	90	90	80 - 88
Heat of evaporation (MJ/kg)	0.71	0.69	0.92	0.36
Vapour Pressure (Pa)	2.2	3.3	16	54 – 103
Solubility in water at 20°C (wt%)	7.7	8.7	miscible	negligible

Ethanol's corrosive action, energy density and oxygen content all limit the proportions in which it can be blended with gasoline in unmodified vehicles (currently 10 vol% in the USA). The superior fuel properties, less corrosive behaviour and lower oxygen content of butanol allows for higher blend ratios, permitting greater production of butanol and increased displacement of fossil-derived gasoline.

In addition to its potential as a drop-in gasoline replacement, butanol has significant potential as a renewable chemical feedstock. Butanol is already produced for use as a bulk chemical, but economic production of renewable butanol would create opportunities to displace petroleum derivatives. For example, *n*-butanol can easily be catalytically dehydrated to butene (Mascal, 2012); similarly *iso*-butanol can be dehydrated to form *iso*-butene. Butenes and their derivatives have a wide range of applications, potentially including the production of jet and diesel fuels (Mascal, 2012).

1.3 Production Routes for Bio-Butanol and Other Replacements for Gasoline

There are three main categories of production pathways for butanol and other replacements for gasoline from biomass: biochemical routes; thermochemical routes; and routes *via* the fermentation of synthesis gas. These three routes to gasoline-replacement biofuels are depicted schematically in Figure 1-1 and are discussed below.

1.3.1 Biochemical Routes

Biochemical routes consist of breaking down biomass into sugars, which are then fermented into products. This is currently the route of choice for ethanol. The century-old ABE process (Acetone – *n*-Butanol – Ethanol) using *Clostridium* bacteria can be used to produce *n*-butanol as a biofuel (Köpke *et al.*, 2011b). *Iso*-butanol is produced by some bacteria and yeasts natively (Green, 2011) and *iso*-butanol pathways have successfully been engineered into *E. Coli* strains (Atsumi *et al.*, 2008).

There has been much commercial interest in this route. Two companies, Gevo Inc. and Butamax Advanced Biofuels LLC – a joint venture created by BP and DuPont – are both engaged in retrofitting existing biochemical ethanol plants in Minnesota in order to produce *iso*-butanol from corn (Butamax Advanced Biofuels LLC, 2014; European Biofuels Technology Platform, 2014) using a variety of proprietary recombinant microorganisms (*e.g.* Feldman *et al.*, 2013). Whilst both companies currently have processes in place for the fermentation of sugar from corn (*i.e.* first-generation biofuels), they are also engaged in research and development to utilise lignocellulosic feedstocks *via* similar routes to cellulosic ethanol production (ethanol from lignocellulosic material).

Amongst others, GreenBiologics is reviving the acetone-butanol-ethanol (ABE) process to produce *n*-butanol, with the goal of utilizing lignocellulosic feedstocks and developing bacterial strains for efficient fermentation.

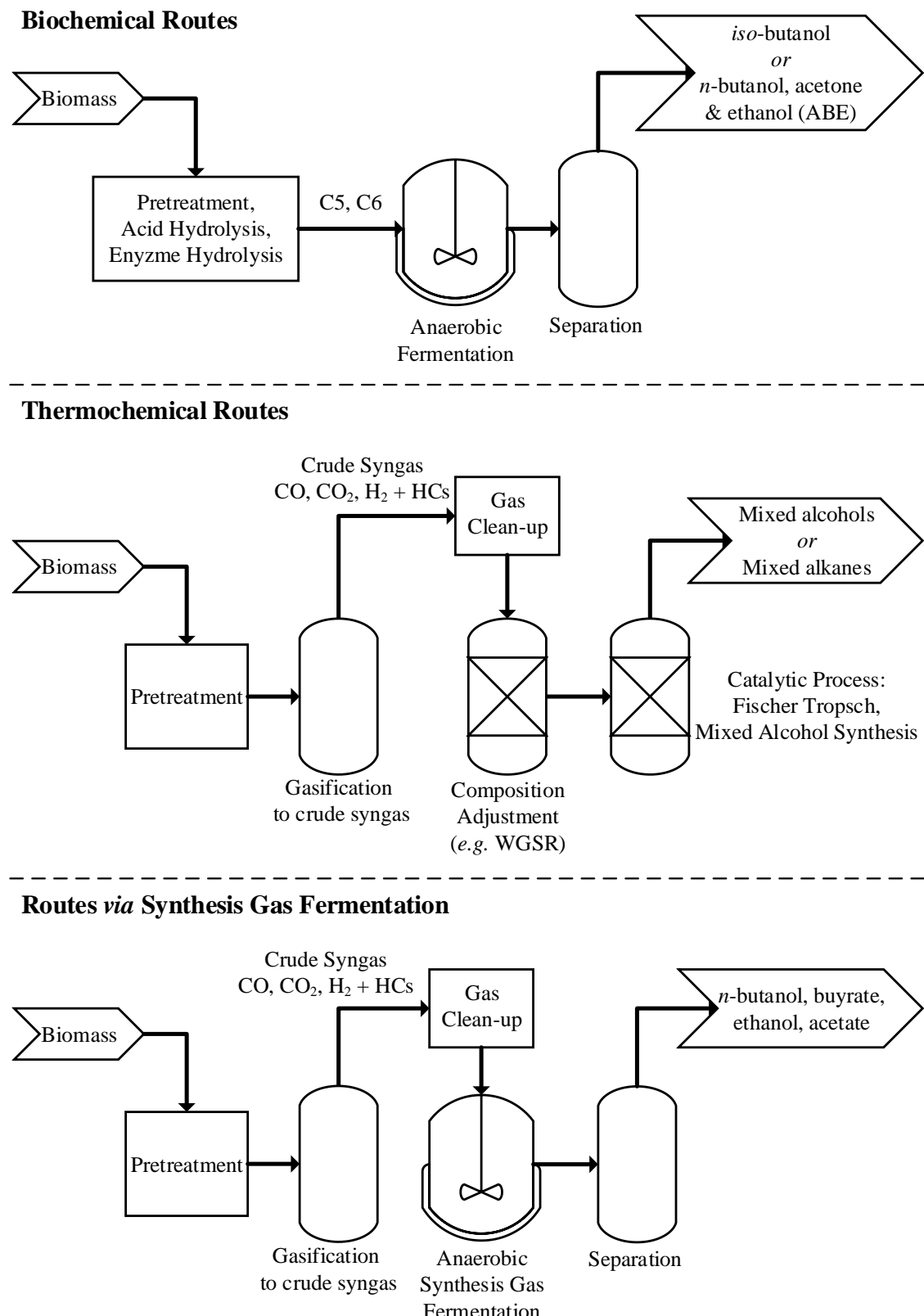


Figure 1-1 – Process Flow Diagrams for Biochemical, Thermochemical and Synthesis Gas Fermentation Routes to gasoline-replacement biofuels

1.3.2 Thermochemical Routes

In thermochemical routes, shown in Figure 1-1, biomass is gasified to crude syngas (CO, CO₂, H₂, H₂O, CH₄ and other impurities). The resulting synthesis gas is cleaned, and its ratio of CO to H₂ adjusted using the water-gas shift reaction. Gas-to-liquid technologies, such as Fischer Tropsch and mixed-alcohol synthesis, are then employed to produce gasoline replacements. This is commonly termed biomass to liquids, ‘BtL’, and in principle is identical to ‘CtL’ (Coal to Liquid) and ‘GtL’ (Gas to Liquid) technologies, except that the synthesis gases in these cases are derived from coal or natural gas.

The gasification step allows for a range of biomass feedstocks to be used. However, extensive gas clean-up is required in order to remove impurities which poison catalysts, notably sulphurous gases and tar. Adjustments to the CO:H₂ composition of the syngas also comes at a substantial cost. These problems, in addition to major issues with product specificity, typically make investment costs for such plants very high (Dürre, 2011a; Köpke *et al.*, 2011b). Nonetheless, there is some commercial interest in this process. Fulcrum Bioenergy have developed a process to convert municipal solid waste (MSW) into ‘synthetic crude oil’, *via* gasification and the Fischer Tropsch process. This product could then be upgraded to diesel or jet fuels. The company are currently in the process of constructing a commercial plant in Nevada for the production of jet fuel from MSW with a planned capacity of 40,000 m³ per year (Lane, 2018).

1.3.3 Fermentation of Synthesis Gas

Routes *via* the fermentation of synthesis gases, depicted schematically in Figure 1-1, are a hybrid of the thermochemical and biochemical routes. Crude synthesis gas is produced by gasification of biomass feedstock and then, after minimal gas clean-up, the synthesis gas is used as the feedstock for a fermentation which converts the gas to liquid fuels. This combines the feedstock flexibility of the thermochemical route with the fermentation step of the biochemical route, which operates at a lower intensity and is much more tolerant to impurities in the synthesis gas. Acetogens, the organisms used in the fermentation, can produce acetate, ethanol, *n*-butyrate, *n*-butanol and 2,3-butanediol naturally, with possibilities for other products *via* synthetic biology.

There has been some commercial interest in this route, although to date efforts have been focussed on ethanol production due to low native butanol titres (Daniell *et al.*, 2012). The commercial leader in this process, LanzaTech, has several pilot and demonstration plants for the production of ethanol from either the CO-rich flue gases from steel manufacture,

or from synthesis gas produced from the gasification of woody biomass (Daniell *et al.*, 2012; LanzaTech, 2015).

Whilst the process of synthesis gas fermentation is significantly less mature than the biochemical or thermochemical production of biofuels, it potentially offers significant benefits, particularly its feedstock flexibility.

1.4 Challenges in the Production of Butanol *via* Fermentation

Technical challenges in the ABE process have been well researched, since this process is over 100 years' old. Frequently-cited issues with this fermentation include: low productivity; poor selectivity for the product, low yield on most carbon substrates, low titre and toxicity of the products to the organism. Additionally, efficient separation of butanol from fermentation broths is a problem (Ezeji *et al.*, 2007; Green, 2011; Köpke *et al.*, 2011b; Outram *et al.*, 2017; Tao *et al.*, 2013a). In contrast, few detailed analyses have been published on *iso*-butanol fermentations or on the production of butanol *via* fermentation of synthesis gases because these routes are much less mature. *Iso*-butanol fermentations are very similar to the ABE process and therefore face similar challenges, although the product selectivity of organisms is generally better than that of organisms used in ABE fermentations (Tao *et al.*, 2014b). Whilst few detailed analyses of butanol production *via* the fermentation of synthesis gases have been conducted, key challenges to the process can be anticipated from ethanol studies, preliminary reviews of biobutanol production options, and extensive studies on the ABE fermentations. In addition to the issues outlined for ABE processes, frequently cited issues during the fermentation of synthesis gases include the scale-up of biomass gasification, gas fermenter design and energy consumption (Daniell *et al.*, 2012; Köpke *et al.*, 2011a; Schiel-Bengelsdorf and Dürre, 2012).

These limitations can be divided into two categories: ‘biochemical challenges’, *i.e.* those surrounding the modification of organisms; and ‘engineering challenges’, *i.e.* those surrounding the design of processes around the fermenter and that of the fermenter itself.

Tackling the biochemical challenges by modifying organisms used in the fermentation of butanol in order to achieve higher yields from substrates, higher productivities, more favourable product ratios, and higher butanol titres is very attractive (Dürre, 2016). However, this is a complex, expensive and time-consuming process, and many high-performing modified organisms are retained by commercial interests. The modification of organisms is beyond the scope of this dissertation.

An improved butanol titre in the broth would be beneficial because it would increase the concentration of butanol before separation, and hence reduce the cost of the separation. However, most organisms are inhibited by butanol concentrations above 10 – 20 g/l. Genetic modification has thus been used to improve the tolerance of organisms to butanol. Even so, the best solventogenic *Clostridia* strains available achieve a butanol titre of around 20 g/l (2 wt%) (Green, 2011), whilst typical butanol titres of such organisms are *circa* 12 g/l. *Iso*-butanol produced by the fermentation organisms such as *E. coli* can be expressed at slightly higher titres because *iso*-butanol is less toxic than *n*-butanol. *E. coli* has consequently been engineered to produce an *iso*-butanol titre of 22 g/l (Atsumi *et al.*, 2008).

The modification of organisms to produce butanol by the fermentation of synthesis gases is less researched than the modifications of those used in ABE and *iso*-butanol fermentations. Butanol titres of 2.7 g/l during the fermentation of CO have been reported by Grethlein *et al.* (1991). The researchers grew *B. methylotrophicum* on CO in a laboratory-scale fermenter at pH 5.5, retaining cells using a membrane separator to increase butanol productivity. Optimisation of the fermenter medium resulted in a butanol titre of 1.1 g/l for synthesis gas fermentation by *Clostridium carboxidivorans* (Phillips *et al.*, 2015). Significantly higher titres of other products produced by the fermentation of synthesis gases have been reported, including *Clostrium ljungdahli* expressing ethanol at > 20 g/l (Gaddy *et al.*, 2007) and *A. woodii* expressing acetate at ~60 g/l (Kantzow *et al.*, 2015). These higher titres suggest that the use of synthesis gas as a feedstock, and its associated mass transfer effects, are not fundamentally limiting factors in product titre, and hence butanol titres similar to those achieved in ABE fermentations might be obtainable by modification of acetogens.

In situ product removal of butanol has been found to greatly improve productivity in ABE and *iso*-butanol fermentations by alleviating product inhibition (Huang *et al.*, 2014; Outram *et al.*, 2017, 2016; Tao *et al.*, 2013b). In addition, selective removal of butanol might improve product ratios, by shifting production towards solventogenesis and away from acidogenesis (production of carboxylic acids). More energy-efficient separation of butanol from dilute aqueous mixtures would also reduce the desire to increase butanol titres achieved by organisms during fermentations. Thus, the biochemical limitations of butanol fermentations could potentially be alleviated significantly by reducing the, arguably less complex, engineering limitations of the fermentation processes.

1.5 Existing Methods for the Separation of Butanol from Aqueous Broths

All routes to producing butanol by fermentation result in its expression in an aqueous broth. Separation of the butanol and any other side products from the fermentation broth is complicated irrespective of the fermentation process. Figure 1-2 depicts a typical separation process for butanol production by fermentation. During both continuous and batch fermentations, *in situ* product removal can be used to remove products from the broth. At the end of batch fermentations, biomass is first removed from the broth, usually by filtration. The aqueous products are then concentrated in a distillation column (often termed the ‘beer’ column), which produces a two-phase mixture in the distillate. The organic phase is sent for further distillation to separate the fermentation products, and the aqueous phase is refluxed.

The separation of the butanol produced by a fermentation is costly in energy consumption. This is due to both the low concentration of butanol in the broth and the complicated phase equilibria of butanol and water. Figure 1-3 shows the vapour-liquid equilibria at atmospheric pressure of both *n*-butanol and *iso*-butanol with water. *Iso*-butanol is slightly less volatile than *n*-butanol and has a slightly higher solubility in water (2.1 mol% vs. 1.9 mol% at 25°C).

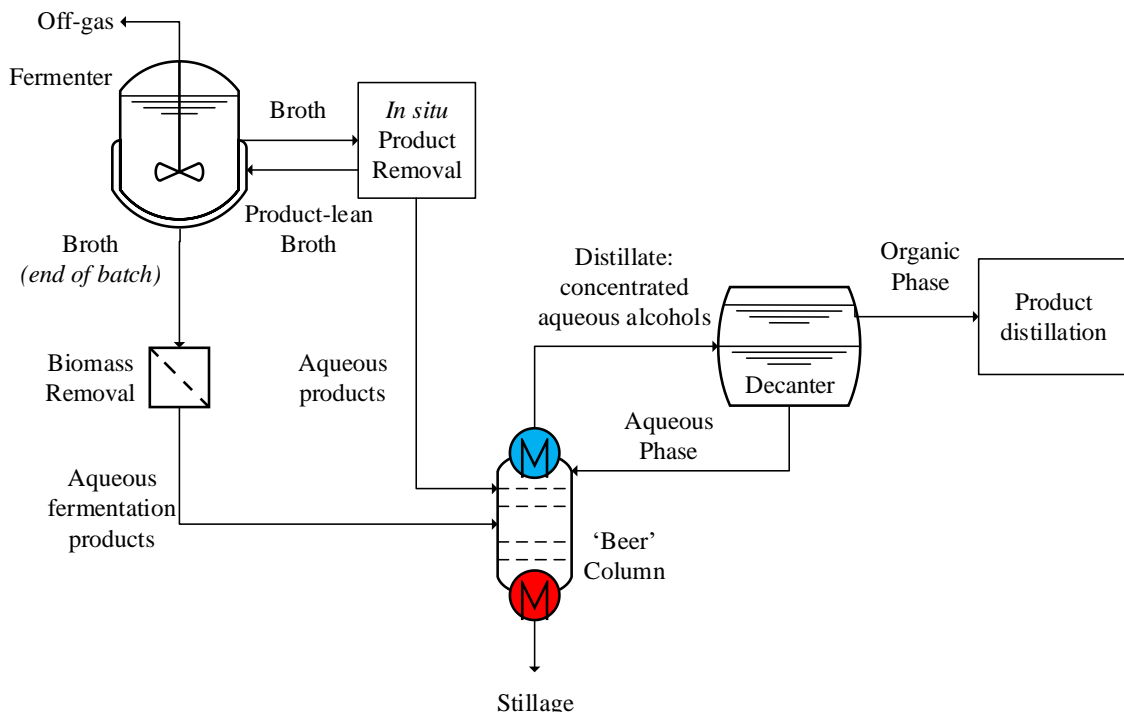


Figure 1-2 – Process flow diagram of a typical separation process for butanol production by fermentation

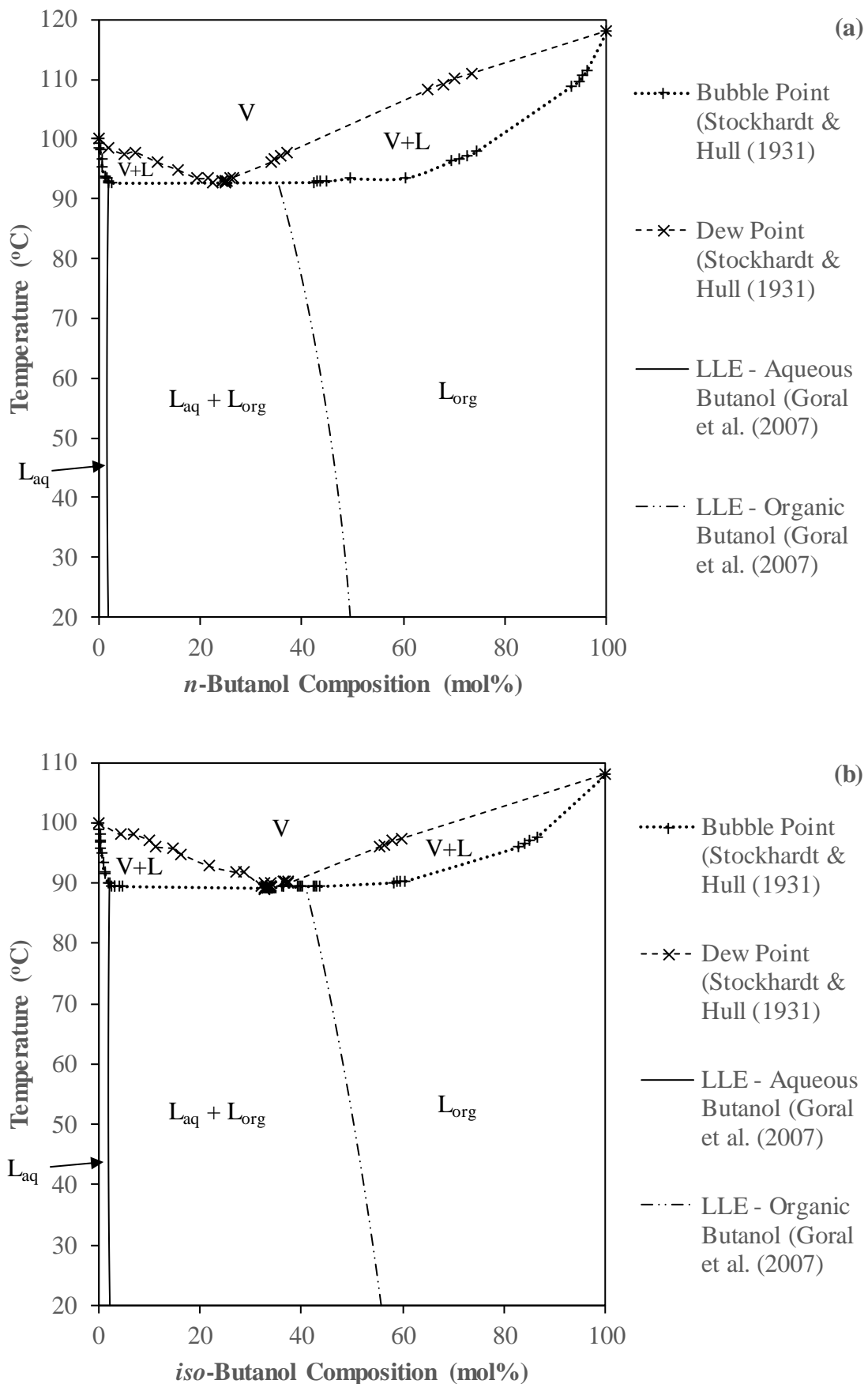


Figure 1-3 – Vapour-Liquid Equilibrium (VLLE) Phase Diagram at 1 bara for (a) n-Butanol/Water; (b) iso-Butanol/Water

Both isomers exhibit very similar vapour-liquid equilibria with water, including a region of immiscibility and a heterogeneous azeotrope. Butanol also has a lower volatility than water. These features, together with its low concentration in the broth, makes the separation of butanol by classical distillation processes not only difficult, but it also requires significant energy input.

Many researchers and manufacturers have investigated a wide range of approaches to reducing the cost of separation. One method is to improve butanol titre in the broth in order to increase the concentration of butanol before separation. Achieving a titre of butanol exceeding its solubility in water (~8 wt%, 2 mol%) would allow a butanol-rich phase to be extracted directly from the broth. However, current research on butanol titres has found that most organisms are inhibited by butanol concentrations above 1 – 2 wt%. Thus, it is unlikely that concentrations exceeding the solubility limit of butanol will be achieved by fermentation soon (González-Peñas *et al.*, 2014). Therefore, efficient methods of separation of butanol remain a significant problem in these processes (Dürre, 2011b).

Since butanol is inhibitory, there has been much interest in *in situ* removal of products from broths. *In situ* product removal (ISPR) effectively achieves continuous removal of products from the fermenter, allowing batch fermentations to run as semi-continuous processes. ISPR can also significantly improve organism productivity per unit fermenter volume by preventing product levels from reaching inhibitory concentrations. For example, Baez *et al.* (2011) produced *iso*-butanol by using *in situ* gas stripping to remove butanol during the fermentation, resulting in a butanol product at 50 g/l. Volumetric productivities of butanol, *i.e.* total rate of butanol production per fermenter liquid volume, of up to 1.4 g/l/h were recorded. Qureshi *et al.* (2005) increased the total solvent productivity of the ABE fermentation from 0.4 g/l/h to 1.7 g/l/h using *in situ* adsorption in a fed-batch ABE process.

Several authors have compared different ISPR techniques for ABE fermentations (Huang *et al.*, 2014; Oudshoorn *et al.*, 2009; Outram *et al.*, 2017, 2016). Commonly-investigated techniques have included flash fermentation, gas and vacuum stripping; pervaporation, liquid-liquid extraction, perstraction and adsorption. Figure 1-4 shows simple process flow diagrams of evaporative techniques for ISPR (flash fermentation, gas and vacuum stripping, pervaporation). Figure 1-5 shows the same for extractive techniques (liquid-liquid extraction and perstraction) and adsorption.

Flash fermentation and vacuum stripping both involve applying reduced pressure to the fermentation broth, causing vaporisation of broth components at the fermentation temperature. As shown in Figure 1-4, during flash fermentation, a vacuum is applied to a liquid stream in a flash tank, thereby producing a vapour stream containing fermentation products and a liquid stream that is recycled back to the fermenter. Conversely, during vacuum fermentation, a vacuum is applied directly to the fermenter, and so the vapour produced contains off-gases from the fermenter as well as fermentation products. In both cases, the low-pressure vapour produced is then compressed and condensed to produce liquid products, at a higher concentration than in the broth.

Vacuum stripping is not suited to gas fermentation because large amounts of off-gas are produced by the fermenter, leading to very large flows through the vacuum pump.

Like flash fermentation, pervaporation also uses low pressure to evaporate broth components, as shown in Figure 1-4. During pervaporation, a permeable membrane is used, with the broth on one side, and low-pressure applied to the other side. Broth components permeate selectively through the membrane and evaporate to form a low-pressure vapour on the vacuum side of the membrane. The retentate left on the broth side of the membrane is recycled back to the fermenter. Due to the use of the selective membrane, pervaporation achieves a greater selectivity towards the fermentation products as compared to flash fermentation. However, the use of a membrane increases capital costs and reduces mass transfer rates.

During gas stripping, the volatile organic products contained in the off-gas from the fermenter are condensed to form liquid products, as shown in Figure 1-4. The remaining gas is recompressed and bubbled back into the fermenter. Recycle rates are kept as high as possible in order to maximise gas flowrate and hence evaporation into the gas stream. During fermentation of synthesis gases, fresh synthesis gas is added to the recycled gas, thus increasing the flowrate of gas through the fermenter. In other fermentation processes, the off-gas can be supplemented with inert gases, such as N₂, or CO₂ to increase the gas flowrate. Gas stripping appears to be ideally suited to the fermentation of synthesis gases, since large quantities of gas must be fed to the fermenter as feedstock as part of the process. Recycle of unreacted gases can be used to increase conversion.

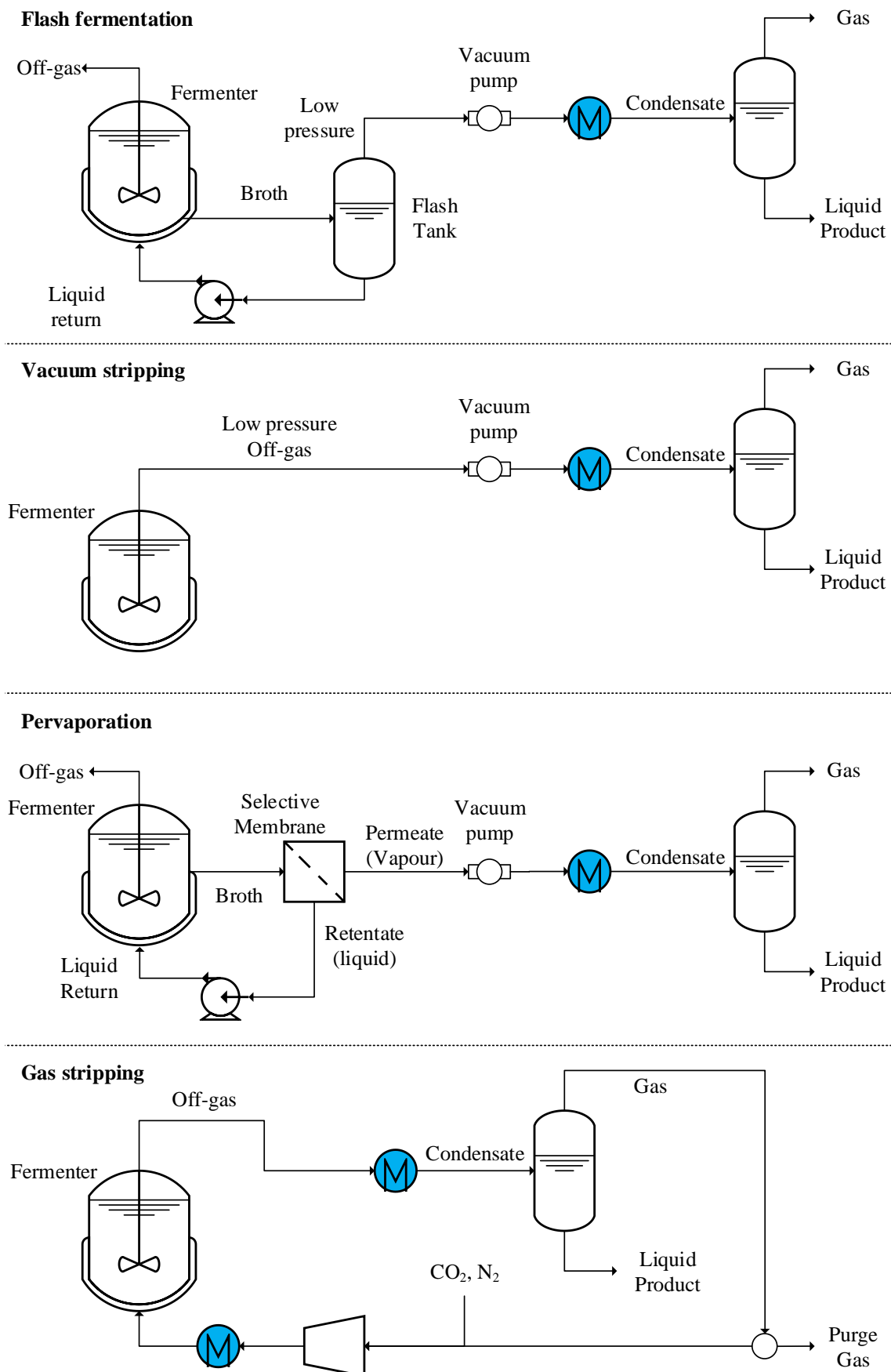


Figure 1-4 – Process Flow Diagrams of evaporative separation techniques for ISPR

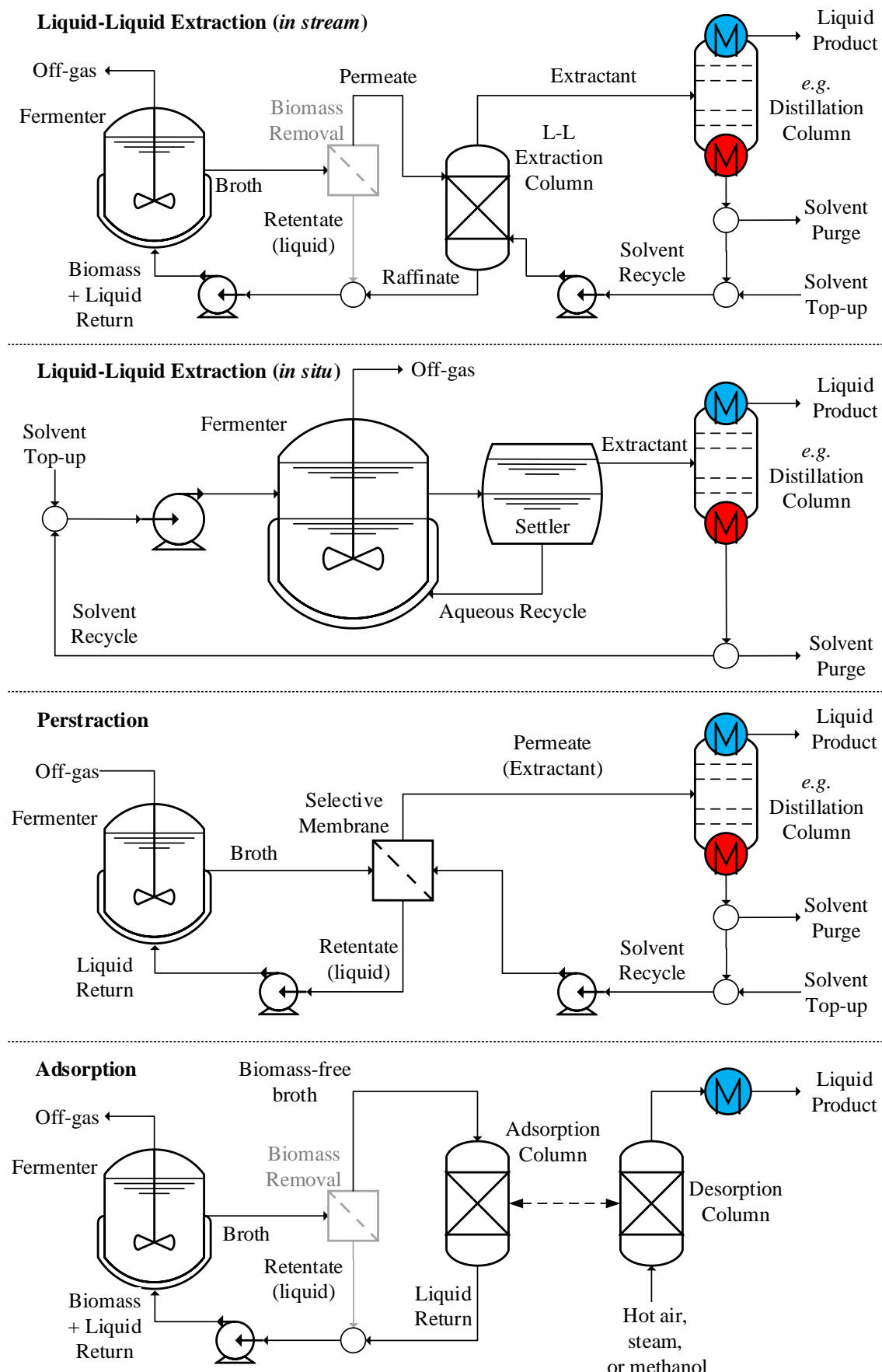


Figure 1-5 – Process Flow Diagrams of extractive and adsorption separation techniques for ISPR

Adsorption has been investigated for selectively binding products from the fermentation broth (Qureshi *et al.*, 2005). As shown in Figure 1-5, in some cases the fermenter broth is first filtered to remove biomass. The broth is then passed through an adsorption column containing the solid adsorbent. Following adsorption, the supernatant is returned to the fermenter. A variety of techniques exist for the regeneration of the adsorbent. In Figure 1-5, a two-column system is used, with one column being regenerated whilst one is used for adsorption. Desorption of the fermentation products can be achieved by increased temperature or reduced pressure. Hot air, steam or methanol can be passed through the column, causing the fermentation products to desorb, and regenerating the adsorbent. The products are then condensed, forming liquid products.

Gas and vacuum stripping, flash fermentation, pervaporation and adsorption all produce an aqueous product stream at a higher concentration than the broth. The products are then purified from this aqueous stream, typically by distillation.

Liquid-liquid extraction is a conventional separation technology employing a solvent of low miscibility with water to extract the products from the aqueous broth into the solvent. As shown in Figure 1-5, the solvent can be contacted with the broth in a number of ways: directly, in the fermenter itself ('*in situ*'); or outside the fermenter ('in stream') in a separate piece of equipment, *e.g.* an extraction column, or a series of mixers and settlers. When a separate unit is used for the extraction, organisms can first be filtered from the broth stream, and then a permeate free from biomass can be fed to the extraction unit. Having separated the solvent and aqueous phases, the resulting extractant, rich in fermentation products, can be purified using conventional separation techniques such as distillation or gas stripping. This also allows the solvent to be recycled. The solvent must be carefully selected so as not to inhibit organism growth, product formation, or cause cell death in the organism. This is because the organism and solvent will either be in direct contact if the organism is present during contact with the solvent; or indirectly *via* droplets of solvent returned to the broth in the aqueous liquid recycle.

As an alternative, perstraction can be used as a separation technique to mitigate a solvent's toxicity to the organism. As shown in Figure 1-5, perstraction employs a selective membrane to separate the aqueous broth from the solvent phase. The membrane can be housed in a separate unit outside the fermenter, as in Figure 1-5, or even built into the fermenter itself. The fermenter products permeate selectively through the membrane into the solvent phase, from which they can subsequently be purified using conventional techniques such as distillation or gas stripping, as *per* liquid-liquid extraction. The

solvent can then be recycled. The membrane in perstraction can improve the selectivity of the separation towards fermentation products compared with liquid-liquid extraction; although the membrane does result in additional capital costs and mass transfer resistance. However, membrane use can reduce solvent toxicity issues and alleviates the requirement for phase separation, which can be a problem with some solvents in liquid-liquid extraction (Groot *et al.*, 1990).

Outram *et al.* (2016) investigated the energy requirements and economic advantages of adding ISPR to an ABE fermentation. It was found that, with the exception of perstraction, ISPR generally increases the overall energy requirement of the plant. In particular, whilst the energy required for distillation was reduced, this was more than offset by the extra energy required for ISPR. Perstraction gave the greatest improvement in economics, although all techniques other than gas stripping resulted in significant profit increases (139 - 175%) owing to increased productivity in the fermenter. Liquid-liquid extraction (using oleyl alcohol) resulted in the greatest proportion (over 70%) of ABE products separated from the broth during ISPR compared with the amount present during the fermentation.

As with other *in situ* product removal techniques, extraction can increase the yield of fermentations by removing inhibitory products. However, the average product yield per unit substrate has been found to be less than those achieved by evaporative techniques such as gas stripping and pervaporation. Indeed, Outram *et al.* (2017) quote average yields of 0.35 g ABE/g substrate for evaporative ISPR techniques, compared with 0.25 g ABE/g substrate for extraction. The reason for this is not clear, as the extractants were selected to be non-toxic. However, it has been postulated that the difference in product yield could be due to substrate or intermediates (such as acids) being removed from the broth by the solvent, or perhaps because of long-term toxic exposure to the solvent. These mechanisms would be specific to the type of fermentation and organism, and so the effect might be different on, for example, fermentation of synthesis gases.

Results from different studies are very difficult to compare directly, since they make very different assumptions about process design, achievable fermentation titre and product stoichiometry. Oudshoorn *et al.* (2009) performed a simple quantitative approach to compare the energy requirement of various techniques. The analysis neglected the specifics of the processes; it used selectivity estimates for each technique and simplified thermodynamics to estimate the energy required for separation of ABE solvents from water. At a total ABE solvent concentration of 20g/l, the analysis found that adsorption

and pervaporation could theoretically require less than 2 MJ/kg butanol, with liquid-liquid extraction requiring 7.7 MJ/kg. Qureshi *et al.* (2005) calculated the energy requirements of adsorption, liquid-liquid extraction and pervaporation to be 8, 9 and 14 MJ/kg respectively. A wide range of separation techniques for ISPR of ABE fermentations was reviewed by Huang *et al.* (2014), who concluded that adsorption, liquid-liquid extraction and pervaporation were the most energy-efficient approaches.

None of the evaporative and adsorption-based separation techniques explored are able to produce reagent- or fuel-grade butanol from aqueous fermentations. These techniques separate butanol from the broth during fermentation, resulting in an increase in the butanol productivity in the fermenter. These techniques often also increase the concentration of butanol in resultant aqueous solution, improving the economics of subsequent purification by distillation. Distillation of aqueous butanol is still therefore a requirement in these processes owing to the relatively poor selectivity of butanol over water of these separation techniques.

In Appendix A, the energy required for the purification of butanol from fermentation broths using distillation was simulated for different fermentation processes to serve as a standard against which other separation methods could be judged.

The separation of butanol from fermenter broths is a known problem in all butanol fermentations (*e.g.* ABE process, *iso*-butanol production, fermentation from synthesis gases). It is particularly expensive in terms of energy consumption as butanol is less volatile than water. Many authors have explored standard techniques to concentrate or separate aqueous butanol broth mixtures, including: distillation; liquid-liquid extractions; perstraction; gas and vacuum stripping; adsorption; as well as other novel techniques. *In situ* removal of butanol can increase the productivity of fermentations by removing the toxic product from the broth during the fermentation process itself, but existing methods are energy-intensive.

1.6 Objectives and Structure of Work

The overall objective of the research presented in this dissertation was to develop and investigate energy efficient techniques to separate dilute butanol from aqueous fermentation broths. The specific objectives were as follows:

1. To develop an energy-efficient technique for the separation of butanol from aqueous fermentation broths, ideally using conventional materials and equipment, which overcomes the limitations of existing techniques
2. To investigate the design of any techniques developed for use in different fermentation processes, *e.g.* ABE process, fermentation from synthesis gases
3. To characterise the performance of any techniques developed for the separation of butanol from aqueous fermentation broths
4. To determine the optimal design and operating conditions for any techniques developed

This chapter has provided a background to the production of butanol *via* fermentation. It has highlighted efficient separation of butanol from the broth as one of the key challenges in the implementation of fermentative production of butanol; improvements in butanol separation would both reduce the energy requirements and alleviate some of the biochemical limitations of such processes. Chapter 2 considers the use of liquid-liquid extraction for the separation of butanol from aqueous broths and proposes a novel extraction method employing C₄ – C₅ hydrocarbons as extractants. The equilibria behaviour of fermentation products with the relevant C₄ – C₅ hydrocarbons were characterised in Chapter 3. Models of the equilibria behaviour of these mixtures were used to evaluate the performance of a liquid-liquid extractor for the separation of butanol from aqueous broths using C₄ – C₅ hydrocarbons in Chapter 4. Chapter 5 evaluates the performance of the entire novel extraction scheme *via* simple flowsheet models. Conclusions drawn from the research are discussed in Chapter 6, whilst Chapter 7 proposes suggestions for further work.

This dissertation also makes use of Appendices for investigations which were essential to achieving the objectives, but which were less novel. For example, a simulation of the distillation of butanol and other fermentation products from aqueous broths is described and discussed in Appendix A. The results of this simulation are employed to compare the energy requirements of alternative processes with those of distillation of the aqueous broth.

Parts of the work presented in this dissertation have been filed in a patent:

Hodgson, P.J., Dennis J.S., 2017 [Publication date: October 2018]. Patent Application Number PCT/GB2018/000057. UK, Intellectual Property Office.

2. Development of a Novel Butanol Separation Method Using Short Hydrocarbons as Extractants

2.1 Introduction

Separation techniques based on solvent extraction exploit butanol's limited miscibility with water. Since extraction produces a butanol-solvent mixture, these techniques present an opportunity to avoid the requirement for energy-intensive distillation of aqueous butanol. Here, liquid-liquid extraction has been investigated using short-chain hydrocarbons. Most research on hydrocarbon solvents has focussed on C₆₊ (Dadgar and Foutch, 1986; González-Peñas *et al.*, 2014; Groot *et al.*, 1990; Kim *et al.*, 1999). However, these hydrocarbons have tended to be dismissed in favour of solvents with larger distribution coefficients. This dissertation proposes the use of volatile hydrocarbons as extractants for the separation of aqueous butanol. These short hydrocarbons (C₄ – C₅) have largely been overlooked in the literature.

There are several ways in which solvent extractions could be performed during the fermentation process. Extraction could take place directly on the broth in the fermenter itself (*in situ*), or outside the broth ('in stream'). 'In stream' extraction could be conducted in the presence of, or following filtration of, fermentation organisms. Finally, permeable membranes could also be used to separate the solvent from the broth using perstraction techniques.

2.1.1 Distribution Coefficient and Selectivity

The distribution coefficient and selectivity are important factors in determining the suitability of solvents for extraction. The distribution coefficient of a solute (butanol) transferred from one solvent (water) to another (the solvent phase) is defined as the ratio of the solute compositions in each phase, *i.e.*:

$$D_i^{molar} = \frac{x_i(\text{organic solvent phase})}{x_i(\text{aqueous phase})} = \frac{x_i^{org}}{x_i^{aq}} \quad (2-1)$$

The distribution coefficient at equilibrium can be related to the activity coefficient of the solute in each phase by considering the chemical potential of both phases. The chemical potentials (μ_i) of two liquid phases, I and II , are equal at equilibrium:

$$\mu_i^I(x_i^I, P, T) = \mu_i^{II}(x_i^{II}, P, T) \quad (2-2)$$

Defining deviation from ideal mixture behaviour through activity coefficient, γ_i as:

$$RT \ln \gamma_i = \left(\frac{\partial G^E}{\partial n_i} \right)_{T, P, n_j} = \overline{G}_i^E \quad (2-3)$$

Where G^E is the excess Gibbs free energy (the difference between the Gibbs free energy and that for an ideal mixture). Hence:

$$\mu_i^I(x_i^I, P, T) = \mu_i^o(x_i = 1, P^o, T) + RT \ln[x_i^I \cdot \gamma_i^I(x_i^I, P, T)] \quad (2-4)$$

Hence, at liquid-liquid equilibrium:

$$x_i^I \cdot \gamma_i^I(x_i^I, P, T) = x_i^{II} \cdot \gamma_i^{II}(x_i^{II}, P, T) \quad (2-5)$$

The molar distribution coefficient, also known as partition coefficient, can therefore be related to the activity coefficients of the solute in each phase at equilibrium:

$$D_i^{molar} = \frac{x_i^{org}}{x_i^{aq}} = \frac{\gamma_i^{aq}(x_i^{aq}, P, T)}{\gamma_i^{org}(x_i^{org}, P, T)} \quad (2-6)$$

Therefore, for liquid-liquid extraction of butanol from an aqueous broth:

$$D_{Bu}^{molar} = \frac{x_{Bu}^{org}}{x_{Bu}^{aq}} = \frac{\gamma_{Bu}^{aq}(x_{Bu}^{aq}, P, T)}{\gamma_{Bu}^{org}(x_{Bu}^{org}, P, T)} \quad (2-7)$$

Distribution coefficients are also frequently expressed as a mass ratio:

$$D_{Bu}^{mass} = \frac{m_{Bu}^{org}}{m_{Bu}^{aq}} = D_{Bu}^{molar} \cdot \frac{\sum_j x_j^{aq} \cdot Mr(j)}{\sum_j x_j^{org} \cdot Mr(j)} \cong D_{Bu}^{molar} \cdot \frac{Mr(aq.)}{Mr(org.)} \text{ (if dilute)} \quad (2-8)$$

The distribution coefficient determines the concentration of the product in the extracted phase and therefore the quantity of solvent required. The costs of purifying the product and of recovering the extractant are proportional to the quantity of solvent used in the extraction.

The selectivity, or separation factor, is defined as the ratio of the distribution coefficient for the desired component (butanol) to the distribution coefficient of an unwanted component (e.g. water):

$$S_{Bu,H_2O} = \frac{D_{Bu}^{molar}}{D_{H_2O}^{molar}} = \frac{x_{Bu}^{org}}{x_{Bu}^{aq}} \cdot \frac{x_{H_2O}^{aq}}{x_{H_2O}^{org}} \approx \frac{D_{Bu}^{Bu}}{x_{H_2O}^{org}} \text{ (if aqueous phase is dilute)} \quad (2-9)$$

The selectivity of component *i* versus component *j*, $S_{i,j}$, can be shown to be identical irrespective of whether mass or molar distribution coefficients are used. Selectivity is the ability of the extractant to separate a component preferentially. Thus, higher values of selectivity for butanol versus water mean that less water enters the solvent stream and therefore a lower number of contacting stages are required (Dadgar and Foutch, 1986; Treybal, 1951).

2.1.2 Previous Research to Identify Suitable Extractants

Much work has been devoted to identifying suitable extractants for separation of dilute aqueous butanol and ABE mixtures. Apart from suitable distribution coefficients and selectivities of butanol over water, suitable solvents need to be biocompatible with fermentation organisms, so that the extracted aqueous stream can be returned to the fermenter. Generally, alkanes have been considered but always been rejected – arguably prematurely – in favour of solvents with higher distribution coefficients. The novel use of short, volatile hydrocarbons as solvents in the extraction of butanol from aqueous broths is proposed here and developed in the rest of this dissertation.

Hydrocarbons (saturated, unsaturated and aromatic), alcohols, ketones, acids, esters and haloalkanes were investigated as solvents by Dadgar and Foutch (1986). The distribution coefficients and selectivities of these solvents were measured in a typical ABE mixture containing acetone, butanol and ethanol in a molar ratio of 3:6:1, with the butanol concentration being 1.6 wt%. The authors concluded that non-polar hydrocarbons had relatively poor distribution coefficients, which worsened as the chain length increased. Substituting non-polar hydrocarbons for hydrocarbons with halide and nitrogen groups gave improved distribution coefficients. Aliphatic alcohols were found to have the highest distribution coefficients ($D_{Bu}^{mass} \sim 5 - 8 \text{ kg/kg}$).

Kim *et al.* (1999) noted that an increased degree of polarity of solvents generally increased the distribution coefficients of polar chemicals such as butanol and ethanol. Their screening process found that carboxylic acids, followed by alcohols, organic phosphates and esters, had higher distribution coefficients than relatively non-polar solvents, such as halocarbons and hydrocarbons. Findings also indicated that branched-chain solvents tended to have higher distributions coefficients and selectivities than straight-chain solvents. Organic acids and esters were highlighted as having high

selectivity and distribution coefficients for butanol. However, an increased polarity of solvent loosely correlated with increased toxicity to the organisms in the fermentation. This was the inverse of the relationship found for distribution coefficient. Thus, alkanes were found to be the most biocompatible.

The distribution coefficients and selectivities of butanol at a typical fermentation temperature (37°C) were measured by Groot *et al.* (1990) for alkanes, alcohols (C₆+), vegetable oils and organic acids, starting with 2 wt% aqueous butanol and using equal volumes of extractant and aqueous solution. The toxicity of the solvents towards *Clostridium beyerinckii* was also determined, resulting in alcohols and several acids being eliminated for *in situ* extraction. Whilst alkanes were found to have high selectivities (of the order of 3,000), their distribution coefficients ($D_{Bu}^{mass} \sim 0.5 \text{ kg/kg}$) were lower than non-toxic vegetable oils and organic acids ($D_{Bu}^{mass} \sim 1 - 4 \text{ kg/kg}$). Oleic acid, castor oil and isopropyl myristate were selected as potential extractants and tested in both a batch and continuous fermentation to produce *iso*-propanol and butanol. Several problems were encountered. All three solvents were contaminated after a period of solvent recycle by medium components, found to be protein precipitates. Oleic acid and castor oil formed stable emulsions. Finally, oleic acid regenerated by distillation became toxic, possibly due to thermal degradation at high temperatures. It is possible that the toxicity difficulties encountered were specific to *Clostridium beyerinckii* and the medium used, since, as the researchers note, successful extractions with these solvents have been published by others.

The problems encountered led Groot *et al.* (1990) to investigate extraction *via* a membrane (perstraction). This is a commonly-favoured solution since it can avoid some of the difficulties encountered in direct extraction of toxicity, emulsion formation and some solvent fouling. In addition, permselective membranes can increase selectivity towards a target product due to faster permeation rates of the target products through the membrane *versus* other components. However, the use of membranes increases capital cost and increases mass transfer resistance (Groot *et al.*, 1990; Huang *et al.*, 2014). The design and selection of suitable membranes for perstraction is an additional key factor for indirect extractions. Groot *et al.* (1990) conducted perstraction on fermentations using oleyl alcohol with silicone, neoprene and latex membranes, and concluded that silicone membranes had the highest mass transfer coefficients. To reduce the energy demands of perstraction, membranes with high flux and separating factors must be found (Outram *et al.*, 2016).

The practical problems encountered by Groot *et al.* (1990) demonstrate that distribution coefficient and selectivity alone are not sufficient to determine solvent suitability. For example, the biocompatibility of solvents with fermentation organisms is also an essential factor in solvent selection, since in many liquid-liquid extraction systems the organisms will come into contact with the extractant directly or indirectly *via* broth recycle. Various authors have attempted to outline selection criteria for extractants in order to identify appropriate solvents. Commonly-found decision criteria are summarised by Huang *et al.* (2014) and Outram *et al.* (2017) as:

- Non-toxic to organism and sterilizable
- High distribution coefficient
- Low mutual miscibility with water, high selectivity (less solvent lost in aqueous phase, less water transferred to solvent phase)
- Large density difference with water (easily separable phases)
- Low viscosity (low energy consumption in phase mixing)
- Large interfacial tension (reduces emulsions and readily phase separates)
- Highly stable, non-reactive with relevant mixtures, and safe
- Readily commercially available at low cost
- Suitable volatility or boiling point (for purification of product)

Of these criteria, distribution coefficient and selectivity appear have been prioritised in most research, along with toxicity tests in some (Huang *et al.*, 2014). However, compromises often have to be made when balancing these properties. Highly polar, hydrophilic solvents have high distribution coefficients, but are also more soluble in water and hence have relatively poor selectivity, whereas non-polar hydrophobic solvents have low mutual solubilities but tend to have a poor affinity with butanol and hence lower distribution coefficients. Low mutual solubilities tend to suggest lower toxicities towards organisms since they result in lower concentrations of the solvent in the aqueous medium in which organisms operate. Hence, if the solvent is toxic to the organism, low solubility in the medium minimises organism contact with the solvent. This relationship between solubility and toxicity is often used in screening processes. Aqueous solubility-related parameters for solvents, such as the Hildebrand solubility parameter or the octanol-water

partition coefficient ($\log P_{oct}$), are often used as basic screening tests for toxicity towards organisms (González-Peñas *et al.*, 2014; Groot *et al.*, 1990).

The biocompatibility of extractants to organisms is a complex phenomenon and depends upon many factors. These include: the precise organism; broth composition; growth phase; and the operation of the extraction equipment. This complexity is evidenced by the differing biocompatibility results produced by a variety of researchers (González-Peñas *et al.*, 2014). There are many differing hypotheses about how and why solvents cause fermentations to stop prematurely. For example, solvents contained in aqueous recycle streams could dissolve in the aqueous medium and be subsequently adsorbed by the organism, causing toxicity directly. This effect is exacerbated by larger solubilities of the solvent in water and, in general, solvents with low molecular masses are more easily adsorbed by organisms (Groot *et al.*, 1990). Other solvents could interfere indirectly with the fermentation process by extracting key nutrients or intermediates (such as butyric acid) from the broth. This is likely to be exacerbated by higher distribution coefficients, leading to an efficient extraction of other organic compounds.

The broth composition, the type of organism and its growth phase have a significant impact on this mechanism. As a result, some high-performing extractants might be unsuitable for direct liquid-liquid extraction of butanol from fermentation broths. Testing extractions on a specific fermentation is required in order to verify the toxicity of a given solvent, especially for solvents with high distribution coefficients or high aqueous solubilities. The toxicity of solvents with high distribution coefficients is a key motivation for the development of perstraction techniques. However, the use of the membrane in perstraction might not prevent the solvent from affecting the fermentation indirectly by extracting key nutrients or intermediates. Toxic solvents might also be adsorbed into the membrane (Groot *et al.*, 1990). Conversely, a review by Outram *et al.* (2017) found no conclusive evidence that toxic extractants with high distribution coefficients cannot successfully be used for perstraction separation in butanol fermentation systems.

Oleyl alcohol has become a standard solvent in investigations of butanol extraction, as well as a benchmark against which other extractants are compared. This is because it has generally been found to be non-toxic to microorganisms and has a relatively high distribution coefficient for butanol of *circa* 4 kg/kg, with a selectivity of *circa* 200 dependant on broth concentrations (Huang *et al.*, 2014; Outram *et al.*, 2016). González-Peñas *et al.* (2014) identified 2-butyl-1-octanol as a potential improvement on oleyl

alcohol. This solvent had previously been little investigated, and a favourable distribution coefficient of ~8 kg/kg and a selectivity of ~650 were recorded at an aqueous concentration of butanol of 1 wt% and 36°C.

Ionic liquids are of particular interest as solvents for three main reasons: (i) their tuneable properties, such as hydrophobicity or affinity to butanol; (ii) their large density difference with water (*e.g.* [BMIM][PF₆] density 1369 kg/m³) which makes organic and aqueous phases easily separable; and (iii) their non-volatility, which allows trivial purification of butanol from the solvent phase (Ha *et al.*, 2010). Ionic liquids with distribution coefficients an order of magnitude higher than oleyl alcohol have been reported (Huang *et al.*, 2014). However, the high viscosity of ionic liquids presents a significant energy barrier to mass transfer rates (Huang *et al.*, 2014), and their biocompatibility needs to be investigated further (Ha *et al.*, 2010).

Roffler *et al.* (1987) considered the use of oleyl alcohol as an extractant, diluted to 50 wt% by decane to reduce the extractant's viscosity and to improve mass transfer and phase separation. A techno-economic analysis was performed on a process design for a fed-batch ABE fermentation with *in situ* extraction using this extractant – resulting in a prediction of a 20% reduction in cost versus a conventional batch fermentation. The potential loss of solvent in the broth, as well as potential contamination of products by the solvent, were highlighted as key issues following the analysis. González-Peñas *et al.* (2014) also proposed that the inclusion of alkanes in solvent mixtures might be beneficial for improving other physical properties of the solvent, such as viscosity. Blends of long-chain, branched alkanes with fatty alcohols, acids and ethers have attracted interest from industrial manufacturers. Butamax has filed patents for the use of such blends as extractants in *iso*-butanol fermentations (Zaher, 2015).

2.2 Employing Volatile Hydrocarbons as Extractants

Whilst simple hydrocarbons do not possess the large distribution coefficients found in longer alcohols, they are, in many other respects, relatively ideal solvents. The benefits of simple hydrocarbons include:

- very low mutual solubilities with water, allowing a highly selective separation, and minimising losses of solvent to the fermenter broth stream;
- non-toxic to organisms (as demonstrated in toxicity trials of C₆+ by Groot *et al.* (1990)), partially due to their very low solubility in aqueous fermenter broths;

- being relatively thermally and chemically stable, improving the safety of the process and preventing the solvent from degrading (and potentially becoming toxic) during butanol purification;
- completely miscibility with butanol owing to butanol's C₄ group
- their compatibility as a fuel, where the product butanol contains trace amounts of hydrocarbons from the extraction;
- favourably low viscosity and density allowing for negligible energy requirements for mixing, faster mass transfer and easier phase separation in liquid-liquid extractions (0.24 and 0.31 mPa s for pentane and hexane respectively at 25°C (Smallwood, 1996) *c.f.* ; 28 mPa s for oleyl alcohol at 25°C (Blahušiak *et al.*, 2013), 7.5 mPa s at 25°C for octanol (Smallwood, 1996));
- a relatively large difference in density compared to aqueous solution, allowing for simple phase separation (611 kg/m³ for pentane and 647 kg/m³ for hexane at 35°C versus *c.f.* 991 kg/m³ for water (Rowley *et al.*, 2008); *c.f.* oleyl alcohol 840 kg/m³ at room temperature (Roffler *et al.*, 1987));
- relatively high interfacial tension with water (49 mN/m for hexane and water at 35°C (Zeppieri *et al.*, 2001), *c.f.* 9 mN/m for octanol and water at 35°C (Cárdenas *et al.*, 2015)), hence reducing the formation of emulsions;
- availability and low-cost;
- in some cases, the fact that some hydrocarbons could be obtained from the product butanol, thereby potentially providing an inexpensive source of make-up solvent.

Turning to C₄ – C₅ hydrocarbons, the materials typically have boiling points at atmospheric pressure below fermentation temperatures and are therefore significantly more volatile than butanol, which boils at 118°C at 1 bara. Thus, after liquid-liquid extraction using such a solvent, the solvent might well be recovered by distillation noting that it is the more volatile component. This is counter to the conventional approach of using an extractant less volatile than butanol, which means that the dilute butanol is vaporised during the subsequent distillation.

On first consideration, the use of such hydrocarbons as extractants would appear significantly more costly in terms of energy consumption than the use of solvents less volatile than butanol. Distilling butanol from a dilute concentration in a heavy solvent should require far less energy than distilling a much larger quantity of a light solvent from

a mixture containing dilute butanol. The high volatility of these hydrocarbons is therefore one of the reasons why they have been ignored. However, since the boiling points of C₄ and C₅ hydrocarbons are relatively low, much of the heat required for boiling could be supplied by low-grade heat sources, such as the heat produced in the fermenter. This heat source would otherwise go to waste – indeed it is often a significant cooling demand on the fermentation system. Large surpluses of low-grade heat are typically available on both direct biochemical and synthesis gas fermentation processes, although such heat is often neglected in simple flowsheet models of these processes (*e.g.* sterilisation requirements).

The enthalpies of vaporisation of non-polar C₄ – C₅ hydrocarbons are significantly lower than that of water due to a lack of polar intermolecular forces. Therefore, for the same molar concentration of butanol, a butanol-hydrocarbon mixture requires significantly less energy to separate by distillation than that required for a butanol-water mixture.

Since C₄ and C₅ hydrocarbons have high volatilities relative to butanol, separation by distillation would be relatively simple. In the case of C₅ hydrocarbons, distillation could, if necessary, be conducted under slightly reduced pressure for suitable heat integration. In the case of C₄ hydrocarbons, distillation and liquid-liquid extraction could be conducted under elevated pressure. C₁ – C₃ hydrocarbons are not suitable extractants as they are significantly more miscible with water and would also require highly elevated pressures at typical broth temperatures since they have very low boiling points. C₆ – C₇ hydrocarbons require significant pressure reduction to separate from butanol using low-grade heat sources, and the relative volatility compared to butanol is significantly reduced, making distillation more costly. Beyond C₆ – C₇, hydrocarbons are less volatile than butanol. Figure 2-1 details atmospheric boiling points for all C₄ – C₅ alkane and alkenes, and relevant butanol isomers. Figure 2-2 details the vapour pressures of these compounds at 25°C, 32°C and 37°C. Boiling points at 1 bara and vapour pressure were calculated from Poling *et al.* (2001), except for *iso*-pentene, 2-methyl-1-butene and (*E*)-2-pentene for which correlations were not available and so were taken from NIST (2016). As detailed in Figure 2-1, C₄ and C₅ hydrocarbons span normal boiling points in the range -12°C – 49°C, with vapour pressures at typical broth temperatures of 0.5 – 5 bara (Figure 2-2). Boiling points increase with chain length, and alkenes generally have lower boiling points than their corresponding saturated alkane.

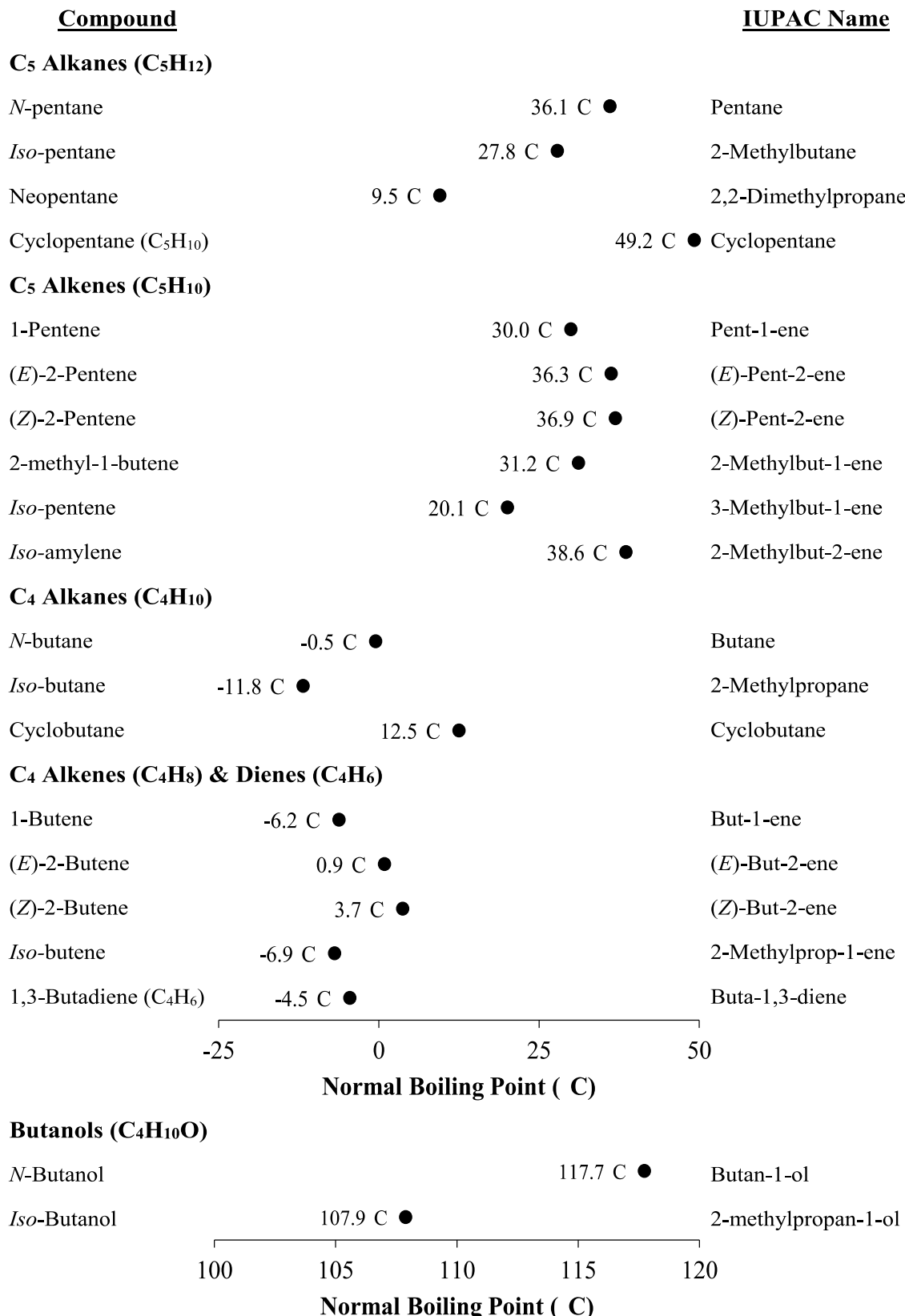


Figure 2-1: IUPAC Names and boiling points at 1 bara for C₄ – C₅ alkanes, alkenes, 1,3-butadiene and relevant butanol isomers

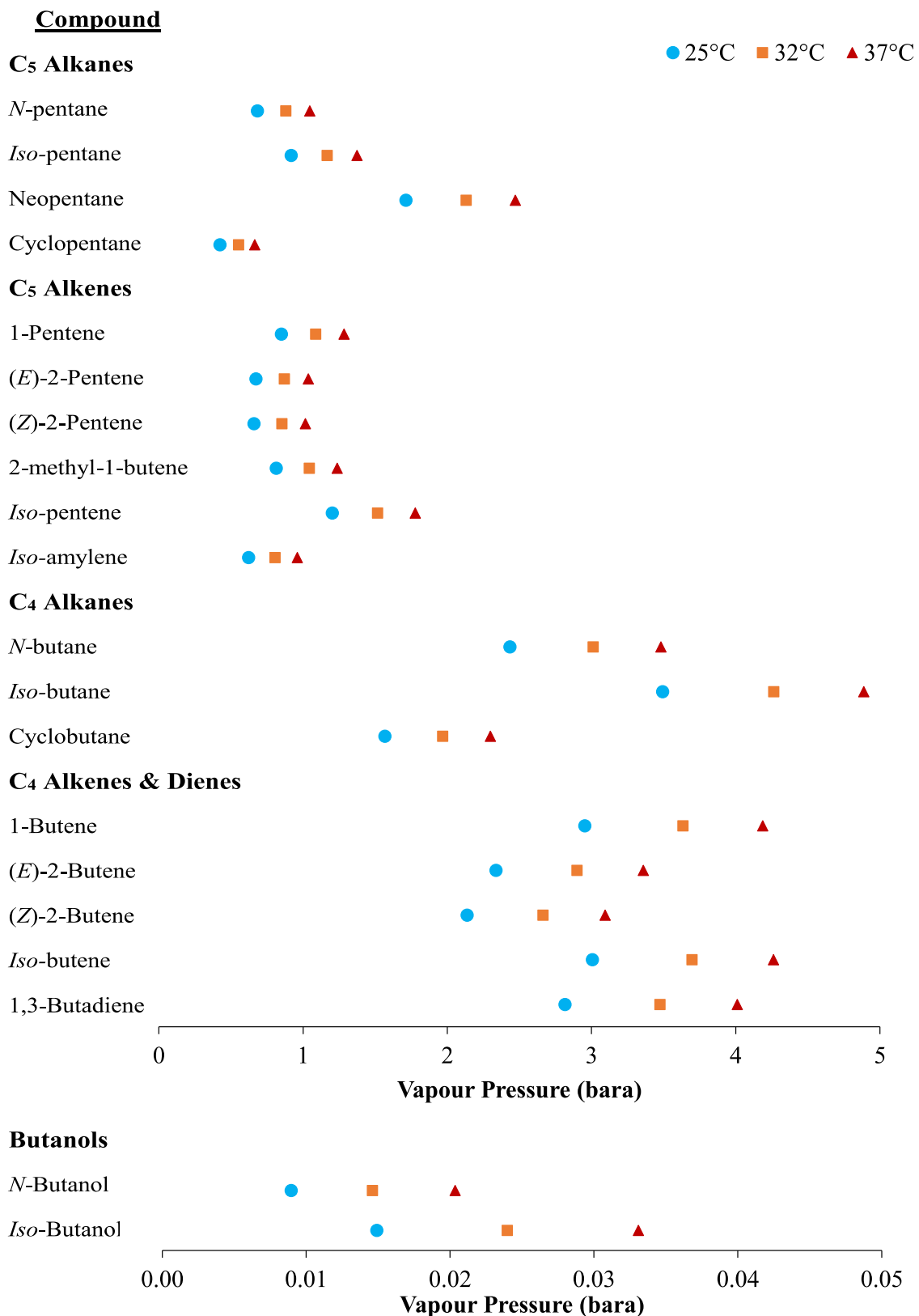


Figure 2-2: Vapour pressures at relevant temperatures for C₄ and C₅ hydrocarbons, and butanol isomers

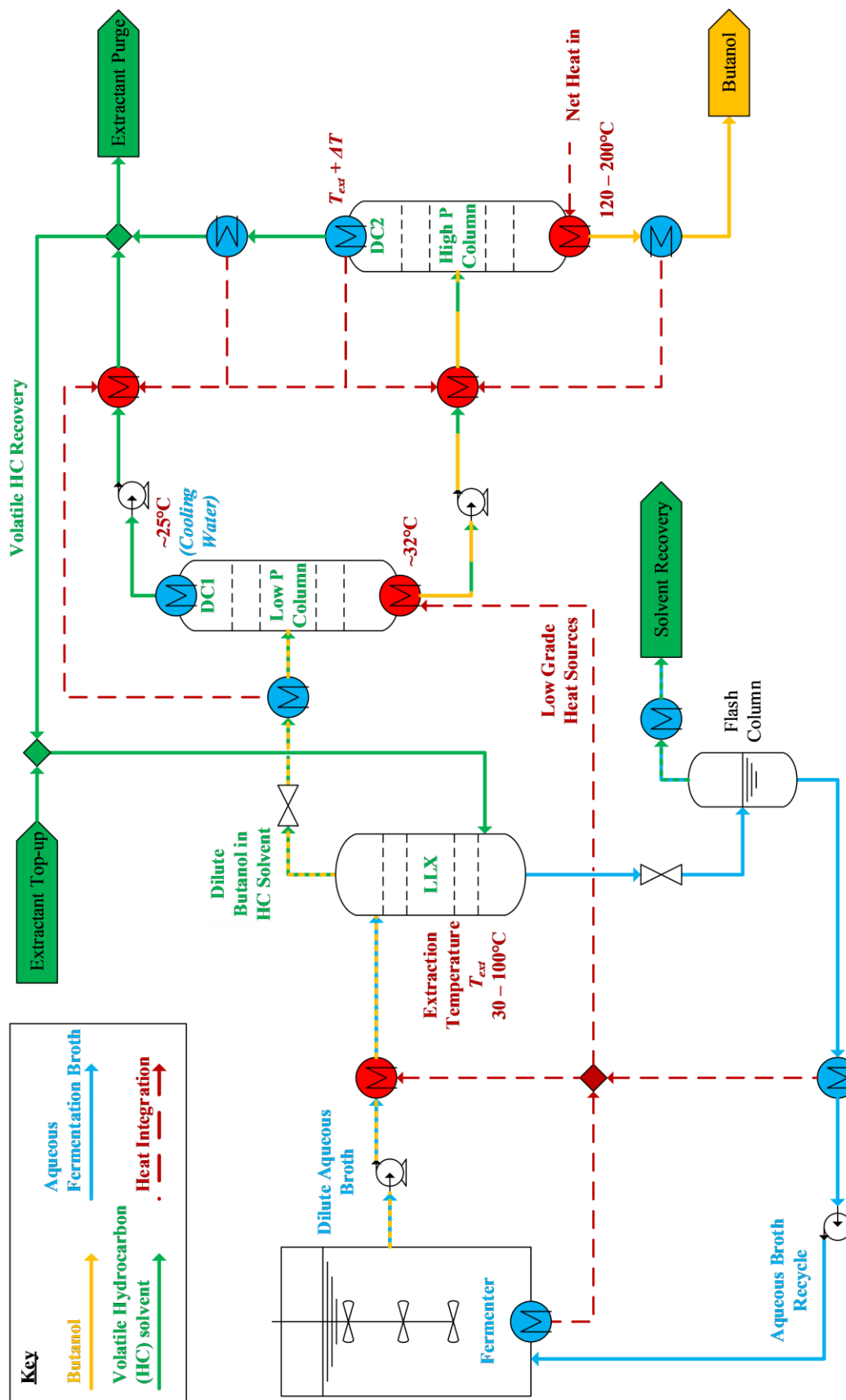
Some of the common pitfalls of LLX of dilute butanol from aqueous fermentation broths identified by Groot *et al.* (1990) could be avoided by using volatile C₄ – C₅ hydrocarbons. One such problem was the build-up of contaminants, including relatively heavy, low volatility compounds from the broth such as protein precipitates in particular. These contaminants foul the recycled solvent stream, thereby demanding high levels of solvent purge. This adds considerable cost, both in replacing lost solvent and in solvent purification. This problem is avoided by using volatile solvents as the solvent is boiled off, and so the recycled solvent remains relatively pure. Some of the heavier or strongly-polar extractants used in other studies (Groot *et al.*, 1990), such as castor oil and oleic acid, formed strong emulsions with the aqueous broth. The use of C₄ – C₅ hydrocarbons might reduce this problem because they have a low viscosity, are non-polar, and have a relatively high interfacial tension with water. However, it would be necessary to test extractions in specific fermentation broths as salts and any surfactants present in the broth would play a significant role in the formation of emulsions.

Finally, it is possible that during distillation, some extractants might degrade or react with trace broth components to form toxic compounds. These toxic compounds would come into contact with the organisms either directly, or indirectly *via* the aqueous broth recycle. For example, oleic acid has been found to become toxic to the broth following separation from butanol by distillation (Groot *et al.*, 1990). This is unlikely to be an issue with C₄ – C₅ hydrocarbons given the low temperatures involved, and stability of C₄ – C₅ hydrocarbons.

This novel method has recently been patented (Hodgson and Dennis, 2017). An illustration of the method is shown in Figure 2-3, confined to the separation of butanol only for the purposes of simplicity. Here, heat from the fermentation would be used to vaporise some of the C₄ or C₅ extractant. A significant advantage of this system is that it uses common industrial chemicals as extractants and relies entirely on the mature technologies of liquid-liquid extraction, and distillation coupled with heat integration. The flow diagram is described in Section 2.3 below.

2.3 Process Design

This scheme, shown in Figure 2-3, uses two distillation columns to separate the solvent and the butanol. The first column operates at low pressure and uses waste heat to concentrate the butanol as much as possible. The second column operates at a higher pressure and completes the separation of butanol from the solvent.


 Figure 2-3 – Separation and heat integration scheme using C₄ and C₅ hydrocarbons as extractants

The two-column approach is necessary because the temperature gradient in the first column is governed by two factors: (i) the temperature of the reboiler, governed by the temperature of the available waste heat; and (ii) the condenser temperature, governed by the temperature of the cooling water. Therefore, the first column cannot necessarily achieve complete separation of butanol from the solvent; the second column consumes high-grade heat to create a temperature gradient large enough to complete the separation.

For example, the fermenter produces heat at 37°C, thereby limiting the reboiler to 32°C – assuming a temperature driving force of 5°C for the reboiler. The pressure of the column is governed by the temperature of the condenser, in which purified solvent condenses. The condenser temperature is determined by the temperature of the coolant (*e.g.* cooling water, giving rise to a condenser temperature of 25°C). Achieving a larger temperature gradient in the column would require a lower temperature in the condenser; this might necessitate refrigeration or recompression of distillate vapour.

Owing to the high volatility of short hydrocarbons relative to butanol, the column would probably require very few stages and so the pressure drop across the column would be minimal. The limited temperature gradient over the first column puts an upper limit on the concentration of butanol obtainable from the bottoms of this column. This maximum concentration equates to the bubble-point composition of a butanol-solvent mixture at the reboiler temperature and pressure. For an ideal mixture, the greater the relative volatility (*i.e.* the more volatile the hydrocarbon), the higher the concentration of butanol obtainable for a given reboiler temperature. Consequently, this limiting butanol concentration puts an upper limit on the amount of low-grade heat that can be utilized by the first column.

The second column uses higher-grade heat to complete the separation of butanol from the solvent. Therefore, the temperature in the reboiler will be equal to the boiling point of the purified butanol at the column pressure. Whilst this column could be operated at the same pressure as the first, there are advantages in operating the second column at a higher pressure. This strategy means that heat from the condenser of the second column, and any heat produced from cooling its bottoms product, can be usefully recovered. The heat can be recycled as low-grade heat for the reboiler of the first column, or used to re-heat the solvent recycle of the first column to the extraction temperature. However, this strategy does come with the penalty that the high-grade heat to the second column must be supplied at a slightly higher temperature – the boiling point of pure butanol at the raised pressure. Furthermore, as relative volatility decreases with increased temperature, a slightly higher pressure in the second column will mean that slightly more stages in the

column will be required. This strategy of recycling heat from the second column will be investigated in Chapter 5.

2.3.1 Multicomponent Broths

The separation scheme proposed thus far has only considered a binary mixture of water and butanol. Other fermentation products such as acetone and ethanol must also be accounted for, including any intermediates such as butyric acid. These chemicals are all more polar than butanol and therefore have a higher affinity with water than butanol. They therefore have relatively poor distribution coefficients when non-polar hydrocarbons are used as extractants.

A number of strategies could be devised for handling volatile side-products such as acetone and ethanol. Two such strategies are depicted in Figure 2-4. One is to attempt to recover the volatile side-products alongside butanol as part of the extraction process. Although the distribution coefficients for these side-products in volatile hydrocarbons are poor, some ethanol and acetone would still be transferred into the solvent phase. Owing to their low concentration and volatility, it is likely that they would evaporate into the vapour phase during distillation. It would then be necessary to separate the side-products from the solvent vapour before recycling the solvent back to the extraction. This could be achieved by condensing the side-product out of the vapour stream *via* refrigeration or *via* re-compression of the vapour and an additional distillation step. Side-draws containing higher side-product concentrations from the butanol-solvent distillation might improve the energy efficiency of this additional separation process. In order to achieve complete separation of these products from the broth, large quantities of solvent would be required due to their low distribution coefficients.

Alternatively, the liquid-liquid extraction could focus on selective removal of butanol from the broth, leaving acetone and ethanol in the aqueous stream. This is also depicted in Figure 2-4. Any small amounts of volatile acetone or ethanol extracted into the solvent stream would be at a low concentration in the solvent, and subsequently would evaporate into the vapour phase during the distillation of the solvent. Acetone and ethanol would therefore be condensed and recycled in the solvent recycle back to the extraction. Since ethanol and acetone would not be removed from the solvent recycle, the ethanol and acetone concentrations in the solvent recycle would equilibrate with the concentrations of these side-products in the broth stream. This would mean that no acetone and ethanol would be transferred from the broth to the solvent during the extraction.

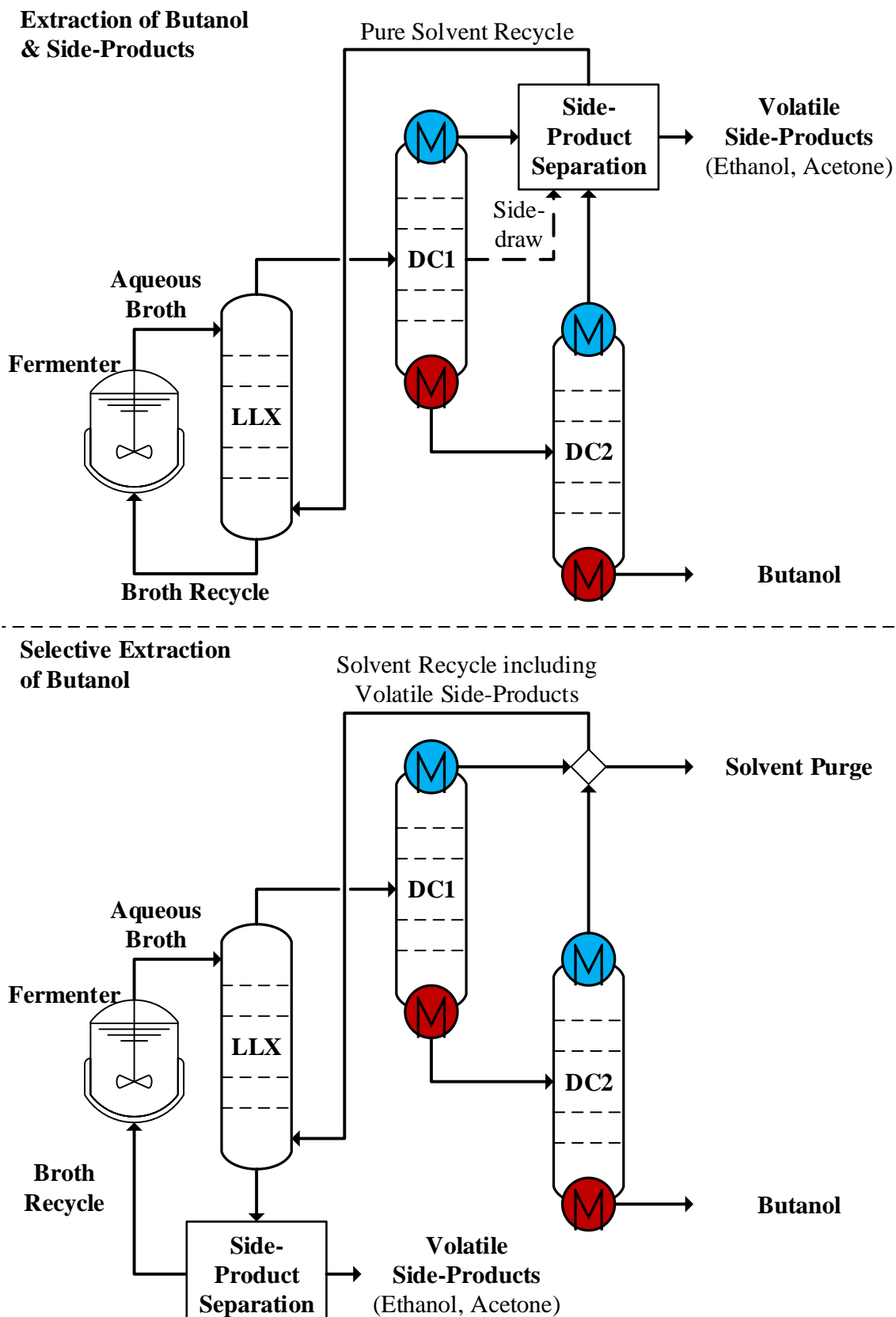


Figure 2-4: Strategies for the extraction of butanol and volatile side-products (ethanol and acetone): extraction of butanol and volatile side-products; and selective extraction of butanol. 'DC' = Distillation Column; 'LLX' = Liquid-Liquid Extraction

In practice, a small quantity would be transferred, an amount equal to the quantity of these side-products lost in a solvent purge stream. Therefore, in this strategy, acetone and ethanol would not be removed from the broth by extraction.

There are other separation methods, such as the evaporative techniques outlined in Section 1.5, for removing these volatile side-products either *in situ*, in stream or at the end of a batch fermentation. Alternatively, ethanol and acetone can be recycled back to the fermenter along with the rest of the broth. Effectively, this would mean that the extraction process would selectively remove butanol from the broth. Since acetone and ethanol are not as toxic as butanol to organisms, it is conceivable that the selective removal of butanol might cause an advantageous shift in organism metabolism favouring butanol production.

Other components in the broth must also be considered. Carboxylic acids, such as butyric acid, and other aqueous broth components are more polar than butanol or are present in very low concentrations in the broth. Therefore, transfer into the non-polar extractant would probably be minimal (depending on the pH). In addition, any broth components less volatile than the solvent transferred in the extraction would not contaminate the solvent recycle in this novel method. This is because the volatile hydrocarbon solvent would be vaporised during the solvent distillation, and the heavy components such as trace carboxylic acids would remain in the liquid phase. This solves one of the difficulties encountered by Groot *et al.* (1990), who found that the heavy components in the broth contaminated their involatile solvents. Conversely, this means that any heavy components extracted into the solvent would remain in the product stream. Depending on the level of this contamination and the intended purpose for the butanol, it might be necessary to complete an additional purification step on the butanol product to remove the contaminants. Such broth components were not considered in this work; equilibria measurements of carboxylic acids with C₄ – C₅ hydrocarbons were scarce and other broth components vary significantly between different fermentations.

2.3.2 Extraction at Elevated Temperature

The literature has shown that the distribution coefficient for solvents used in the extraction of butanol from fermentation broths can be strongly temperature dependent (Kraemer *et al.*, 2010). This is often insufficiently addressed in measurements of distribution coefficients in the literature since many studies conduct measurements at ambient rather than broth temperatures. This is one reason why significant disagreement can exist

amongst measurements in the literature. For example, mesitylene has a much lower distribution coefficient for butanol extraction at fermentation temperatures (~ 0.8 kg/kg) than *e.g.* oleyl alcohol (~ 4 kg/kg), but increases to ~ 2.2 kg/kg at 80°C (Kraemer *et al.*, 2010). This effect can be exploited by extracting at elevated temperatures. Mesitylene has a higher selectivity and a much lower viscosity and boiling point than oleyl alcohol. The improvements in the distribution coefficient of mesitylene at higher temperatures resulted in a lower energy requirement for an extraction using mesitylene at 80°C followed by distillation, compared with the same process using oleyl alcohol (4.8 vs. 13.3 MJ/kg butanol).

The extraction process using volatile hydrocarbons could thus be modified to capitalise on higher distribution coefficients obtained by elevating the extraction temperature, as shown in Figure 2-5. To prevent thermal shock to the fermenter organism, this type of extraction would probably have to be carried out ‘in stream’, *i.e.* in an extraction unit outside the fermenter. In this instance, the fermentation organisms would first have to be removed from the broth stream *via* a filtration process prior to the extraction. Following

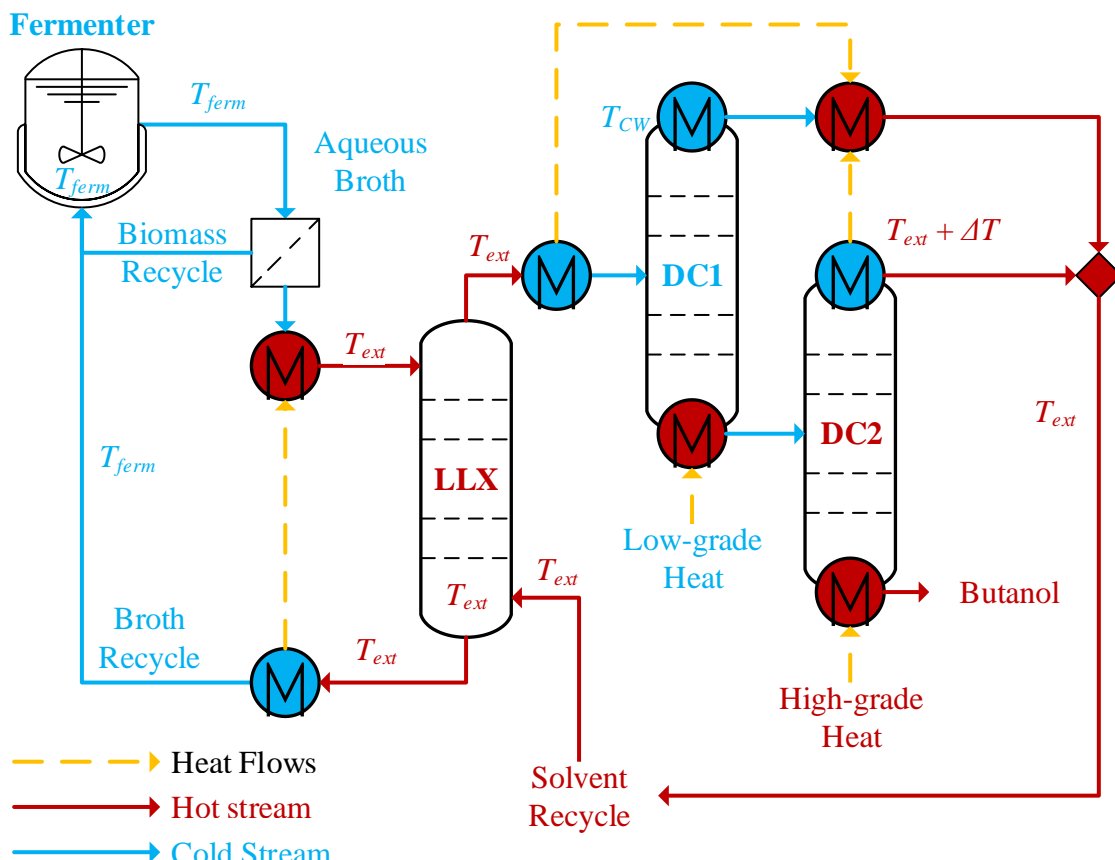


Figure 2-5: Heat integration strategy for performing liquid-liquid extraction of butanol by volatile hydrocarbons from aqueous broths at elevated temperatures
 ‘DC’ = Distillation Column; ‘LLX’ = Liquid-Liquid Extraction

removal of the organisms, the broth would then require heating to the elevated extraction temperature. This additional heat could mostly be recovered from the cooling required on the butanol-lean broth following extraction, and before recycle back to the fermenter, as shown in Figure 2-5. In this scenario, the condensed solvent from the first distillation column (DC1) would also need to be re-heated to the extraction temperature before solvent recycle back to the extractor. However, this additional heat could also mostly be provided *via* heat integration with the butanol-solvent mixture produced by the extraction. As shown in Figure 2-5, this butanol-solvent mixture could be cooled from the elevated extraction temperature *en route* to DC1, which operates at the low-grade temperature. In addition, the pressure of DC2 could be increased further so that the heat from condensing the solvent in the second column were hot enough to use to heat the solvent and aqueous broth feeds for the elevated temperature extraction. The operating conditions and heat integration of such a system is considered further in Chapter 5.

2.3.3 Other Design Modifications

The core premise of this novel separation scheme is the use of low-grade waste heat to vaporise a volatile hydrocarbon extractant. This technique can be used in a range of designs. For example, the system could be applied as part of a process to produce a butanol-gasoline blend for use as a liquid fuel.

One motivation for the research of butanol fermentations is the possibility of using butanol as a liquid fuel. In such an application, the produced butanol could be blended with existing hydrocarbon fuels, such as gasoline. Therefore, rather than purifying butanol from a hydrocarbon solvent in order to re-mix it with another hydrocarbon mixture (*i.e.* the hydrocarbon fuel), the prospect of using the hydrocarbon fuel as an extractant directly is very attractive.

Gasoline has been investigated as a potential butanol extractant (Evanko *et al.*, 2013; Groot *et al.*, 1990; Huang *et al.*, 2014). Its use as an extractant has the advantage of not requiring subsequent separation, although being alkane-based, it also has a much lower distribution coefficient for butanol (~0.3 kg/kg at 37°C (Groot *et al.*, 1990)) than other extractants such as oleyl alcohol. Whilst the distribution coefficient of butanol in gasoline is relatively poor at dilute aqueous compositions, it does rise significantly at higher butanol concentrations (Evanko *et al.*, 2013; Letcher *et al.*, 1986). However, the butanol titres realisable in fermentation processes (< 2 wt% butanol) mean that obtaining butanol

concentrations typical of gasoline blends (10 vol% butanol) are not achievable by using gasoline as extractants directly.

One solution to the above is to concentrate, before extraction with gasoline, the aqueous solution of butanol using a different separation technique. The concentration step would also alleviate concerns about the toxicity of gasoline to the broth, since the extraction is not performed on the broth directly. This solution has been outlined by Leeper and Wankat (1982) who investigated the same proposal for ethanol (rather than butanol) to produce gasohol. The authors extracted aqueous ethanol directly into gasoline, *via* a distillation step to concentrate the aqueous ethanol before extraction. Alternatively, Kurkijärvi and Lehtonen (2014) used an approach that engages common gasoline additives MTBE, ETBE and *iso*-octane as extractants. These extractants can also be used as liquid fuel or directly blended with gasoline, thereby saving energy on the purification of butanol from the extraction solvent. However, these extractants also suffer from relatively poor distribution coefficients, limiting the proportion of butanol in the product.

Instead of employing energy-intensive distillation as the concentrating step, as proposed by Leeper and Wankat (1982), extraction by volatile hydrocarbons could be used to concentrate butanol to a higher aqueous concentration before extraction by gasoline. Thus, a volatile hydrocarbon would first be used to extract butanol from the broth. The resulting dilute butanol-solvent mixture would be concentrated by a distillation, using low-grade waste heat to supply the reboiler. Since hydrocarbons and gasoline are miscible, gasoline cannot be used directly to extract butanol from the concentrated butanol-solvent mixture produced in the distillation. Therefore, the butanol would have to be extracted back into a polar solvent, *i.e.* a solvent immiscible with gasoline.

An obvious candidate for this polar solvent is water, since it is readily available, non-toxic and highly immiscible with gasoline. The butanol could therefore be extracted from the concentrated butanol-solvent mixture by water to form an aqueous mixture of concentrated butanol. This concentrated aqueous butanol could then be extracted directly into gasoline, forming the liquid fuel blend. This scheme is shown in Figure 2-6.

Here, the concentration of butanol produced by the distillation step effectively controls the concentration of butanol achieved in the subsequent extraction steps, and so could be used to control the resulting concentration of butanol in the gasoline blend. This strategy would be advantageous during the production of a gasoline-butanol blend, because no high-grade heat is required in the process.

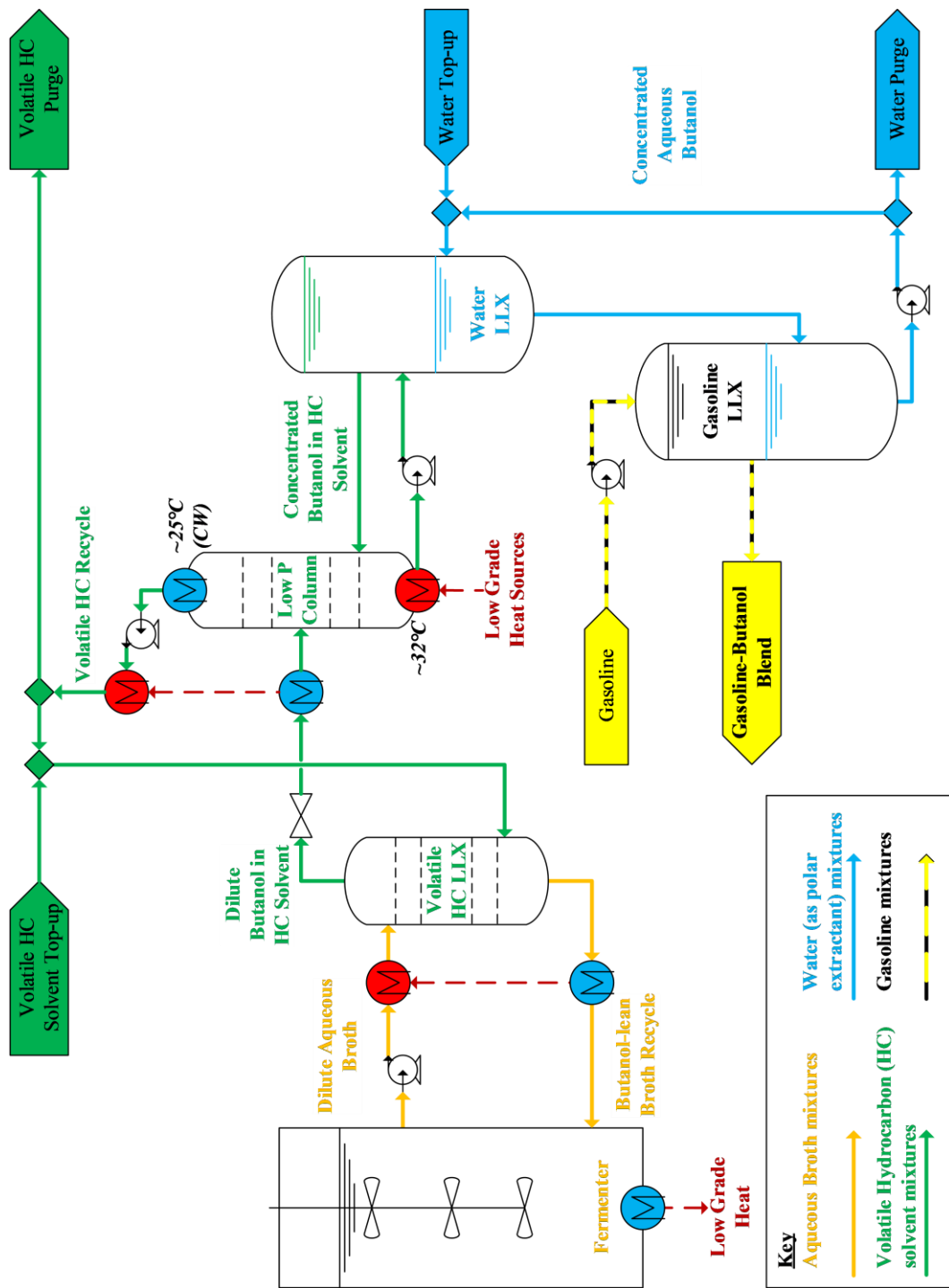


Figure 2-6 – Separation of aqueous butanol to produce a gasoline-butanol blend via extraction using C₄ & C₅ hydrocarbons

2.4 The Mutual Solubility of Short Hydrocarbons and Water

Low mutual solubility of the extraction solvent and the feed solvent is imperative in any extraction process. Low mutual solubility prevents the feed solvent from being transferred into the extractant phase, and similarly prevents the extractant from being lost in the raffinate; it also reduces the complexity of downstream separation of butanol from the extracting solvent. Low solubility of the extraction solvent in water reduces losses of the extraction solvent into the product-lean broth recycled to the fermenter. This lower solubility of the solvent in the aqueous broth also reduces the likelihood of solvent toxicity towards the fermentation organism, since the solvent would therefore be present at trace concentrations in the broth. Hydrocarbons exhibit low mutual solubilities with water; however, this solubility is higher in shorter hydrocarbons. In addition, as well as altering the distribution coefficient, the temperature of the extraction affects the mutual solubility of the hydrocarbon solvent and water. The mutual solubility of volatile hydrocarbons with water is therefore an important criterion in the selection of such a solvent.

2.4.1 The Solubility of Volatile Hydrocarbons in Water

Since their solubilities are very low, experimental results for the solubility of hydrocarbons in water are inconsistent (Góral *et al.*, 2004). Góral *et al.* (2004) developed a correlation for the solubility of saturated and unsaturated hydrocarbons in water as a function of temperature, based on an evaluation of all solubility measurements reported in the available literature for C₅ – C₁₀ saturated and unsaturated hydrocarbons, thus:

$$\ln(x_{HC}^{sol}) = \ln(x_{HC}^{sol,min}) + \frac{\Delta_{soln}C_p}{R} \left(\frac{T_{min}}{T} + \ln\left(\frac{T}{T_{min}}\right) - 1 \right) \quad (2-10)$$

$$\ln(x_{HC}^{sol,min}) = c_1 + c_2 b + c_\pi L \quad (2-11)$$

$$\frac{\Delta_{soln}C_p}{R} = c_3 b \quad (2-12)$$

$$b = 0.08664 \frac{RT_c}{P_c} \quad (2-13)$$

Here $c_1 = -4.08$; $c_2 = -0.073 \text{ mol/cm}^3$; $c_\pi = 1.10$; $c_3 = 0.376 \text{ mol/cm}^3$. The parameter L represents the number of π bonds in the hydrocarbon (*i.e.* $L = 0$ for alkanes; $L = 1$ for alkenes; $L = 2$ for alkadienes). The solubility of the hydrocarbon (HC), x_{HC}^{sol} , is given as the mole fraction of the hydrocarbon as a function of temperature, T (kelvin). The critical temperature and pressure of the hydrocarbon are denoted T_c and P_c respectively. The

temperature, T_{min} (K), corresponds to the mole fraction of the hydrocarbon at minimum solubility, $x_{HC}^{sol,min}$ which was found to be 298 K for cyclic hydrocarbons and 306 K for all other hydrocarbons. Góral *et al.* (2004) demonstrated the validity of this correlation on solubility measurements between 273 K and over 400 K for saturated hydrocarbons, and at up to ~333 K for unsaturated hydrocarbons.

The solubility of volatile hydrocarbons can also be estimated from Henry's Law at the saturation pressure of the hydrocarbon. As the solubility of liquids is not a strong function of pressure, this solubility does not significantly increase above the saturation pressure of the hydrocarbon. The effect of pressure on solubility between the saturation pressure of the solvent and the critical pressure was found to be minimal in experimental work on 1-butene (Leland and McKetta, 1955), one of the more volatile C₄ – C₅ solvents investigated. Hence:

$$c_{org}^{aq} = \mathcal{H}_{HC} P_{HC}^{sat} \quad (2-14)$$

where c_{HC}^{aq} is the solubility of the hydrocarbon in water (kmol/m³) and \mathcal{H}_{HC} is the Henry's Law constant (kmol/m³/Pa) for the hydrocarbon.

A comprehensive database of Henry's Law constants at 25°C for substances in water has been compiled by Sander (2015). Temperature dependence was reported for a few short hydrocarbons, but the values quoted were found to be inconsistent with the correlation of Góral *et al.* (2004) and measurements by others. The solubilities of C₄ – C₅ alkanes and alkenes in water at 25°C were calculated using the correlation of Góral *et al.* (2004) using critical temperatures and pressures from NIST (2016) and were compared to those calculated by Henry's Law constants compiled by Sander (2015). was used to calculate the solubilities for C₄ – C₅ alkanes and alkenes in water at a range of temperatures. This comparison is presented in Figure 2-7.

As shown in Figure 2-7, the correlation of Góral *et al.* (2004) loosely corresponds to the solubilities calculated by the Henry's Law constants of Sander (2015) at 25°C. However significant disagreement exists for certain compounds, *e.g.* *iso*-amylene and *iso*-butene, for which the predictions by Henry's Law are far higher than the correlation.

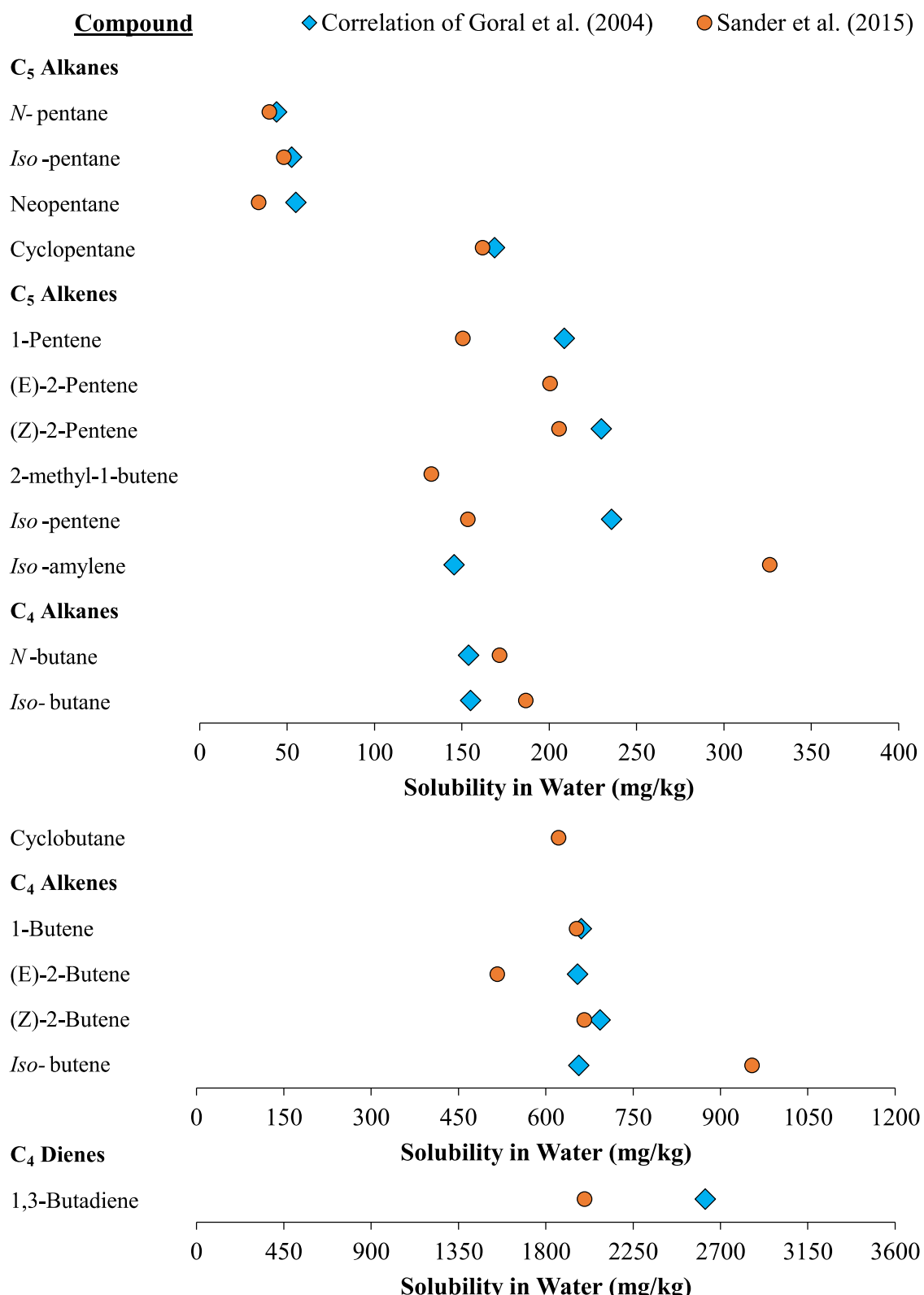


Figure 2-7: Solubility of relevant hydrocarbons in water at 25°C, as calculated by the correlation of Goral *et al.* (2004) and by Henry's Constant (Sander, 2015)

As would be expected, solubility increased with addition of (slightly polar) π bonds from alkanes to alkenes and decreased with chain length. The solubility of C₅ alkanes was ~50 mg/kg¹ at 25°C. As a rule of thumb, this solubility approximately tripled for either a reduction in chain length (*e.g.* to a C₄ alkane), or an increase in the number of π bonds (*e.g.* C₅ alkane to C₅ alkene), or in the equivalent cyclic alkane (*e.g.* C₅ alkane to cyclopentane). Therefore, the solubility in water at 25°C was ~150 mg/kg for C₄ alkanes, C₅ alkenes and cyclopentane; ~600 mg/kg for C₄ alkenes and cyclobutane; and ~2400 mg/kg for 1,3-butadiene (a C₄ diene).

The solubilities of C₄ – C₅ hydrocarbons in water, correlated by the equation of Góral *et al.* (2004) at temperatures of 25°C – 100°C, are detailed in Figure 2-8. For comparison, a number of experimental measurements are also presented, either published since the work of Góral *et al.* (2004) or not included in their correlation, produced by Leland and McKetta, (1955); Mokraoui *et al.* (2007); Polak and Lu (1973) and Serra and Palavra (2003). Most notably, the solubility of 1-butene was measured in water and in a bacterial medium at 25°C – 50°C by Serra and Palavra (2003), who found that the measured solubilities of 1-butene in the medium were very close to those obtained in pure water (maximum 4% deviation in mole fraction). This would indicate that measurements of solubility of hydrocarbons in pure water are similar to those in aqueous broths. However, the measured solubilities were much lower than those estimated by the correlation, Henry's constant or from other experimental measurements, as shown in Figure 2-8. This highlights the inconsistency of measurements of solubilities of volatile hydrocarbons in the literature.

¹ Solubilities have been reported in this dissertation in mg/kg, *i.e.* as mass fractions $\times 10^{-6}$. The molar masses of C₄ and C₅ hydrocarbons (54 – 58 and 70 – 72 kg/kmol) are approximately 3× and 4× that of water (18 kg/kmol) respectively. Thus, as a rule of thumb, to convert dilute mole fractions of C₄ and C₅ hydrocarbons in water to mass fractions, multiply the mole fraction by 3 and 4 respectively. To convert mole fractions of dilute water in C₄ and C₅ hydrocarbons into mass fractions, divide by 3 and 4 respectively. Similarly, to convert mole fractions of dilute butanol (74 kg/kmol) in water to mass fractions, multiply the mole fractions by 4. Hence, to convert mole fractions of butanol in C₄ and C₅ hydrocarbons to mass fractions, multiply by 4/3 and 1 respectively.

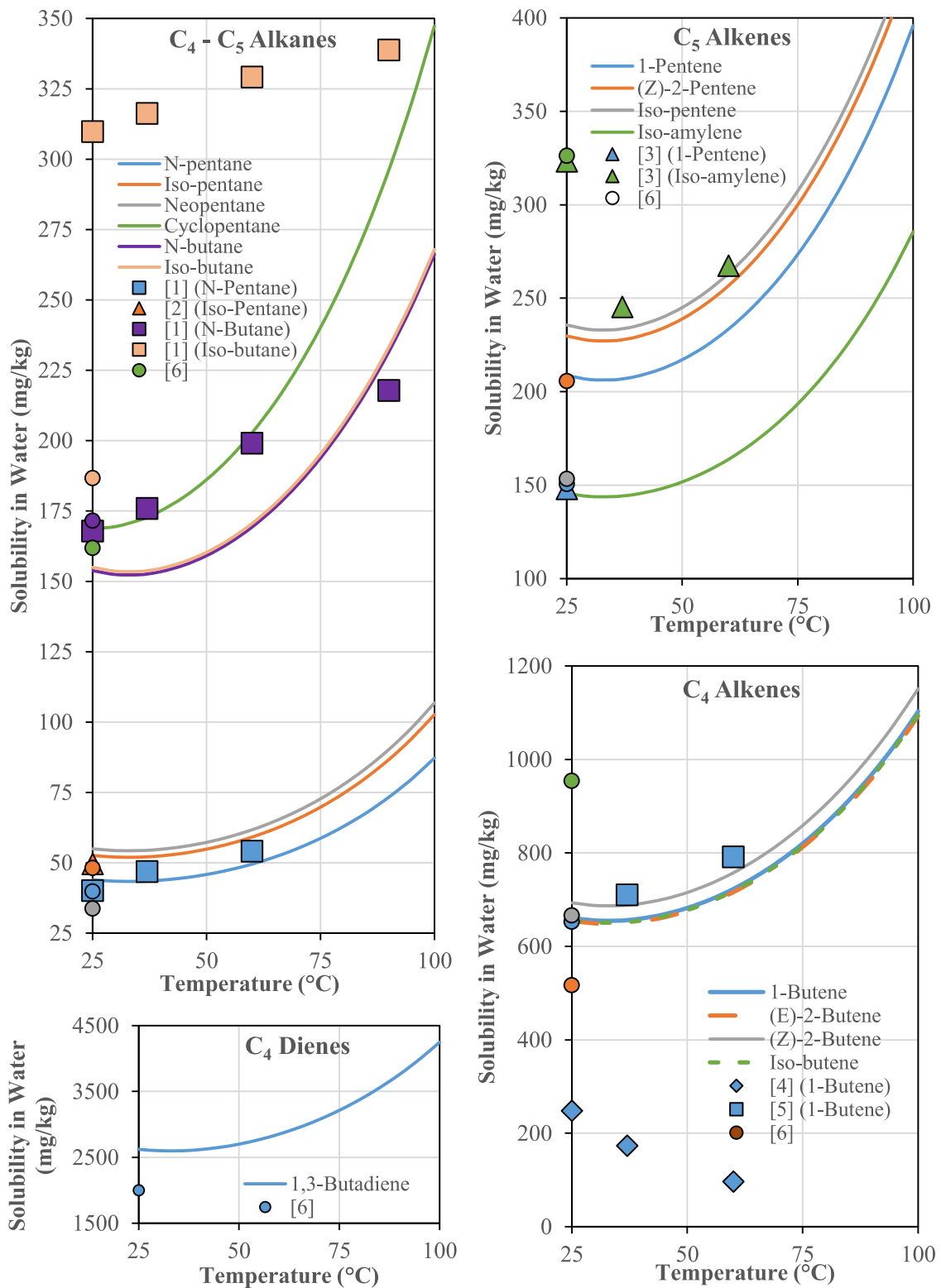


Figure 2-8: Solubility of relevant hydrocarbons in water at 25°C – 100°C, as calculated by the correlation of Goral *et al.* (2004) (lines), by Henry's Constant (Sander, 2015) (circles, ○), and experimental measurements ([ref], other points)

[1] = Mokraoui *et al.* (2007); [2] = Polak and Lu (1973); [3] = Góral *et al.* (2004);
 [4] = Serra and Palavra (2003); [5] = Leland and McKetta (1955); [6] = Sander (2015)

The correlation of Góral *et al.* (2004), suggested that typical fermentation temperatures (305 – 310 K) conveniently correspond to the around point of minimum solubility of the hydrocarbons ($T_{min} = 306$ K for the correlation of Góral *et al.* (2004)). The correlation and measurements obtained from the literature suggest that solubilities of C₄ – C₅ hydrocarbons in water do not vary significantly between 25°C and 50°C, as shown in Figure 2-8. The correlation of Góral *et al.* (2004) predicted that temperatures above this point cause solubility to increase. Solubilities of hydrocarbons presented in Figure 2-8 approximately doubled between 25 – 50°C and 100°C. Therefore, performing extractions at elevated temperature could result in greater concentrations of solvent lost in the aqueous stream leaving the extraction.

Steps could be taken to recover the volatile solvent from the broth recycle if the loss of the solvent into the aqueous broth recycle, or toxicity to the organism in the broth, were of concern. Figure 2-9 details a scheme to recover the volatile solvent from the aqueous stream following extraction. First, organisms could be removed from the broth by a filtration. The biomass-free broth could then be heated to the extraction temperature (for extractions at elevated temperature). This would cause some dissolved fermentation gases (e.g. CO₂) to evaporate; these should be removed (in ‘ T_{ext} Flash Tank’ in Figure 2-9) before liquid-liquid extraction. This process would therefore result in a biomass-free and de-gassed aqueous broth for extraction. Following extraction of butanol, if

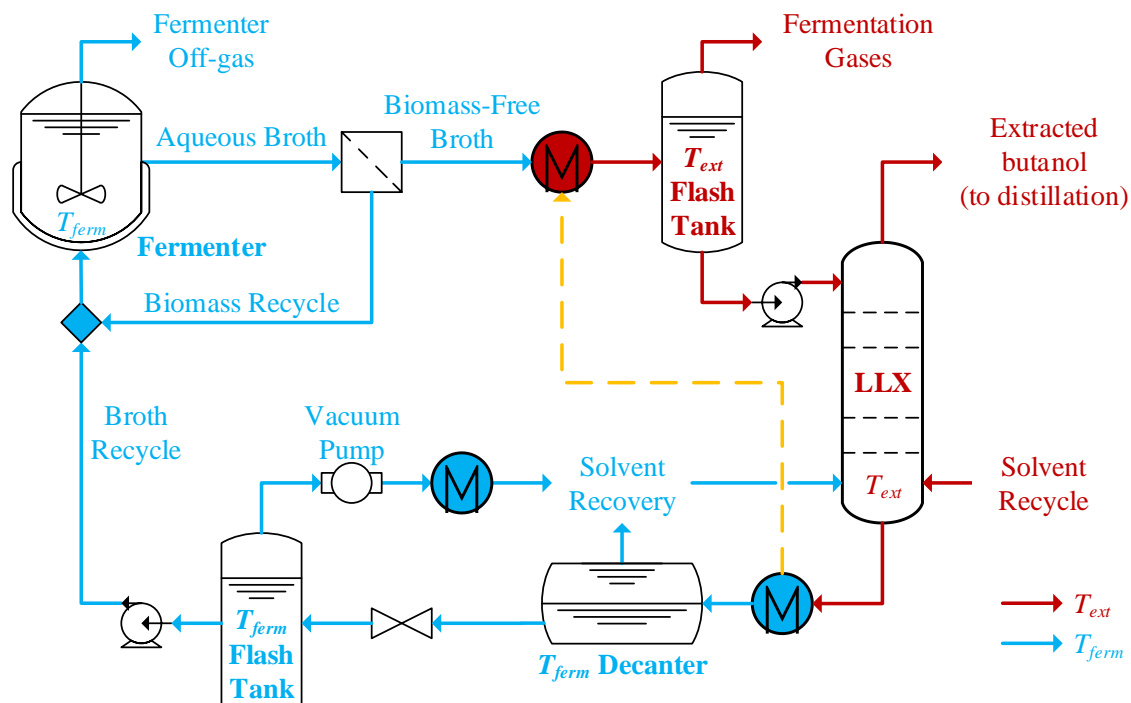


Figure 2-9: Recovery of volatile hydrocarbons from aqueous broth recycle following extraction. T_{ext} = extraction temperature; T_{ferm} = fermentation temperature

extraction were performed at an elevated temperature, the aqueous broth would need cooling back to the fermentation temperature. This would cause solvent to separate as an immiscible phase (in ‘ T_{ferm} Decanter’) as the solubility of the hydrocarbon decreases with temperature. In order to recover more solvent from the broth, a flash tank at reduced pressure, *e.g.* 0.5 bara, could be employed (‘ T_{ferm} Flash Tank’) prior to pumping back to the fermenter. The solvent vapour from the flash could be re-compressed and condensed, or condensed using refrigeration, and returned to the extraction column. Lower flash pressures would reduce the concentration of solvent in the broth recycle but would result in more energy requirements for refrigeration or re-compression, and would result in more evaporation of water and volatile fermentation products.

The solubility of volatile hydrocarbons in water at a reduced pressure can be estimated by assuming Henry’s Law applies, *i.e.* that below the vapour pressure of the hydrocarbon, the solubility is proportional to the pressure:

$$x_{HC}^{sol}(P < P_{HC}^{sat}, T) = \left(\frac{P}{P_{HC}^{sat}} \right) \cdot x_{HC}^{sol}(P \geq P_{HC}^{sat}, T) \quad (2-15)$$

The solubilities calculated by the correlation of Góral *et al.* (2004) at a typical fermentation temperature of 37°C were used to calculate the solubilities of C₄ – C₅ hydrocarbons in water at 0.5 bara. These are presented in Figure 2-10, alongside solubilities of hydrocarbons in water at 0.5 bara, 37°C, calculated from Henry’s constants obtained from Sander (2015). The Henry’s constants were at 25°C, but solubilities at 37°C were predicted to be similar to those at 25°C. The vapour pressures of C₄ – C₅ hydrocarbons presented in Figure 2-2 were employed in the calculations. As shown in Figure 2-2, the reduced pressure decreases the solubility of C₄ and C₅ alkanes to around the same magnitude - ~20 mg/kg (~5 – 10 ppm). Roughly, solubility increases by a factor of 4 for each additional π bond, *i.e.* ~80 mg/kg for C₄ and C₅ alkenes and ~300 mg/kg for C₄ dienes. These solubilities are very low, thus minimising solvent loss to the aqueous recycle and minimising interaction between the solvent and the organism in the broth.

To summarise, solvent loss to the aqueous stream is not likely to be a significant problem in the extraction scheme, since the solubilities at ambient and fermentation temperatures are all significantly under 1 g/kg, as detailed in Figure 2-8. The sole exception is butadiene, the solubility of which was found to exceed 2 g/kg and therefore would probably cause significant solvent losses without solvent recovery from the broth recycle and hence potentially increase the risk of organism toxicity issues due to the higher

quantity of solvent present in the broth recycle. The C₅ alkanes demonstrate very low solubilities of under 100 mg/kg, even at elevated temperatures. Solvent recovery could be employed to reduce the solvent composition in the broth recycle further if required.

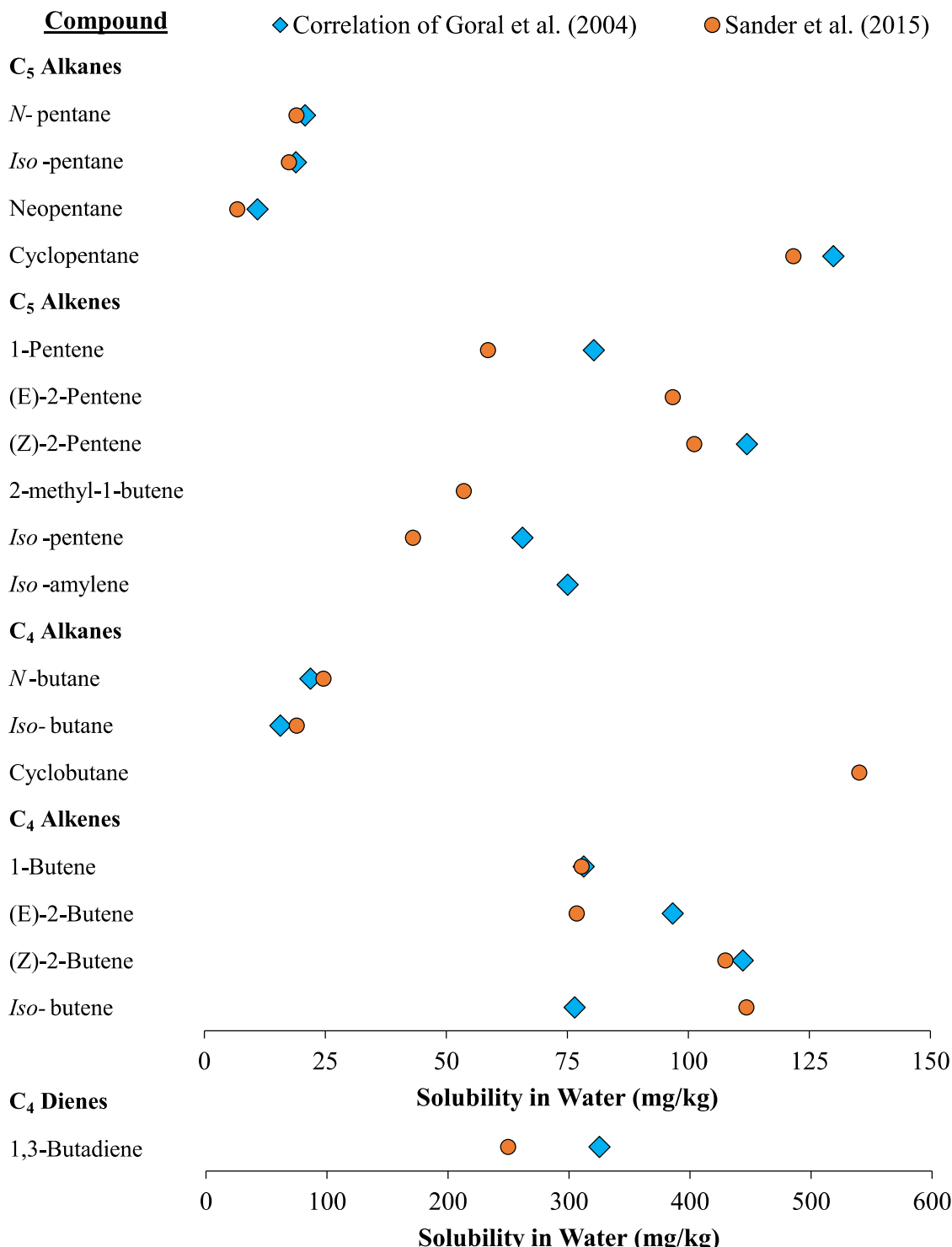


Figure 2-10: Solubility of relevant hydrocarbons in water at 0.5 bara, 37°C, as calculated by the correlation of Goral *et al.* (2004) and by Henry's Constant (Sander, 2015)

2.4.2 The Solubility of Water in Volatile Hydrocarbons

The solubility of water in the extractant affects the selectivity of butanol over water in the extraction. The solubilities of water in hydrocarbons are relatively insensitive to carbon chain-length (Tsonopoulos, 1999), in contrast to the dependence on chain length of the solubility of hydrocarbons in water. However, solubility of water in hydrocarbons increases slightly with chain-length. Several (Black *et al.*, 1948; Hibbard and Schalla, 1952; Tsonopoulos, 1999) have investigated the effect of temperature on the solubility of water in hydrocarbons and have formed simple correlations, all of the form:

$$\ln(x_{H_2O}^{sol}) = A + \frac{B}{T} \quad (2-16)$$

where $x_{H_2O}^{sol}$ is the solubility of water in the hydrocarbon, given as a mole fraction of water and T is the temperature. The constants A and B (and units of T) depend on the particular correlation and hydrocarbon.

Figure 2-11 shows the solubility of water in C₄ – C₅ hydrocarbons calculated by these various correlations at 20 – 100°C on semi-log plots. Also shown in Figure 2-11 are the results of the correlations for specific hydrocarbons of Góral *et al.* (2004), as well as and some measurements of water solubility from the literature. As with measurements of the solubility of hydrocarbons in water, the measurements of the solubility of water loosely fitted the various correlations. The results in Figure 2-11 demonstrate that the solubility of water is sparing at fermentation temperatures, especially in alkanes. However, as shown in Figure 2-11, the solubility of water increases drastically between typical fermentation temperatures and elevated temperatures. Solubility of water in C₄ – C₅ hydrocarbons was predicted to increase by a factor of 3 between 20°C and typical fermentation temperatures (37°C), and a factor of ~10 between typical fermentation temperatures and 100°C.

In a similar manner to the increased solubility of hydrocarbons in water, the effect of this increase in solubility on the extraction system could be mitigated. If the extracted butanol stream were cooled prior to entering the distillation system, as proposed for extraction at elevated temperatures in Figure 2-5, water should separate as an immiscible phase. This should leave water in the solvent at a solubility equivalent to that at around fermentation temperatures.

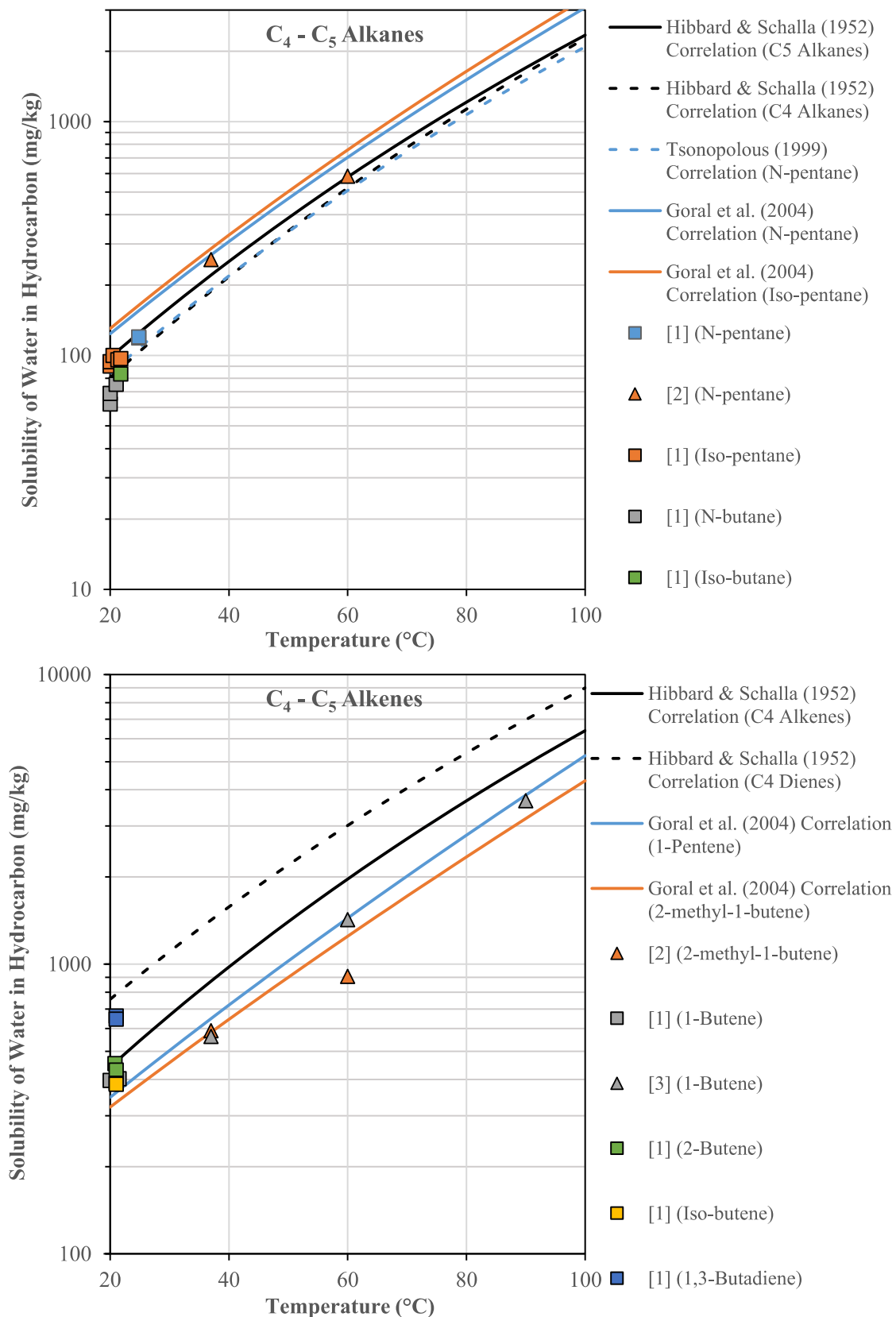


Figure 2-11: Solubility of water in relevant hydrocarbons at 20°C – 100°C, as calculated by the various correlations (lines) and experimental measurements ([ref], points)

[1] = Black *et al.* (1948); [2] = Góral *et al.* (2004); [3] = Leland and McKetta (1955)

The solubilities of water in C₄ alkanes were found to be the lowest of the hydrocarbons investigated, with a solubility of approximately 200 mg/kg (~600 ppm) at typical fermentation temperatures. The solubilities in C₅ alkanes were slightly higher (~250 mg/kg, ~1000 ppm). There were no correlations or measurements from a consistent source to compare C₄ and C₅ alkenes, as shown in Figure 2-5. The solubility of water in C₄ – C₅ alkenes was around 2 – 4 times higher than the equivalent alkanes (approximately 500 – 800 mg/kg, 1500 – 3000 ppm), due to the slight dipole moment introduced by the π bond. The solubility of water in C₄ dienes was predicted to be around double that of C₄ alkenes due to the additional π bond. These solubilities of water in hydrocarbons are all very low and therefore transfer of water into the solvent phase from the broth would probably be minimal, resulting in high selectivities over water for the extraction process.

2.5 Estimating the Performance of the Distillation System for the Separation of Butanol from Volatile Hydrocarbons

The distillation system used in the extraction of butanol from aqueous broths using volatile hydrocarbons dominates the heat requirements for the overall separation scheme depicted in Figure 2-3. It is possible to estimate, approximately, the heat requirements of this distillation system using some simplifying assumptions. These estimates can be used to compare C₄ and C₅ hydrocarbons as potential candidates for the extracting solvent.

2.5.1 Assumptions

In order to simplify the analysis, the distillation system was approximated as a binary system, containing only the major components, the hydrocarbon solvent and butanol. In addition, to produce rough estimates for the operating conditions and energy consumption of the distillation columns, the distillate of both columns was approximated as pure solvent, and the reflux of both columns was neglected. Given the relative volatility of C₄ – C₅ hydrocarbons *versus* butanol, obtaining a high purity of the solvent in the distillate with minimal reflux and a practical number of stages is feasible. This also justifies neglecting the pressure difference over the column.

In order to approximate the vapour-liquid equilibria (VLE) in the distillation columns, Raoult's Law was used, assuming both the liquid and vapour mixtures of butanol and the solvent behave ideally. This is unlikely to be accurate, since butanol and volatile hydrocarbons have very different polarities and so are likely to show positive deviation from Raoult's Law. A positive deviation would lead to an increase in the butanol

concentration produced by the first distillation column. Hence, Raoult's Law provides a conservative approximation of the VLE. A more rigorous analysis of the VLE of mixtures of hydrocarbons and butanol is presented in Chapter 3, and was employed to conduct a more accurate assessment of the performance of the distillation system in Chapter 5.

The *n*-butanol isomer was selected for the analysis. The results of the analysis would be very similar for *iso*-butanol.

2.5.2 Methodology

The two column, distillation system of separation of the solvent from butanol is shown in Figure 2-12. The pressure in the first distillation column (DC1) was estimated from the vapour pressure of the pure solvent at the condenser temperature. The temperature of the condenser is limited by the temperature of the available coolant, *e.g.* cooling water. Hence, the vapour pressure of the solvent at 25°C is indicative of a typical pressure for DC1. Figure 2-2 details the vapour pressures of C₄ – C₅ hydrocarbons at 25°C. The second distillation column (DC2) should be designed to produce solvent vapour in the condenser at a temperature that is at least equal to the fermentation temperature (*e.g.* 37°C). Hence, the vapour pressure of C₄ – C₅ hydrocarbons at 37°C, given in Figure 2-2, indicates the typical pressure of the second distillation column. If necessary, the design could employ a higher condenser temperature if significant re-heating of the solvent produced in the distillate of DC1 were required before solvent recycle.

The vapour pressures of the solvent at the condenser and reboiler temperatures can be used to estimate the typical concentration of butanol produced by the first column. Assuming Raoult's Law:

$$y_i P = x_i P_i^{sat} \quad (2-17)$$

Hence, for a binary mixture of butanol and hydrocarbon, the bubble-point pressure (*P*) at a mole fraction of butanol (*x_{Bu}*) and temperature (*T*) can be calculated as:

$$P(T) = x_{Bu} P_{Bu}^{sat}(T) + (1 - x_{Bu}) P_{org}^{sat}(T) \quad (2-18)$$

The composition in the reboiler is given by the bubble-point composition at the reboiler temperature (*T_{reboil}^{DC1}*) and pressure (*P_{reboil}^{DC1}*). Therefore, the maximum mole fraction of the butanol produced by the first distillation column (*x_{Bu,DC1}^{max}*) is given by:

$$x_{Bu,DC1}^{max} = \frac{P_{org}^{sat}(T_{reboil}^{DC1}) - P_{reboil}^{DC1}}{P_{org}^{sat}(T_{reboil}^{DC1}) - P_{Bu}^{sat}(T_{reboil}^{DC1})} \quad (2-19)$$

This mole fraction of butanol, $x_{Bu,DC1}^{max}$, is a ‘maximum’ since sufficient low-grade heat must be available to reach this composition. As described by eq. (2-19), this maximum is ultimately limited by the temperature gradient of the column.

Assuming a negligible pressure drop across the column, the reboiler pressure is equal to the condenser temperature. The condenser temperature is equal to the vapour pressure of the pure solvent at the condenser temperature (T_{cond}^{DC1}). Therefore:

$$x_{Bu,DC1}^{max} = \frac{P_{org}^{sat}(T_{reboil}^{DC1}) - P_{org}^{sat}(T_{cond}^{DC1})}{P_{org}^{sat}(T_{reboil}^{DC1}) - P_{Bu}^{sat}(T_{reboil}^{DC1})} \quad (2-20)$$

$$\therefore x_{Bu,DC1}^{max} = \frac{1 - \frac{P_{org}^{sat}(T_{cond}^{DC1})}{P_{org}^{sat}(T_{reboil}^{DC1})}}{1 - \frac{1}{\alpha_{org,Bu}(T_{reboil}^{DC1})}}, \quad \alpha_{org,Bu}(T) = \frac{P_{org}^{sat}(T)}{P_{Bu}^{sat}(T)} \quad (2-21)$$

where $\alpha_{org,Bu}$ is the volatility of the hydrocarbon solvent relative to butanol.

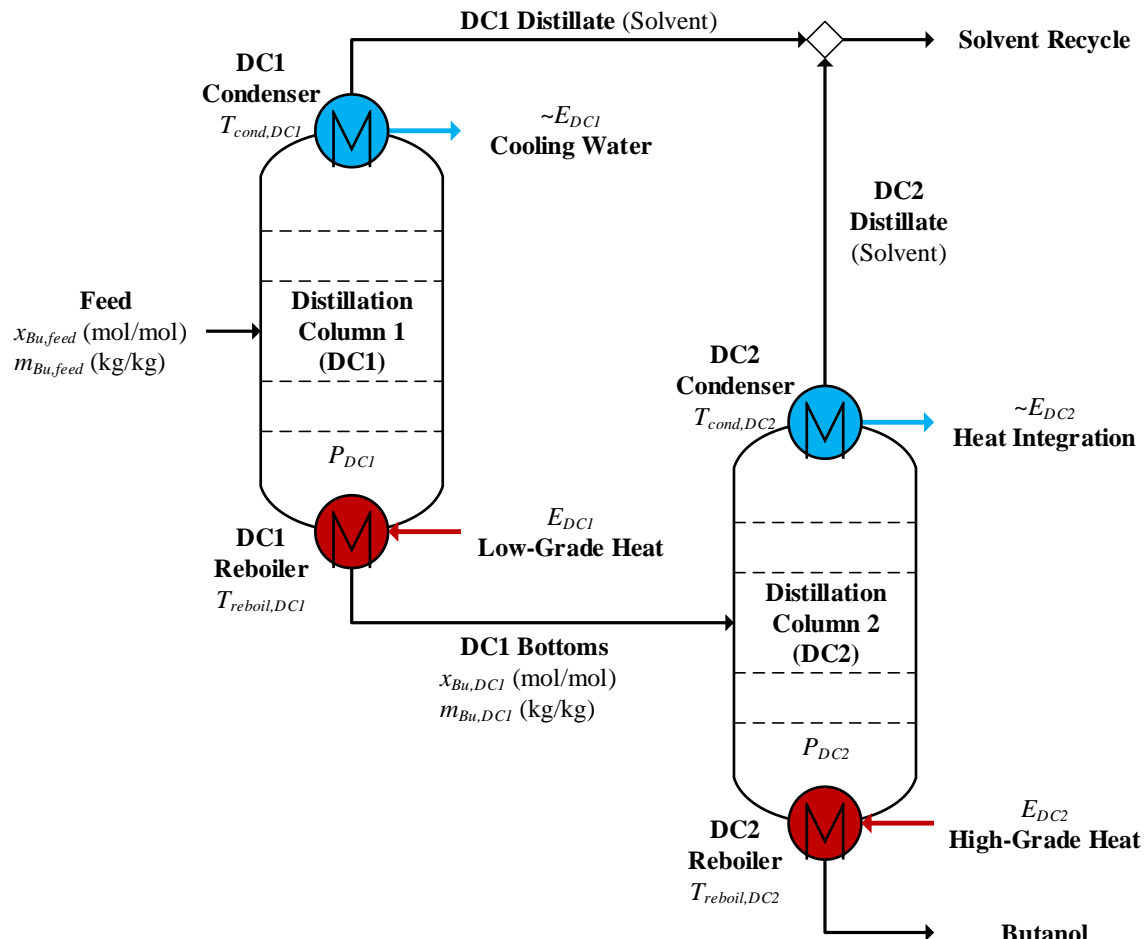


Figure 2-12: Schematic diagram of the distillation system for the separation of butanol from volatile hydrocarbons

Equation (2-21) can be simplified further, noting that the Clausius-Clapeyron equation can be used to predict the temperature variation of a compound's saturation pressure (P^{sat}) using its enthalpy of vaporisation ($\Delta\underline{H}_{org}^{vap}$). The enthalpy of vaporisation was assumed to be independent of temperature over the small temperature gradient of the first distillation column. In addition, the volatilities of C₄ – C₅ hydrocarbons relative to butanol ($\alpha_{org,Bu}$) are large ($\gg 1$). For example, the relative volatility of the least volatile candidate, cyclopentane, at 32°C is ~38. Hence for C₄ – C₅ hydrocarbons, the denominator in eq. (2-21) is negligible. Thus, $x_{Bu,DC1}^{max}$ can be approximated as:

$$x_{Bu,DC1}^{max} \cong 1 - \exp\left(-\frac{\Delta\underline{H}_{org}^{vap}}{R}\left(\frac{1}{T_{cond}^{DC1}} - \frac{1}{T_{reboil}^{DC1}}\right)\right) \quad (2-22)$$

Hence, the exact volatility of the C₄ – C₅ hydrocarbon does not impact significantly on the maximum mole fraction of butanol obtainable in the first column ($x_{Bu,DC1}^{max}$). This maximum butanol concentration increases with the enthalpy of vaporisation of the solvent and the temperature gradient of the distillation column.

The high-grade heat required by the second distillation column initially appears to be proportional to the enthalpy of vaporisation of the solvent. The heat required for the second column per kg of recovered butanol, E_{DC2} , can be approximated as the energy required to vapourise the mass of:

$$E_{DC2} \cong \frac{1}{Mr(BuOH)} \frac{(1 - x_{Bu,DC1}^{max})}{x_{Bu,DC1}^{max}} \Delta\underline{H}_{org}^{vap} \quad (2-23)$$

However, the mole fraction of butanol fed to the second distillation column, $x_{Bu,DC1}^{max}$, is also a function of enthalpy of vaporisation through eq. (2-22). Thus, the dependence of the energy required for the second distillation column on the enthalpy of vaporisation of the solvent is more complicated than it initially appears. This can be demonstrated by substituting the expression for $x_{Bu,DC1}^{max}$ (eq. 2-22) into eq (2-23):

$$E_{DC2} \cong \frac{\left(\frac{\Delta\underline{H}_{org}^{vap}}{74.12}\right)}{\exp\left(\frac{\Delta\underline{H}_{org}^{vap}}{R}\left(\frac{1}{T_{cond}^{DC1}} - \frac{1}{T_{reboil}^{DC1}}\right)\right) - 1} \quad (2-24)$$

The low-grade heat required for the first distillation column can be calculated by considering the total heat requirement of both columns. The total heat required for both

columns, E_{DC} , is approximately equal to the energy required to evaporate the solvent, per kg of recovered butanol:

$$E_{DC} \cong \frac{(1 - m_{Bu}^{feed})}{m_{Bu}^{feed}} \Delta \hat{H}_{org}^{vap} \quad (2-25)$$

The mass fraction of butanol fed into the overall distillation system (*i.e.* into the first column), m_{Bu}^{feed} , depends on the effective mass distribution coefficient of the extraction, D_{mass}^{Bu} , and the concentration of butanol in the aqueous broth, m_{Bu}^{aq} :

$$m_{Bu}^{feed} = D_{mass}^{Bu} m_{Bu}^{aq} \quad (2-26)$$

The low-grade heat required by the first distillation column, E_{DC1} , is then simply given by:

$$E_{DC1} \cong E_{DC} - E_{DC2} \quad (2-27)$$

2.5.3 Results

The vapour pressure of the C₄ – C₅ hydrocarbons given in Figure 2-2 were used to estimate their enthalpies of vaporisation at 25°C – 32°C using the Clausius-Claperyon equation. These estimates are shown in Figure 2-13 for each hydrocarbon, given on both a molar and mass basis. As shown in Figure 2-13, the molar enthalpy of vaporisation clearly increases with molecular weight. This relationship is approximately linear, because the specific enthalpy of vaporisation is approximately constant (0.4 MJ/kg, ±10%) for all the C₄ and C₅ hydrocarbons. Alkenes have slightly higher specific enthalpies of vaporisation compared to their corresponding alkanes, whilst branching slightly reduces enthalpy of vaporisation.

The maximum mass fraction of *n*-butanol obtainable in the first distillation column ($m_{Bu,DC1}^{max}$) and the energy consumption of the second distillation column (E_{DC2}) were calculated using eqs. (2-22) and (2-24) respectively under two scenarios. In both scenarios, a condenser temperature of 25°C was assumed for the first distillation column (DC1). In the first scenario ('Case A'), a reboiler temperature of 32°C was assumed in DC1. The second scenario ('Case B') considered a narrower temperature gradient in DC1, by assuming a reboiler temperature of 27°C. The resulting estimates of the butanol concentrations produced by DC1, and the corresponding estimates of the high-grade heat required by the second distillation column (DC2), are detailed in Figure 2-14. It can be seen that a heat requirement for DC2 of 1.2 MJ/kg butanol was estimated for all C₄ and

C_5 hydrocarbons for a reboiler at 32°C (*i.e.* a temperature gradient of 7°C). This requirement corresponded to an estimated maximum butanol concentration of 20 – 25 wt% in DC1. The narrow 2°C temperature gradient across DC1 in Case B, with the reboiler at 27°C, reduced the maximum butanol concentration in DC1 to 7 – 8 wt% for all C_4 and C_5 hydrocarbons. This resulted in an estimated energy consumption 4.8 – 4.9 MJ/kg butanol for DC2.

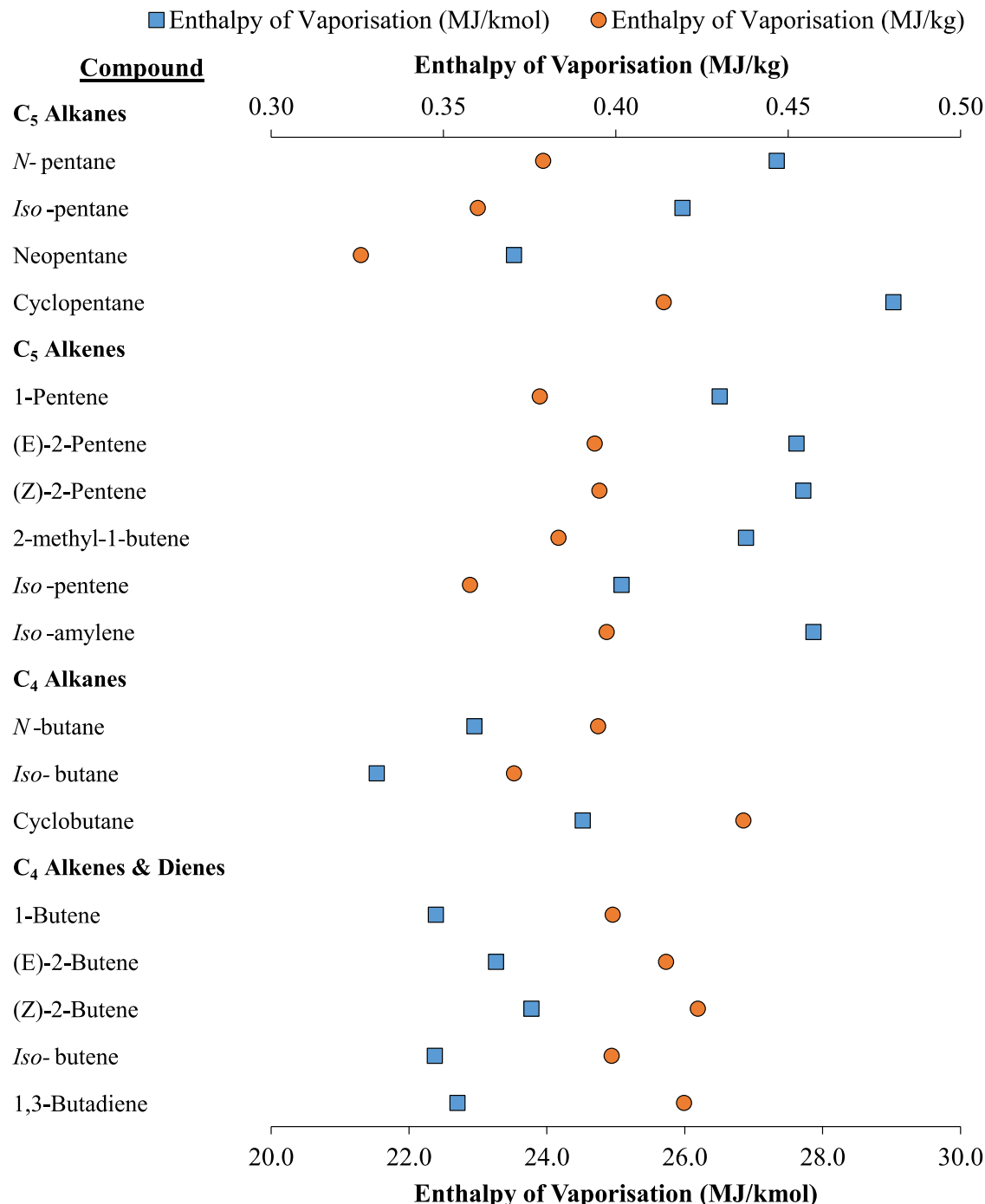


Figure 2-13: Enthalpies of vaporisation of C_4 – C_5 hydrocarbons on a molar and mass basis at 25 – 32°C, calculated by the Clausius-Claperyon equation from vapour pressures obtained from Poling *et al.* (2001)

2.5.4 Discussion

Owing to the almost identical predictions for energy consumption for all candidate solvents, these estimates do not help to narrow the field of solvent candidates. However, they do suggest that only very low quantities of high-grade heat are required for the separation process, *e.g.* a requirement of only ~1.4 MJ/kg butanol high-grade heat is predicted in the first scenario (*c.f.* butanol enthalpy of vaporisation, ~0.7 MJ/kg, enthalpy of combustion ~36 MJ/kg). It is important to note that these estimates are based on Raoult's Law, assuming ideal gas and liquid mixtures. Non-ideal gas and liquid mixtures might make a significant difference to the possible butanol concentration obtainable in DC1, and hence the energy requirements of DC2. Measurements of VLE will be analysed in Chapter 3 in order to investigate the effect of these non-idealities.

Assuming sufficient low-grade heat is available to maximise the butanol concentration produced in DC1, the high-grade heat requirements of the distillation system depends only on the enthalpy of vaporisation of the solvent and the temperature gradient across DC1. It does not depend on the distribution coefficient of the solvent in the extraction.

However, the distribution coefficient affects the total heat requirements of the distillation system. The total heat required by the distillation system, E_{DC} , can be estimated using eq. (2-25). For short-chain hydrocarbons, a rough estimate of a distribution coefficient of *circa* 0.5 kg/kg can be made, based on measurements of the extraction of butanol using hexane from a broth with mass fraction of 2 wt% butanol (Groot *et al.*, 1990). Groot *et al.* (1990) measured similar distribution coefficients of butanol in hexane and heptane, suggesting the distribution coefficient of C₄ – C₅ hydrocarbons might be similar. However, this is a very rough estimate based on one broth concentration from the limited measurements available in the literature. The specific enthalpy of vaporisation for C₄ – C₅ hydrocarbons is ~0.4 MJ/kg (as outlined in Figure 2-13). Using these estimates, eq. (2-25) predicts a total heat requirement of *ca.* 40 MJ/kg butanol for the distillation system, for an extraction of 2 wt% butanol from an aqueous broth.

This estimate of total heat consumption of the distillation system can then be used to calculate the low-grade heat required by DC1 *via* eq. (2-27). The low-grade heat required is therefore *ca.* 35 – 39 MJ/kg butanol, depending on the temperature gradient (and hence butanol concentration) in DC1. Whilst this figure is large (*c.f.* butanol enthalpy of combustion ~36MJ/kg), large quantities of low-grade waste heat are often available on fermentation plants, most notably from the fermenter itself. The low-grade heat required

is also heavily influenced by the value of the distribution coefficient. Doubling the distribution coefficient to 1 kg/kg would reduce the predicted low-grade heat requirement

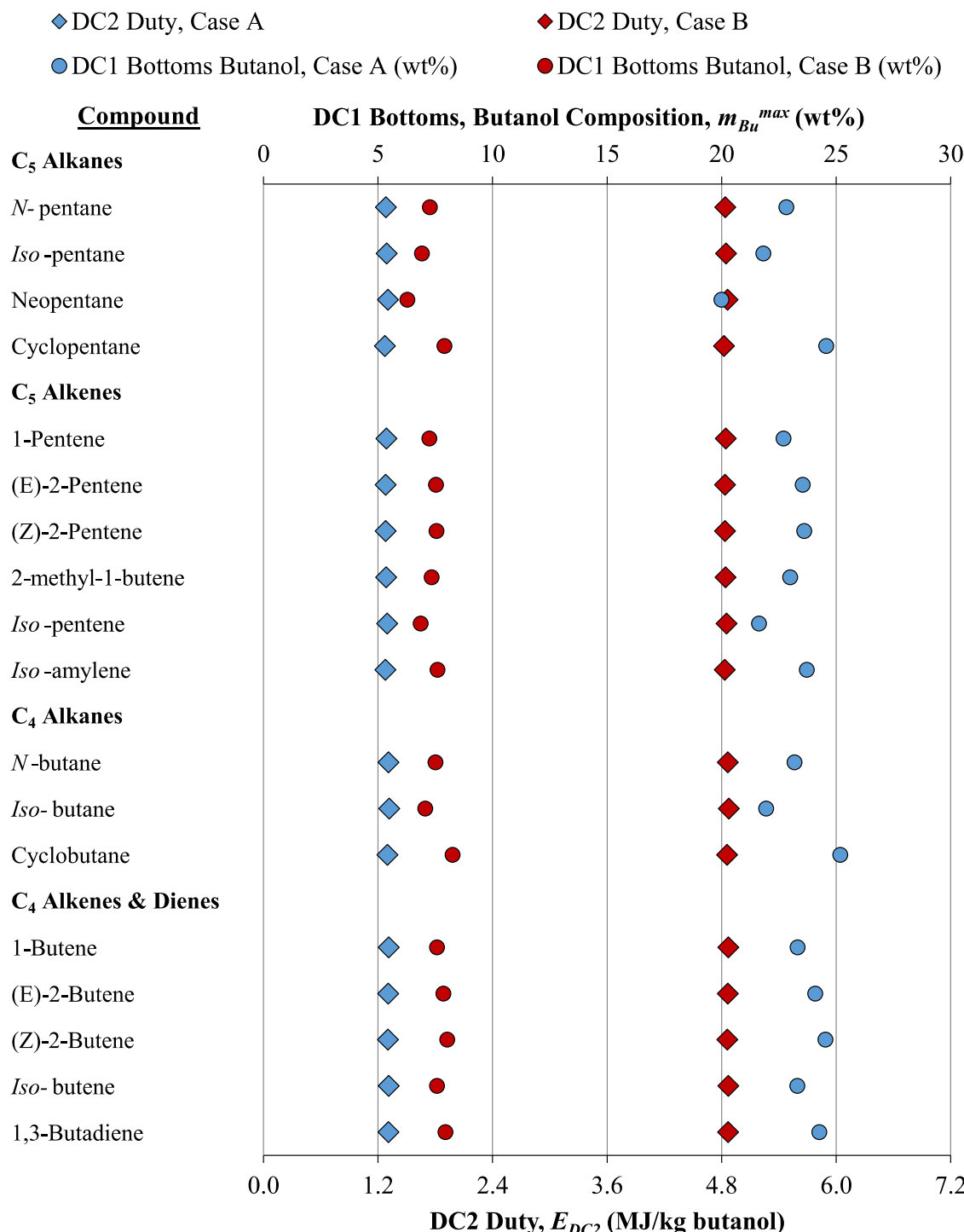


Figure 2-14: Estimates for the maximum *n*-butanol composition produced by DC1 (m_{Bu}^{max} , wt%) and the duty of DC2 (E_{DC2}) for extraction of aqueous butanol employing C₄ and C₅ hydrocarbons for two temperature gradients in DC1:

- Case A: $T_{reboil}^{DC1} = 27^\circ\text{C}$; $T_{cond}^{DC2} = 25^\circ\text{C}$ (2°C temperature gradient)
- Case B: $T_{reboil}^{DC1} = 32^\circ\text{C}$; $T_{cond}^{DC2} = 25^\circ\text{C}$ (7°C temperature gradient)

to 15 – 18 MJ/kg butanol for the extraction of butanol from the same 2 wt% butanol broth. Hence, the distribution coefficient of the hydrocarbon solvent is an important property in minimising the low-grade heat required by the first distillation column.

2.6 Estimating the Distribution Coefficient of Butanol at Infinite Dilution between Water and Selected Hydrocarbons

As noted in Section 2.5, estimates of the performance of the distillation system have found that the low-grade heat requirements can be substantial, depending on the distribution coefficient. In addition, secondary heating and pumping energy requirements are proportional to the quantity of solvent required for the extraction. These secondary energy requirements could be significant if an elevated temperature were employed for the extraction to improve distribution coefficient.

Distribution coefficient is a function of both composition and temperature and the thermodynamic activity in the two phases. Nonetheless, it is possible to estimate the distribution coefficient for the volatile hydrocarbons as a function of temperature at infinite dilution by making some simplifying assumptions. This should provide an indication of the distribution coefficient of the hydrocarbons for extraction of butanol from dilute aqueous broths. Given that fermentation broths are dilute in butanol, the distribution coefficient during extraction will probably be close to that at infinite dilution.

2.6.1 Theory

A model has been devised for the purposes of estimating the limiting distribution coefficients at infinite dilution. It uses the co-existence equation, which relates the dew-point to the bubble-point curve in vapour-liquid equilibria. The co-existence equation therefore requires an equation of state to model the vapour phase; the virial equation of state was selected for the purpose of this approximation. The virial equation is valid at the low to moderate pressures at which the relevant volatile hydrocarbons (containing butanol at infinite dilution) vaporise. In addition, the two solvents in each phase (in this case, water and the hydrocarbon) were assumed to be completely immiscible, allowing the activities of butanol in each phase to be approximated as the activity of butanol in binary mixtures. Given the low mutual solubility of butanol with the relevant hydrocarbons (as explored in Section 2.4), this was a valid assumption.

The limiting distribution coefficient at infinite dilution can be found from the ratio of the activity coefficients at infinite dilution:

$$D_i^{\infty,molar} = \frac{\gamma_i^{\infty,aq}(P, T)}{\gamma_i^{\infty,org}(P, T)} \quad (2-28)$$

The activity coefficient of butanol at infinite dilution in hydrocarbons can be found by considering the binary vapour-liquid equilibria (VLE) of butanol with the relevant hydrocarbon. By considering the co-existence equation, which relates the dew-point curve to the bubble-point curve, an estimate of the activity coefficient of butanol can be found. The vapour phase was modelled using the virial equation of state. Hence an estimate of the distribution coefficient of butanol can be made. The derivation is given in Appendix B, from which:

$$D_{Bu}^{\infty,molar}(T) = \frac{\gamma_{Bu}^{\infty,aq}(T)}{\gamma_{Bu}^{\infty,org}(T)} = \frac{\gamma_{Bu}^{\infty,aq}(T)}{\left(\alpha_{org,Bu} - (\alpha_{org,Bu} - 1)\mathcal{M} \frac{P_{org}^{sat}(V_{org}^V - V_{Bu}^L)}{RT} \right) \epsilon} \quad (2-29)$$

where:

$$\epsilon = \exp\left(\frac{P_{Bu}^{sat}}{RT}\left((\alpha_{org,Bu} - 1)(B_{Bu-Bu} - V_{Bu}^L) + \alpha_{org,Bu}\delta_{Bu-org}\right)\right) \quad (2-30)$$

Here \mathcal{M} is the gradient of the bubble-point pressure with respect to composition at infinite dilution of butanol ($x_{Bu} \rightarrow 0$), relative to that of Raoult's Law:

$$\mathcal{M} = \frac{\left(\frac{dP}{dx_{Bu}}\right)_{x_{Bu} \rightarrow 0}}{(P_{Bu}^{sat} - P_{org}^{sat})} \quad (2-31)$$

Hence \mathcal{M} is a measure of non-ideality at infinite dilution. This parameter, \mathcal{M} has been devised to separate out the effect of the relative volatility (α) on the activity coefficient at infinite dilution. In some cases, the activity coefficient is not very sensitive to the value of \mathcal{M} , allowing a reasonable estimate of the distribution coefficient to be found, based on rough analysis of the VLE behaviour of butanol and relevant hydrocarbons.

The effect of \mathcal{M} on $D_{Bu}^{\infty,molar}$ is difficult to analyse in equation (2-29) due to its complexity. To illustrate the effect of \mathcal{M} , equation (2-29) can be simplified by approximating the vapour phase as ideal (*i.e.* $B_{Bu-Bu} = \delta_{Bu-org} = 0$) and by neglecting

the Poynting correction (by assuming liquid molar volume, V_{Bu}^L , is negligible compared to vapour molar volume):

$$D_{Bu}^{\infty,molar}(T) = \frac{\gamma_{Bu}^{\infty,aq}(T)}{\gamma_{Bu}^{\infty,org}(T)} = \frac{\gamma_{Bu}^{\infty,aq}(T)}{(\mathcal{M} + \alpha_{org,Bu}(1 - \mathcal{M}))} \quad (2-32)$$

In the ideal vapour case, when $\mathcal{M} = 1$, $\gamma_{Bu}^{\infty,org} = 1$.

For systems with large relative volatilities (*e.g.* for C₄ hydrocarbons, $\alpha_{org,Bu} = 0(200)$ at 37°C), $D_{Bu}^{\infty,molar}$ is extremely sensitive to values of \mathcal{M} when \mathcal{M} is close to unity. This can be seen in the simplified eq. (2-32), which assumes the vapour phase to be ideal. This sensitivity is clearer than in eq. (2-29), which models the non-ideality in the vapour phase using the virial equation of state (as well as accounting for the Poynting correction).

Figure 2-15a-d shows the general form of plots of vapour-liquid equilibria of butanol with volatile hydrocarbons for different values of \mathcal{M} , at fixed temperature. Figure 2-15a shows the VLE behaviour for the reference case using Raoult's Law, *i.e.* $\mathcal{M} = 1$ and $\gamma = 1$, in which the bubble-point pressure is linear between the two pure vapour pressures.

For binary systems such as butanol with C₄ – C₆ hydrocarbons (where $P_{org}^{sat} > P_{Bu}^{sat}$ and $\alpha_{org,Bu} > 1$), if $\mathcal{M} < 1$ and $\gamma_{Bu}^{\infty} > 1$, assuming the vapour phase is ideal, the system will show positive deviations from Raoult's Law. The VLE of a solvent with these properties is shown in Figure 2-15b. In this case, the species show a net repulsive force between dissimilar molecules. This means that distillation requires fewer stages than for the ideal mixture shown in Figure 2-15a, and higher concentrations of butanol can be obtained for a given temperature gradient.

For $\mathcal{M} = 0$, the gradient of bubble-point pressure with respect to composition is zero at infinite dilution ($x_{Bu} \rightarrow 0$). For $\mathcal{M} < 0$, the gradient of the bubble-point curve is positive at infinite dilution (for systems with $P_{org}^{sat} > P_{Bu}^{sat}$). In these systems, the vapour pressure initially increases with addition of the less volatile component (butanol) and hence the system forms a minimum boiling point azeotrope. This case is shown in Figure 2-15c.

Conversely, if $\mathcal{M} > 1$ and $\gamma_{Bu}^{\infty} < 1$, the system will show negative deviation from Raoult's Law.

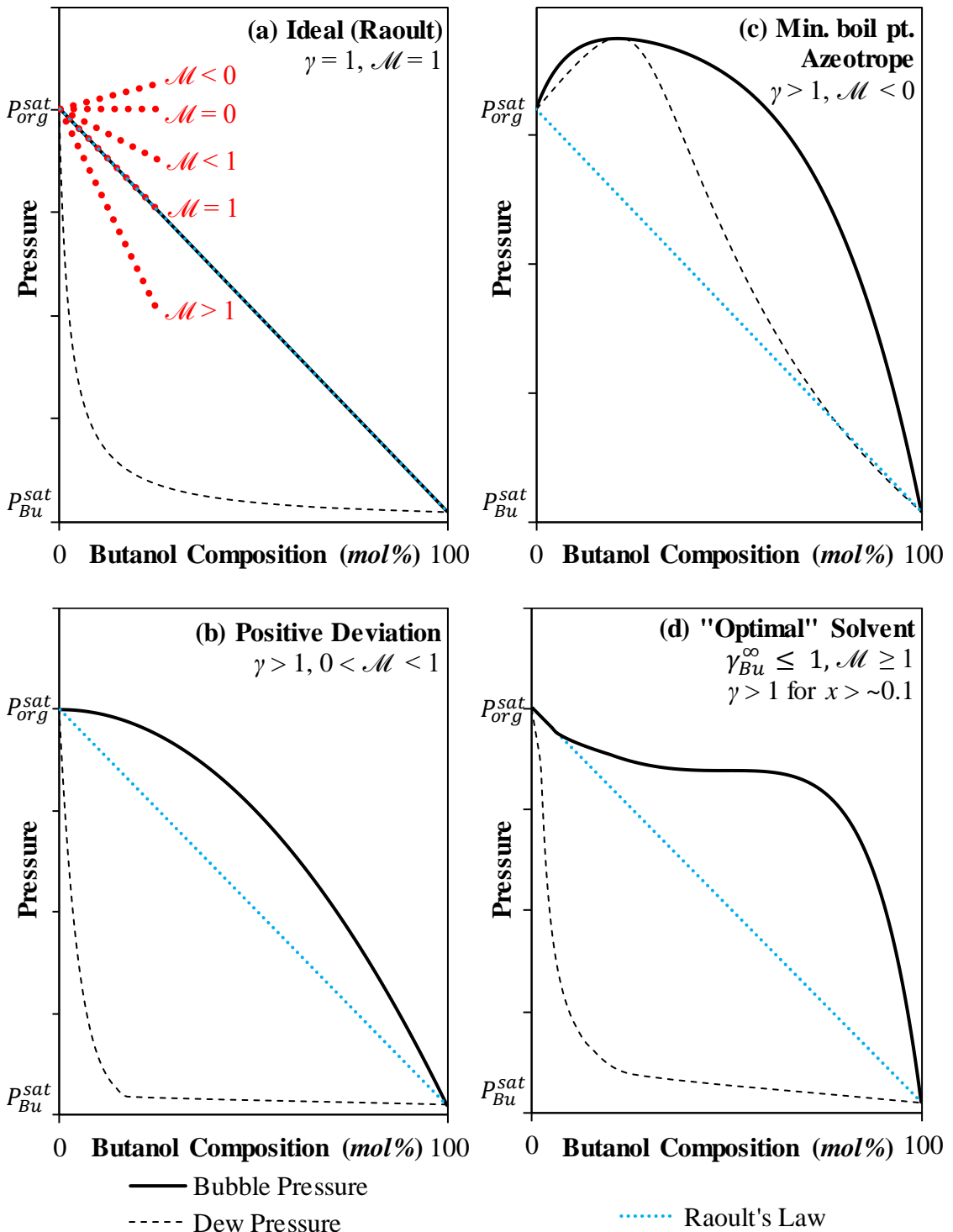


Figure 2-15a-d: Example isothermal vapour-liquid equilibria of butanol with volatile solvents for different values of \mathcal{M}

(a) Raoult's Law ($\mathcal{M} = 1$)

(b) Positive deviation from Raoult's Law ($\mathcal{M} < 1$)

(c) Minimum boiling point (maximum pressure) azeotrope ($\mathcal{M} < 0$)

(d) A theoretical 'optimal' volatile solvent for extraction of butanol

Figure 2-15d shows the vapour-liquid equilibria for a binary mixture of butanol and volatile solvent with theoretically optimal thermodynamics where the value of \mathcal{M} ($\mathcal{M} \geq 1$) minimises the activity coefficient of butanol in the solvent at low concentration and hence maximises the distribution coefficient for dilute extractions. This value of \mathcal{M} corresponds to Raoult's Law behaviour, or negative deviation from Raoult's Law at infinite dilution. However, a negative deviation from Raoult's Law is the result of net attractive forces between dissimilar molecules, which therefore increases the energy and number of stages required in a distillation separation. Therefore, an optimal volatile solvent for use in a butanol extraction would also exhibit large positive deviations from Raoult's Law at higher concentrations, above the dilute concentrations found in the extraction. Aside from reducing the number of stages in the distillation column, this characteristic would also increase the concentration of butanol produced in the first distillation column, where the temperature gradient is limited. For an optimal solvent, only a small temperature increase above the saturation temperature of the solvent would be required to produce a highly concentrated butanol in the reboiler. This is equivalent to a small pressure decrease from the saturation pressure of the solvent on an isothermal plot such as Figure 2-15d. A high relative volatility of the solvent also reduces the number of stages required in distillation, and so is another characteristic of an optimal solvent.

In summary, the binary vapour-liquid equilibrium characteristics of an optimal solvent with butanol would constitute effectively a combination of large positive deviations from Raoult's Law (Figure 2-15b), allowing simple separation using low-grade heat; and ideal mixture behaviour at low butanol concentration (Figure 2-15a), which would produce a very high distribution coefficient for the extraction.

Minimum boiling point azeotropes (Figure 2-15c) are undesirable in the solvent-butanol vapour-liquid equilibrium (VLE). In addition to resulting in a low distribution coefficient (since $\mathcal{M} < 0$), the presence of an azeotrope would cause difficulties during distillation, similar to those encountered in butanol-water distillation. If a minimum boiling point azeotrope were present in the VLE, butanol would be boiled into the vapour phase below the azeotrope concentration. This would therefore require a two-column system, or another azeotropic separation technique, in order to separate the azeotrope in place of one of the distillation columns, depending on the composition of the azeotrope. A two-column system used to separate the azeotrope must operate at two difference pressures. It would therefore potentially become difficult to achieve a high degree of separation

using low-grade heat, which has specific column pressure requirements, in addition to the requirement of additional separation equipment.

Experimental measurements of the binary VLE of butanol with various C₄ – C₆ hydrocarbons (detailed in section 3.2) demonstrate that these binaries show positive deviation from Raoult's Law and that most do not form an azeotrope. Therefore, for these systems, 0 < \mathcal{M} < 1. The only exception is *n*-hexane, which shows a minimum boiling point azeotrope at a dilute butanol concentration at higher temperatures. This means that for *n*-hexane at higher temperatures, \mathcal{M} is slightly negative. At lower temperatures, bubble-point curves show $\mathcal{M} \sim 0$. When $\mathcal{M} \sim 0$, $D_{Bu}^{\infty,molar}$ will decrease with relative volatility ($\alpha_{org,Bu}$). For systems with $\mathcal{M} \sim 0$, unless $\alpha_{org,Bu}$ is very large (or very small), $D_{Bu}^{\infty,molar}$ is not very sensitive to the value of \mathcal{M} since, if $\mathcal{M} \sim 0$, approximately:

$$D_{Bu}^{\infty,molar}(T) \cong \frac{\gamma_{Bu}^{\infty,aq}(T)}{\alpha_{org,Bu}} \quad (2-33)$$

2.6.2 Estimates of \mathcal{M} and Methodology

In order to approximate \mathcal{M} , raw measurements of bubble-point taken from the literature for a range of binary mixtures C₄ – C₆ hydrocarbons with butanol were used. These measurements are detailed in the Supplementary Material included with this dissertation. Rough estimates of the gradient of the bubble-point curve at $x_{Bu} \rightarrow 0$ was made using only measurements of bubble-point with $x_{Bu} < 0.1$:

$$\left(\frac{dP}{dx_{Bu}} \right)_{x_{Bu} \rightarrow 0} \approx \frac{P(x_{Bu}, T) - P_{Bu}^{sat}(T)}{x_{Bu}}, \quad x_{Bu} < 0.1 \quad (2-34)$$

The gradient of Raoult's Law, ($P_{Bu}^{sat} - P_{HC}^{sat}$), for each set of VLE measurements were calculated using the measured pure vapour pressures in reported in each set of VLE measurements. These were subsequently used to estimate \mathcal{M} (' \mathcal{M}_{est} ') for each set of VLE measurements:

$$\mathcal{M}_{est} \approx \frac{1}{N_{VLE}} \sum_i^{N_{VLE}} \frac{P(x_{Bu,i}, T) - P_{Bu}^{sat}(x_{Bu} = 0, T)}{x_{Bu,i}(P_{Bu}^{sat}(x_{Bu} = 0, T) - P_{HC}^{sat}(x_{Bu} = 1, T))}, \quad x_{Bu,i} < 0.1 \quad (2-35)$$

Where N_{VLE} is the number of measurements of bubble-point pressure in the set of measurements for which $x_{Bu} < 10$ mol%. This gave a rough estimate of the bubble-point gradient at low butanol compositions as compared with that of Raoult's Law.

These estimates found that \mathcal{M}_{est} was a slight function of temperature, but averages across sets of measurements in the range 25 – 120°C found estimates for \mathcal{M}_{est} of -0.1 for *n*-hexane and 0.2 for 1-hexene. The value of \mathcal{M}_{est} estimated for *n*-pentane (0.3) was assumed to be valid for all C₅ hydrocarbons. Similarly, the value of \mathcal{M}_{est} estimated for *n*-butane and *iso*-butane (0.55, the same value for both isomers) was assumed to be valid for all C₄ alkanes, whilst the value estimated for 1-butene (0.9) was assumed to be valid for all C₄ alkenes.

These estimates of \mathcal{M}_{est} were employed in equation (2-29) to predict distribution coefficients at infinite dilution of *n*- and *iso*-butanol in C₄ – C₅ hydrocarbons, hexane and 1-hexene. The values of \mathcal{M}_{est} were calculated using binary *n*-butanol VLE measurements but were assumed to be valid for binary mixtures of *iso*-butanol with volatile hydrocarbons. The limiting activity of butanol in water at infinite dilution, $\gamma_{Bu}^{\infty,aq}$, was calculated from correlations of Dohnal *et al.* (2006) (*n*-butanol) and Fenclova *et al.* (2007) (*iso*-butanol) (given in Appendix B.5). virial coefficients were estimated using the Tsonopolous model (detailed in Appendix D), using critical properties from Poling *et al.* (2001).

2.6.3 Results

Figure 2-16 details the estimates of the limiting distribution coefficient of butanol at infinite dilution in C₄ – C₅ hydrocarbons, hexane and 1-hexene at a range of temperatures. Estimates are detailed for both *n*- and *iso*-butanol for comparison, using estimates of \mathcal{M} (\mathcal{M}_{est}) calculated as described in the preceding section.

In addition, estimates of the limiting distribution coefficient of *n*-butanol are detailed in Figure 2-16, assuming $\mathcal{M} = 0$. This equates to a minimum estimate of the limiting distribution coefficient, given that $\mathcal{M} \geq 0$ for binary mixtures of butanol and volatile hydrocarbon solvents.

Finally, the total energy required for the distillation system, E_{DC} , was calculated using eqs. (2-25) and (2-26). The estimates of the total energy required were based on distribution coefficients predicted for *n*-butanol using estimates of \mathcal{M} calculated from literature VLE measurements. These energy consumption estimates are presented in Figure 2-17.

As shown in Figure 2-16, the distribution coefficient of butanol in C₄ – C₆ hydrocarbons is predicted to rise dramatically with temperature, typically increasing by a factor of ~4

between 37°C and 90°C. This increase in distribution coefficient is reflected in much smaller values of the total energy required for distillation (E_{DC}) for extractions performed at 90°C *versus* 37°C in Figure 2-17. This means that if the availability of low-grade heat

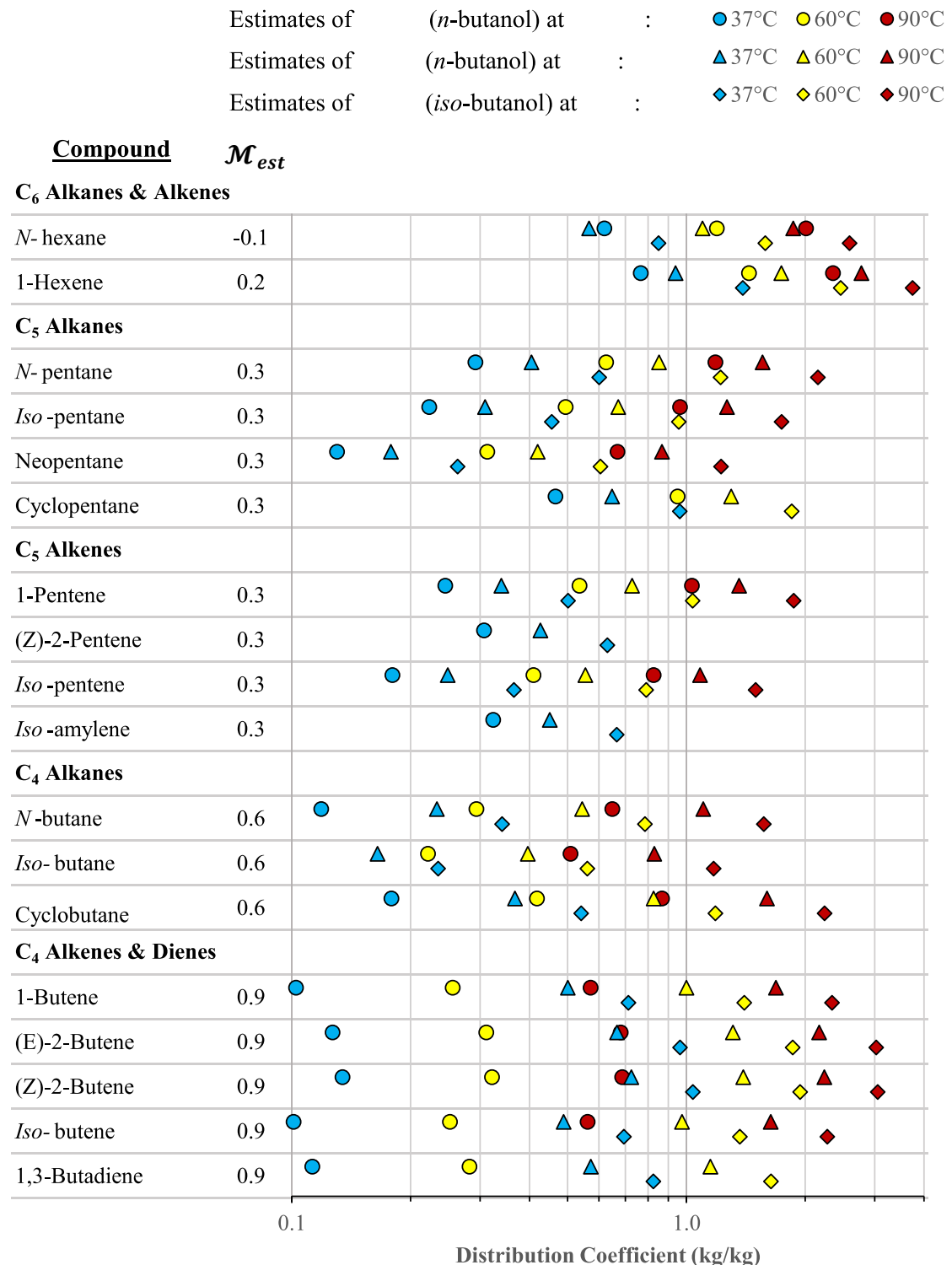


Figure 2-16: Estimates for the mass distribution coefficient of dilute *n*-butanol and *iso*-butanol in C_4 – C_6 hydrocarbons *versus* water at 37°C, 60°C and 90°C. Estimates were calculated for both $\mathcal{M} \sim 0$ and for $\mathcal{M} = \mathcal{M}_{est}$.

were limited, increasing the extraction temperature might reduce the amount of low-grade heat required significantly.

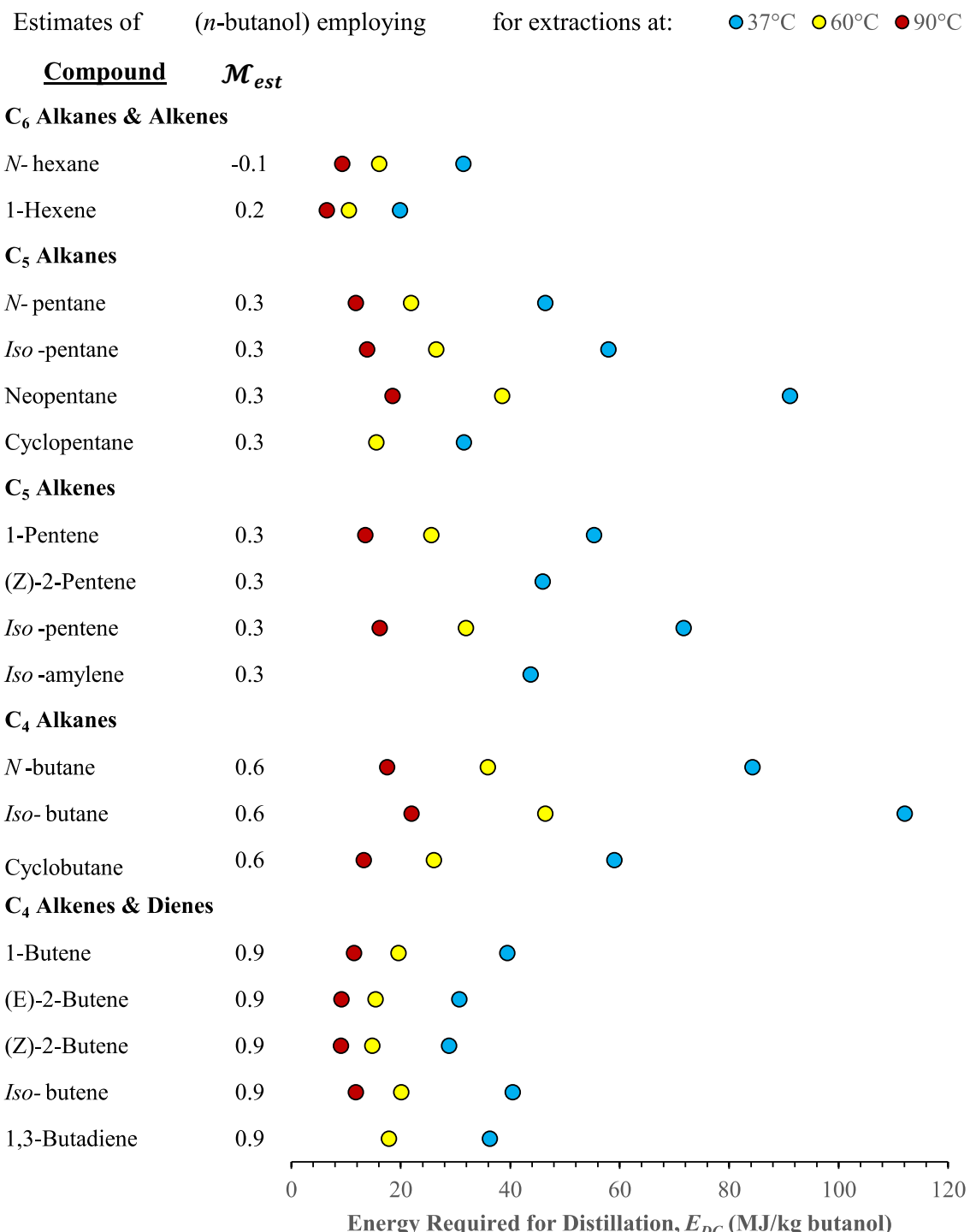


Figure 2-17: Estimates of the total energy required for distillation of *n*-butanol and C₄–C₆ hydrocarbons (E_{DC}) following extraction of butanol from a 2 wt% aqueous mixture, employing estimates of the distribution coefficient at \mathcal{M}_{est} (Figure 2-16)

2.6.4 Discussion

As demonstrated by eq. (2-32), D_{Bu}^{∞} is insensitive to the value of \mathcal{M} for $\mathcal{M} \sim 0$, especially for less volatile hydrocarbons. This is confirmed by the similarity of values predicted for D_{Bu}^{∞} at $\mathcal{M} = 0$ for C₅ – C₆ hydrocarbons *versus* values predicted when values of \mathcal{M} calculated from literature VLE measurements were employed ($\mathcal{M} = -0.1$ to 0.3). This suggests that the estimated values of D_{Bu}^{∞} are relatively accurate for these hydrocarbons, since the accuracy of \mathcal{M} is not important.

Estimates for these hydrocarbons also agree with the limited measurements available in the literature for distribution coefficients. For example:

- an estimated value of $D_{Bu}^{\infty, mass} \sim 0.6$ kg/kg for *n*-hexane at 37°C (c.f. 0.5 kg/kg Groot *et al.* (1990));
- an estimated value of $D_{Bu}^{\infty, mass} \sim 0.2$ kg/kg for *iso*-pentane at 25°C (c.f. 0.21 kg/kg Dadgar and Foutch (1986))

Conversely for the comparatively volatile C₄ hydrocarbons, the values of D_{Bu}^{∞} are highly sensitive to the value of \mathcal{M} since \mathcal{M} is close to unity. Therefore, these estimates contain a large degree of uncertainty, especially for C₄ alkenes where $\mathcal{M}_{est} = 0.9$

Estimates for the distribution coefficients for dilute *iso*-butanol are slightly higher than those for *n*-butanol at all temperatures, with predicted distribution coefficients at 90°C up to 50% higher, as shown in Figure 2-16. This is because the slightly higher volatility of *iso*-butanol compared to that of *n*-butanol results in slightly lower relative volatilities of hydrocarbons *versus* *iso*-butanol compared to those *versus* *n*-butanol. The effect of this reduced relative volatility is large enough to counteract the effect of the lower activity coefficient of *iso*-butanol at infinite dilution in water, which is slightly lower than that of *n*-butanol. However, since estimates of \mathcal{M} used in the prediction of distribution coefficients of *iso*-butanol are based on those of *n*-butanol, the estimates of distribution coefficient for *iso*-butanol contain a large degree of uncertainty. This uncertainty is exacerbated for predictions of distribution coefficients in C₄ hydrocarbons, for which \mathcal{M} is not close to zero.

This analysis identifies C₄ alkenes as having the highest distribution coefficients amongst the C₄ – C₅ hydrocarbons, with mass distribution coefficients exceeding 0.5 kg/kg at 37°C, rising to ~2 kg/kg at 90°C. These equate to total energy requirements for distillation ~36 MJ/kg butanol (coincidentally, the enthalpy of combustion of butanol) for

extracting 2 wt% aqueous butanol at 37°C. This falls to ~10 MJ/kg for extractions performed at 90°C. *N*-pentane is also promising, with a mass distribution coefficient of 0.4 at 37°C and 1.6 at 90°C, close to those of the C₄ alkenes. The distribution coefficient estimated for *n*-pentane is also likely to be relatively accurate since $\mathcal{M} \sim 0$, and so the exact value of \mathcal{M} is not significant.

However, of all the hydrocarbons investigated, the predicted distribution coefficients are highest for 1-hexene, for which mass distribution coefficients of 0.9 at 37°C and 2.8 at 90°C are predicted. These distribution coefficients equate to a total energy requirement for distillation of 20 and 6 MJ/kg butanol for extraction at 37°C and 90°C respectively. The predicted distribution coefficients of 1-hexene are around 50% higher than those predicted for its alkane equivalent, *n*-hexane, for which predicted distribution coefficients are similar to those of the C₄ alkenes. This suggests that the slight polarity of alkenes due to the presence of the C=C bond can increase distribution coefficient significantly. Despite their more favourable distribution coefficients, C₆ hydrocarbons are probably not suitable candidates for extraction of butanol since they would require highly reduced pressure in order to conduct distillation of the solvent and butanol using low-grade heat.

The estimates produced were also for butanol at infinite dilution, and so only provide a guide to the equilibria at dilute butanol concentrations. The activity coefficient of butanol in both water and the solvent will change as butanol concentration increases. A more thorough analysis of the vapour-liquid equilibria measurements in the literature is required to calculate distribution coefficients of butanol in hydrocarbon solvents *versus* water as a function of composition and temperature. Distribution coefficients for side-products such as ethanol and acetone should also be calculated. This analysis of literature VLE measurements will be explored in Chapter 3.

2.7 Conclusion

A novel liquid-liquid extraction technique has been devised, which uses simple, short (C₄ or C₅) hydrocarbons as extractants. These extractants have been ignored by previous authors as they are more volatile than butanol. At first inspection, this would appear to be a drawback, as it means boiling off the large quantity of solvent rather than the comparatively small quantity of butanol in the extracted phase. Longer (C₆₊), less volatile hydrocarbons have also been rejected by previous authors, as whilst their selectivity over water is very high for the extraction of butanol, their distribution coefficients are lower than other potential extractants. However, since C₄ – C₅

hydrocarbons are relatively volatile, they can be boiled off using plentiful supplies of very low-grade heat, for example, the heat given off by the fermentation at ~37°C.

The use of low-grade waste heat means that separation of the extracted phase can be achieved at a minimal net energy cost, and so the low distribution coefficient of volatile hydrocarbons is not a determining factor. Short hydrocarbons have many advantages as extractants, including very low mutual solubilities with water; low organism toxicity; low viscosities; high density difference; high interfacial tensions (reducing emulsion formation and reducing phase separation costs); low-replacement cost; stability and product compatibility.

Short hydrocarbons do not possess high distribution coefficients compared with other extractants. Estimations following a thermodynamic analysis found distribution coefficients were highest for C₄ alkenes, and that their distribution coefficient rise with temperature. By using low-grade waste heat to concentrate the butanol-solvent mixture, high-grade requirements were found to be minimal, estimated to be 1 – 5 MJ/kg butanol. However, the low-grade heat requirements could be substantial, and depend mostly on the aqueous broth concentration and the distribution coefficient of the solvent.

A more thorough analysis of VLE measurements in the literature is required to find distribution coefficients for butanol and other fermentation products in hydrocarbons *versus* water as a function of composition and temperature. The following chapter outlines this analysis of VLE and excess enthalpy measurements for butanol, ethanol and acetone with C₄ – C₆ hydrocarbons.

3. Analysis of Binary Thermodynamic Data of Short Hydrocarbons with Fermentation Products

3.1 Introduction

Estimates of the energy consumption of the extraction of butanol using volatile hydrocarbons have been made based on approximations of the equilibria of binary mixtures of butanol with one of a number of C₄ – C₆ hydrocarbons. This chapter uses thermodynamic data found in the literature to determine the vapour-liquid equilibria of these mixtures. Activities of dilute butanol in C₄ – C₆ hydrocarbons were also calculated so as to predict distribution coefficients for butanol between a hydrocarbon and water. The latter is important because the low-grade heat required in the extraction process using volatile hydrocarbons is highly sensitive to the distribution coefficient of butanol.

Measurements of liquid-liquid equilibria (LLE) for the ternary system involving the partition of butanol between water and a hydrocarbon are scarce, although some measurements of distribution coefficients of *n*-butanol with water and *n*-hexane are available in the literature. A search of the available literature did not identify any ternary data for butanol (*n*- or *iso*-) with water and C₄ or C₅ hydrocarbons. Nonetheless it did find measurements of vapour-liquid equilibrium (VLE), excess enthalpy of mixing and excess volume of mixing for binary mixtures of butanol with C₄ and C₅ hydrocarbons. Measurements of VLE can be used to calculate activity coefficients for these binary pairs since at vapour-liquid equilibrium:

$$\phi_i(y_i, T, P) \cdot y_i P = \gamma_i(x_i, T, P) \cdot x_i (\phi_i^{sat} \cdot P_i^{sat}) \cdot \exp\left(\frac{V_i^L(P - P_i^{sat})}{RT}\right) \quad (3-1)$$

where $\phi_i(y_i, T, P)$ is the fugacity of species *i* at vapour mole fraction of species *i*, y_i , temperature *T* and pressure *P*, calculated by a suitable equation of state. The liquid phase activity coefficient is denoted by $\gamma_i(x_i, T, P)$, a function of temperature, pressure and the liquid mole fraction of species *i*, x_i . The superscript ‘sat’ denotes conditions at pure *i*. The molar volume of pure species *i* is denoted V_i^L and *R* is the universal gas constant.

Measurements of the excess volume (\underline{V}^E) and excess enthalpy of mixing (H^E) can be used to calculate the variation of activity coefficient (γ_i) with pressure and temperature respectively (the full derivation is detailed in Appendix E), thus:

$$\left(\frac{\partial \ln \gamma_i}{\partial P}\right)_{T,x} = \frac{\overline{V}_i^E}{RT} \quad (3-2)$$

$$\left(\frac{\partial \ln \gamma_i}{\partial T}\right)_{P,x} = -\frac{\overline{H}_i^E}{RT^2} \quad (3-3)$$

where \overline{V}_i^E and \overline{H}_i^E are the partial molar excess volume and enthalpy of species i respectively. It was assumed that the activities of the species in equilibrium are independent of pressure. This assumption was verified for mixtures of butanol with volatile hydrocarbons by examining the effect of pressure on the activity coefficient of *n*-butanol in *n*-pentane, using measurements of the excess molar volume of mixing, as described in Appendix E.

3.2 Binary Thermodynamic Measurements Available in the Literature

Measurements from the available literature of VLE and excess enthalpy of mixing at constant temperature, taken to be within the range 0 – 100°C, the approximate range of interest for the extraction temperature, were compiled into a database. An extensive search was conducted for binary mixtures of *n*-butanol with any C₄ or C₅ hydrocarbon, *n*-hexane, 1-hexene, or water. VLE measurements of butanol with C₄ and C₅ hydrocarbons were identified for pentane, *n*-butane, *iso*-butane and 1-butene. Thermodynamic data for some of these binary mixtures of butanol with hydrocarbons, containing measurements of excess enthalpy of mixing, were also found. A similar search was then conducted for VLE measurements of binary mixtures comprising *iso*-butanol, ethanol and acetone with solvents for which VLE measurements of binaries with *n*-butanol had been identified. These VLE measurements, together with any associated measurements of excess enthalpy of mixing, were added to the database. The resultant database of thermodynamic measurements of relevant binary mixtures is detailed in the Supplementary Material included with this dissertation.

Searches excluded isobaric VLE measurements. Isobaric VLE measurements are relatively common, since many separation processes (*e.g.* distillation) operate at constant pressure. However, analysis of isobaric VLE measurements is not feasible without

associated measurements of excess enthalpy to calculate activity coefficients at a given temperature (Islam and Rahman, 2012). In any case, isobaric VLE measurements were scarce for the desired binary mixtures. An exception was made for acetone and 1-hexene, for which no other VLE measurements could be found. However, the temperature range of the isobaric VLE measurements identified for this pair (Ogorodnikov *et al.*, 1961) was very narrow, and so the Clausius-Clapyron equation was used to approximate these measurements as isothermal ones.

The lowest (non-zero) concentration of the product (butanol, acetone *etc.*) recorded in each dataset is noted in the summary of the database (Table S-1, given in the Supplementary Material included with this dissertation). This minimum concentration is relevant to the investigation of liquid-liquid equilibria of a dilute product (*c.f.* < 0.5 mol% butanol in the aqueous broth). Since the activity coefficient can vary significantly at very low concentrations, it is imperative that there are measurements around this range for accurate analysis of equilibria of dilute mixtures.

In total, 107 isothermal datasets, consisting of *ca.* 2000 individual measurements, were identified for binary mixtures of the six hydrocarbons with the fermentation products, of which 34 datasets were for binaries containing *n*-butanol.

3.3 Regression of VLE and Excess Enthalpy Measurements

3.3.1 Types of VLE Datasets and Correction of Liquid Phase Compositions

VLE data can be categorised by the type of measurements recorded at equilibrium in the equilibrium ‘cell’. In isothermal VLE measurements, the total pressure (P) is always recorded. Measurements are made at discrete liquid phase compositions (x) to produce the bubble-point curve on the $P - x$ diagram. For the sake of simplicity in experimental design, the overall composition of the mixture injected into the cell (z), rather than liquid composition at equilibrium (x) was recorded in many cases. Thus, such measurements are termed ‘ $P - z$ ’ datasets.

If the volume of the cell is known (V^{cell}), and the number of moles of each species injected into the cell is known (N_1, N_2), then the vapour compositions calculated during the regression of VLE datasets (y^{calc}) can be used to back-calculate the original liquid composition (x). This can be achieved by a simple mole balance, derived in Appendix C:

$$x_1 = \frac{z_1 \underline{V}^V - y_1 \underline{V}^{cell} + (y_1^{calc} - z_1)(\underline{V}_2^L + \underline{V}_E^L)}{\underline{V}^V - \underline{V}^{cell} - (y_1^{calc} - z_1)(\underline{V}_1^L - \underline{V}_2^L)} \quad (3-4)$$

where:

$$z_1 = \frac{N_1}{N_1 + N_2} \quad (3-5)$$

$$\underline{V}^{cell} = \frac{V^{cell}}{N_1 + N_2} \quad (3-6)$$

Excess volume on liquid mixing (\underline{V}_E^L) is a function of liquid composition (x_1) but is usually neglected since it is small compared to \underline{V}_2^L and \underline{V}_1^L .

Initially, the regression procedure can be conducted by approximating the liquid mole fraction (x_1) as the overall mole fraction (z_1). The compositions in the vapour phase, determined by the regression of the bubble-point curve, can then be used in the above mass balance to correct the overall mole fractions to the liquid compositions at equilibrium. The regression procedure is then iterated with the corrected liquid compositions until the compositions converge. This procedure usually converges very quickly, as the overall cell compositions are normally very close to the liquid compositions (as approximated during the first iteration). This proximity is because the vapour headspace in the equilibrium cell is small, and the density of the vapour phase at sub-critical conditions is negligible compared to that of the liquid phase.

For this reason, many studies in the literature have assumed that the mole fraction of the overall cell is equal to the liquid mole fraction. Frustratingly, this means that authors have often neglected to publish the necessary information required to perform the correction of the liquid composition. Datasets for which the necessary measurements to perform this correction are reported (*i.e.* measurements of cell volumes and quantity of moles injected into the equilibrium cell) have been referred to as ‘ PzV ’ datasets in this work. The publication of this type of dataset and its subsequent reduction (using the Barker method) has been undertaken for VLE measurements of many binary alcohol-alkane mixtures by researchers at Helsinki University of Technology. Their data-reduction methodology is detailed in Uusi-Kyyny *et al.* (2002).

Finally, the composition of both the liquid (x) and vapour (y) phases at equilibrium is recorded in some datasets. These types of VLE datasets are termed here ‘ Pxy ’ datasets.

3.3.2 Correction of Temperature Variation in Isothermal Datasets

For VLE data that are nominally isothermal, small temperature variations are often measured in the equilibrium cell (T_{exp}). Datasets that include measurements of the actual temperature (T) in the equilibrium cell, as opposed to datasets which merely quote the target isothermal temperature of the equilibrium cell, here have ‘ T ’ included in their type designation, *e.g.* PTz , $PTzV$. Any temperature variations from the target temperature quoted for the isothermal measurements (T_{target}) should be removed from the raw VLE measurements. This can be achieved by employing the Clausius-Clapeyron equation to correct experimental bubble-point pressures (P_{exp}) to isothermal (‘adjusted’) bubble-point pressures (P_{adj}):

$$\frac{d \ln P^{sat}}{d T} = -\frac{\Delta\underline{H}^{vap}}{RT^2} \quad (3-7)$$

$$\therefore P_{adj}(T_{target}) = P_{exp}(T_{exp}) \cdot \exp\left(\frac{\Delta\underline{H}^{vap}}{R}\left(\frac{1}{T_{exp}} - \frac{1}{T_{target}}\right)\right) \quad (3-8)$$

This version of the Clausius-Clapeyron equation assumed that the volume of the vapour phase could be represented by the ideal gas law, and that the liquid molar volume was negligible compared to the molar volume of the vapour phase. This was valid for the purposes of correcting the small temperature variations as the pressures were low. The temperature dependence of enthalpy of vaporisation ($\Delta\underline{H}^{vap}$) was neglected, because the variation from the target temperature was typically $\ll 1$ K. The molar enthalpy of vaporisation can be approximated as the sum of the pure enthalpies of vaporisations, weighted by overall cell compositions:

$$\Delta\underline{H}^{vap} \cong \sum y_i \Delta\underline{H}_i^{vap} \approx \sum z_i \Delta\underline{H}_i^{vap} \quad (3-9)$$

3.3.3 Regression Methodologies

Regression was used to describe vapour-liquid equilibria, and to determine activity coefficients at dilute concentrations. The authors of the datasets in the database conducted a variety of different analyses to regress the raw measurements in their isothermal VLE datasets. Three main approaches were identified: the ‘Barker method’; the ‘Mixon method’; and direct measurements of vapour-liquid equilibrium (P_{xy} measurements).

3.3.4 The ‘Barker Method’

The ‘Barker method’ regresses P_x , P_z , or P_{zV} measurements (*i.e.* measurements of the bubble-point curve) by fitting parameters of an activity coefficient model to the measurements. Popular choices of activity coefficient model are Redlich-Kister or Margules (equivalent models); Wilson; NRTL; UNIQUAC and Van Laar (Islam and Rahman, 2012).

The vapour composition and pressure at equilibrium can be calculated at a given liquid composition and corresponding activity coefficients by:

$$P_{calc} = \sum_i \gamma_i(x_i, T, P) \cdot x_i \cdot \left(\frac{\phi_i^{sat}}{\phi_i(y_i, T, P)} \cdot P_i^{sat} \right) \cdot \exp \left(\frac{V_i^L(P - P_i^{sat})}{RT} \right) \quad (3-10)$$

$$y_{i,calc} = \gamma_i(x_i, T, P) \cdot x_i \cdot \left(\frac{\phi_i^{sat}}{\phi_i(y_i, T, P)} \cdot \frac{P_i^{sat}}{P_{calc}} \right) \cdot \exp \left(\frac{V_i^L(P - P_i^{sat})}{RT} \right) \quad (3-11)$$

This calculation of vapour composition and pressure is iterative. This is because fugacity (ϕ_i) depends on the calculated vapor composition ($y_{i,calc}$) and pressure (P_{calc}); similarly, the Poynting correction (the exponential term) depends on the vapour pressure (P_{calc}). The first iteration can be conducted by neglecting the Poynting correction and assuming the vapour phase is ideal ($\phi_i = 1$). In subsequent iterations, an equation of state for the vapour phase is used to calculate fugacity, such as the virial equation or variations on Redlich-Kwong.

The parameters of the activity coefficient model are optimised to fit the calculated vapour pressures to the bubble-point measurements by minimising an objective function. The objective function employed for this optimisation is usually a variant on the pressure deviation between the values of vapour pressure calculated by the activity model (P_{calc}), and those of the measurements in the dataset (P_{exp}). Activity coefficients are then simply calculated from the activity model using the optimised parameters.

The Barker method is popular, as it produces parameters for commonly-used activity coefficient models. Subsequently, parameters of these activity models are easy to use in process simulation software and other investigations. Different activity coefficient models used in regressions are often compared for optimal fit to the VLE measurements for a given system. These activity coefficient models often have a theoretical basis, with 2-3 temperature-dependent parameters. However, such models with only 2 or 3 parameters cannot describe the rapid changes in the gradient of the bubble-point curve

(dP/dx) that can occur at low concentrations. A rapid change in the gradient of the bubble-point curve at dilute concentrations corresponds to rapid changes in activity coefficient. This dependence can be demonstrated by inspecting the form of the activity coefficient at infinite dilution as a function of the gradient of the bubble-point curve at $x_1 \rightarrow 0$. This can be derived from the co-existence equation, employing the virial equation of state (derived in Appendix C):

$$\gamma_1^\infty(T, P_2^{sat}) = \left(\frac{(\underline{V}_2^V - \underline{V}_2^L)}{RT} \cdot \left(\frac{dP}{dx_1} \right)_{x_1 \rightarrow 0} + 1 \right) \cdot \alpha_{2,1} \cdot \epsilon$$

$$\epsilon = \exp \left(\frac{P_1^{sat}}{RT} \left((\alpha_{2,1} - 1)(B_{11} - \underline{V}_1^L) + \alpha_{2,1} \delta_{12} \right) \right) \quad (3-12)$$

Hence the value of activity coefficient (γ_i) is highly sensitive to the gradient of the bubble-point curve (dP/dx_1). Therefore, inflexible activity models with only 2 – 3 parameters do not accurately represent activity coefficient at low concentrations (Fischer and Gmehling, 1994).

The sensitivity of activity coefficient to the gradient of the bubble-point curve is a problem when attempting to model the activity coefficient accurately at low concentrations. Indeed, the activity coefficient of butanol in C₄ hydrocarbons at infinite dilution was found to be particularly sensitive to the bubble curve gradient as $x_{Bu} \rightarrow 0$ in Section 2.6. In addition, Islam and Kabadi (2009) found that the limiting molar distribution coefficient at infinite dilution for butanol in hexane versus water was found to be 14.6 when using activity coefficients calculated by experimental VLE measurements regressed using the UNIQUAC activity model. However, when activity coefficients were calculated using eq. (3-12) from VLE measurements obtained from the literature, a value of 1.4 was calculated for the limiting distribution coefficient at infinite dilution. A similar value (1.2) was calculated from the author's own measurements using eq. (3-12). These two values are an order of magnitude lower than the value calculated by the activity model. This discrepancy highlights the problems with employing activity coefficient models at dilute concentrations, such as found in aqueous fermentation broths.

Excess enthalpy measurements can also be included in the Barker method by using temperature-dependant parameters in the activity coefficient model. Activity coefficient models can be rearranged using equation (3-3) to calculate excess enthalpy.

The Barker method is a popular and powerful method for regressing VLE measurements of the bubble-point curve by fitting the measurements to an activity coefficient model.

However, the use of inflexible activity coefficient models with only 2 – 3 parameters often results in significant errors at dilute concentrations.

3.3.5 The ‘Mixon Method’

The ‘Mixon method’, originally developed by Mixon *et al.* (1965) does not assume an activity coefficient model. Instead, the co-existence equation (Appendix C) is employed to integrate the bubble-point curve to find the dew-point curve (P_y). To conduct this integration, the measurements of bubble-point pressure taken at discrete compositions must first be smoothed into a continuous curve. This is normally achieved by fitting a cubic spline to the measurements. The Mixon method has the advantage of not assuming an activity coefficient model, which restricts the shapes of the bubble and dew-point curves. As a result, the Mixon method can achieve a more accurate fit across the entire composition range. This is beneficial for modelling dilute compositions where gradients of bubble-point curves can change rapidly.

Therefore, regression of the datasets containing VLE measurements in the database described in section 3.2 was attempted using the Mixon method. However, drawbacks similar to those experienced by Plank *et al.* (1981) were encountered. It was found that the procedure selected to smooth the measurements at discrete compositions into a continuous curve had a significant impact on the resulting activity coefficient at low concentrations. It was found that significant intervention and experience of using the method was required in order to achieve a smooth curve without overfitting. The Mixon method was extremely sensitive to scatter and experimental error (including in P_i^{sat} values) at dilute compositions. Without careful selection of splines, the Mixon method overfitted datasets, causing sharp changes in the bubble curve gradient. In addition, using the Mixon method to combine multiple VLE datasets at different temperatures with excess enthalpy measurements was cumbersome and inconsistent. In practice, it required significant manual intervention in the selection of datasets used for a datum temperature and temperature-dependence portions of the analysis.

The method used in Section 2.6 to estimate distribution coefficients for butanol at infinite dilution is analogous to the Mixon method. Instead of a cubic spline fit across the entire composition range, a straight-line was fitted to measurements of the bubble-point pressure close to $x_{Bu} = 0$ in order to determine the gradient of the bubble curve as $x_{Bu} \rightarrow 0$. The co-existence equation with the virial equation of state was then used to calculate activity coefficient of butanol at infinite dilution from the gradient.

3.3.6 Direct Measurement of Vapour-Liquid Equilibrium (P_{xy} Measurements)

In the Barker and Mixon methods, the composition of the vapour phase is calculated from measurements of bubble-point pressures *via* either an activity coefficient model (the Barker method); or the co-existence equation (the Mixon method). Alternatively, the vapour phase composition can be measured at equilibrium. A recirculating still is used to measure equilibrium concentrations in both the liquid and vapor phases (yielding ' P_{xy} ' measurements). Several datasets from the compiled database containing VLE measurements have been measured using this method. Activity coefficients are calculated at each datapoint by employing eq. (3-1). The experimental activity coefficients can either be fitted to an activity coefficient model (as employed in the Barker method) or smoothed using a spline fit (as employed in the Mixon method).

Whilst theoretically this method should be very effective, in practice it is difficult to obtain accurate measurements of the liquid and vapour phase simultaneously at equilibrium. As demonstrated by Kuschel *et al.* (1977), the inclusion of vapour compositions in regressions of VLE measurements is not advisable, especially in systems with high relative volatility (such as those containing C₄ – C₆ hydrocarbons) due to the experimental error in vapour phase measurements at equilibrium. The authors therefore recommended that only bubble-point measurements from P_{xy} datasets are used in reductions of VLE measurements. This approach retains the benefit that the measured bubble-point curve comprises true liquid compositions, rather than overall cell compositions (*i.e.* true P_x measurements rather than P_z).

3.4 Methodology for the Regression of VLE and Excess Enthalpy

The datasets for each binary mixture in the database were regressed in this work using a consistent methodology. The Barker method was selected for the regression of the datasets, in order to avoid the inconsistencies produced by the smoothing of the data as found when attempting the regression using the Mixon method both in this work and others (Plank *et al.*, 1981). The Barker method is more consistent in its reproduction of γ_i^∞ values (Plank *et al.*, 1981). However, modern activity models with 2 - 3 parameters are not flexible enough to represent the activity coefficient at low concentrations accurately. To avoid this problem, the flexible Legendre activity coefficient model was employed. This model is based on the Legendre polynomial, which can use any number

of coefficients. Although it has no physical basis, unlike modern activity models, its unlimited number of coefficients allow it to represent rapid changes in the slope dP/dx , and hence accurately represent activity coefficient at low concentrations. This is a popular solution to this problem, with researchers at Helsinki University of Technology using this method throughout their work (Uusi-Kyyny *et al.*, 2002). Indeed, many authors have used the Legendre polynomial to calculate activity coefficients at infinite dilution (Fischer and Gmehling, 1994; Islam and Kabadi, 2011; Islam *et al.*, 2011). However, one problem introduced by the unlimited number of coefficients available in the Legendre activity model is that of over-fitting the measurements with excessive coefficients.

Optimising a large number of unknown Legendre coefficients proved computationally challenging in the present work. To resolve this, each regression was initially performed with only 4 Legendre coefficients. These coefficients were then used as initial estimates to regress the system with 5 coefficients. This process was iterated for an increasing number of coefficients. The value of the objective function following each regression was used to prevent over-fitting. Once the objective function no longer decreased by at least 10% upon addition of another Legendre coefficient, the regression was stopped. This was a somewhat crude approach to finding the number of Legendre coefficients necessary without resulting in over-fitting. A more rigorous method using the experimental error was described by Pokki (2004). However, this more rigorous method was impossible to perform on the range of datasets used in this work, since the experimental error was not consistent, or even recorded, in every dataset.

3.4.1 Development of the Legendre Activity Coefficient Model

The Legendre activity model for a binary mixture is given by Uusi-Kyyny *et al.* (2002):

$$g^E = \frac{G^E}{RT} = x_1(1 - x_1) \sum_{k=0}^{k_{max}} A_k L_k \quad (3-13)$$

where:

$$\begin{aligned} L_0 &= 1 \\ L_1 &= (2x_1 - 1) \\ L_k &= \frac{1}{k} [(2k - 1)(2x_1 - 1)L_{k-1} - (k - 1)L_{k-2}] \quad (k > 1) \end{aligned} \quad (3-14)$$

Taking the derivative of the Legendre polynomial with respect to mole fraction x_1 yields:

$$g^{E'} = \left(\frac{\partial g}{\partial x_1} \right)_{P,T} = (1 - 2x_1) \sum_{k=0}^{k_{max}} A_k L_k + x_1(1 - x_1) \sum_{k=0}^{k_{max}} A_k \left(\frac{dL_k}{dx_1} \right) \quad (3-15)$$

Where:

$$\begin{aligned} \frac{dL_0}{dx_1} &= 0 \\ \frac{dL_1}{dx_1} &= 2 \\ \frac{dL_k}{dx_1} &= \frac{1}{k} \left[(2k - 1) \left(2L_{k-1} + \frac{dL_{k-1}}{dx_1} (2x_1 - 1) \right) - (k - 1) \frac{dL_{k-2}}{dx_1} \right] \quad (k > 1) \end{aligned} \quad (3-16)$$

Employing the definition of activity coefficient:

$$RT \ln \gamma_i = \overline{G_i^E} \quad (3-17)$$

Thus, the activity coefficients can be calculated as:

$$\gamma_1 = \exp(g^E + (1 - x_1)g^{E'}) \quad (3-18)$$

$$\gamma_2 = \exp(g^E - x_1g^{E'}) \quad (3-19)$$

Since excess Gibbs energy (\underline{G}^E) is a function of temperature, the Legendre coefficients (A_k) in the model are also functions of temperature. Uusi-Kyyny *et al.* (2002) used the following temperature dependence (where T is in K):

$$A_k = a_{k,0} + T a_{k,1} + T^2 a_{k,2} \quad (3-20)$$

However, this simple polynomial relationship does not model the effect of temperature on excess enthalpy and excess heat capacity effectively, and so a more rigorous model for temperature dependence was developed. Noting the relationship between excess Gibbs free energy and enthalpy, and the definition of excess heat capacity:

$$\left(\frac{\partial g^E}{\partial T} \right)_{P,x} = - \frac{\underline{H}^E}{R T^2} \quad (3-21)$$

$$C_p^E = \left(\frac{\partial H^E}{\partial T} \right)_{P,x} \quad (3-22)$$

Therefore, excess enthalpy and heat capacity in the Legendre activity model are given by:

$$\frac{\underline{H}^E}{R T} = x_1(1 - x_1) \sum_{k=0}^{k_{max}} B_k L_k \quad (3-23)$$

$$\frac{C_p^E}{R} = x_1(1 - x_1) \sum_{k=0}^{k_{max}} C_k L_k \quad (3-24)$$

where B_k and C_k are dimensionless and are given by:

$$B_k = -T \left(\frac{\partial A_k}{\partial T} \right)_{P,x} \quad (3-25)$$

$$C_k = \left(\frac{\partial [TB_k]}{\partial T} \right)_{P,x} = -2T \left(\frac{\partial A_k}{\partial T} \right)_{P,x} - T^2 \left(\frac{\partial^2 A_k}{\partial T^2} \right)_{P,x} \quad (3-26)$$

Using the polynomial relationship for A_k of Uusi-Kyyny *et al.* (2002) yields:

$$B_k = -T(a_{k,1} + 2Ta_{k,2}) = -Ta_{k,1} - 2T^2a_{k,2} \quad (3-27)$$

$$C_k = -2T(a_{k,1} + 2Ta_{k,2}) - T^2(2a_{k,2}) = -2Ta_{k,1} - 6T^2a_{k,2} \quad (3-28)$$

This is a problem, because C_k (and hence C_p^E) is an arbitrary quadratic function of temperature. Alternatively, excess heat capacity could be assumed to be constant with respect to temperature over the temperature range in question, *i.e.* assume that C_k is constant with temperature:

$$C_k(T) = C_k(T_{ref}) = c_k \quad (3-29)$$

Employing this assumption, integration of equation (3-26) between T_{ref} and T gives B_k as:

$$TB_k(T) - T_{ref}B_k(T_{ref}) = C_k(T - T_{ref}) \quad (3-30)$$

$$\therefore B_k(T) = \left(\frac{T_{ref}}{T} \right) b_k + \left(\frac{(T - T_{ref})}{T} \right) c_k \quad (3-31)$$

where $b_k = B_k(T_{ref})$.

Similarly, integration of equation (3-25) between T_{ref} and T gives A_k as:

$$A_k(T) - A_k(T_{ref}) = \int_{T_{ref}}^T -\frac{B_k(T)}{T} dT = \int_{T_{ref}}^T -\left(\frac{T_{ref}}{T^2} \right) b_k - \left(\frac{1}{T} - \frac{T_{ref}}{T^2} \right) c_k dT \quad (3-32)$$

$$\therefore A_k(T) = a_k + \left(\frac{1}{T} - \frac{1}{T_{ref}} \right) T_{ref} b_k - \left[\ln \left(\frac{T}{T_{ref}} \right) + \left(\frac{1}{T} - \frac{1}{T_{ref}} \right) T_{ref} \right] c_k \quad (3-33)$$

Where $a_k = A_k(T_{ref})$.

The choice of T_{ref} is arbitrary, and so has been set to 298.15 K.

3.4.2 Vapour Phase Equation of State

The virial equation of state was assumed for the vapour phase during the regression procedure on the basis that the pressures considered are relatively low. This simple equation of state is commonly used in the literature, and there are many models available to calculate the second virial coefficient. Here, it was calculated using the method of Tsonopoulos (1974). Appendix D details and justifies this choice of method for the calculation of second virial coefficients.

The choice of equation of state can have a significant impact on the regression. The impact of using the Soave-Redlich-Kwong equation of state instead of the virial equation, was investigated. The effect of approximating the vapour phase as ideal was also investigated. These equations of states and the calculation of molar volume of the vapour phase and fugacity coefficients are given in Appendix D.

3.4.3 Physical Properties of Pure Fermentation Products and Hydrocarbon Solvents

Pure component physical properties (liquid density, enthalpy of vaporisation, pure vapor pressures) were obtained from the DIPPR database as functions of temperature (Rowley *et al.*, 2008). Where these were unavailable for a component, the NIST Webbook (NIST, 2016) or Poling *et al.* (2001) were used. The parameters and equations from these sources used for the calculation of pure component properties are given in the Supplementary Material included with this dissertation.

It is imperative that, where possible, experimental values of P_i^{sat} are used during the regression of each dataset, rather than those from a correlation, *e.g.* the Antoine equation. Kuschel *et al.* (1977) demonstrated that the use of P_i^{sat} values obtained from correlations increased the error between calculated and measured pressures significantly compared to using experimental values obtained during the measurement of the bubble-point curve.

3.4.4 Objective Function

Different authors have used various objective functions (*OF*) for regression of VLE and excess enthalpy measurements (Holderbaum *et al.*, 1991; Usui-Kyyny *et al.*, 2002). Common choices are variations on relative error $((P_{exp,k} - P_{calc,k})/P_{exp,k})$ and least-squares (Islam and Rahman, 2012). More complex formulations for the objective function are available if an estimate of the experimental errors in the measurements are known (Islam and Rahman, 2012). This accounts for the error in the experimental

measurements when fitting the activity model and can therefore reduce over-fitting. However, estimates of experimental error were not available for many of the datasets in the database.

When relative error was used as an objective function to regress the measurements the database, large deviations from measurements of excess enthalpy were often identified. Therefore, a normalised least-squares method was employed. This type of objective function penalises large deviations from experimental measurements more heavily. The objective function used in the regression of the datasets was given by:

$$OF = \sum_{k=1}^{N_{VLE}} \left(\frac{P_{exp,k} - P_{calc,k}}{P_{exp,k}} \right)^2 + \sum_{l=1}^{N_{HE}} \left(\frac{H_{exp,l}^E - H_{calc,l}^E}{H_{exp,l}^E} \right)^2 \quad (x_1 \neq 0, 1) \quad (3-34)$$

Datasets and individual datapoints are not weighted in this objective function, and so every datapoint in each dataset is weighted equally. Weighting different datasets has been used by some authors (Islam and Kabadi, 2011; Islam *et al.*, 2011), however it is often highly subjective and would have been impractical due to the number of datasets. Weighting the objective function in order to prioritise datapoints measured at dilute concentrations was trialled, but this was found to be unnecessary when employing the flexible Legendre polynomial.

3.4.5 Regression Procedure

The regression was programmed and performed in MathWorks® MATLAB. The optimisation function *fminsearch* was employed to optimise a set of temperature-dependent Legendre coefficients for each binary. Figure 3-1 summarises the entire procedure employed for the regression of the datasets, based on the Barker method. First, the VLE datasets in the database were conditioned, by removing any temperature variations recorded in the datasets using the Clausius-Claperyon equation. Pure vapour pressures from DIPPR correlations were also added to complete any VLE datasets which did not include measurements of vapour pressure for pure components. Combined with any datasets of excess enthalpy measurements in the database, the conditioned VLE datasets formed a database of isothermal datasets of VLE and excess enthalpy measurements for each binary.

The Legendre activity model, initially with 4 coefficients ($k_{max} = 3$), was then employed to regress the database of VLE and excess enthalpy measurements for each binary. During each iteration of the optimisation process, vapour compositions and pressures

were calculated for each VLE dataset, and the liquid compositions at equilibrium were corrected for PzV datasets. This necessitated an iteration loop within the iterative optimisation process. Once optimal Legendre activity coefficients were found using the objective function (OF), another set of Legendre activity coefficients were added and the entire regression process repeated. This was repeated until the objective function did not

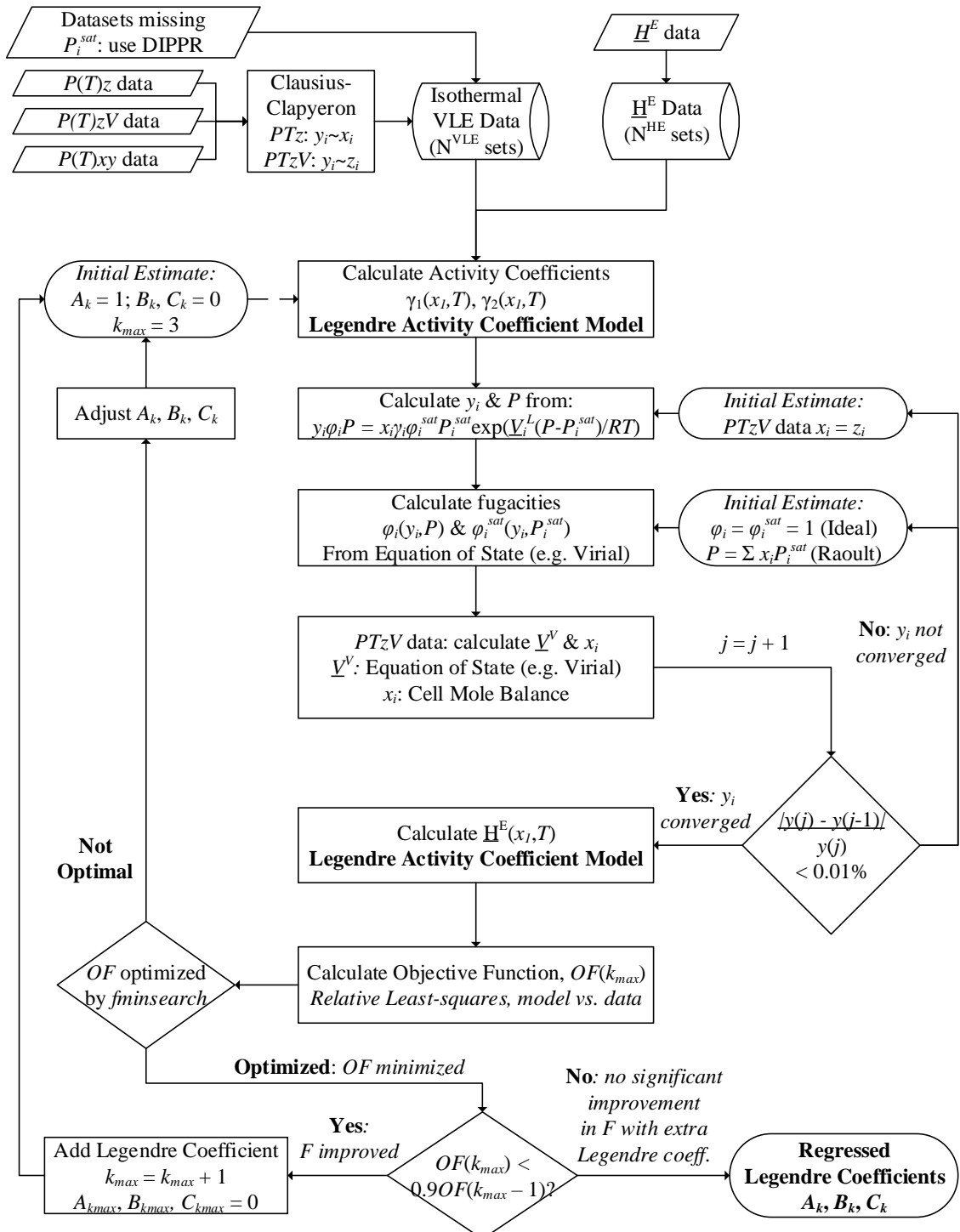


Figure 3-1: Regression procedure for the calculation of Legendre model coefficients from datasets containing VLE and excess enthalpy measurements of binary mixtures of volatile hydrocarbons and fermentation products

decrease by more than 10% when an additional set of Legendre activity coefficients was employed for the regression.

3.5 Activity Model Regression Results

The datasets in the database were regressed using the Barker method. This determined a set of temperature-dependent Legendre activity coefficients for each binary mixture of *n*-butanol, acetone and ethanol with six hydrocarbon solvents: *n*-hexane, 1-hexene, *n*-pentane, *n*-butane, *iso*-butane and 1-butene. In addition, a set of Legendre activity coefficients were determined for the binary of *iso*-butanol and *n*-hexane. The regressions were conducted by modelling the vapour phase with the virial equation of state. The temperature dependent Legendre coefficients resulting from these regressions are given in the Supplementary Material. These regressions were repeated using the SRK equation of state, and assuming the vapour phase was ideal. For the sake of clarity, the Legendre activity models produced by each of these regressions have been termed here the ‘Leg-virial’, the ‘Leg-SRK’, and the ‘Leg-IGL’ (Ideal Gas Law) models respectively.

3.5.1 Model Predictions of Activity Coefficients

Figure 3-2 shows the activity coefficients predicted by the Leg-virial Models of *n*-butanol in each of the six hydrocarbon solvents investigated. Activity coefficients are plotted for a range of temperatures between 25°C and 100°C, including at 37°C (a typical fermentation temperature). Figures 3-3 and 3-4 show the equivalent predictions for acetone and ethanol respectively. In each of these three figures, activity coefficients are shown for low concentrations (< 20 mol%) of the fermentation product. Activity coefficient decreases with composition. As can be seen in Figure 3-2 to Figure 3-4, the activity coefficients of the fermentation products in each of the binaries decreases rapidly between infinite dilution and 10 mol%, especially at lower temperatures, and for binaries with alcohols.

Activity coefficients were predicted to decrease with increasing temperature. This trend can be seen across all fermentation products and all solvents in Figure 3-2, Figure 3-3 and Figure 3-4. The effect of temperature on the predicted activity coefficients is largest at infinite dilution and decreases with composition. At infinite dilution, the activity coefficient of the fermentation product increases by a factor of 2 – 4 between 25°C and 100°C. As shown in Figures 3-2 and 3-4, at an alcohol composition of 20 mol%, the effect of temperature on the predicted activity coefficients of the alcohols is negligible for the binaries of with the six hydrocarbons.

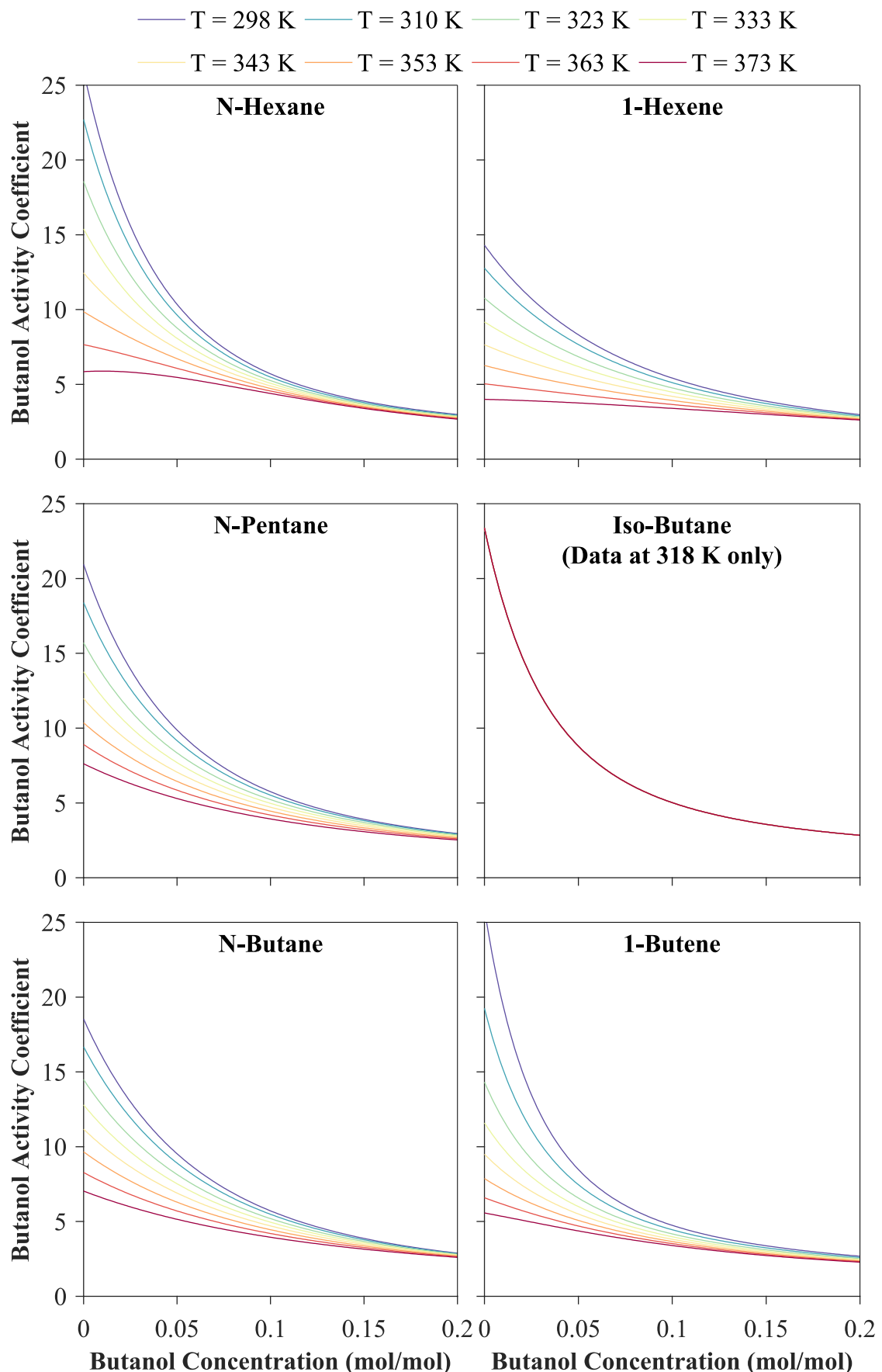


Figure 3-2: Activity coefficients of *n*-butanol at low concentration in six hydrocarbons at 298 – 373 K, predicted by the Leg-virial models

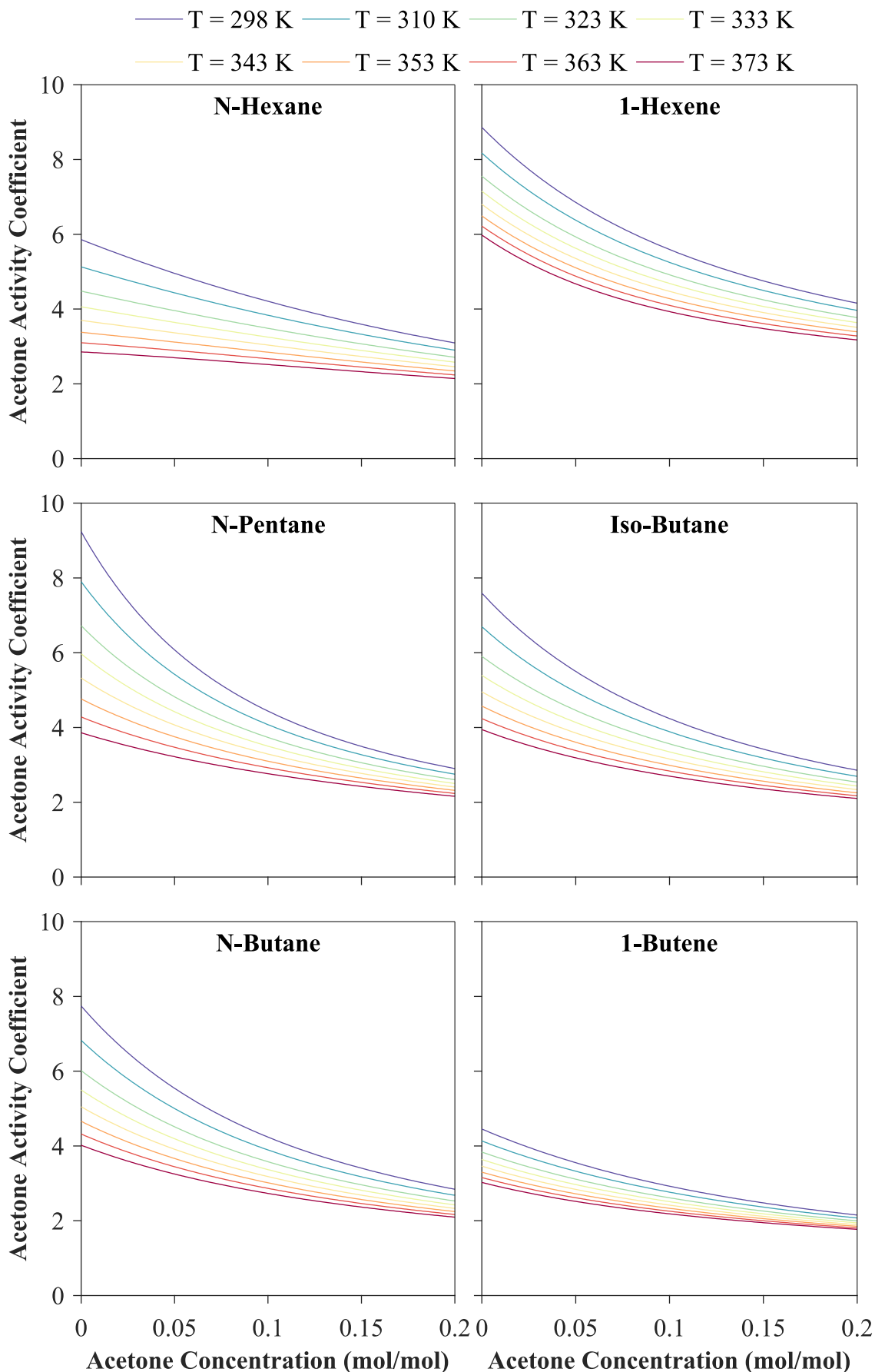


Figure 3-3: Activity coefficients of acetone at low concentration in six hydrocarbons at 298 – 373 K, predicted by the Leg-virial models

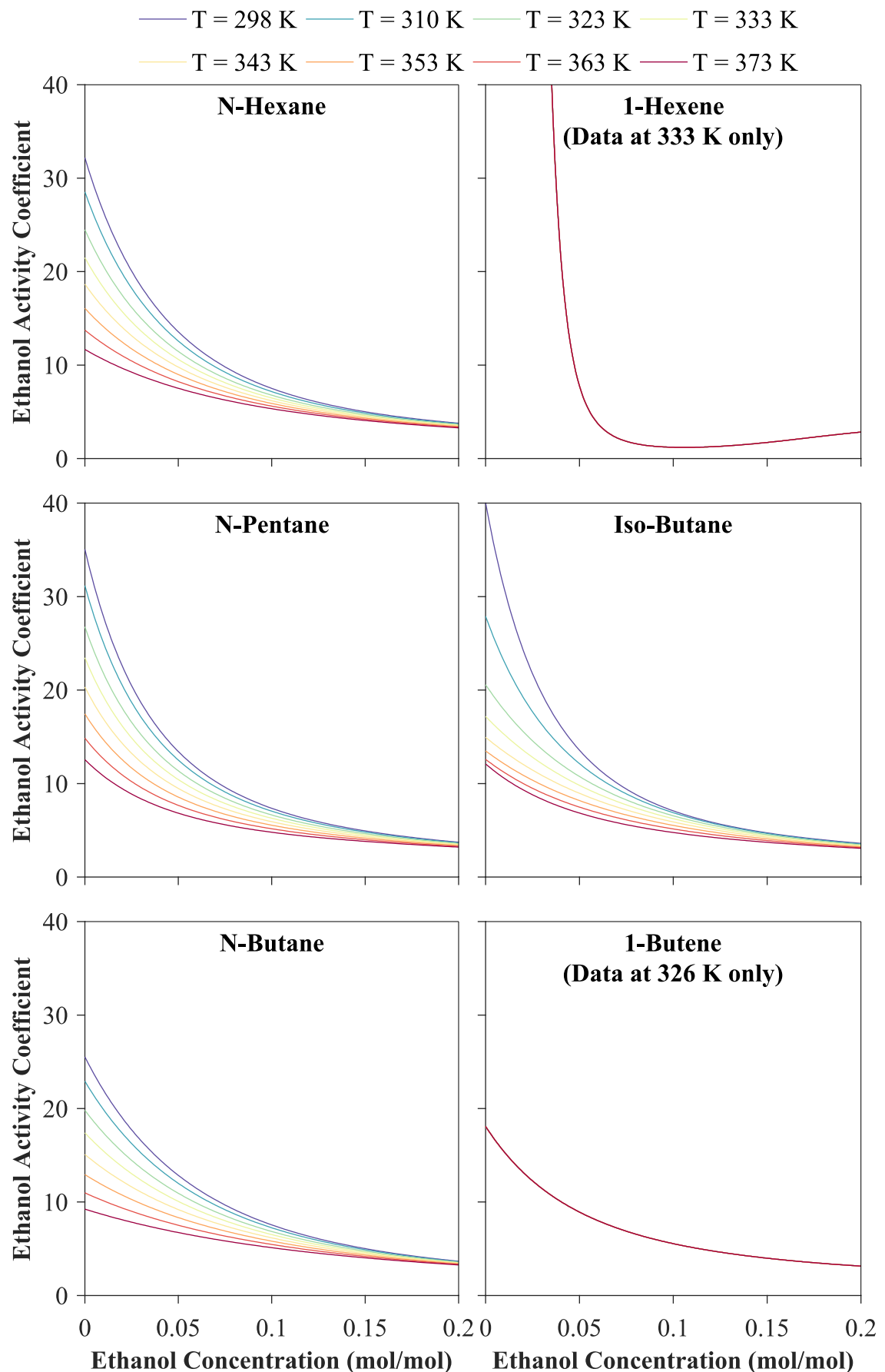


Figure 3-4: Activity coefficients of ethanol at low concentration in six hydrocarbons at 298 – 373 K, predicted by the Leg-virial Models

For acetone at 20 mol% (Figure 3-3), the predicted activity coefficients of acetone increase with temperature, although the effect is smaller than at infinite dilution.

Figure 3-5 shows the activity coefficients predicted by the Leg-SRK Models for ethanol in the six hydrocarbon solvents. This can be compared with Figure 3-4 in order to observe the impact of the equation of state that was employed in the regression of the binary datasets on the prediction of ethanol activity coefficients. As shown in Figure 3-5, the impact was minimal for some solvents. However, for pentane and *iso*-butane, the Leg-SRK Models predict a minimum in the activity coefficient of ethanol at infinite dilution at a temperature below 100°C. This is in contrast to the predictions of the Leg-virial Models, for which activity coefficients decreased with temperature up to at least 100°C. The Leg-SRK Models of 1-hexene and ethanol yields plausible activity coefficients for this binary. Conversely, the regression of the single VLE dataset available for this binary using the virial equation of state was unsuccessful. Thus, the Leg-virial Models predicted unphysical activity coefficients at dilute concentrations for this binary (Figure 3-4). The minimum ethanol concentration in this sole VLE dataset was 14 mol%, meaning that measurements at low concentrations were not available.

For *iso*-butanol, binary VLE datasets were only available with hexane. Figure 3-6 shows activity coefficients for *iso*-butanol with hexane predicted using the Leg-virial Models; the Leg-SRK Models; and Leg-IGL Models. The figure compares these with the equivalent predictions for *n*-butanol. As shown in Figure 3-6, the predicted behaviour of the activity coefficient of *iso*-butanol in hexane is very similar to that of *n*-butanol. However, the activity coefficients of *iso*-butanol are slightly lower than those of *n*-butanol, particularly at lower temperatures. For these binaries, the impact of employing different equations of state in the regressions was minimal. However, Leg-IGL Models consistently predicted slightly lower activity coefficients than those predicted by the Leg-virial Models or the Leg-SRK Models.

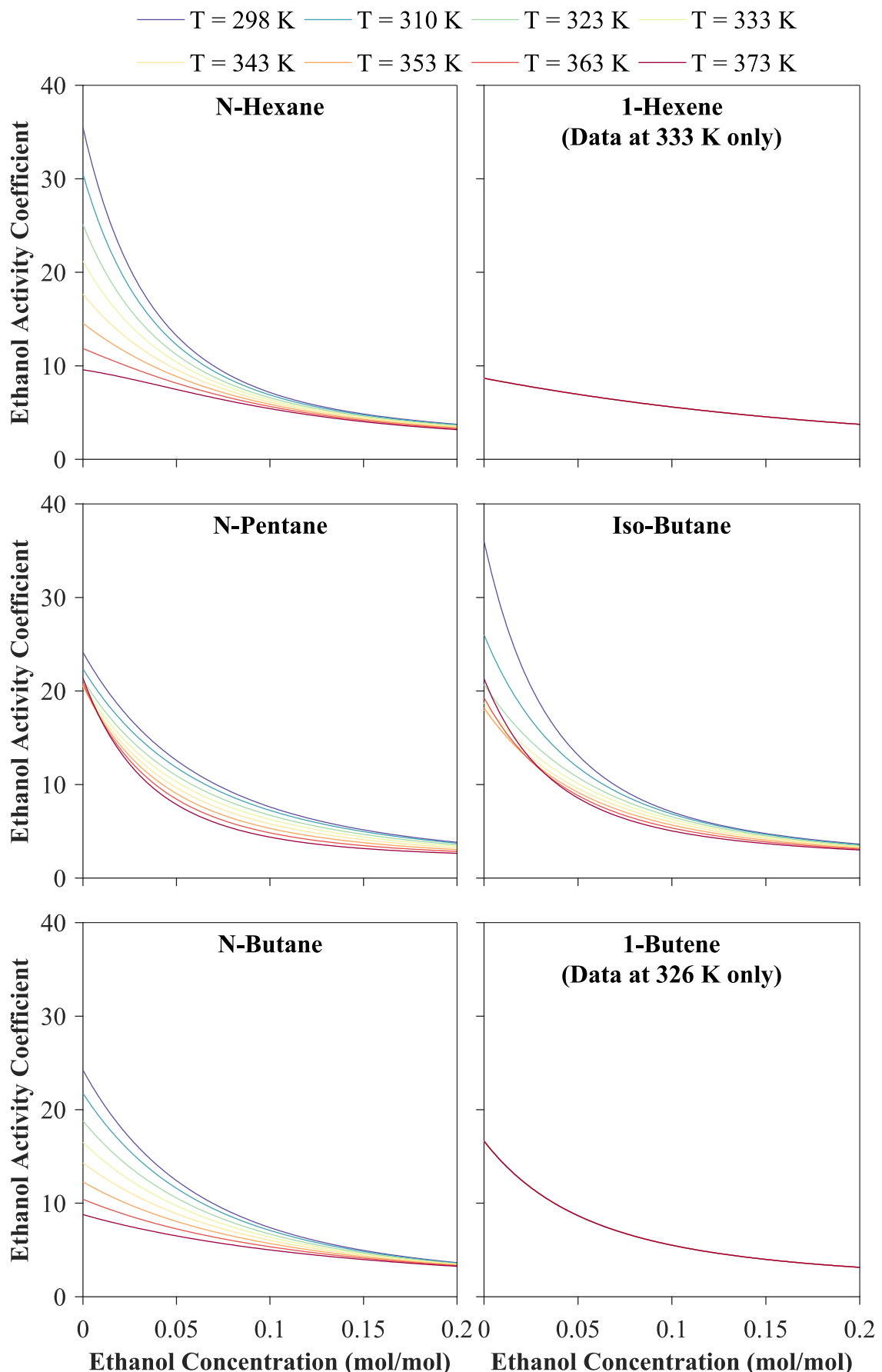


Figure 3-5: Activity coefficients of ethanol at low concentration in six hydrocarbons at 298 – 373 K, predicted by the Leg-SRK Models

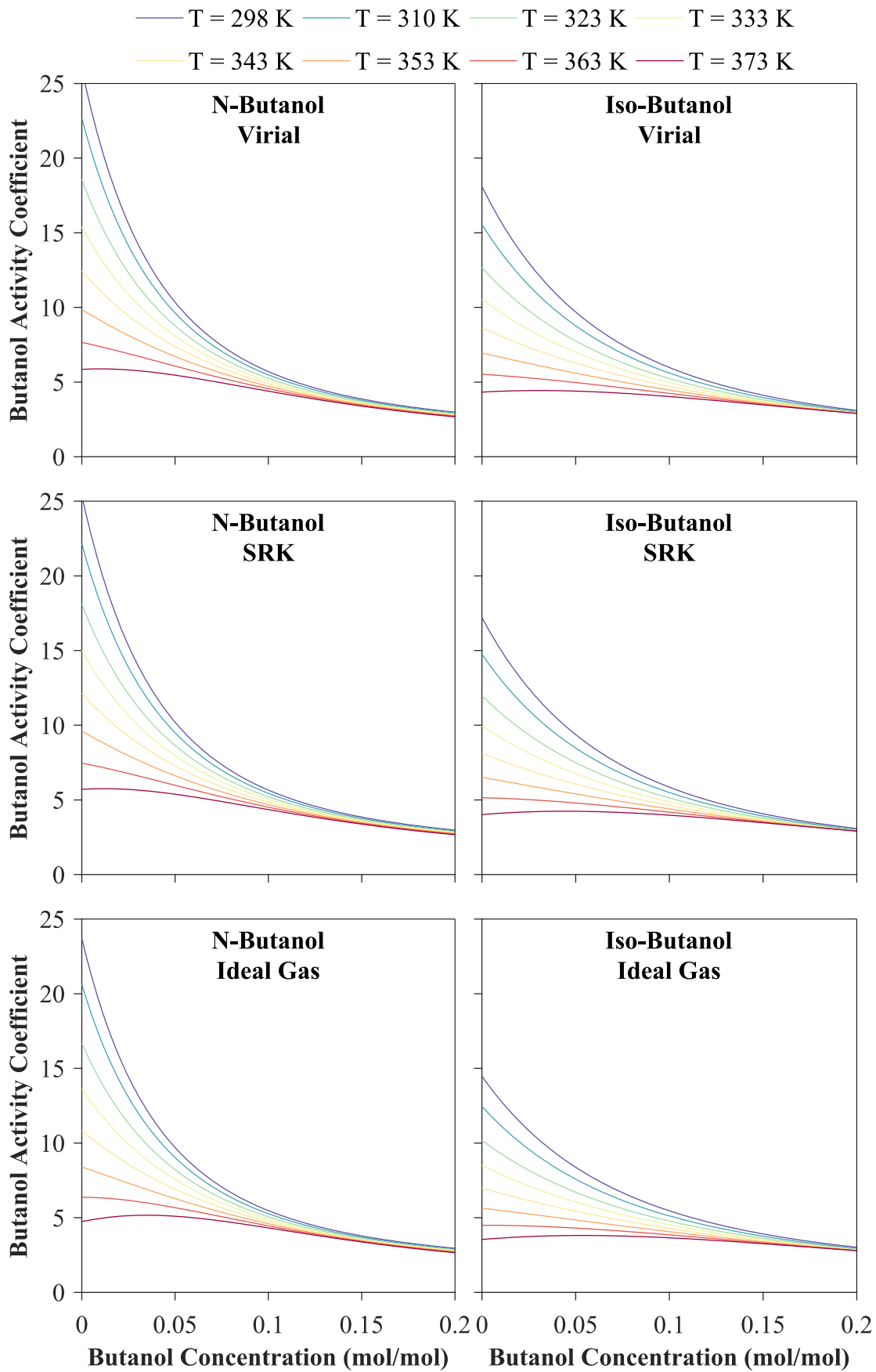


Figure 3-6: Activity coefficients of *n*- and *iso*- butanol at low concentration in *n*-hexane at 298 – 373 K, predicted by the Leg-Virial Models, the Leg-SRK Models and the Leg-IGL Models

3.5.2 Deviation of Model Predictions from Literature Datasets

The fit of the three models to the experimental measurements, from which the models were regressed, has been summarised by Figures 3-7, 3-8 and 3-9. Figure 3-7 details the average relative deviation of the model predictions from each binary dataset containing measurements of bubble-point pressures or excess enthalpy. The figure compares the deviations of each of the three models in box and whisker plots, separating datasets by hydrocarbon solvent.

The average relative deviation of the model predictions from each dataset was defined as:

$$\frac{100\%}{N_{VLE}} \sum_{k=1}^{N_{VLE}} \left| \frac{P_{calc,k} - P_{exp,k}}{P_{exp,k}} \right| \text{ or } \frac{100\%}{N_{HE}} \sum_{k=1}^{N_{HE}} \left| \frac{H_{calc,k}^E - H_{exp,k}^E}{H_{exp,k}^E} \right| (x_k \neq 0) \quad (3-35)$$

Where P_{calc} and H_{calc}^E are the bubble-point pressure or excess enthalpy predicted by the models respectively, and P_{exp} and H_{exp}^E are the bubble-point pressure or excess enthalpy measurements contained in the dataset respectively. The number of datapoints (k) in the VLE or excess enthalpy dataset are denoted N_{VLE} or N_{HE} respectively. It should be noted that this deviation function is not the same as the objective function used in the regression procedure (which was based on a least-squares approach).

As shown in Figure 3-7, the deviations of model predictions were generally lowest for the Leg-virial Models, although predictions by the Leg-SRK Models yielded similar deviations from the datasets. The deviations of predictions by all three models for binaries containing 1-butene was very low.

Figure 3-8 shows the relative average deviations of the predictions made by the Leg-virial Models from each dataset, separated by binary mixture. The deviations were smallest for binaries containing acetone, followed, for most solvents, by those containing butanol. This trend corresponded to the number of datasets available for each binary, with larger numbers of datasets for a binary corresponding to larger deviations.

The deviation of model predictions from the datasets are analysed further in Figure 3-9. Rather than considering the average deviation of predictions for each dataset, Figure 3-9 instead details the relative deviation of predictions using the Leg-virial Models from each individual datapoint within each dataset, *i.e.*:

$$\frac{P_{calc} - P_{exp}}{P_{exp}} \text{ or } \frac{H_{calc}^E - H_{exp}^E}{H_{exp}^E} (x \neq 0) \quad (3-36)$$

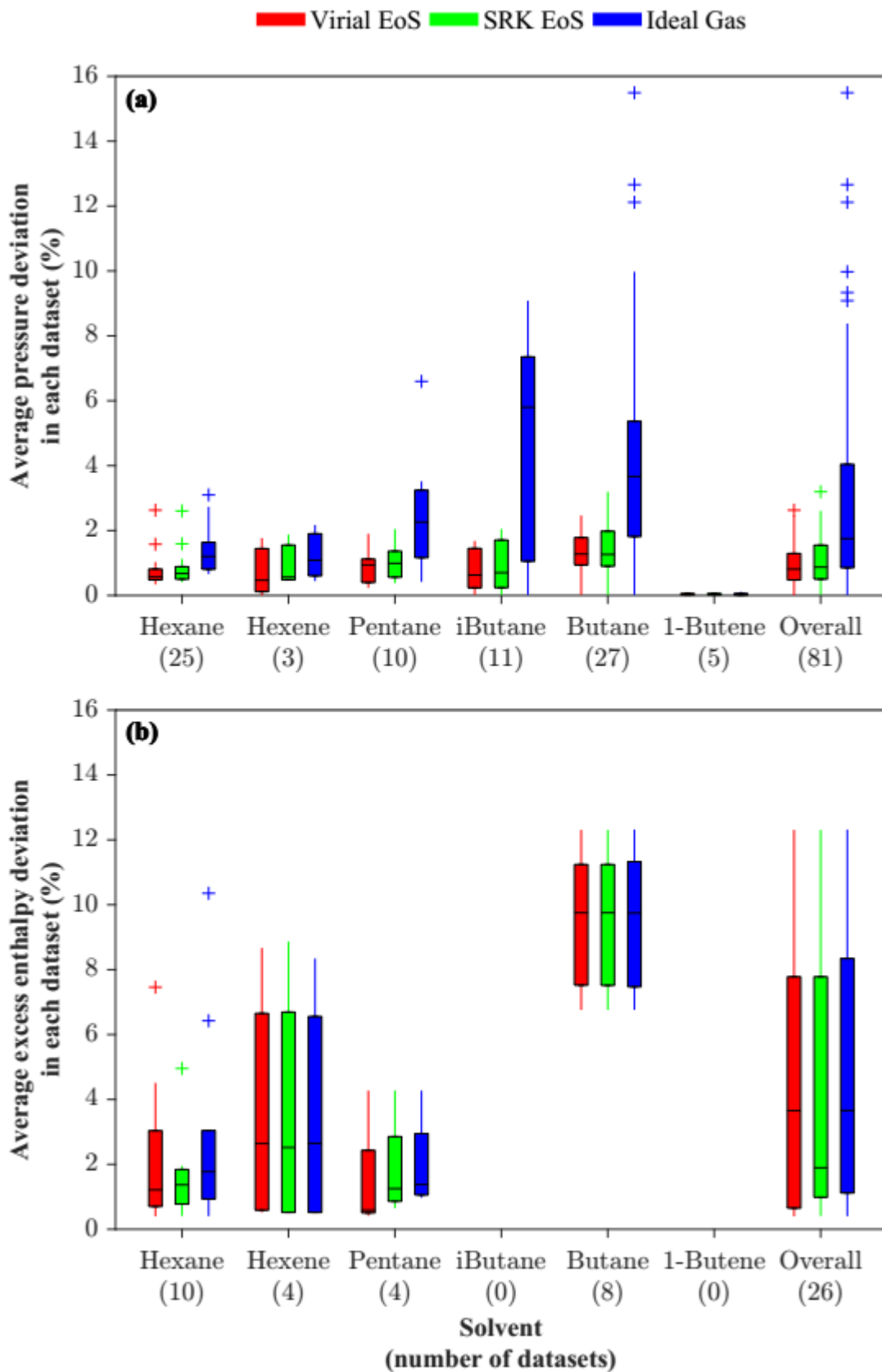


Figure 3-7a-b: Box and whisker plots of average relative deviation from: (a) bubble-point pressure (VLE datasets); and (b) excess enthalpy datasets of predictions made using the Leg-virial Models; the Leg-SRK Models; and the Leg-IGL Models. Whisker limit: 1.5x interquartile range.

■ Acetone ■ n-Butanol ■ Ethanol

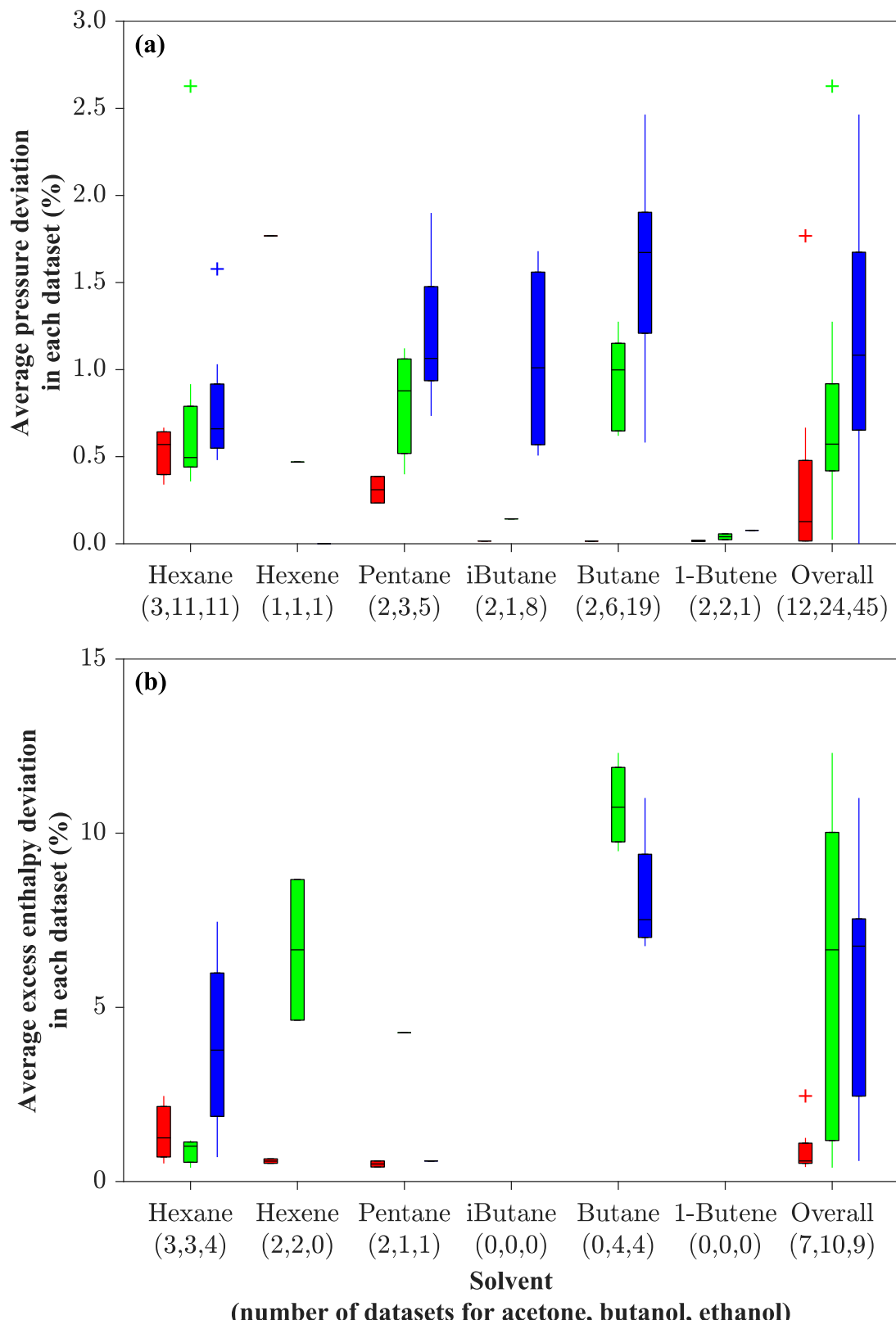


Figure 3-8a-b: Box and whisker plots of average relative deviation from (a) bubble-point pressure (VLE datasets); and (b) excess enthalpy datasets of predictions made using the Leg-virial Models, broken down by fermentation product. Whisker limit: 1.5x interquartile range.

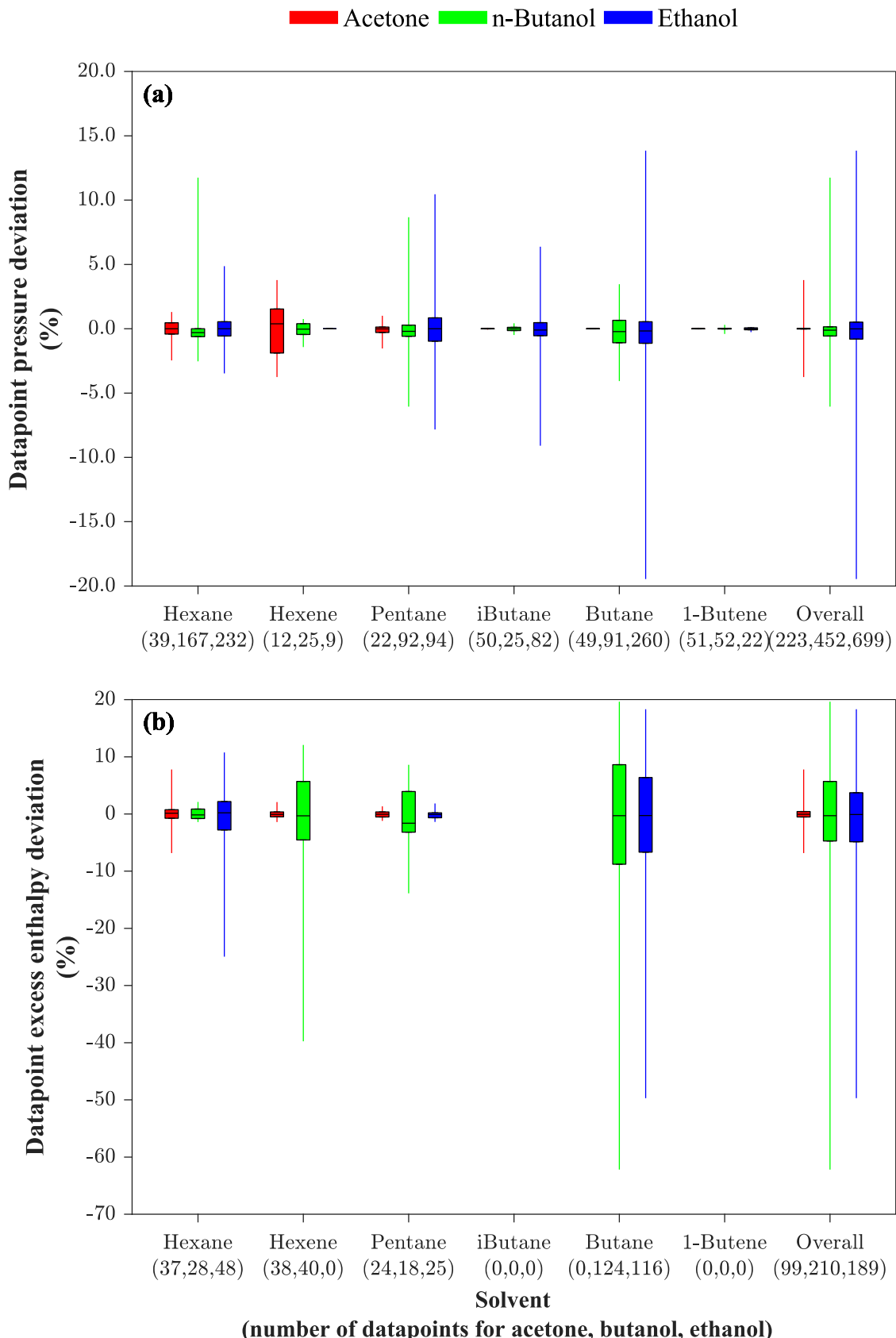


Figure 3-9a-b: Box and whisker plots of relative deviation of predictions calculated by the Leg-virial Models from (a) individual measurements of bubble-point pressure; and (b) individual measurements of excess enthalpy, broken down by fermentation product. Whisker limit: full range of datapoints.

As shown in Figure 3-9a, deviations of the Leg-virial Model predictions from measurements of VLE and excess enthalpy were relatively symmetrical (*i.e.* equal magnitudes of positive and negative deviations), with deviation in predicted datapoints of ranging from -20 – +15 %. This suggests that deviation is largely due to scatter of experimental data. The majority of model predictions of VLE datapoints fall within the range of experimental error, with the quartiles of the relative deviation being smaller than $\pm 2 - 3 \%$ for every mixture.

The relative deviation of predictions for all 125 VLE bubble-point pressures of binaries containing 1-butene were very low ($<< 1\%$). The largest deviations were for predictions of VLE for mixtures of ethanol and *n*-butane, where deviations of up to 20% were predicted for individual measurements. However, this binary also contained the largest number of VLE measurements (260).

Relative deviations of predicted excess enthalpies were larger than those of bubble-point pressures. The deviations of predictions of excess enthalpy from experimental measurements (Figure 3-9a) were also relatively uniform around zero, with the quartiles being less than $\pm 10\%$ for every mixture. However, there were several outliers for which model predictions of excess enthalpy were significantly lower than experimental datapoints (up to ~60% lower). The existence of these outliers with large deviations was not surprising since excess enthalpies with absolute values close to zero show large relative deviations for a small absolute error.

3.5.3 Model Predictions of Vapour-Liquid Equilibria and Excess Enthalpy

Figure 3-10 compares the VLE and excess enthalpy predictions made by the Leg-virial Models to the experimental measurements contained in the datasets for *n*-butanol and *n*-hexane. As can be seen in Figure 3-10, the Leg-virial Model accurately represented the bubble and dew-point curves and excess enthalpy measurements for a large number of datasets across a wide range of temperatures. At higher temperatures, butanol was predicted to form a minimum boiling point azeotrope with hexane at a dilute butanol composition.

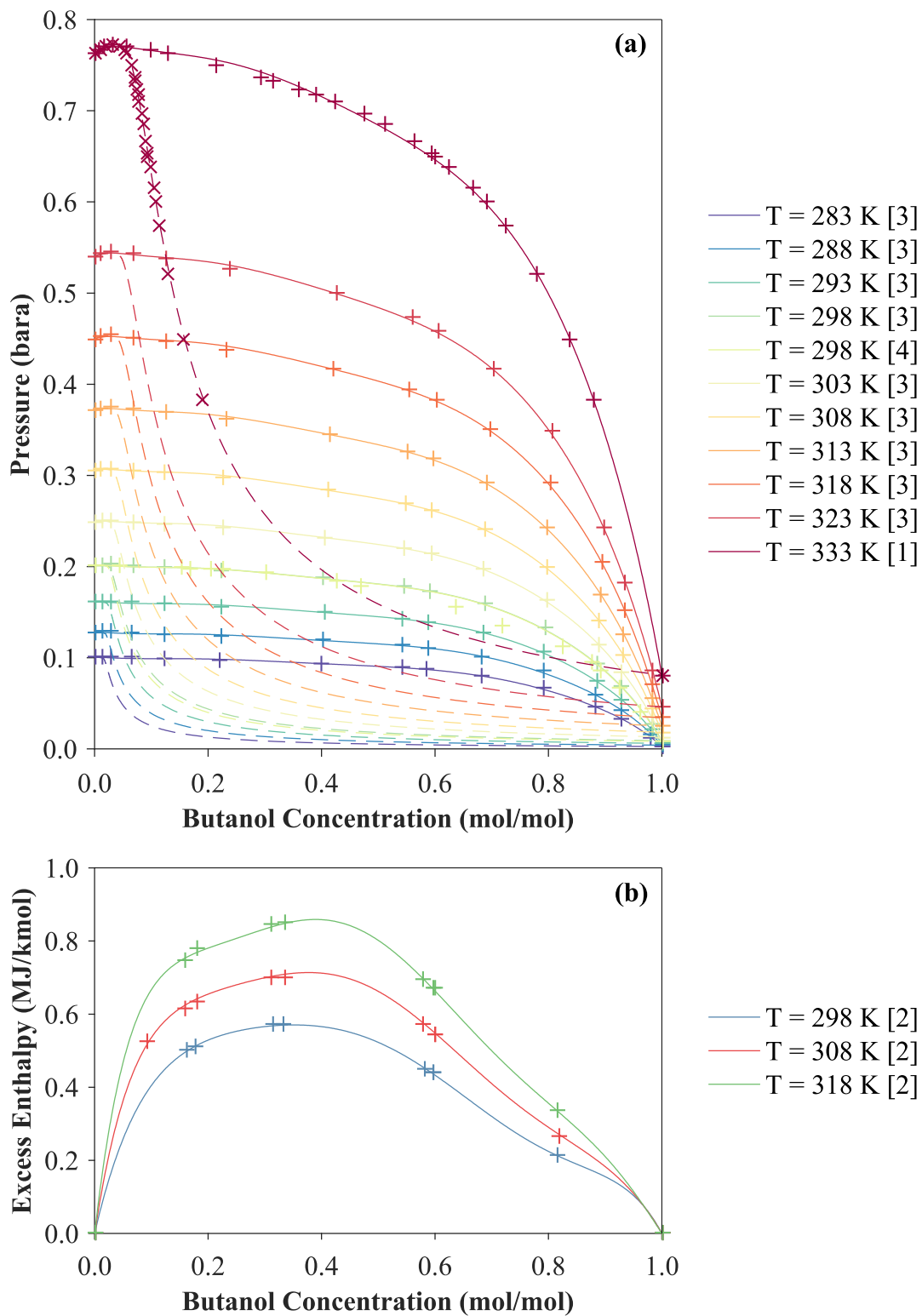


Figure 3-10a-b: Leg-virial Model predictions and measurements from dataset [ref#] for (a) vapor-liquid equilibrium; (b) excess enthalpy of *n*-hexane and *n*-butanol

Model Lines: Solid line (-) = P - x or H_E; Dashed Line (--) = P - y

Dataset measurements: + = P - x or H_E^E; x = P - y; o = P - z

[1] = Berro *et al.* (1982); [2] = Brown *et al.* (1964); [3] = Gracia *et al.* (1992)

[4] = Rodriguez *et al.* (1993)

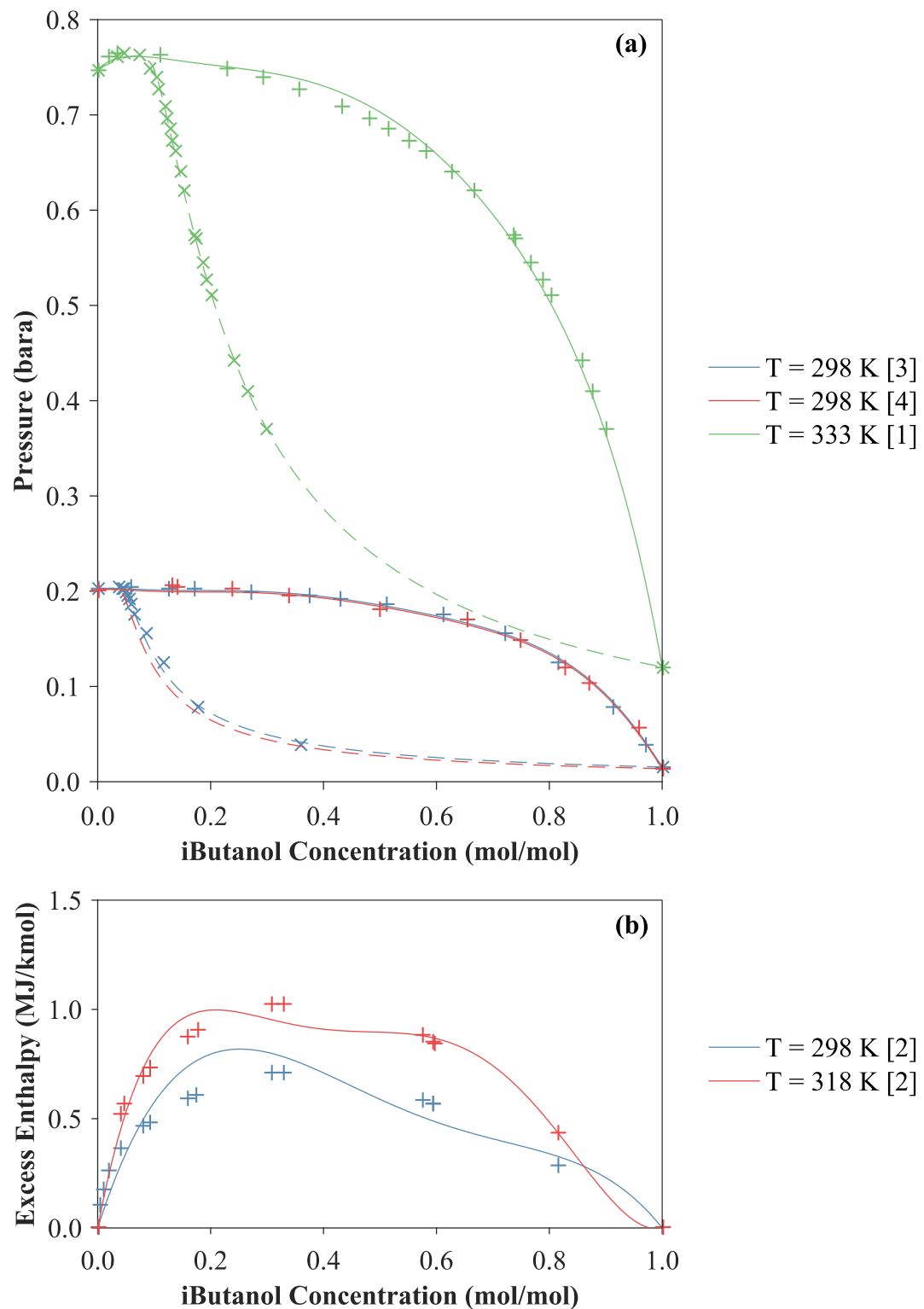


Figure 3-11a-b: Leg-virial Model predictions and measurements from dataset [ref#] for (a) vapor-liquid equilibrium; (b) excess enthalpy of *n*-hexane and *iso*-butanol

Model Lines: Solid line (–) = $P - x$ or H_E ; Dashed Line (--) = $P - y$

Dataset measurements: + = $P - x$ or H_E^E ; \times = $P - y$; \circ = $P - z$

[1] = Berro *et al.* (1982); [2] = Brown *et al.* (1964); [3] = Guerrero *et al.* (2010)

[4] = Rodriguez *et al.* (1993)

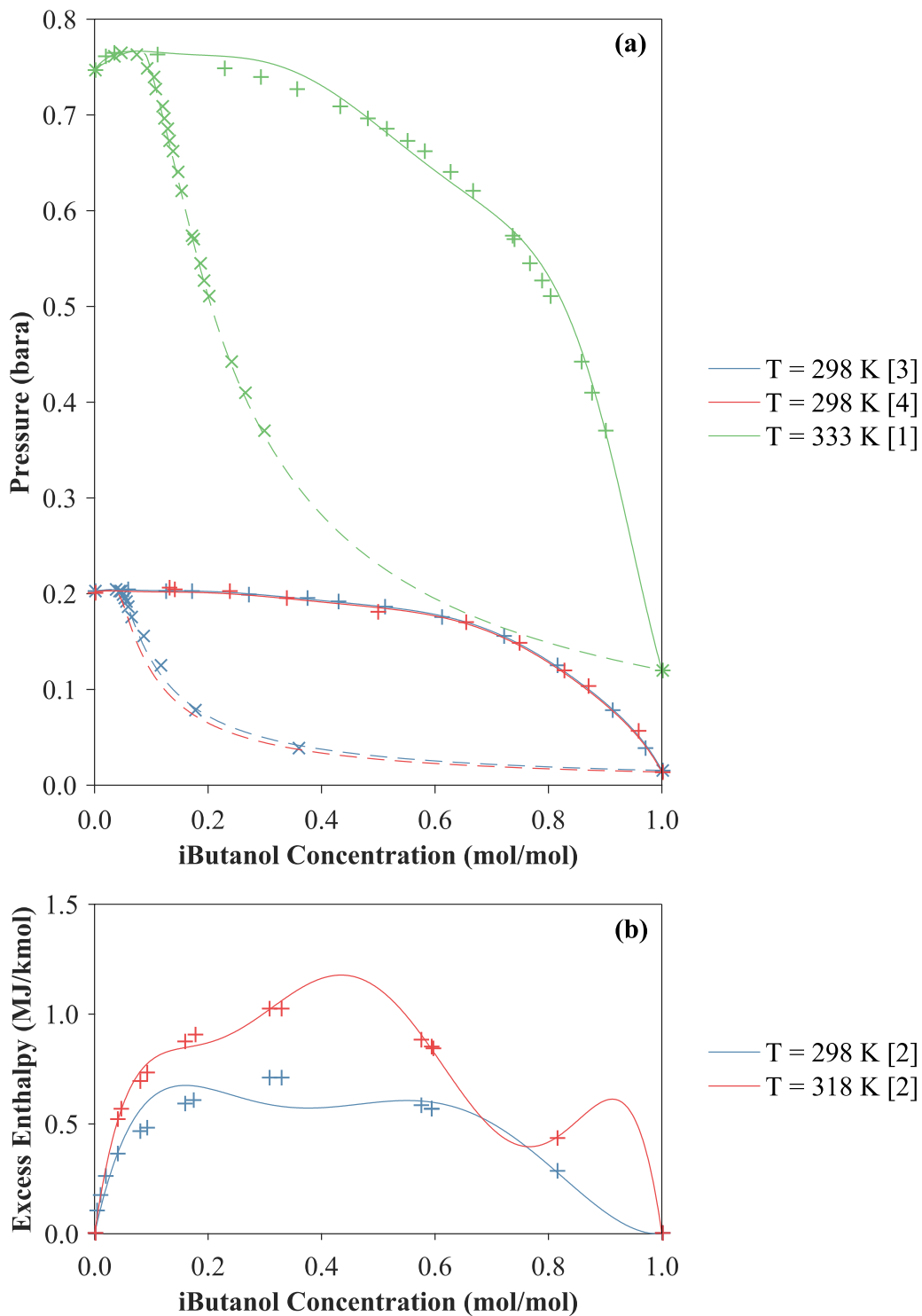


Figure 3-12a-b: Leg-virial Model predictions and measurements from dataset [ref#] for (a) vapor-liquid equilibrium; (b) excess enthalpy of *n*-hexane and *iso*-butanol with an additional Legendre coefficient employed during regression (over-fitted)

Model Lines: Solid line (—) = P – x or H_E; Dashed Line (--) = P – y

Dataset measurements: + = P – x or H_E; × = P – y; ○ = P – z

[1] = Berro *et al.* (1982); [2] = Brown *et al.* (1964); [3] = Guerrero *et al.* (2010)

[4] = Rodriguez *et al.* (1993)

Figure 3-11 shows the equivalent predictions for *iso*-butanol with *n*-hexane. A similar azeotrope to that of *n*-butanol with *n*-hexane was predicted. The model accurately represents the measurements of the VLE datasets, but the predictions of the excess enthalpy measurements were less accurate than those for *n*-butanol.

This inaccuracy was exacerbated in Figure 3-12. Like Figure 3-11, this figure details model predictions of VLE and excess enthalpy compared with the experimental measurements contained in the datasets for *iso*-butanol and *n*-hexane. However, in Figure 3-12 a Leg-virial Model was regressed using one additional set of Legendre coefficients (*i.e.* one further than the algorithm would have stopped at). Hence, this figure demonstrates the problems that can arise from overfitting measurements in regressions using the Legendre activity model. The deviations of the model predictions detailed in Figure 3-12 from the measurements of excess enthalpy are slightly smaller than those in Figure 3-11. However, the stationary points predicted by the overfitted model between measurements are unlikely to be accurate, leading to spurious predictions.

Figures 3-13, 3-14 and 3-15 compare predictions of VLE and excess enthalpy calculated by Leg-virial Models with datasets containing measurements for *n*-butanol with 1-hexene, *n*-pentane, and *n*-butane respectively. The measurements of VLE for each solvent were accurately predicted by the Leg-virial Models. As shown in Figures 3-13, 3-14 and 3-15, predictions of the excess enthalpy were slightly less accurate. However, the model correctly predicted the shape and magnitude of the excess enthalpy curve. The excess enthalpy of mixing was found to be positive for all hydrocarbon-fermentation product binaries.

Figure 3-16 shows the comparison between the VLE predicted by the Leg-virial Models and the measurements contained in datasets for *n*-butanol with *iso*-butane and 1-butene. No excess enthalpy measurements were available for these binaries. All VLE datasets for these binaries were of the *PTzV* type. This resulted in highly accurate fits of the model to the experimental measurements. The experimental measurements plotted are at overall cell compositions (*z*), and so if accurately predicted, should lie between the model dew and bubble-point curves, close to the bubble-point curve.

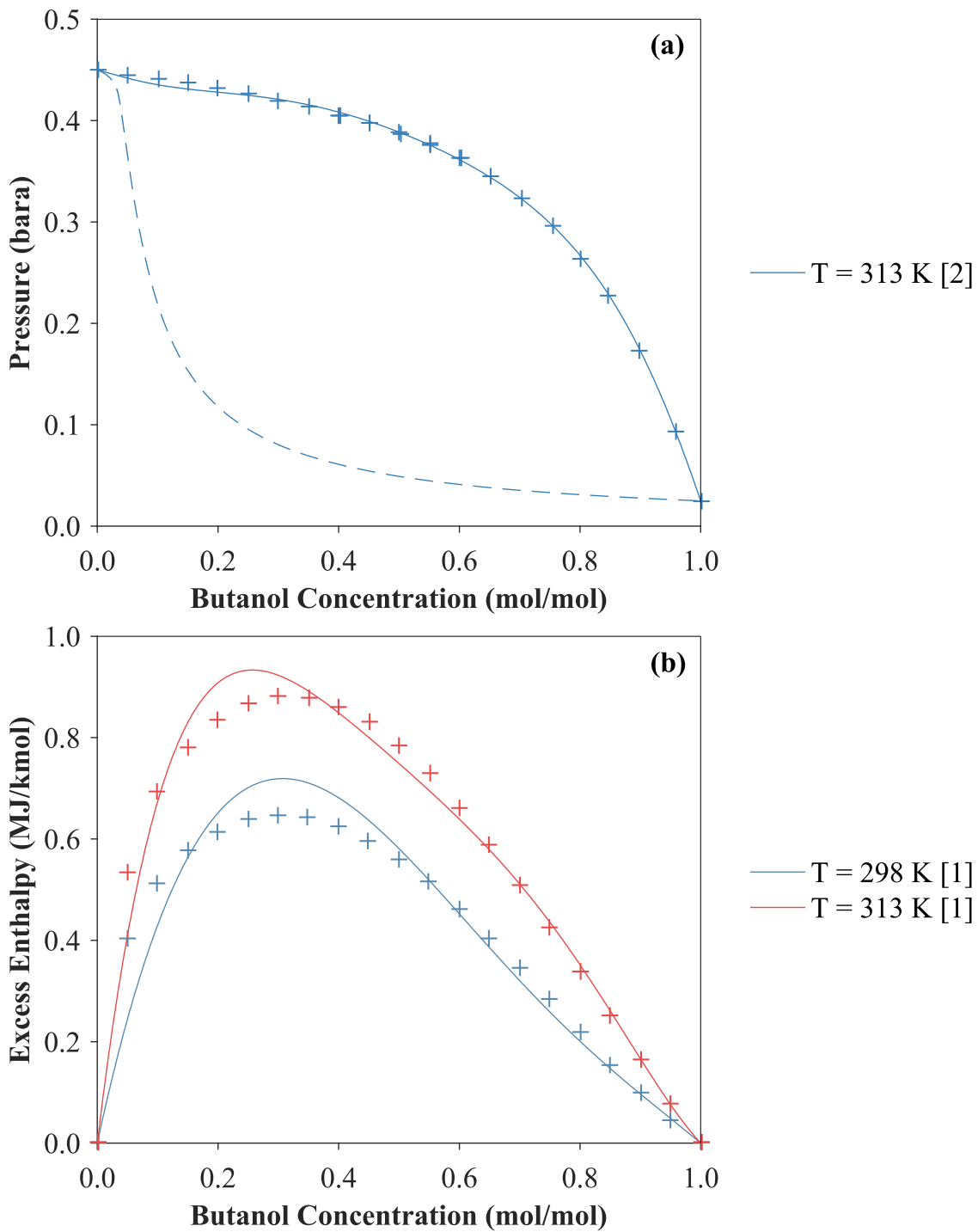


Figure 3-13a-b: Leg-virial Model predictions and measurements from dataset [ref#] for (a) vapor-liquid equilibrium; (b) excess enthalpy of 1-hexene and *n*-butanol

Model Lines: Solid line (–) = $P - x$ or H_E ; Dashed Line (--) = $P - y$

Dataset measurements: + = $P - x$ or H_E^E ; \times = $P - y$; \circ = $P - z$

[1] = Aguilar *et al.* (2012); [2] = Ghellai *et al.* (2013)

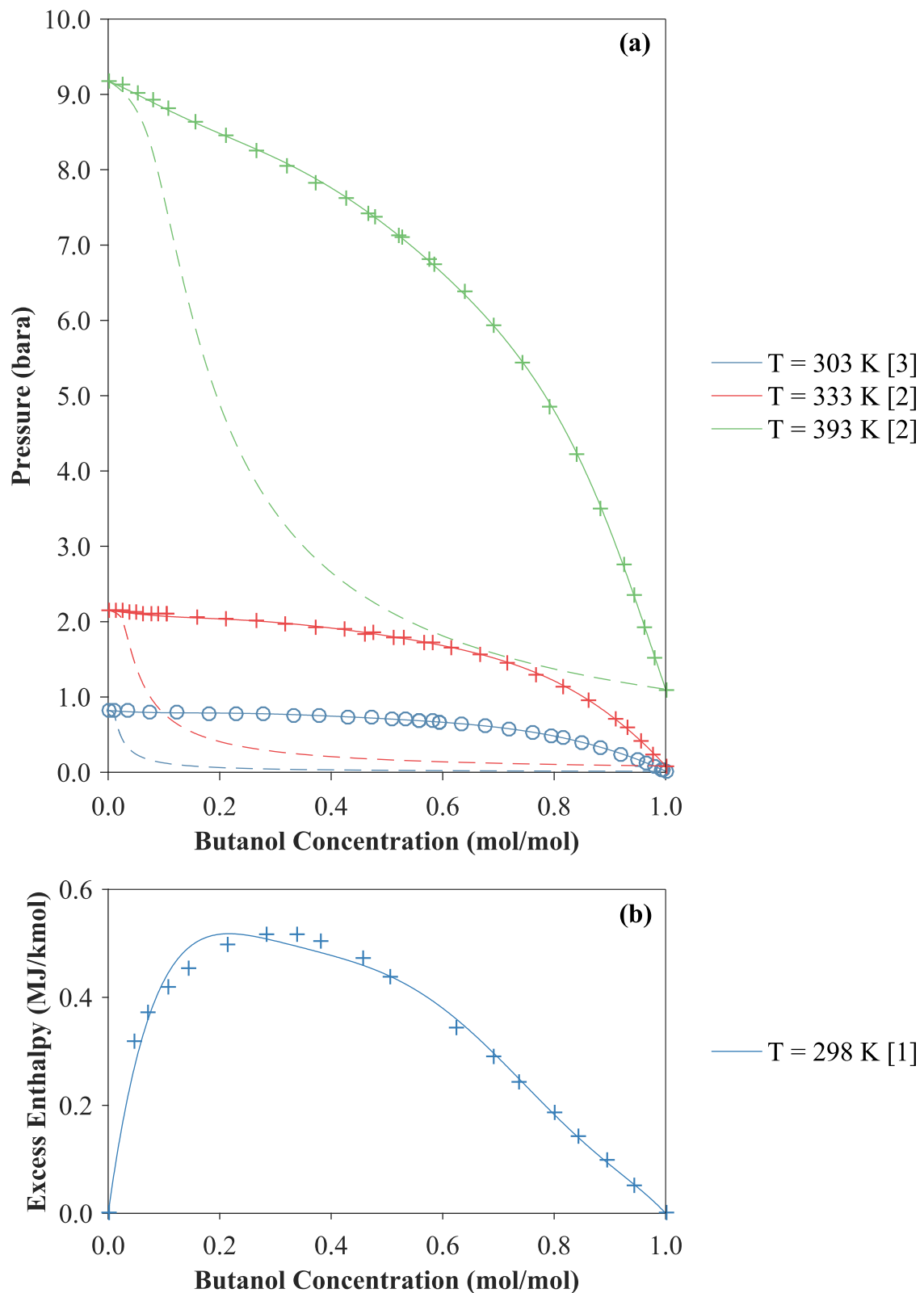


Figure 3-14a-b: Leg-virial Model prediction (lines) and measurements from [ref #] for (a) vapor-liquid equilibrium; (b) excess enthalpy of *n*-pentane and *n*-butanol

Model Lines: Solid line (—) = P - x or H_E; Dashed Line (--) = P - y

Dataset measurements: + = P - x or H_E; × = P - y; ○ = P - z

[1] = Collins *et al.* (1980); [2] = McDougal *et al.* (2014); [3] = Ronc and Ratcliff (1976)

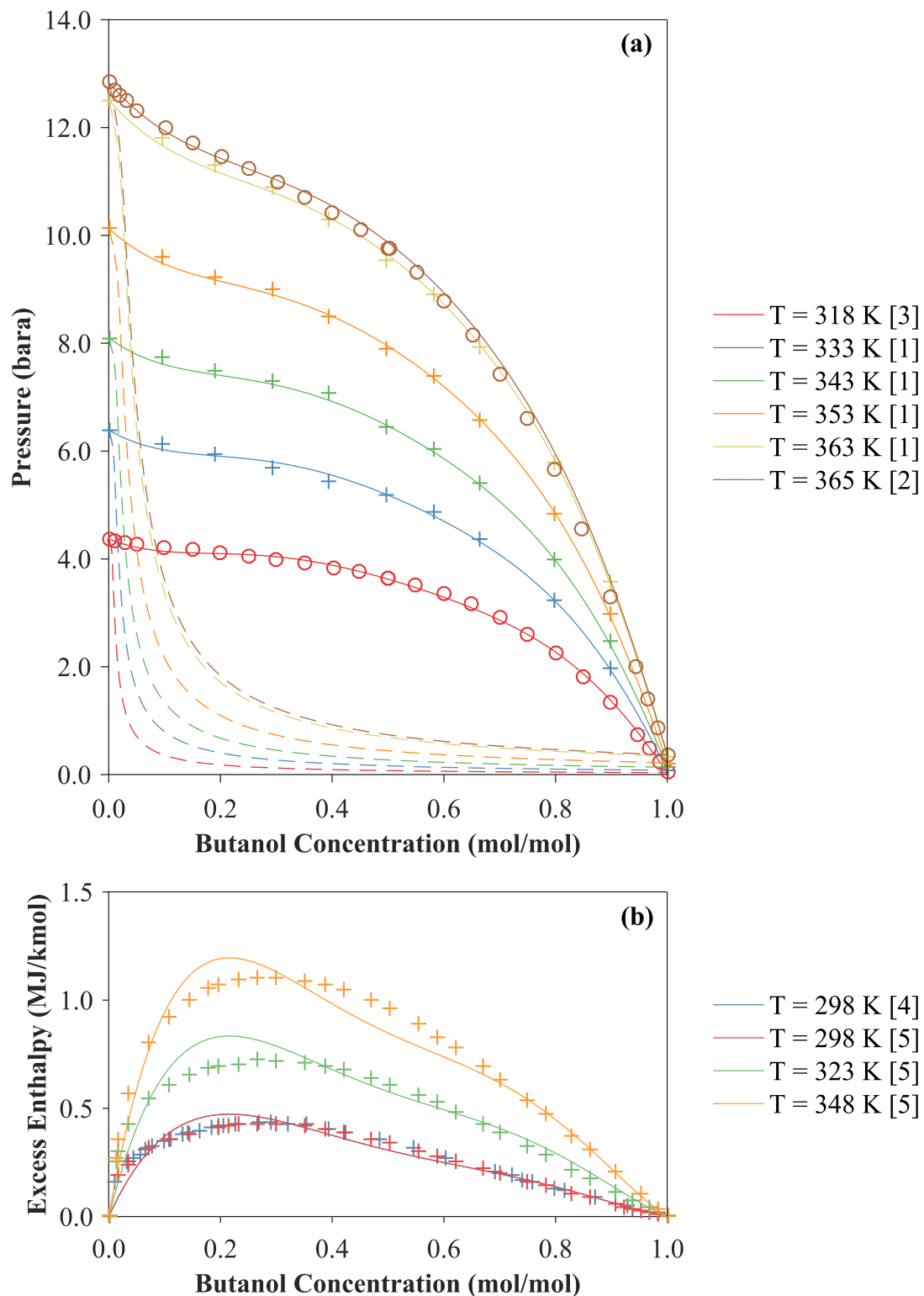


Figure 3-15a-b: Leg-virial Model prediction (lines) and measurements from [ref#] for (a) vapor-liquid equilibrium; (b) excess enthalpy of *n*-butane and *n*-butanol

Model Lines: Solid line (-) = $P - x$ or H_E ; Dashed Line (--) = $P - y$

Dataset measurements: + = $P - x$ or H_E ; \times = $P - y$; \circ = $P - z$

[1] = Deak *et al.* (1995); [2] = Dell'Era *et al.* (2007); [3] = Kuitunen *et al.* (2008)

[4] = McFall *et al.* (1981); [5] = Sipowska *et al.* (1994)

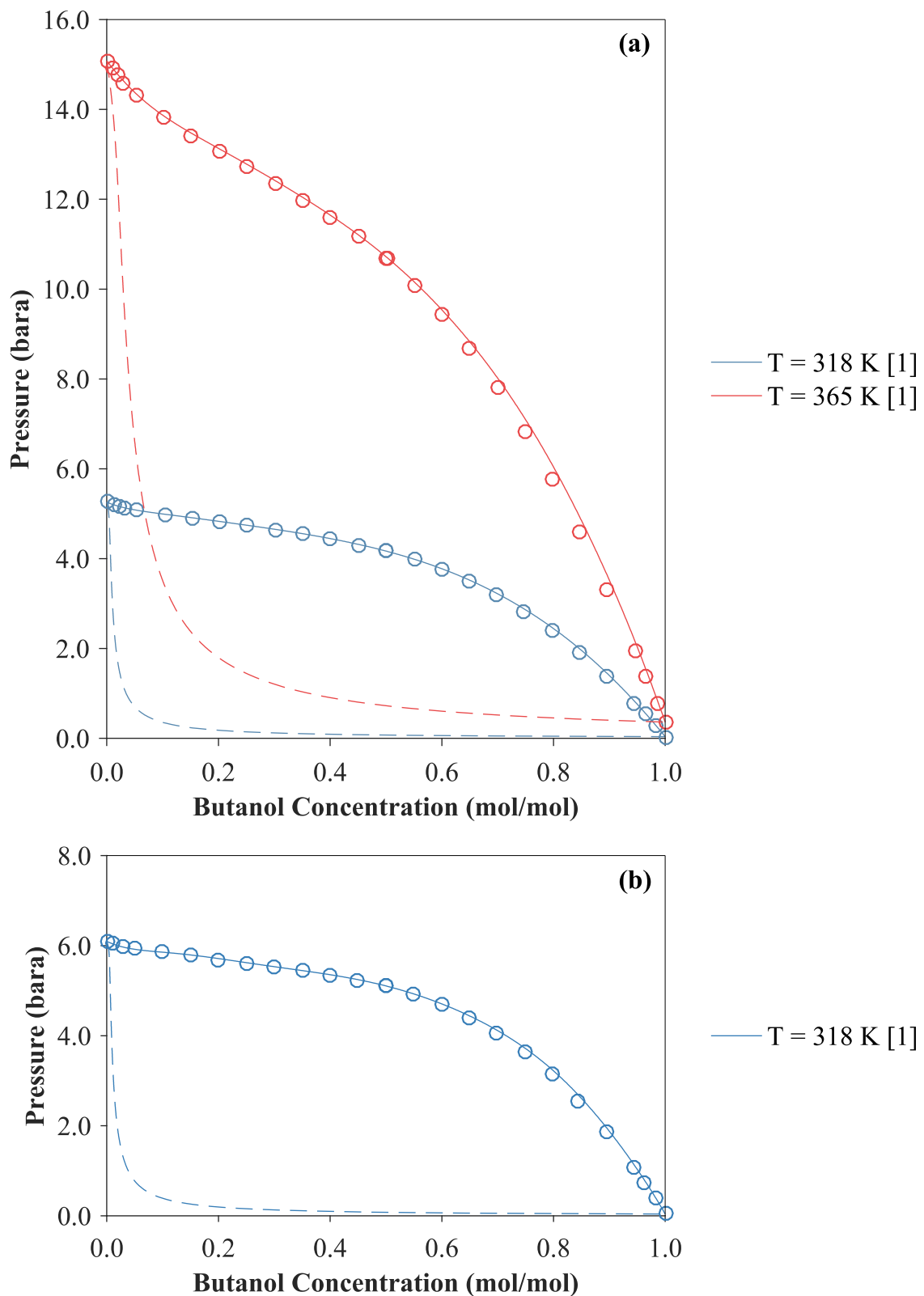


Figure 3-16a-b: Leg-virial Model prediction (lines) and measurements from [ref#] for vapor-liquid equilibrium of (a) 1-butene and (b) iso-butane with *n*-butanol

Model Lines: Solid line (–) = $P - x$ or H_E ; Dashed Line (--) = $P - y$

Dataset measurements: + = $P - x$ or H_E ; $\times = P - y$; $\circ = P - z$

[1] = Kuitunen *et al.* (2008)

Figures 3-17 and 3-18 contrast regressions performed using different equations of state. Figure 3-17 compares the predictions of VLE and excess enthalpy calculated using the Leg-virial Models with measurements from datasets containing ethanol with *n*-pentane. Figure 3-18 details the same comparison for predictions made using the Leg-SRK Models. Both models accurately represent the VLE and excess enthalpy measurements. Both models also predict the formation of a minimum boiling-point azeotrope at low ethanol concentrations at higher temperatures. However, as shown in Figure 3-17, the Leg-virial Model represents the measurements of both VLE and excess enthalpy at low ethanol concentrations more accurately than the Leg-SRK Model (Figure 3-18).

3.6 Discussion

The choice of the equation of state used to model the vapour phase was found to have a significant impact on the results of the regressions. As Figure 3-7 demonstrates, the deviation of model predictions from measurements contained in the binary datasets varies depending on the choice of equation of state. VLE measurements predicted using the Leg-IGL models (which approximated the vapour phase as ideal) resulted in significantly more deviation from VLE measurements than using either the Leg-virial or Leg-SRK models. This suggested that the binary mixtures of one hydrocarbon with one of the various fermentation products exhibit some non-ideal behaviour, even at low pressures. The Leg-virial and Leg-SRK models predicted similar deviations for the VLE measurements, although the Leg-virial Models produced slightly lower deviations. This was possibly because the Leg-virial Models employed an estimate of the binary interaction parameter, whereas for the Leg-SRK Models, the binary interaction parameter was neglected, as explained in Appendix D. Unsurprisingly, the deviation of predictions from measurements of excess enthalpy was not as significantly affected by the vapour equation of state employed in the regression. The influence of the equation of state employed on excess enthalpy is indirect, caused by a compromise between the temperature dependence of activity coefficients predicted by measurements of excess enthalpy, and by measurement of VLE at different temperatures.

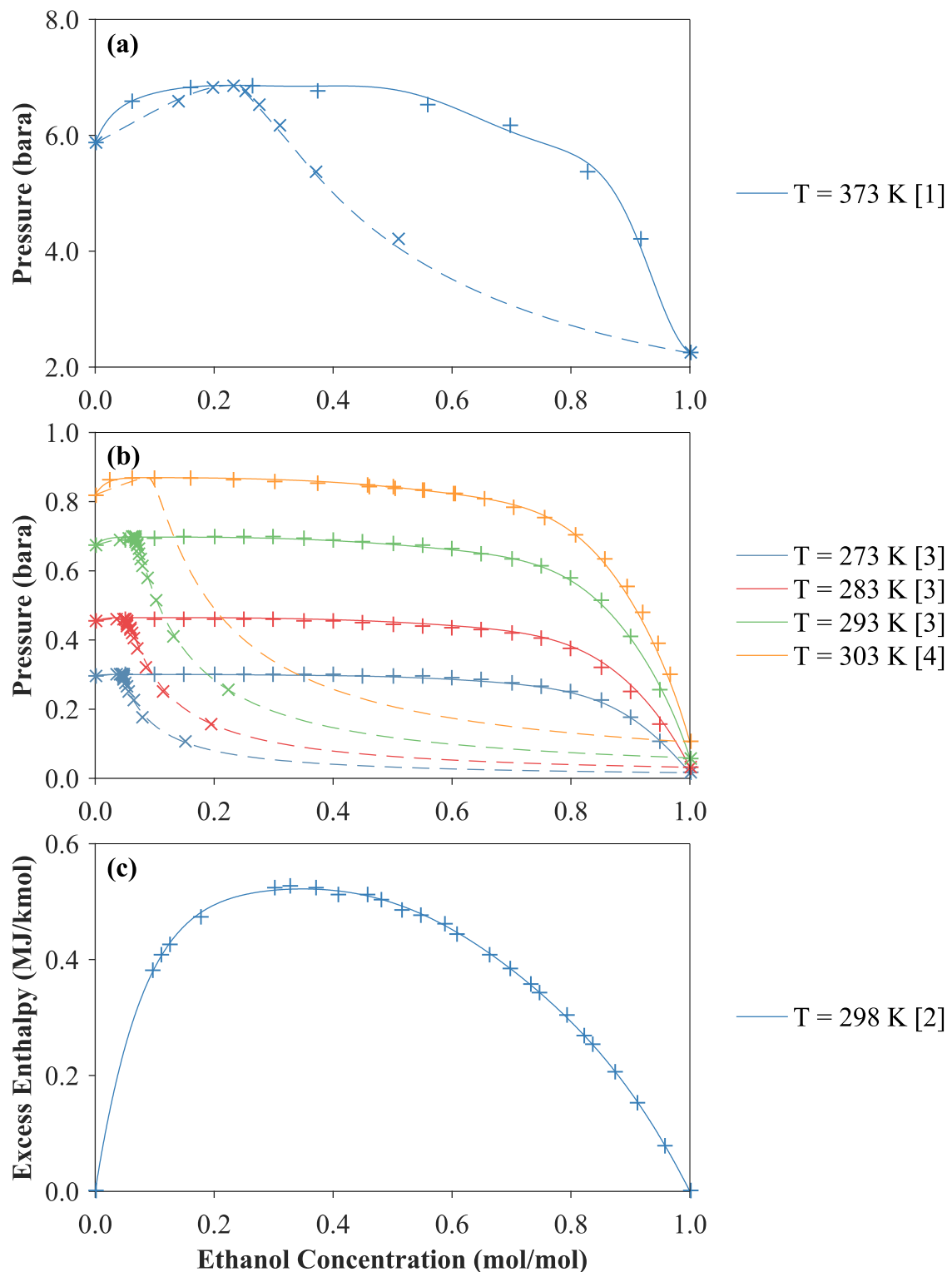


Figure 3-17a-c: Leg-virial Model prediction (lines) and measurements from [ref#] for (a, b) vapor-liquid equilibrium; (c) excess enthalpy of pentane with ethanol

Model Lines: Solid line (—) = $P - x$ or H_E ; Dashed Line (--) = $P - y$

Dataset measurements: + = $P - x$ or H_E ; \times = $P - y$; \circ = $P - z$

[1] = Campbell *et al.* (1987); [2] = Collins *et al.* (1980); [3] = Ishii (1935)

[4] = Reimers *et al.* (1992)

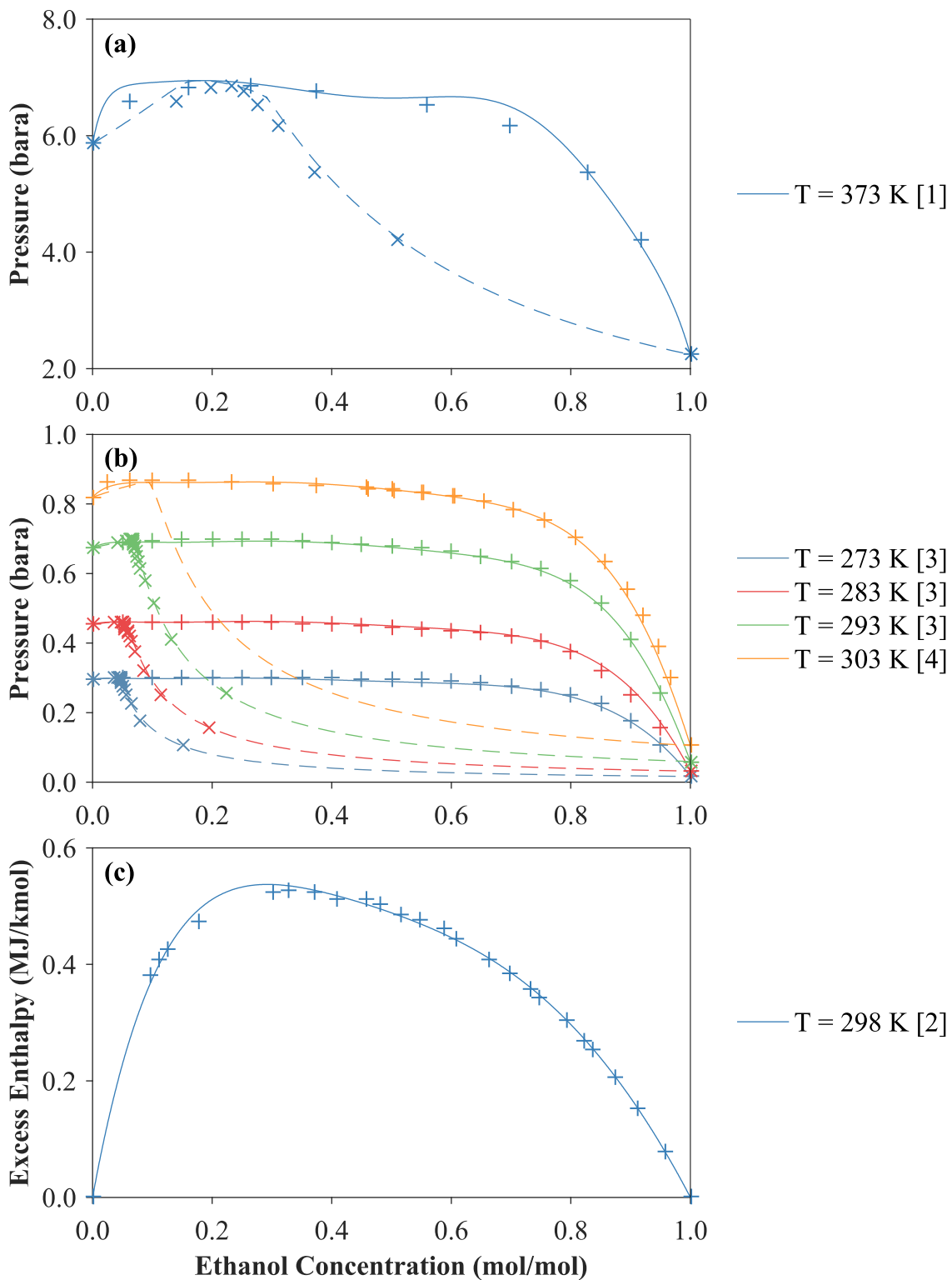


Figure 3-18a-c: Leg-SRK Model prediction (lines) and measurements from [ref#] for (a, b) vapor-liquid equilibrium; (c) excess enthalpy of pentane with ethanol

Model Lines: Solid line (—) = $P - x$ or H_E ; Dashed Line (--) = $P - y$

Dataset measurements: + = $P - x$ or H_E ; \times = $P - y$; \circ = $P - z$

[1] = Campbell *et al.* (1987); [2] = Collins *et al.* (1980); [3] = Ishii (1935)

[4] = Reimers *et al.* (1992)

Figures 3-17 and 3-18 further illustrate the effect of choice of equation of state on the regression on the prediction of VLE and excess enthalpy. Predictions made by the Leg-virial Models (Figure 3-17) result in a closer fit of VLE measurements of ethanol with *n*-pentane than that displayed in Figure 3-18, which displays the equivalent predictions using the Leg-SRK models. The difference is most notable at low ethanol concentration. The Leg-SRK model does not accurately predict the gradient of the bubble-point pressure at low ethanol concentrations, and consequently this model will produce inaccurate activity coefficients of ethanol at low concentration. The effect of the inaccurate prediction of the bubble-point gradient at low ethanol concentration by the Leg-SRK model can be seen in Figure 3-5, when comparing the activity coefficients of ethanol in *n*-pentane predicted by the Leg-SRK Model with equivalent predictions by the Leg-virial model shown in Figure 3-4. The Leg-SRK model predicted lower activity coefficients of ethanol than the Leg-virial model and predicted a minimum in activity coefficient at infinite dilution at a temperatures <100°C. This is contrary to results seen for the effect of temperature on activity coefficient for other solvents and for other products, for which a reduction in activity coefficient with temperature was predicted in the range 20 – 100°C. Figure 3-5 also suggests that the predictions made by the Leg-SRK model were inaccurate for ethanol with *iso*-butane, because this model also predicts a minimum in activity coefficient at infinite dilution for a temperature lower than 100°C for this mixture. However, Figure 3-4 shows that the Leg-virial model did not successfully predict activity coefficients for ethanol in 1-hexene at low ethanol concentrations. This was probably because the minimum ethanol concentration available in the sole dataset available for this binary mixture was 14 mol%. The average deviation of ~0% shown in Figure 3-8a for the Leg-virial Model predictions of the VLE of ethanol and 1-hexene from the measurements of this dataset suggests that the model has been over-fitted. Further experimental measurements of VLE, especially at low ethanol concentration, are needed for this system in order to accurately predict activity coefficients.

Figure 3-6 further demonstrates the impact of equation of state on the regressions at low concentration by comparing the predictions made by the Leg-virial Models, the Leg-SRK Models and the Leg-IGL Models of the VLE of *n*-butanol and *iso*-butanol binary mixtures with hexane. For these binaries, the impact of the equation of state used in the regression is not as marked as in other binaries, with the three models yielding similar predictions. The Leg-IGL Models did however result in activity coefficients at infinite dilution around 10 – 20% lower than equivalent predictions by the Leg-virial Models.

Regressions employing the virial equation of state, *i.e.* the Leg-virial Models, were therefore deemed to be the most appropriate models, on the basis that these models produced predictions with the lowest deviation from experimental measurements.

Average deviations of predictions by the Leg-virial Models of each VLE dataset were low, being <3% for all 81 datasets, and <1.5% for butanol and acetone VLE data. The broader range of VLE datasets containing ethanol increased the deviation compared with butanol and acetone datasets. Deviation of predictions from excess enthalpy datasets was larger, ranging from around 1 – 12%. This was unsurprising, since excess enthalpy measurements are often difficult to predict (Islam and Rahman, 2012). However, the modifications made to the temperature dependence of the Legendre activity model, described in section 3.4.1, and employing an objective function based on the relative least-squares in the regression, as noted in section 3.4.4, greatly improved the fit of the model to the measurements. A greater deviation of predictions from excess enthalpy measurements was also to be expected, since it is the derivative of excess enthalpy (\overline{H}_i^E) that determines the temperature dependence of activity coefficient. Hence, small deviations in absolute value of excess enthalpy have a negligible effect on activity coefficient, especially since excess enthalpy is fixed at zero at each end of the composition range.

Models regressed from VLE datasets of the type $PTzV$ resulted in predictions with very low deviations from the measurements. For example, all VLE data containing 1-butene were of this type. Here, average deviations of model predictions from each dataset were <0.1%. This type of VLE measurement is optimal because it avoids the experimental error associated with attempting to measure vapour and liquid compositions simultaneously in a recirculating cell (as done within Pxy data) because it simply measures quantities injected into the cell. Recording the cell volume and number of moles injected into the cell allows the regression procedure to determine the equilibrium vapour and liquid compositions by a mass balance on the equilibrium cell. The close fit of the models to $PTzV$ datasets can be seen in Figures 3-15 and 3-16 (Leg-virial model predictions compared to VLE measurements of *n*-butanol in *n*-butane, and in *iso*-butane and 1-butene respectively). It should be noted that, by definition, overall cell mole fraction z_i is between y_i and x_i . These two figures, along with Figure 3-15 (*n*-butanol and *n*-pentane) and Figure 3-16 (*n*-butanol and *n*-butane) demonstrate the accuracy of the Leg-virial Model in predicting VLE measurements, and the slightly poorer predictions of the model for measurements of excess enthalpy.

The relatively low deviations of predictions of $PTzV$ datasets suggested that the inaccuracy of models regressed from Pz datasets was partially due to being unable to correct Pz measurements to the liquid mole fractions at equilibrium, in addition to normal experimental error.

The issue of over-fitting model parameters faced by using an activity model such as the Legendre model, which has an infinite number of coefficients available, is demonstrated in Figures 3-11 and 3-12. These figures compare the predictions of the Leg-virial Models to datasets containing measurements of *iso*-butanol and *n*-hexane. Figure 3-11 was produced by regression of the datasets, employing the Legendre activity model and the crude criteria to prevent over-fitting detailed in Section 3.4.1. Conversely, the regression to produce the predictions in Figure 3-12 was designed to employ one further set of Legendre coefficients in the regression. This additional set of coefficients resulted in the overfitting that can be seen in the prediction of excess enthalpy in Figure 3-12. This also demonstrates that the over-fitting criteria utilised, whilst crude, was at least partially successful.

However, the scatter in measurements of excess enthalpy generally caused over-fitting of excess enthalpy measurements. This can be seen in the predictions of excess enthalpy of *iso*-butanol and *n*-hexane (Figure 3-11), and in other predictions of other binaries, such as for *n*-butanol and *n*-hexane (Figure 3-10). In these examples, the regression appears to have over-fitted the excess enthalpy measurements. This was also partially due to the form of the Legendre activity model for prediction of excess enthalpy data. When the Legendre activity model is used to model excess enthalpy data only, a high number of coefficients are required in order to predict a smooth excess enthalpy curve without erroneous stationary points. The modifications made to the temperature dependence of the Legendre activity coefficients reduced this problem significantly, but other polynomial expressions are better suited for the purpose of modelling the simple curves found for excess enthalpy. However, the impact of over-fitting measurements of excess enthalpy was thought to be small. The temperature dependence of activity coefficients derives from the gradient of the excess enthalpy with respect to composition, which is less significantly affected by the over-fitting.

Figures 3-10 and 3-11 demonstrate accurate predictions of the vapour-phase composition at equilibrium with experimental measurements from Pxy datasets. Figure 3-11 also demonstrates the importance of using the vapour pressures from the datasets where possible (as opposed to those from a correlation) when comparing the model predictions

to the measurements. This figure compares the predictions of the Leg-virial Models with two different datasets at 298 K. The slight difference in the experimental pure vapour pressures contained in the two datasets at 298 K caused a notable difference in the prediction of the vapour phase composition. Employing measurements of pure vapour pressure contained in each dataset during the regression reduces systematic experimental error in the measurement of bubble-point pressure.

Figures 3-10 and 3-11 also compare the model predictions of hexane and *iso*-butanol with those of hexane and *n*-butanol. Binary data for *iso*-butanol could not be found for any short hydrocarbons other than *n*-hexane. Therefore, these data provided the only comparison between the two butanol isomers. As can be seen both in Figure 3-10 and Figure 3-11, the shape of the VLE and excess enthalpy curves are similar for the two isomers. Thus, the assumption that the gradient of $P - x$ at $x_{Bu} \rightarrow 0$ relative to that of Raoult's Law (' \mathcal{M} ') is similar for both isomers (Section 2.6) is reasonable, based on the available measurements. Similar values of \mathcal{M} for the two butanol isomers will result in predictions of a slightly lower value for the activity coefficient of *iso*-butanol than that of *n*-butanol since the relative volatility of *iso*-butanol is slightly higher. The figures also show that $\mathcal{M} \sim 0$ at lower temperatures for hexane and increases to a slightly positive value at higher temperatures, resulting in the formation of a minimum boiling point azeotrope at low butanol concentration. This increase in repulsive intermolecular forces between butanol and hexane at higher temperature is not enough to prevent the activity coefficient of butanol from continuing to decrease as temperature increases, as seen in Figure 3-6, since the effect of the reduced relative volatility at higher temperatures is enough to outweigh this.

The values of \mathcal{M} estimated for the six solvents in section 2.6 can be shown to be relatively accurate based on the regressions by considering the gradient at $x_{Bu} \rightarrow 0$ in the VLE plots in Figures 3-10 – 3-16. Binary mixtures of butanol with all six hydrocarbons demonstrated positive deviation from Raoult's Law. Only the binary mixture of butanol with hexane showed some azeotropic behaviour at higher temperatures. Most notably, the C₄ hydrocarbons demonstrated VLE behaviour (Figures 3-15 and 3-16) similar to that outlined for an 'optimal' solvent for use in extraction of butanol, outlined in Figure 2-15d. For butanol in C₄ hydrocarbons, \mathcal{M} , a measure of ideality at infinite dilution compared to Raoult's Law, was close to unity. Values of \mathcal{M} close to unity result in lower activity coefficients, for a fixed relative volatility. Conversely, above 5-10 mol% butanol, C₄ hydrocarbons with butanol demonstrate significant positive deviation from Raoult's Law.

This would allow C₄ hydrocarbon to be readily distilled off the mixture using low-grade heat and only small temperature gradients in a distillation set-up.

The value of \mathcal{M} for a mixture of butanol in pentane is lower than unity, and \mathcal{M} is ~0 for C₆ hydrocarbons. However, the relative volatility of these solvents *versus* butanol is also lower. The consistency of activity coefficient across the chain lengths suggests that the effect of increased non-ideality and hence increased deviation from Raoult's Law with chain length at dilute butanol concentration is balanced by the effect of decreasing relative volatility as chain length increases. This suggests that an activity model based on theoretical interactions between butanol and these simple hydrocarbons, based on the volatility of the hydrocarbon, could be built and used to fit the data better and, in turn, used to predict activity coefficients for other C₄ – C₆ hydrocarbons.

3.7 Conclusions

A modified Legendre activity model was employed in the Barker method to regress measurements of VLE and excess enthalpy of binary mixtures of butanol, ethanol and acetone with six C₄ – C₆ hydrocarbons. An extensive search of the published literature was conducted in order to compile database of datasets containing isothermal VLE and excess enthalpy measurements of these binaries at 20 – 100°C.

The flexible Legendre activity model employed in the regression of data was able to model the rapid changes in the gradient of the bubble-point curve. This was imperative, as popular activity models, such as the NRTL model, only have 2 – 3 parameters, which limits the ability of these models to predict rapid changes in the gradient of the bubble-point curve. These rapid changes often occur at dilute concentrations, such as those found in fermentation broths, and result in rapid changes in activity coefficient.

The equation of state employed to model the vapour phase in the regression of datasets was found to have a significant impact on the activity coefficients predicted. The virial equation of state was found to be most suitable for the regression of the hydrocarbon datasets. The Legendre activity models produced by the regression of datasets where the virial equation of state was employed were termed the 'Leg-virial Models'.

Activity coefficients of low concentration fermentation products in hydrocarbons predicted by the Leg-virial Models was found to decrease dramatically with temperature in the range 25°C – 100°C; activity coefficient at infinite dilution was predicted to vary by a factor of 2 – 4 between 25°C and 100°C. Activity coefficients were also found to

decrease with product concentration. By fermenter product concentrations of 20 mol%, activity coefficients were predicted to have decreased significantly from values at infinite dilution, and the effect of temperature was minimal.

Activity coefficients of *iso*-butanol in *n*-hexane (the only dataset for which VLE measurements with *iso*-butanol were available) were predicted to be slightly lower activity coefficients than those of *n*-butanol.

Each binary mixtures of butanol with the six hydrocarbon solvents exhibited positive deviation from Raoult's Law. The vapour-liquid equilibria of butanol in C₄ hydrocarbons demonstrated the characteristics of an optimal solvent for extraction: behaviour was close to Raoult's Law at dilute butanol concentrations, whilst positive deviation from Raoult's Law was predicted above low butanol concentrations, without forming any azeotropes.

The application of the results to the design and performance of liquid-liquid extraction and distillation is examined, respectively, in Chapters 4 and 5.

4. Modelling the Extraction of Fermentation Products using Volatile Hydrocarbons

4.1 Introduction

This chapter models the liquid-liquid equilibria (LLE), and hence the distribution coefficients, of dilute fermentation products between volatile hydrocarbons and water, using the activity coefficients determined in Chapter 3.

The distribution (or partition) coefficient of a solute being transferred from one solvent (here, water) to another (here, an alkane) is defined as the ratio of the mole fractions in each phase at equilibrium, *i.e.*:

$$D_i^{molar} = \frac{x_i^{org}}{x_i^{aq}} = \frac{\gamma_i^{aq}(x_i^{aq}, P, T)}{\gamma_i^{org}(x_i^{org}, P, T)} \quad (4-1)$$

where i is the solute of interest (*e.g.* butanol); x_i^{org} and x_i^{aq} are the solute mole fractions in the extractant (organic hydrocarbon) and the aqueous phases respectively. The ternary activity coefficients of the solute in the organic and aqueous phases, γ_i^{org} and γ_i^{aq} respectively, are at the ternary concentrations in each phase at equilibrium, and at the temperature and pressure of the extraction. However, Appendix E demonstrated that the effect of pressure on activity coefficients can be neglected.

Ternary activity coefficients must therefore be predicted in order to calculate distribution coefficients. No measurements could be found for ternary equilibria of butanol in water and C₄ – C₅ hydrocarbons, although a limited number of measurements were available for butanol in water and hexane (Islam and Kabadi, 2011; Sugi and Katayama, 1977). In the absence of ternary equilibria measurements, the ternary liquid-liquid equilibria had to be predicted from the activity coefficients of the three constituent binary mixtures, *i.e.*:

- the fermentation product and the relevant hydrocarbon (determined in Chapter 3)
- the relevant hydrocarbon and water, which are highly immiscible (investigated in Section 2.4)
- the fermentation product and water (investigated in this Chapter).

4.1.1 Models for the Prediction of Ternary LLE from Binary Activity Coefficients

One approach to modelling ternary LLE is to use a multicomponent activity model, such as the NRTL or UNIQUAC models. These activity models can be used to predict ternary equilibria from their constituent binary activity models. However, this approach was found to be problematic when modelling activity coefficients at dilute concentrations, as these often change rapidly and are therefore poorly predicted by inflexible activity models with only 2 - 3 parameters per binary system.

An alternative approach is to employ combination models (*e.g.* Talley *et al.*, 1993), which can employ any combination of binary activity models, including flexible models such as the Legendre activity model. Combination models extrapolate ternary compositions to three binary compositions. The excess Gibbs free energy at each of these three binary compositions can be calculated using any activity model of each binary. These are combined to calculate the excess Gibbs free energy at the ternary composition, from which the activity coefficients of the ternary mixture can be calculated. However, there are an infinite number of methods to perform the extrapolation of the ternary mixture into the three binary mixtures, and hence an infinite number of ways to perform the combination. Without a sizeable number of measurements of ternary liquid-liquid equilibria to validate any given method, it was found to be impossible to ascertain reliably which extrapolation models would yield accurate results for any given ternary mixture.

Both approaches described above also rely upon an activity coefficient model of the solvent pair, *i.e.* of mixtures of water and the relevant hydrocarbon. It is trivial to produce an activity coefficient model that predicts the mutual solubilities of the solvent pair. However, since it is not possible to measure the equilibria in the binary miscibility gap, it is therefore not possible to verify the accuracy of the binary activity model in the miscibility gap without measurements on the ternary mixture, where the pair are able to coexist in ratios that are immiscible in the binary mixture.

This is problematic for combination models as it adds another unknown factor into the model: the activity model employed for the solvent pair. This is also problematic in practice for the prediction of the ternary equilibria using the NRTL model. Islam *et al.* (2011) regressed binary and ternary equilibria measurements for hexane, water and butanol in order to produce an NRTL model for the ternary system at 20 – 100°C. Since the NRTL activity model is a three-parameter model, and only two equilibrium

measurements exist for the hexane-water binary (the mutual solubilities), one parameter for this binary is left as a free variable. The authors effectively used this third free variable to fit the NRTL model to ternary equilibria measurements for the system. The fact that the activity model for the immiscible solvent pair cannot be validated without measurements of ternary equilibria therefore limits the ability of multicomponent activity models to predict ternary equilibria from its three constituent binaries. Islam *et al.* (2011) have also discussed elsewhere the limitations of multicomponent activity models, such as the NRTL model, for predicting ternary equilibria at dilute solute concentrations, due to their inflexibility (Islam and Kabadi, 2009).

Ternary systems which have limited mutual solubility for two binary pairs, such as butanol-water-hydrocarbon mixtures, are termed ‘Type II’ systems. Another crude method to estimate ternary equilibria for Type II systems is the use of interpolation methods (Treybal, 1951). Interpolation methods can be used to predict the location of the ternary solubility lines. In Type II systems the two solubility lines, by definition, must each join the two pairs of binary solubilities. For example, in the case of a butanol-water-hydrocarbon system, the solubility line for the organic phase must connect the solubility of water in the hydrocarbon to the solubility of water in butanol. Similarly, the solubility line for the aqueous phase must connect the solubility of the hydrocarbon in water to the solubility of butanol in water. However, these interpolation methods are not able to predict the distribution coefficient (*i.e.* the position of tie-lines between the two solubility curves); they can only predict the position of ternary solubility, although this could still be very useful. For example, interpolation methods could be used to predict the solubility of water in the organic phase as a function of butanol concentration. Despite attempts to employ several interpolation models, including those outlined by Brown (1948) and Varteressian and Fenske (1937), none were able to successfully predict the ternary solubilities of the only ternary equilibria measurements available for butanol (butanol-water-hexane).

4.1.2 Approximating Ternary LLE of Dilute Mixtures using Binary Activity Coefficients

For systems where the two solvents (here, the hydrocarbon and water) are close to immiscible, neglecting their mutual solubility can give relatively accurate predictions for the distribution coefficient at low concentrations of the solute (butanol, ethanol or acetone) (Treybal, 1951). This means that the ternary effects on the activity coefficient of the solvent can be neglected, since the concentrations of the solute and the solvent from

the opposing phase (*e.g.* water in the hydrocarbon phase) are very low. Thus, at low solute concentrations, binary activity coefficients (rather than ternary coefficients) can be used to predict distribution coefficients at low solute concentrations for highly immiscible system, such as hydrocarbon-water extractions. This approach is advantageous since the methods investigated for the prediction of ternary LLE were found to be problematic, and no measurements of ternary VLE or LLE for C₄ and C₅ hydrocarbons with butanol and water were available.

The approach of neglecting the miscibility of the solvents can be further justified on the basis that a ternary system itself is also a simplification of the real extraction system, which extracts butanol from a multicomponent fermentation broth. Hence solutes in the extraction are subject to ternary interactions not only with the two solvents (water and the hydrocarbon), but also from each other (ethanol, acetone) and any other components in the broth (*e.g.* carboxylic acids, intermediates, nutrients). It was posited that the influence of ternary interactions due to the presence of trace concentrations of water or the hydrocarbon was likely to be as small as the influence of the ternary interactions due to the presence of any other dilute components in a fermentation broth. Therefore, it was concluded that attempting to account for ternary interactions of water and the hydrocarbon theoretically by using a ternary model would not improve the accuracy of predictions of distribution coefficients in a fermentation broth, compared with neglecting these interactions. However, these ternary models are essential when exploring the equilibria of more concentrated systems. In systems containing higher concentrations of butanol, the presence of butanol increases the solubility of water in the organic phase significantly, and hence these ternary interactions become significant. In order to predict the distribution coefficients of fermentation products by neglecting the miscibility of water and the relevant hydrocarbons, the activity coefficients of aqueous acetone, ethanol and butanol were required and this is described in Chapter 3.

Finally, liquid-liquid thermodynamic equilibrium is not the only factor in the performance of an extractor; rate processes in the form of mass transfer also play a significant role. Some of the kinetic constraints were considered in the design of an extraction unit for this system, and a basic model built to evaluate the performance of the extractor.

4.2 Calculation of Activity Coefficients of Aqueous Butanol

Despite being a relatively common mixture, published VLE measurements of butanol isomers with water were surprisingly scarce, especially at dilute concentrations of

butanol. Therefore, it was not possible to produce accurate predictions of the activity coefficients of dilute butanol isomers in water based on VLE measurements. An activity coefficient model was instead devised based on the limiting activity coefficients of butanol and water at infinite dilution in butanol-water mixtures and the mutual solubility of butanol and water. Correlations of these properties have been well documented for mixtures of butanol and water as a function of temperature (Dohnal *et al.*, 2006; Fenclova *et al.*, 2007; Maczynski *et al.*, 2007)

4.2.1 Development of an Activity Coefficient Model

The mutual solubilities of butanol (1) and water (2) represent the position of a binary liquid-liquid equilibrium, and therefore must satisfy two conditions by equating the chemical potential of water and butanol in each phase:

$$\mu_1^I = \mu_1^{II} \rightarrow \therefore \ln(x_1^I \gamma_1^I) = \ln(x_1^{II} \gamma_1^{II}) \quad (4-2)$$

$$\mu_2^I = \mu_2^{II} \rightarrow \therefore \ln(x_2^I \gamma_2^I) = \ln(x_2^{II} \gamma_2^{II}) \quad (4-3)$$

where I and II represent each phase (aqueous and organic), x_i^I is the mole fraction of species i in phase I at the solubility limit (*i.e.* at LLE) and γ_i^I is the activity coefficient of species i in phase I at the solubility limit.

Hence, the mutual solubilities of butanol and water supply two constraints (eqs. (4-2) and (4-3)) on the activity model. The limiting activity coefficients of both butanol and water at infinite dilution provide two further constraints on the activity model. Therefore, a four-parameter model is required to satisfy fully all four constraints. Due to its simplicity, a four-parameter Margules model was used to represent the butanol (1)-water (2) mixture:

$$\frac{G^E}{RT} = g^E = x_1 x_2 (A_{21} x_1 + A_{12} x_2 + x_1 x_2 (B_{21} x_1 + B_{12} x_2)) \quad (4-4)$$

where A_{12} , A_{21} , B_{12} and B_{21} are Margules coefficients. The Margules model is of polynomial form, and so it would be possible to convert the four-parameter Margules model into an equivalent Legendre polynomial.

It is trivial to demonstrate that $A_{12} = \ln \gamma_1^\infty$ and $A_{21} = \ln \gamma_2^\infty$. Given the condition of equal activity at liquid-liquid equilibrium (*i.e.* eqs. (4-2) and (4-3)) it is also possible to prove that B_{12} and B_{21} can be calculated from the binary LLE position x_1^I , x_1^{II} :

$$B_{12} = \frac{(\Delta a_2)(\Delta d_2) - (\Delta a_1)(\Delta c_1)}{(\Delta c_1)(\Delta c_2) - (\Delta d_1)(\Delta d_2)} \quad (4-5)$$

$$B_{21} = \frac{(\Delta a_1)(\Delta d_1) - (\Delta a_2)(\Delta c_2)}{(\Delta c_1)(\Delta c_2) - (\Delta d_1)(\Delta d_2)} \quad (4-6)$$

where Δ represents the difference between the parameter in liquid phase I and that in liquid phase II:

$$\Delta a_i = (a_i^I - a_i^{II}) \quad (4-7)$$

$$\Delta c_i = (c_i^I - c_i^{II}) \quad (4-8)$$

$$\Delta d_i = (d_i^I - d_i^{II}) \quad (4-9)$$

and parameters a_i^J , c_i^J and d_i^J for species i (binary mixture $i - j$) for phase J are given by:

$$a_i^J = (1 - x_i^J)((1 - 2x_i^J)A_{ij} + 2x_i^J A_{ji}) + \ln x_i^J \quad (4-10)$$

$$c_i^J = 2(x_i^J)^3 x_j^J (1 - 2x_i^J) \quad (4-11)$$

$$d_i^J = (x_i^J x_j^J)^2 (4x_i^J - 1) \quad (4-12)$$

4.2.2 Correlations of Limiting Activity Coefficients at Infinite Dilution and Correlations of Mutual Solubilities for Butanol and Water

Dohnal *et al.* (2006) and Fenclova *et al.* (2007) obtained the limiting activity coefficients of at infinite dilution of, respectively, *n*-butanol and *iso*-butanol in water (γ_i^∞) over the temperature range 273 - 373 K. Their correlations are given in Appendix F. In the present research, an analogous correlation for the limiting activity coefficient of water in butanol isomers was developed using the method of Dohnal *et al.* (2006) and Fenclova *et al.* (2007) and is described in Appendix F. These correlations were used to calculate A_{12} and A_{21} at any given temperature.

The mutual solubility of butanol isomers and water were investigated by Maczynski *et al.* (2007), who conducted an analysis of the available measurements for *n*-butanol and *iso*-butanol respectively, leading to correlations of the form:

$$\ln x_i^{sol} = \ln x_{i,min}^{sol} + C_i \left(\frac{T_{i,min}}{T} - \ln \left(\frac{T_{i,min}}{T} \right) - 1 \right) + D_i \exp \left(\alpha_i \left(1 - \frac{T}{T_{cs}} \right) \right) \quad (4-13)$$

where x_i^{sol} is the solubility of species i (given as a mole fraction) and $x_{i,min}^{sol}$ is the minimum solubility of species i at temperature $T_{i,min}$. The variables C_i , D_i and α_i are correlation parameters specific to the relevant species. Table 4-1 details the parameter

values for water and butanol isomers. The correlation is valid from 273 K to the critical solution temperature (T_{cs}), above which complete miscibility occurs.

The correlations of Maczynski *et al.* (2007) were used to calculate B_{12} and B_{21} at any given temperature. The four-parameter Margules model therefore interpolates between the activities at infinite dilution (as predicted by the correlations detailed in Appendix F) and the position of the binary LLE given by the correlations of Maczynski *et al.* (2007) for the mutual solubilities of butanol and water.

Table 4-1 – Parameters for the correlations of Maczynski *et al.* (2007) for the mutual solubilities of butanol isomers and water

Solubility	$\ln x_{i,min}^{sol}(T_{i,min})$	C_i	D_i	α_i	T_{cs} (K)	$T_{i,min}$ (K)
<i>N</i> -butanol in water	-4.12	27.71	0.911	-30	398.0	330
Water in <i>n</i> -butanol	-0.702	6.082	0.126	-30	398.0	270
<i>Iso</i> -butanol in water	-4.03	32.34	0.858	-30	406.3	330
Water in <i>iso</i> -butanol	-0.968	4.136	0.140	-30	406.3	220

4.2.3 Model Validation

As butanol exhibits a heterogeneous azeotrope with water, a liquid phase containing butanol at its solubility in water would be in vapour-liquid equilibrium with the butanol-water azeotrope. The four-parameter Margules model was used to predict the pressure and vapour composition of this azeotrope. The virial equation of state was employed to model the vapour phase, using second virial coefficients estimated using the Tsonopolous method, described in Appendix D. These predictions of the azeotrope were used to validate the model.

Gmehling (2014a) provided a compilation of measurements of the pressure and vapour composition of *n*-butanol-water. Measurements of the VLE of *iso*-butanol and water were employed to obtain measurements of *iso*-butanol-water azeotropes (Ellis and Garbett, 1960; Fischer and Gmehling, 1994; Lyzlova *et al.*, 1979; Stockhardt and Hull,

1931). Figure 4-1 plots the measurements of the compositions and pressures of the *n*-butanol-water and *iso*-butanol-water azeotropes, compared with those predicted by the four-parameter Margules model. As shown in Figure 4-1, the four-parameter Margules model, based on correlations of the activity coefficients of butanol and water at infinite dilution and the mutual solubilities of butanol and water, produced valid predictions of the measurements of the pressure and composition of the butanol-water azeotropes.

The model was further validated using a set of VLE measurements for mixtures of *n*-butanol and water and mixtures of *iso*-butanol and water at 50°C (Fischer and Gmehling, 1994). This set of VLE measurements was compared to model predictions of VLE in Figure 4-2, again employing the virial equation of state for the vapour phase. As can be seen in Figure 4-2, the four-parameter Margules model accurately predicts the VLE measurements, including at low butanol concentrations. The largest discrepancy between the VLE measurements and the model was the prediction of the mutual solubility. The model's prediction is fixed to that of the correlation of Maczynski *et al.* (2007), which does not agree with the mutual solubility of butanol and water obtained from the VLE measurements of Fischer and Gmehling (1994) at 50°C. However, given that Fischer and Gmehling (1994) were measuring bubble-point pressures, it is likely that their values of mutual solubilities in this complex vapour-liquid-liquid equilibrium are inaccurate.

4.2.4 Model Results

The four-parameter Margules model was employed successfully for binary aqueous mixtures of *n*- and *iso*-butanol between 20°C and 90°C. The activity coefficients predicted by the model for butanol isomers in water are shown in Figure 4-3. The limiting activity coefficient for butanol in water at infinite dilution peaked at around 60 – 70°C. The activity coefficient decreased more rapidly with butanol concentration at higher temperatures than at lower temperatures: between zero concentration and typical fermenter broth concentrations (~0.5 mol%), the activity coefficient of *n*-butanol decreased by ~15% at 90°C, but only by ~6% at 20°C. Unsurprisingly, *iso*-butanol behaved very similarly to *n*-butanol, although it was predicted to possess a slightly lower activity coefficient (~5% lower).

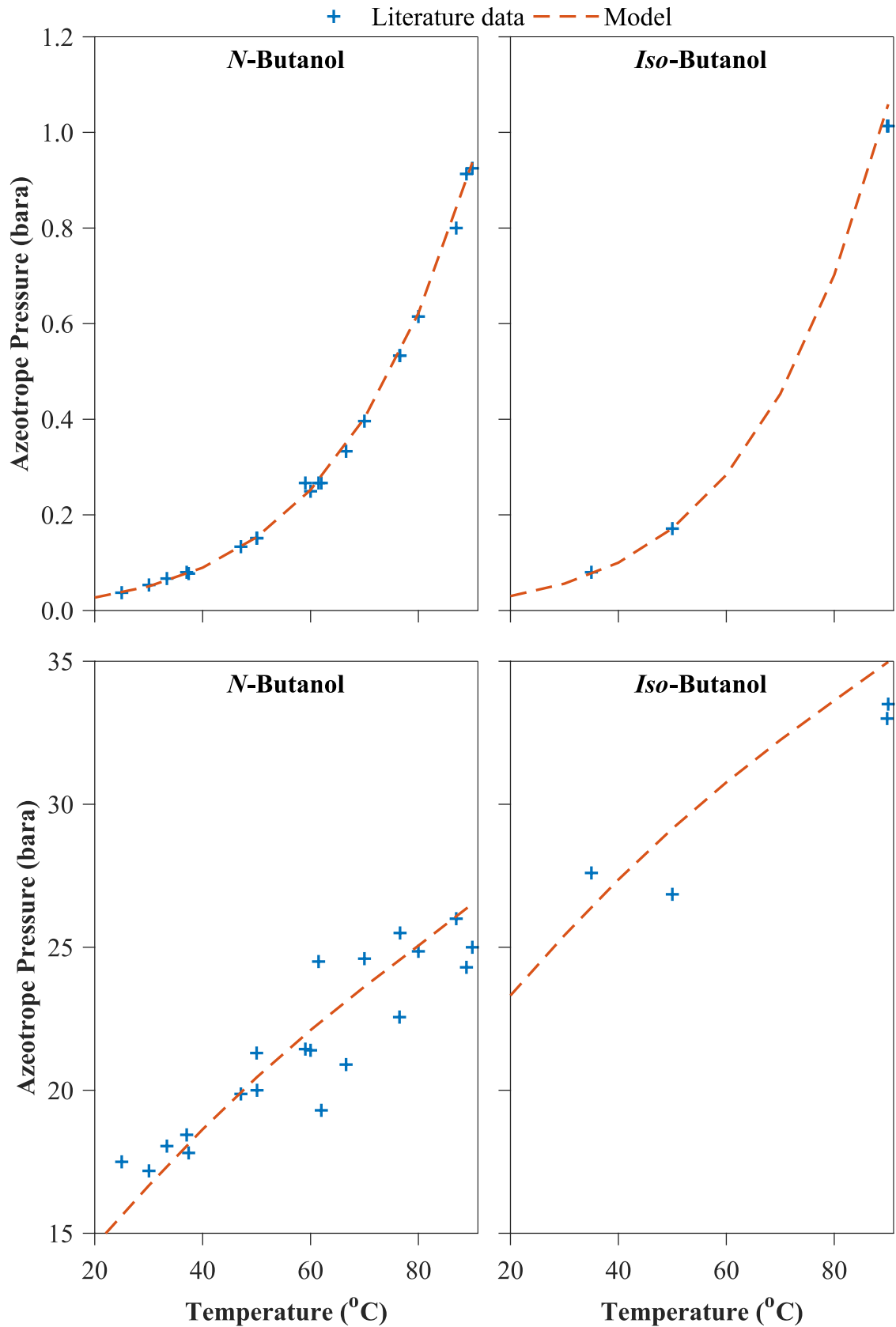


Figure 4-1a-b: Model prediction *versus* literature measurements of azeotrope vapour mole fraction and azeotrope pressure as a function of temperature for *n*-butanol-water and *iso*-butanol-water binary mixtures

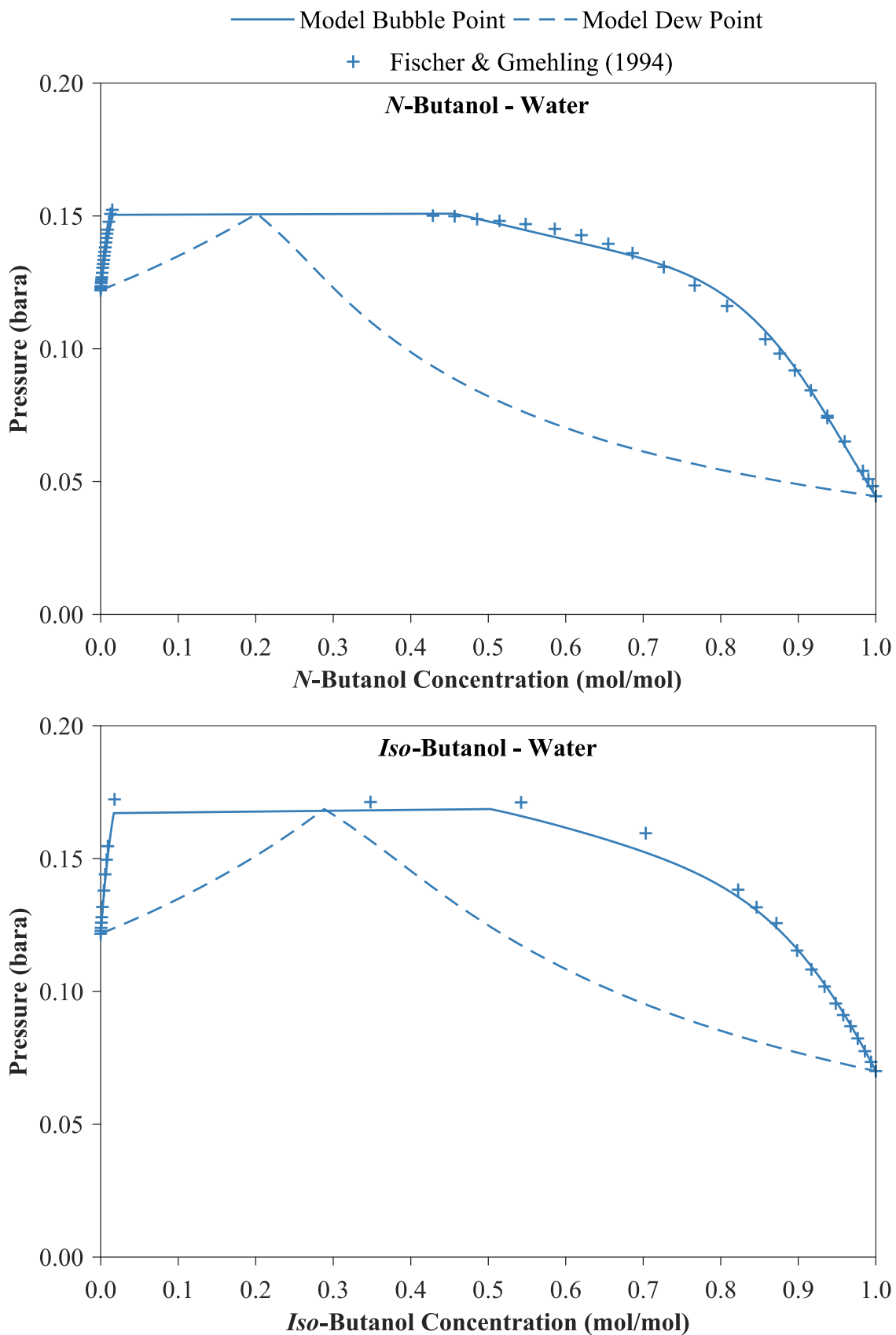


Figure 4-2a-b: Model bubble-point and dew-point predictions versus $P - x$ VLE measurements of Fischer & Gmehling (1994) for *n*-butanol-water and *iso*-butanol-water

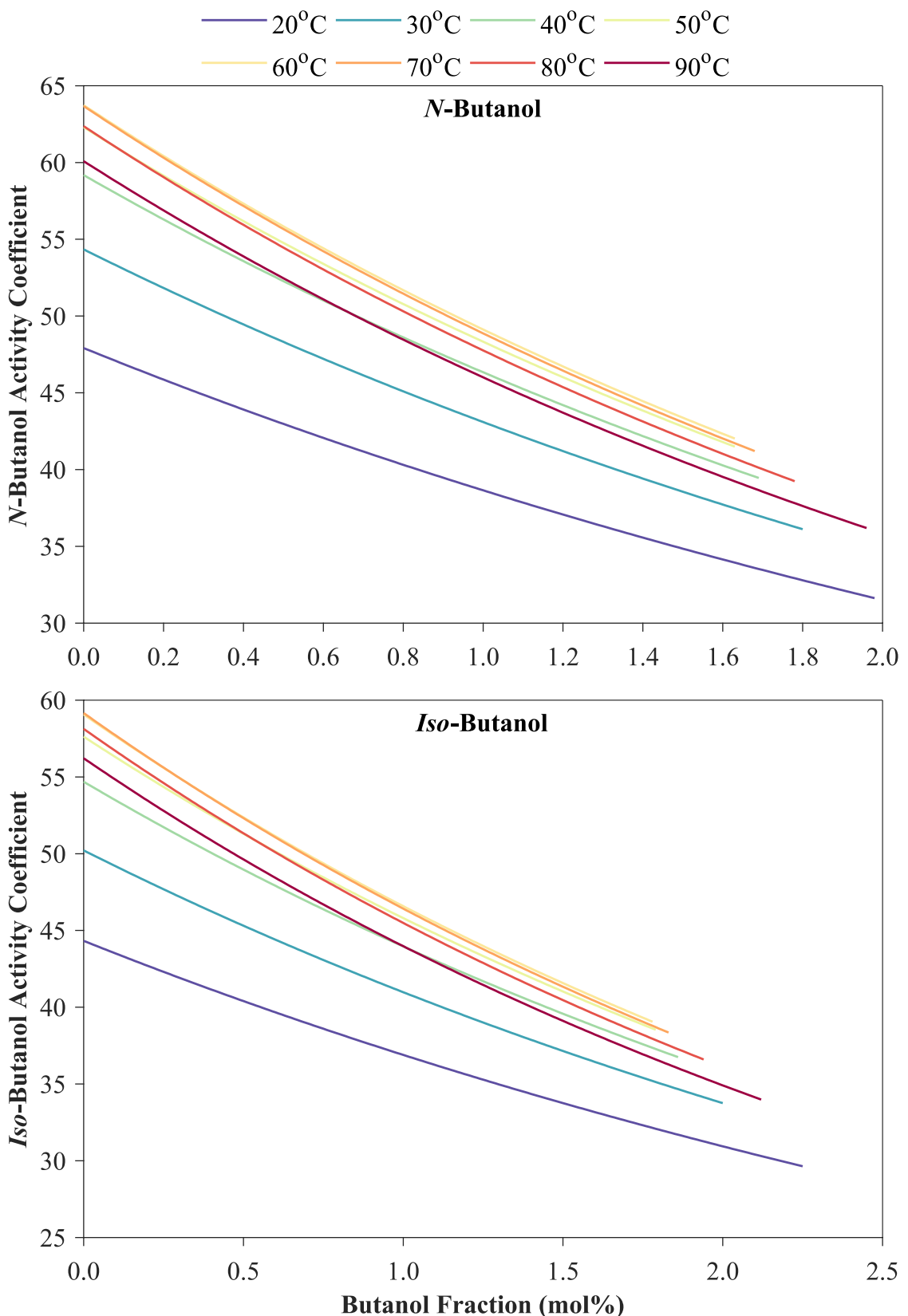


Figure 4-3a-b: Model results for activity coefficient of (a) *n*-butanol and (b) *iso*-butanol in water up to the solubility limit of butanol, at a range of temperatures

The benefit of employing more reliable limiting activity coefficients from the correlations of Dohnal *et al.* (2006) and Fenclova *et al.* (2007) is also apparent. Based on VLE measurements at 50°C, a limiting activity coefficient for *n*-butanol of 78 is predicted (Fischer and Gmehling, 1994). This is in contrast to the correlation of Dohnal *et al.* (2006), which was based on a large compilation of literature values for the activity coefficient of butanol at infinite dilution, which predicted a value of 62 at the same temperature, ~20% lower.

Above 90°C, the miscibility gap of butanol and water reduces significantly. At these temperatures, the Margules model produced erroneous predictions of a second miscibility gap in the butanol-rich phase. This might be due to the limited capacity of a four-parameter Margules model to replicate the equilibria of the binary at this temperature; or it could be due to inaccuracies in the underlying correlations at these temperatures. Solutions to improve the validity of a model of aqueous butanol include:

- using a different model with a theoretical basis (*e.g.* the NRTL model, which has 3 parameters and so could accurately represent 3 of the 4 constraints used in the four-parameter Margules model);
- developing a model with a higher number of Margules parameters;
- developing more accurate correlations for the limiting activity coefficients and mutual solubilities above 90°C.

For the purposes of this work, the activity model of aqueous butanol up to 90°C was considered sufficient. In addition, for the purposes of calculating activity coefficients of dilute aqueous butanol, the model still predicts activity coefficients for butanol between infinite dilution and the butanol solubility limit beyond 90°C.

4.3 Calculation of the Activity Coefficient of Aqueous Ethanol

4.3.1 Methodology

The NRTL activity model of Voutsas *et al.* (2011) for ethanol and water was used as a basis to predict the activity coefficient of ethanol in water. The activity coefficient of ethanol in water in this NRTL model ($\gamma_{Et}^{Voutsas}$) was given by:

$$RT \ln \gamma_{Et}^{Voutsas} = x_2^2 \left[\frac{\tau_{21}G_{21}^2}{(x_1 + x_2 G_{21})^2} + \frac{\tau_{12}G_{12}}{(x_2 + x_1 G_{12})^2} \right]$$

$$G_{12} = \exp(-\alpha_{12}\tau_{12}); G_{21} = \exp(-\alpha_{12}\tau_{21}) \quad (4-14)$$

where 1 = ethanol and 2 = water, and:

$$\begin{aligned}\tau_{12} &= (-508.37 + 3.3910 T - 0.005840 T^2)/T \\ \tau_{21} &= (-763.53 + 5.1484 T - 0.003320 T^2)/T \\ \alpha_{12} &= 0.3\end{aligned}\quad (4-15)$$

However, the NRTL model is inflexible and therefore does not accurately predict activity coefficients at dilute concentrations. The correlation by Dohnal *et al.* (2006) can provide the limiting activity coefficient of ethanol in water at infinite dilution ($\gamma_{Et}^{\infty, Dohnal}$) as a function of temperature in the temperature range 273 - 373 K:

$$\ln \gamma_{Et}^{\infty, Dohnal} = -2.2437 + \frac{6.9054}{\tau} - \frac{34.0965}{\tau} e^{-2.3357\tau} \quad (4-16)$$

where $\tau = T/(298.15 \text{ K})$.

In order to improve the accuracy of predictions of γ_{Et} at dilute concentrations of ethanol below 10 mol%, the predictions of the NRTL model of Voutsas *et al.* (2011), $\gamma_{Et}^{Voutsas}$, were crudely adjusted using the limiting activity coefficient of ethanol predicted by the correlation of Dohnal *et al.* (2006) ($\gamma_{Et}^{\infty, Dohnal}$). This was achieved by scaling the activity coefficients of ethanol predicted by the NRTL model at mole fractions < 10 mol% linearly, from a multiplier of unity at 10 mol% ethanol to a multiplier of $\gamma_{Et}^{\infty, Dohnal}/\gamma_{Et}^{\infty, Voutsas}$ at 0 mol% ethanol, *i.e.* by applying the following formula:

$$\gamma_{Et}(x_{Et}, T) = \gamma_{Et}^{Voutsas}(x_{Et}, T) + S_F \left(\gamma_{Et}^{Voutsas}(x_{Et}, T) - \gamma_{Et}^{10\%, Voutsas}(T) \right) \quad (4-17)$$

where $\gamma_{Et}^{\infty, Voutsas}$; $\gamma_{Et}^{10\%, Voutsas}$; and $\gamma_{Et}^{Voutsas}$ are the activity coefficients of ethanol in water predicted by the NRTL model of Voutsas *et al.* (2011) at, respectively, infinite dilution, an ethanol mole fraction of 10 mol%, and at ethanol mole fraction of x_{Et} . The scaling factor, S_F , is given by:

$$S_F = \left(\frac{\gamma_{Et}^{\infty, Dohnal} - \gamma_{Et}^{\infty, Voutsas}}{\gamma_{Bu}^{\infty, Voutsas} - \gamma_{Bu}^{10\%, Voutsas}} \right) \left(1 - \frac{x_{Et}}{10 \text{ mol\%}} \right) \quad (4-18)$$

4.3.2 Results

The activity coefficients resulting from the adjustment of the NRTL model of Voutsas *et al.* (2011) were fitted to a flexible Legendre activity model with 10 coefficients, with results given in Table 4-2. Table 4-2 also shows the deviation of the Legendre activity coefficient model for ethanol and water from the NRTL model of Voutsas *et al.* (2011). This deviation was based on the relative difference in predicted bubble-point pressures in each model. The virial equation of state was employed to model the vapour phase for the

purpose of these calculations. The maximum deviation was very small, *ca.* 1-2%, occurring at around 2.5 mol% ethanol. Conversely, the difference in the predictions of the limiting activity coefficient of ethanol between the NRTL model of Voutsas *et al.* and the correlation of Dohnal *et al.* was significantly higher: up to ~17% higher at lower temperatures (based on $\ln \gamma_{Et}^{\infty, Dohnal}$ vs. $\ln \gamma_{Et}^{\infty, Voutsas}$). This demonstrates the significant effect that small deviations in bubble-point pressure have on activity coefficients. This further illustrates that inflexible activity models often do not accurately predict activity coefficients at low concentrations, highlighting the need to employ the correlation of Dohnal *et al.* (2006) to correct the activity coefficients of ethanol at low compositions. The method used to adjust the NRTL model was crude and would not predict accurate activity coefficients of water containing dilute ethanol. The method could be improved by altering the gradient of the excess Gibbs free energy (g^E) at dilute ethanol compositions; however this was deemed unnecessary for the purpose of calculating distribution coefficients of dilute ethanol.

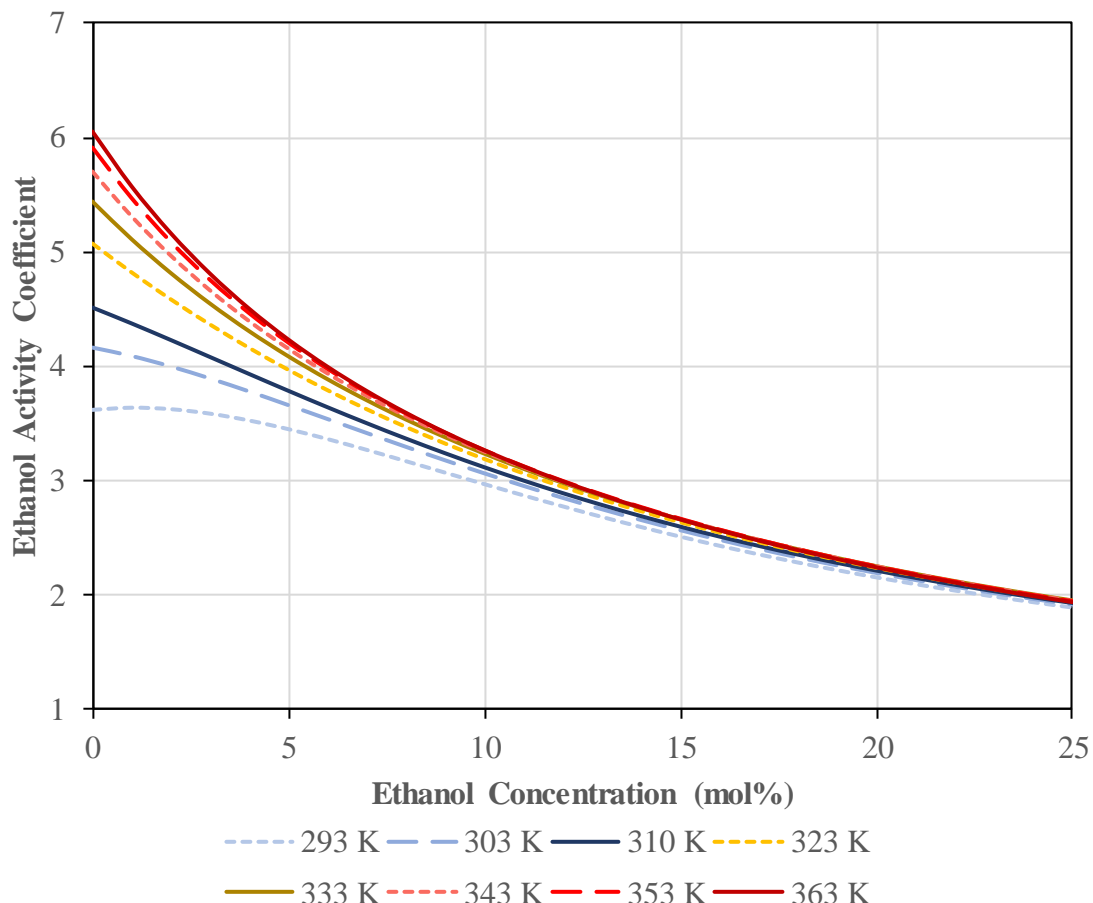


Figure 4-4: The activity coefficient of ethanol in water predicted by the Legendre model

Table 4-2 – Legendre activity coefficients for model of ethanol activity coefficient in water at select temperatures, and maximum deviation of predictions of bubble-point pressure from those of the NRTL model of Voutsas *et al.* (2011)

Temperature (K)	A_0	A_1	A_2	A_3	A_4	A_5	A_6	A_7	A_8	A_9	Max. P_{bubble} Deviation from Voutsas (%)
293.15	1.14878	-0.23856	-0.00432	0.03358	-0.02835	0.01859	-0.01065	0.00436	-0.00128	-0.00072	2.3
298.15	1.16951	-0.25735	0.00790	0.02503	-0.02234	0.01478	-0.00849	0.00348	-0.00102	-0.00057	1.9
303.15	1.18771	-0.27463	0.01897	0.01738	-0.01697	0.01138	-0.00655	0.00269	-0.00079	-0.00044	1.5
310.15	1.20926	-0.29651	0.03271	0.00801	-0.01043	0.00724	-0.00420	0.00173	-0.00051	-0.00028	1.0
313.15	1.21717	-0.30512	0.03801	0.00443	-0.00795	0.00567	-0.00331	0.00136	-0.00040	-0.00022	0.8
323.15	1.23831	-0.33076	0.05346	-0.00581	-0.00088	0.00120	-0.00077	0.00032	-0.00010	-0.00005	0.2
333.15	1.25208	-0.35221	0.06589	-0.01379	0.00457	-0.00223	0.00119	-0.00048	0.00014	0.00007	0.3
343.15	1.25932	-0.37002	0.07580	-0.01992	0.00869	-0.00481	0.00266	-0.00109	0.00033	0.00016	0.6
353.15	1.26072	-0.38467	0.08360	-0.02454	0.01172	-0.00671	0.00373	-0.00154	0.00046	0.00023	0.9
363.15	1.25690	-0.39655	0.08968	-0.02793	0.01390	-0.00805	0.00450	-0.00186	0.00056	0.00027	1.1
373.15	1.24836	-0.40604	0.09434	-0.03034	0.01538	-0.00897	0.00502	-0.00208	0.00063	0.00030	1.2

The activity coefficients of ethanol in water predicted by the Legendre model are shown in Figure 4-4. As the figure shows, the activity coefficient of ethanol at infinite dilution was predicted to increase with temperature between 20°C and 90°C, although the effect was strongest at lower temperatures. The activity coefficient of ethanol was predicted to decrease with composition, to a value of ~3 at all temperatures.

4.4 Calculation of the Activity Coefficient of Aqueous Acetone

Activity coefficients for binary mixtures of acetone and water were regressed from measurements of VLE and excess enthalpy for this binary mixture, given in Table S-1 in the Supplementary Material included with this dissertation. This was performed using the same method presented for binary mixtures of hydrocarbon and alcohol given in Chapter 3. The virial equation of state was employed to model the vapour phase, as detailed in Appendix D. The temperature dependent Legendre coefficients resulting from the regression are given in the Supplementary Material included with this dissertation. The resulting activity coefficients of acetone predicted by the Legendre model are shown in Figure 4-5. As shown, the activity coefficient of acetone at infinite dilution was predicted to increase with temperature, with predictions at 90°C around double those at 20°C. The activity coefficient of acetone was also predicted to decrease with acetone composition; the model predicted a value of ~3.5 at 15 mol% acetone for all temperatures.

Figure 4-6 compares VLE and excess enthalpy measurements with the predictions of the Legendre model. As shown, the model accurately represents the VLE behaviour demonstrated by the measurements across a range of temperatures. The model predicts the formation of an azeotrope with water at a high concentration of acetone at the end of the temperature range (100°C). The model also accurately represents the behaviour of the measurements of excess enthalpies, which demonstrate negative excess enthalpies of mixing a lower acetone compositions and positive excess enthalpies at higher acetone compositions.

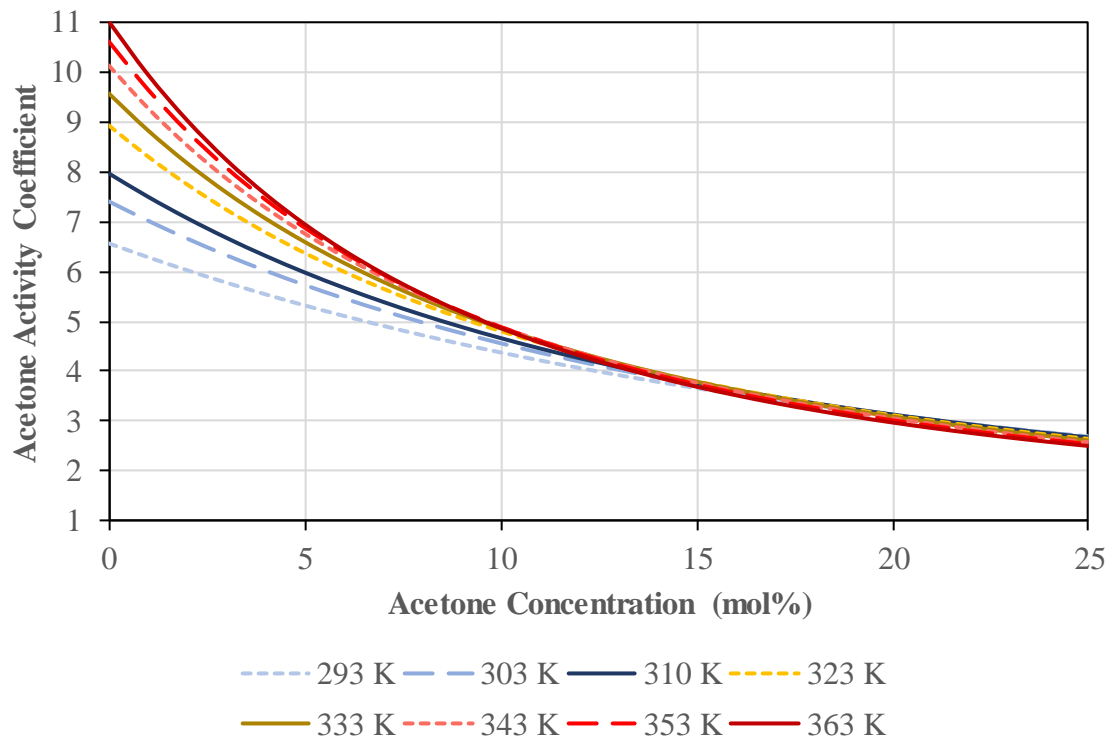


Figure 4-5: Model results for activity coefficient of acetone in water

The average deviation between the model and the corresponding measurements for each dataset ranged from 0.7 – 5.1%, with maximum errors within each dataset being ~4% for VLE measurements and ~7 – 16% for measurements of excess enthalpy. These deviations were probably within the bounds of experimental error for each dataset, although experimental error was difficult to obtain from source literature.

4.5 Predictions of Distribution Coefficients for Dilute Fermentation Products

The distribution coefficients at equilibrium of *n*-butanol, acetone and ethanol in six C₄ – C₆ hydrocarbons *versus* water were predicted at 25 – 100°C. These predictions were made by neglecting the mutual solubility of the hydrocarbons and water, as discussed in Section 4.1.2. The activity coefficients of the fermentation products in the organic, hydrocarbon phase were predicted by employing the Leg-virial Models, developed in Chapter 3. The activity coefficients of *n*-butanol, ethanol and acetone in the aqueous phase were predicted by employing the models developed in Sections 4.2, 4.3 and 4.4 respectively.

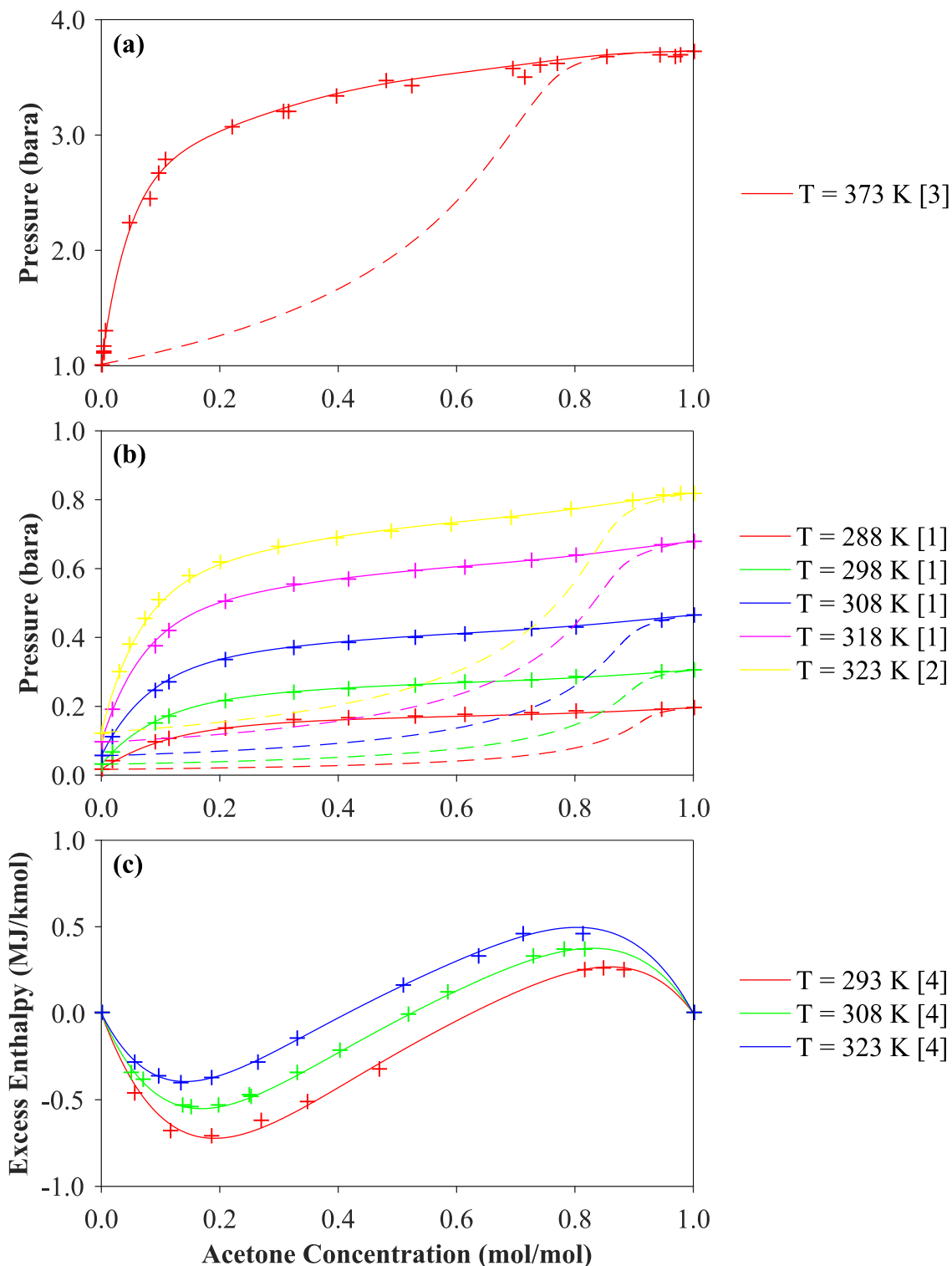


Figure 4-6a-c: Legendre Model predictions and measurements from datasets [1] – [4] for (a,b) vapor-liquid equilibrium; (b) excess enthalpy of acetone and water

Model Lines: Solid line (–) = $P - x$ or H_E ; Dashed Line (--) = $P - y$

Dataset measurements: + = $P - x$ or H_E^E ; \times = $P - y$; \circ = $P - z$

[1] = Rhim *et al.* (1974); [2] = Chaudhry *et al.* (1980); [3] = Griswold and Wong (1952)

[4] = Belousov and Sokolova (1966)

4.5.1 Predicted Distribution Coefficients

The resulting mass distribution coefficients at equilibrium for dilute *n*-butanol in C₄ – C₆ hydrocarbons *versus* water (D_{Bu}^{mass}) are shown in Figure 4-7. These are shown for dilute concentrations of butanol in the aqueous phase, at a range of temperatures. As shown in Figure 4-7, distribution coefficients for *iso*-butane could only be predicted at 318 K because this was the only temperature for which activity coefficients could be determined for binary mixtures with *n*-butanol.

As shown in Figure 4-7, the distribution coefficient of butanol is a strong function of temperature. Distribution coefficients in all six solvents were predicted to increase by a factor of 3-4 between 25°C and 100°C. This increase was to be expected, due to the effects of temperature on the activity coefficients of butanol in water and hydrocarbons. Whilst the activity coefficient of butanol at low concentrations in water was predicted to increase with temperature to a peak at ~60°C, the activity coefficient of butanol in volatile hydrocarbons was predicted to decrease with temperature. Both these effects cause the distribution coefficient of butanol between hydrocarbons and water phases to increase with temperature. Above 60°C, the activity coefficient of butanol in water was predicted to decrease slightly. However, the effect of the decrease in activity coefficient of butanol in hydrocarbons was large enough that the distribution coefficient was predicted to continue increasing above 60°C. A peak in the distribution coefficient of butanol can be seen at the upper end of the temperature range investigated (100°C) for *n*-hexane, 1-hexene and 1-butene for aqueous concentrations of butanol of around 2 – 3 wt%.

In general, predictions of D_{Bu}^{mass} were also found to increase with butanol composition (shown in Figure 4-7 as the mass fraction in the aqueous phase). For example, D_{Bu}^{mass} was predicted to increase by ~50% between infinite dilution and 2 wt% in 1-butene. The predicted increase of D_{Bu}^{mass} with butanol composition was smaller for the larger hydrocarbons. Indeed, for C₆ hydrocarbons, values of D_{Bu}^{mass} at 100°C were actually predicted to slightly decrease with butanol concentration.

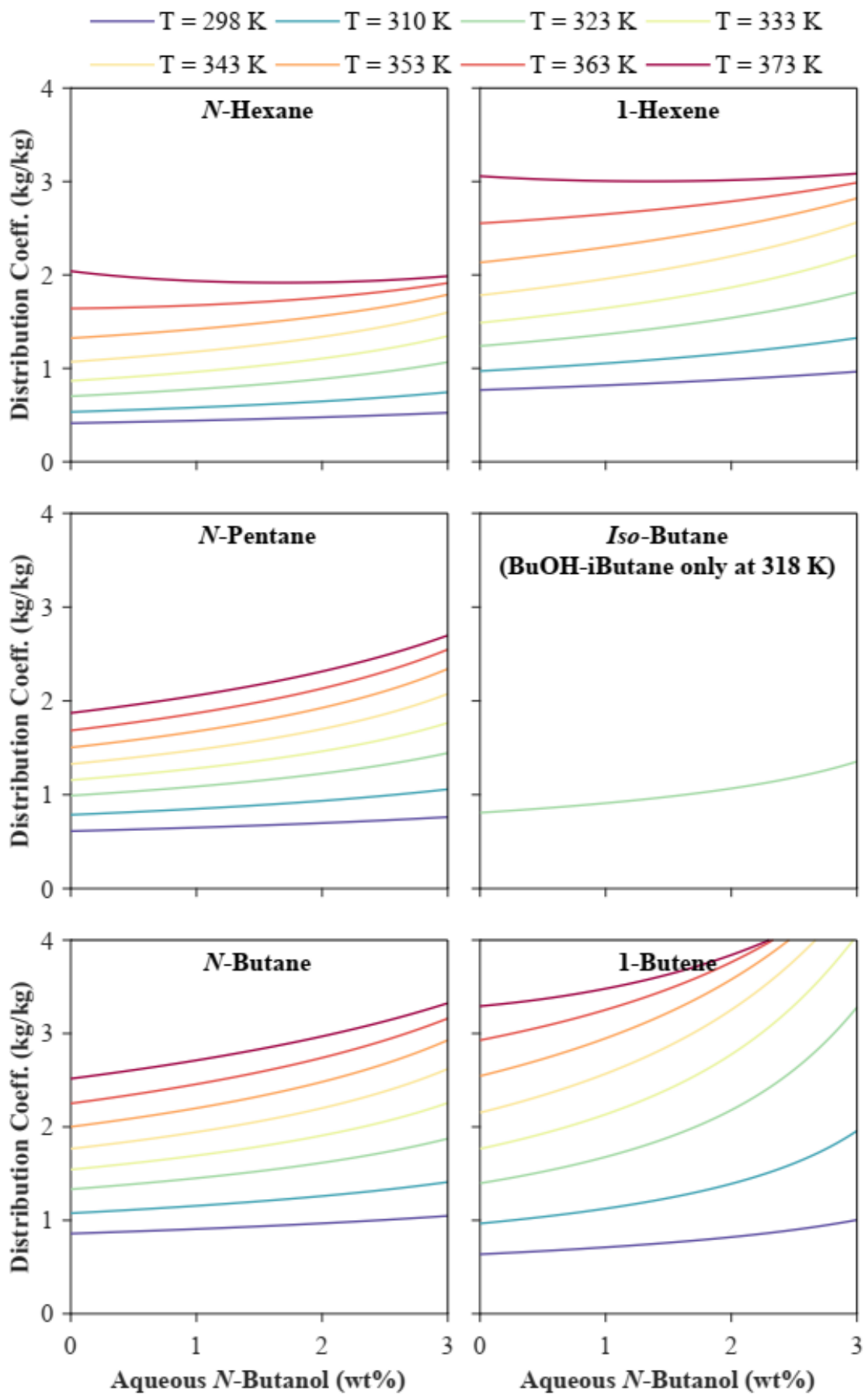


Figure 4-7: Predictions of the mass distribution coefficient of *n*-butanol in six hydrocarbons *versus* water at 298 – 373 K

N-butane, 1-butene and 1-hexene produced the highest distribution coefficients, with values at infinite dilution ranging from 0.65 kg/kg at 25°C to 3.4 kg/kg at 100°C. Of these solvents, 1-butene displayed a greater increase in distribution coefficient with temperature and concentration, reaching 3.6 kg/kg at 100°C, for 2 wt% butanol in the aqueous phase. All three hydrocarbons were predicted to perform similarly at typical fermentation temperatures, producing distribution coefficients of around 1 kg/kg at infinite dilution, and *ca.* 1.2, 1.3 and 1.5 kg/kg in 1-hexene, *n*-butane and 1-butene respectively at 37°C, for 2 wt% butanol in the aqueous phase. *N*-pentane and *n*-hexane performed similarly, producing distribution coefficients ranging from ~0.5 kg/kg at ambient to temperatures to a maximum of 2.4 kg/kg for *n*-pentane at 100°C, 2 wt%.

Figure 4-8 compares the mass distribution coefficients predicted for *n*-butanol in *n*-hexane *versus* water, with those predicted for *iso*-butanol. As can be seen in Figure 4-8, *iso*-butanol was predicted to behave very similarly to *n*-butanol. Predictions of distribution coefficients at infinite dilution at higher temperatures were up to 25% higher for *iso*-butanol than *n*-butanol, although the difference in predicted distribution coefficients between the two isomers was much smaller at lower temperatures and higher butanol compositions.

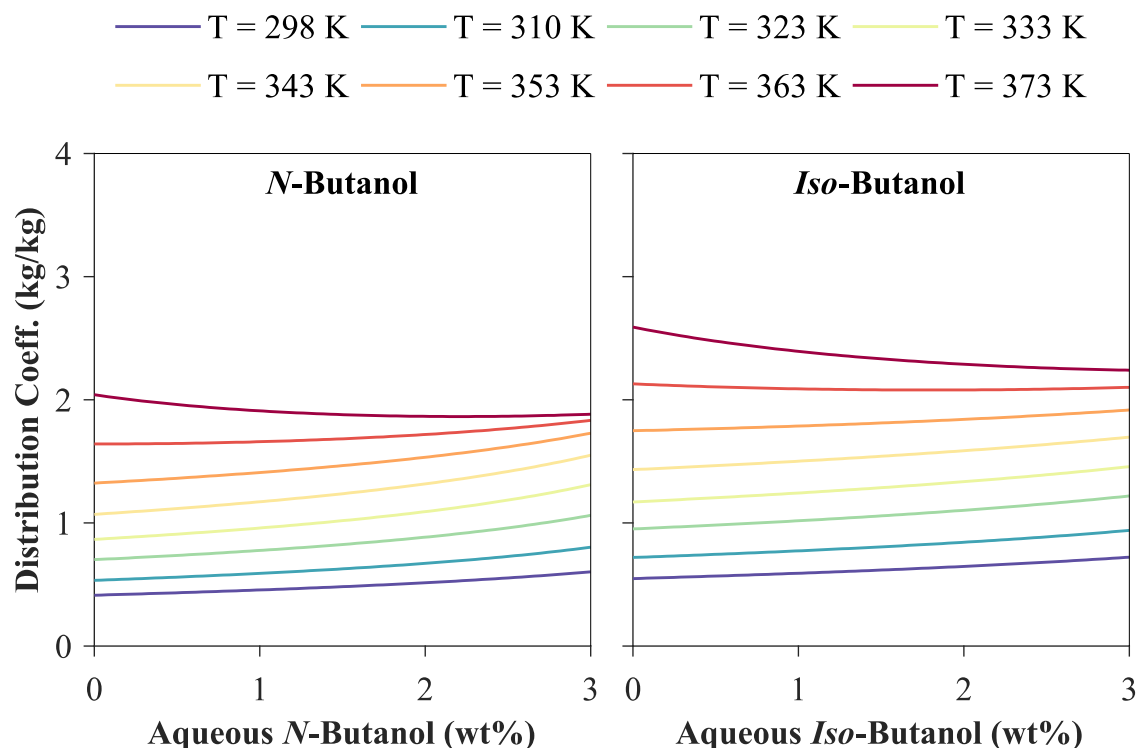


Figure 4-8: Predictions of the mass distribution coefficient of *n*-butanol and *iso*-butanol in *n*-hexane *versus* water at 298 – 373 K

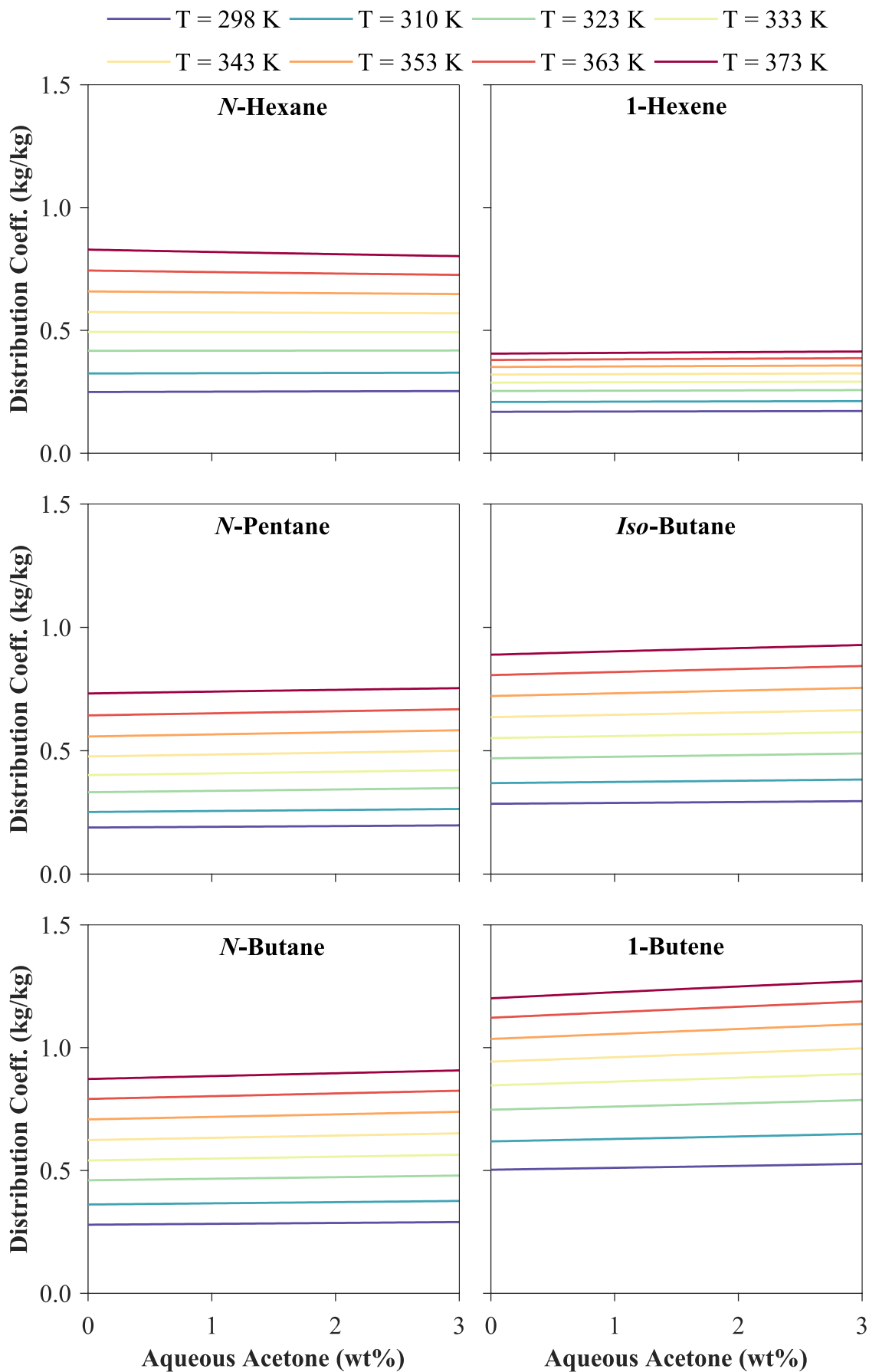


Figure 4-9: Predictions of the mass distribution coefficient of acetone in six hydrocarbons *versus* water at 298 – 373 K

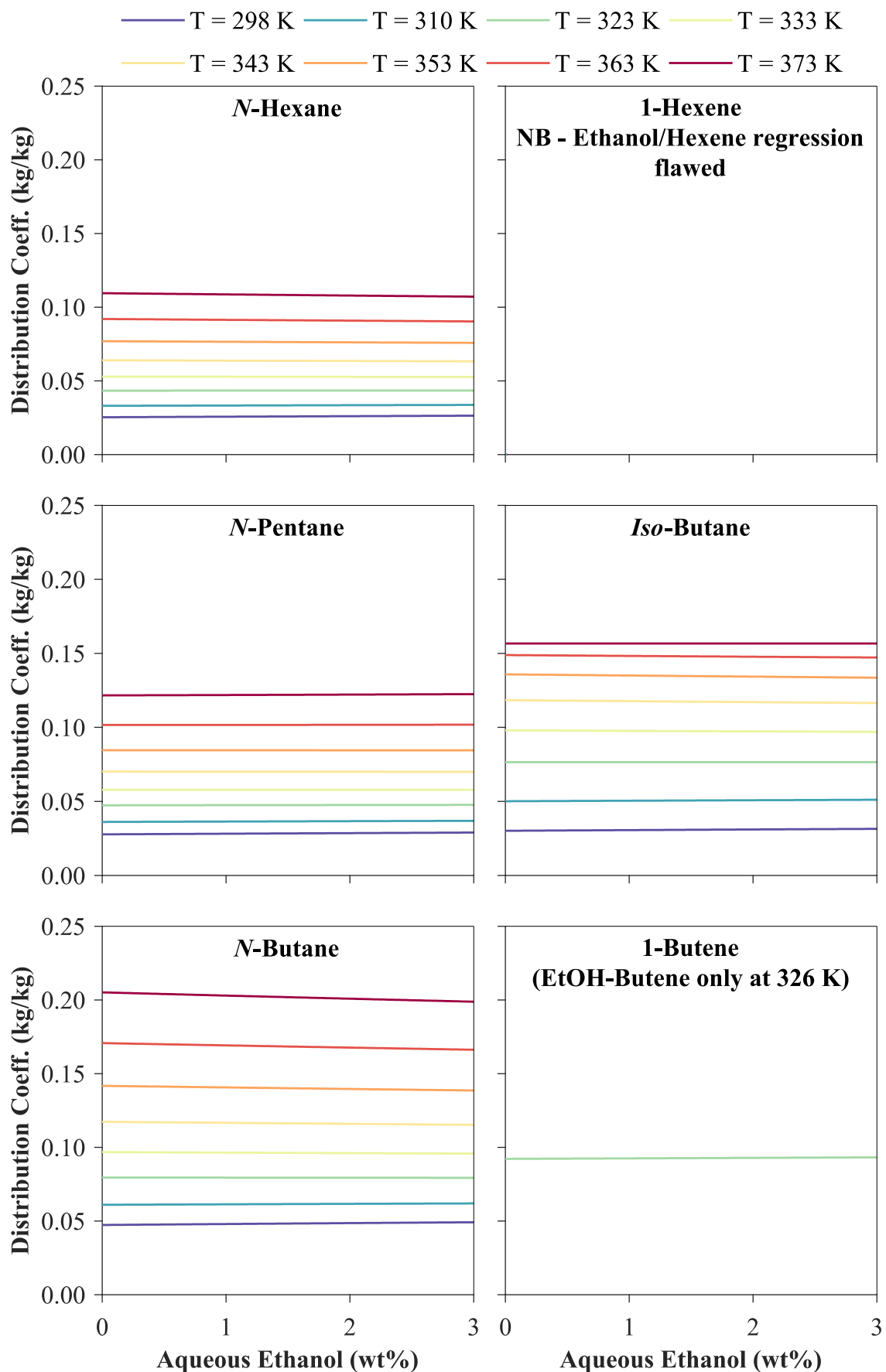


Figure 4-10: Predictions of the mass distribution coefficient of ethanol in six hydrocarbons versus water at 298 – 373 K

The predictions of mass distribution coefficients for dilute acetone and ethanol in C₄ – C₆ hydrocarbons *versus* water (D_{Ace}^{mass} and D_{Et}^{mass} respectively) are shown in Figure 4-9 and Figure 4-10 respectively. These are shown for dilute compositions in the aqueous phase at a range of temperatures. Figure 4-9 and Figure 4-10 show similar trends for the distribution coefficients of both acetone and ethanol in volatile hydrocarbons. Distribution coefficients increased with temperature for both products. This was to be expected, because the activity coefficients of both ethanol and acetone in water were predicted to increase with temperature, whilst they were predicted to decrease with temperature in hydrocarbons. The combination of these effects led to predictions of an increase in distribution coefficient by a factor of 3-4 between 25°C and 100°C, similar to the increase predicted for butanol. Unlike butanol, the distribution coefficients of acetone and ethanol were not predicted to reach a maximum in this temperature range because the activity coefficients of ethanol and acetone in water do not pass through a maximum. The concentration of ethanol and acetone does not appear to have a significant effect on distribution coefficient.

For acetone, predicted values of distribution coefficients were relatively low compared to those of butanol: distribution coefficients of acetone ranged from ~0.25 kg/kg at 25°C to ~0.8 kg/kg at 100°C for most of the hydrocarbons. The exception was 1-butene, which was predicted to perform slightly better, with distribution coefficients ranging from 0.5 kg/kg at 25°C to 1.2 kg/kg at 100°C. Ethanol distribution coefficients were very low compared to butanol, with distribution coefficients ranging from around 0.025 kg/kg at 25°C to 0.12 kg/kg at 100°C for *n*-hexane and *n*-pentane respectively; and 0.03–0.05 kg/kg at 25°C to 0.15–0.20 kg/kg at 100°C for the C₄ solvents.

4.5.2 Predicted Selectivity of Butanol over Side-Products

Figure 4-11 uses the predictions of distribution coefficients to calculate the selectivity of *n*-butanol over ethanol and acetone in hydrocarbon solvents *versus* water as a function of temperature and aqueous butanol composition. Selectivity was calculated as:

$$S_{Bu,Ace}(m_{Bu}^{aq}, T) = \frac{D_{Bu}^{mass}(m_{Bu}^{aq})}{D_{Ace}^{mass}(m_{Ace}^{aq})}; \quad S_{Bu,Et}(m_{Bu}^{aq}, T) = \frac{D_{Bu}^{mass}(m_{Bu}^{aq})}{D_{Et}^{mass}(m_{Et}^{aq})} \quad (4-19)$$

where $S_{Bu,j}$ is the selectivity of butanol over fermentation product *j*, *T* is the extraction temperature (K) and m_i^{aq} is the mass fraction of fermentation product *i* (wt%).

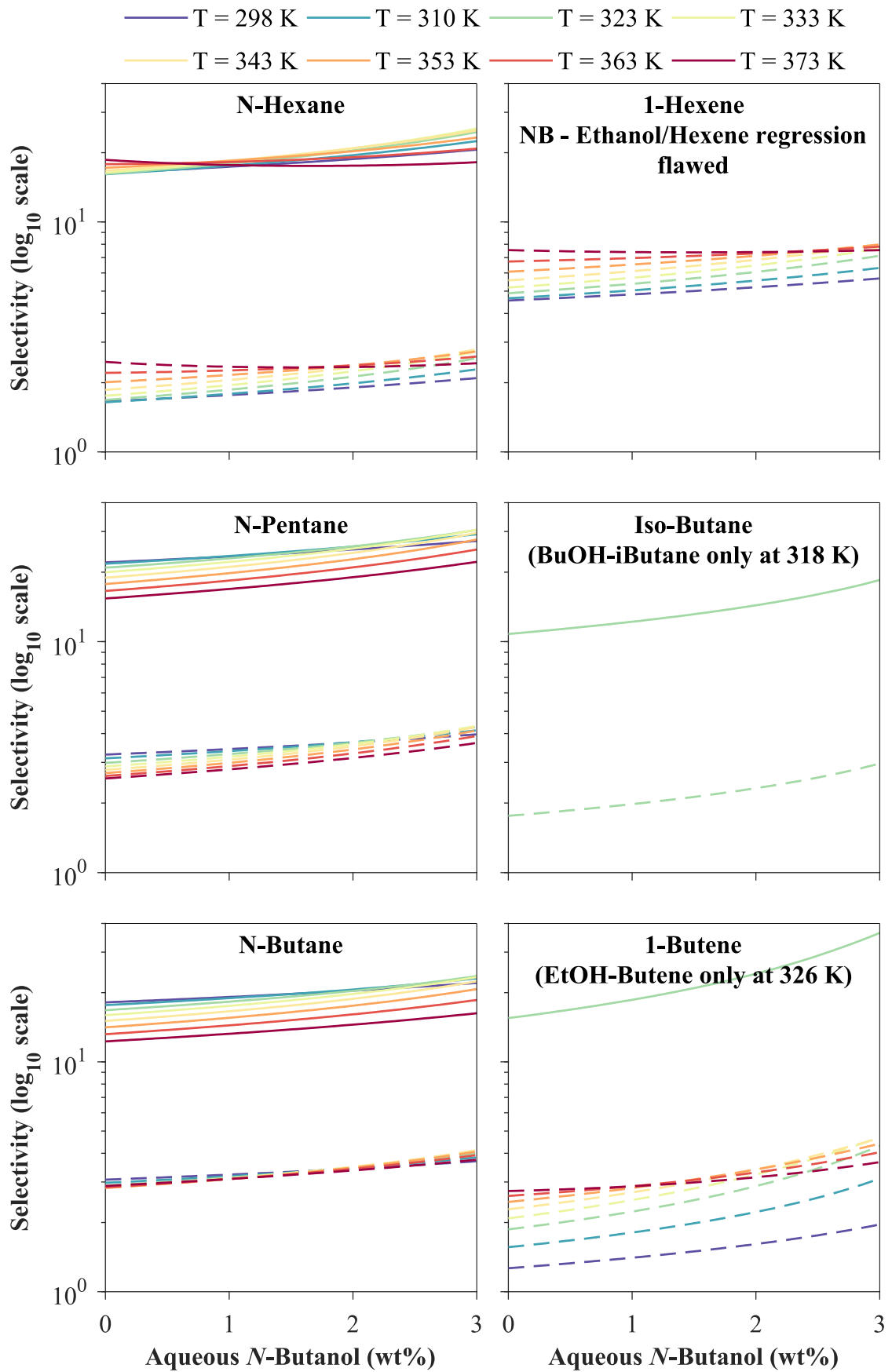


Figure 4-11: Predictions of selectivity of *n*-butanol over ethanol (solid lines) and acetone (dashed lines) in six hydrocarbons versus water at 298 – 373 K, for aqueous ABE mixtures in molar ratio 0.5 : 1: 0.167 (acetone: butanol: ethanol)

Acetone, butanol and ethanol were assumed to be present in the aqueous phase in the molar ratio of 0.5 : 1 : 0.167, typical for ABE broths (Green, 2011), which equate to a mass ratio of 0.4 : 1 : 0.1.

The predictions of low distribution coefficients for ethanol compared with those of *n*-butanol is reflected in the selectivity of butanol over ethanol in Figure 4-11. Predictions of the selectivity of butanol over ethanol ranged from around 10 – 30, with selectivity over ethanol generally predicted to decrease with temperature for the *n*-alkanes (the only solvents for which the temperature dependence of selectivity over ethanol was available). However, selectivity over ethanol in *n*-hexane demonstrated the opposite relationship with temperature at very low butanol concentration.

Predictions of the selectivity of *n*-butanol over acetone showed considerably more variation across the solvents. *N*-butane and *n*-pentane were predicted to produce butanol selectivities over acetone of ~3, with a small negative gradient with temperature. Conversely, butanol selectivities over acetone in *n*-hexane, 1-hexene and 1-butene were predicted to display larger, and mostly positive, gradients with temperature. However, the selectivity over acetone was predicted to peak at 100°C for aqueous compositions of 1 – 2 wt% butanol in these solvents. The selectivity over acetone was found to be highest in 1-hexene (values of 4 - 8), and lowest in 1-butene and *n*-hexane (values of 1 – 3).

4.5.3 Comparison with Experimental Measurements

Published measurements of ternary LLE, or alternatively of liquid-liquid extraction (LLX) trials, for relevant systems were scarce, especially at low concentrations. Three sources of ternary LLE for *n*-butanol in *n*-hexane and water were identified, in addition to a distribution coefficient of 0.5 kg/kg measured for butanol extraction by *n*-hexane at 37°C (Groot *et al.*, 1990). The measurements of LLE were converted into distribution coefficients for comparison with model predictions of the distribution coefficient for *n*-hexane. This comparison is shown in Figure 4-12. As shown in the figure, the model predictions loosely correspond with the measurements of Groot *et al.* (1990) and Islam and Kabadi (2011). However, predictions are much lower than those of Sugi and Katayama (1977) and Gomis *et al.* (2012).

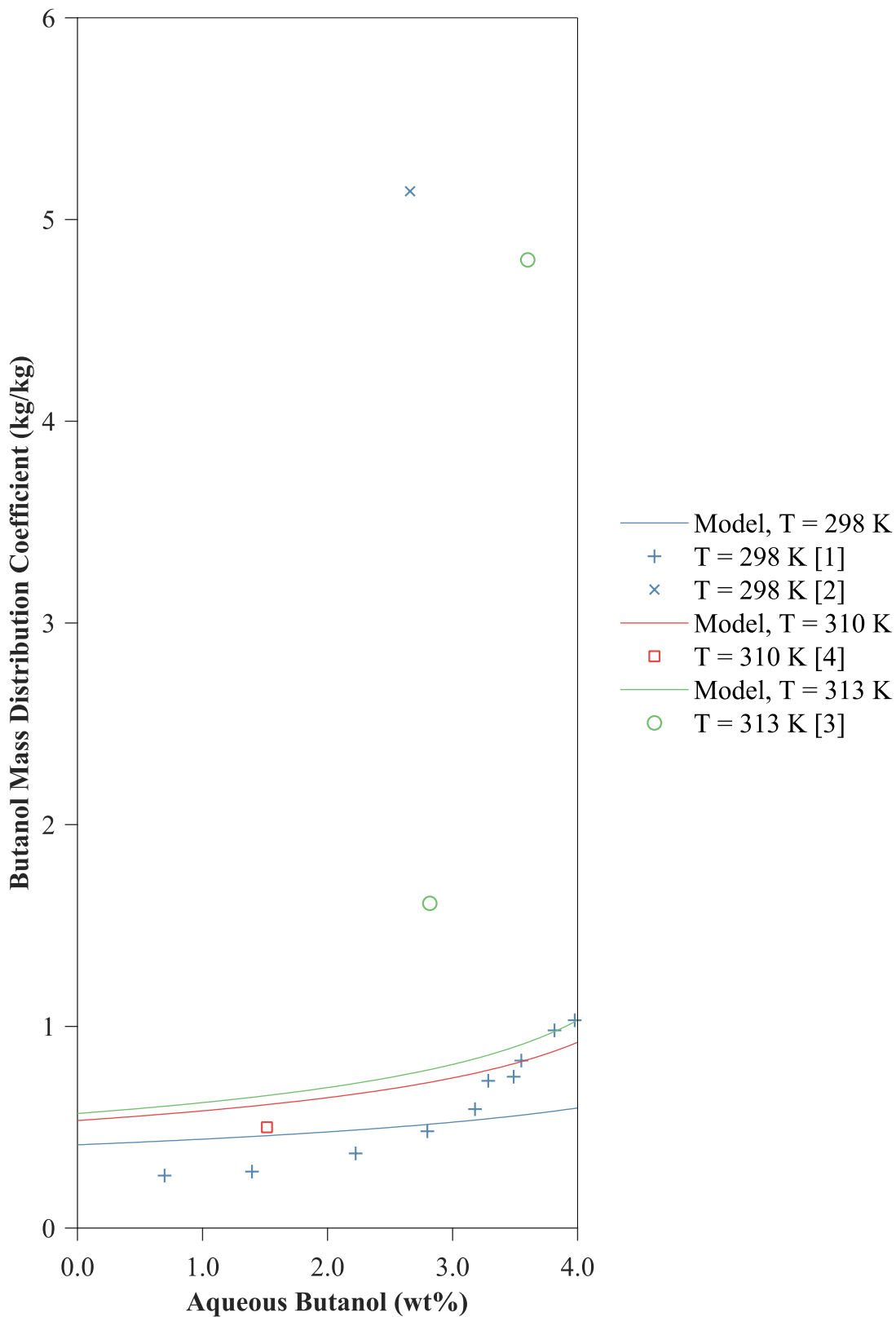


Figure 4-12: Comparison of predictions of the mass distribution coefficient of *n*-butanol in *n*-hexane *versus* water with experimental measurements of ternary LLE and liquid-liquid extraction tests

[1] = Islam and Kabadi (2011); [2] = Sugi and Katayama (1977);

[3] = Groot *et al.* (1990); [4] = Gomis *et al.* (2012)

Figure 4-13 and Figure 4-14 compare predictions of distribution coefficients of ethanol with those calculated from ternary LLE measurements available in the literature for ethanol in *n*-hexane and *n*-pentane *versus* water respectively. However, the lowest compositions of ethanol available in the measurements of LLE were ~10 - 20 wt%. At these ethanol compositions, the dilute assumptions of the model are not likely to be valid.

As shown in Figure 4-13 and Figure 4-14, the distribution coefficients predicted for ethanol were of a similar order of magnitude to those calculated from experimental measurements of LLE. However, significant disagreement existed between the scarce measurements of LLE for ethanol, even between those obtained from the same source.

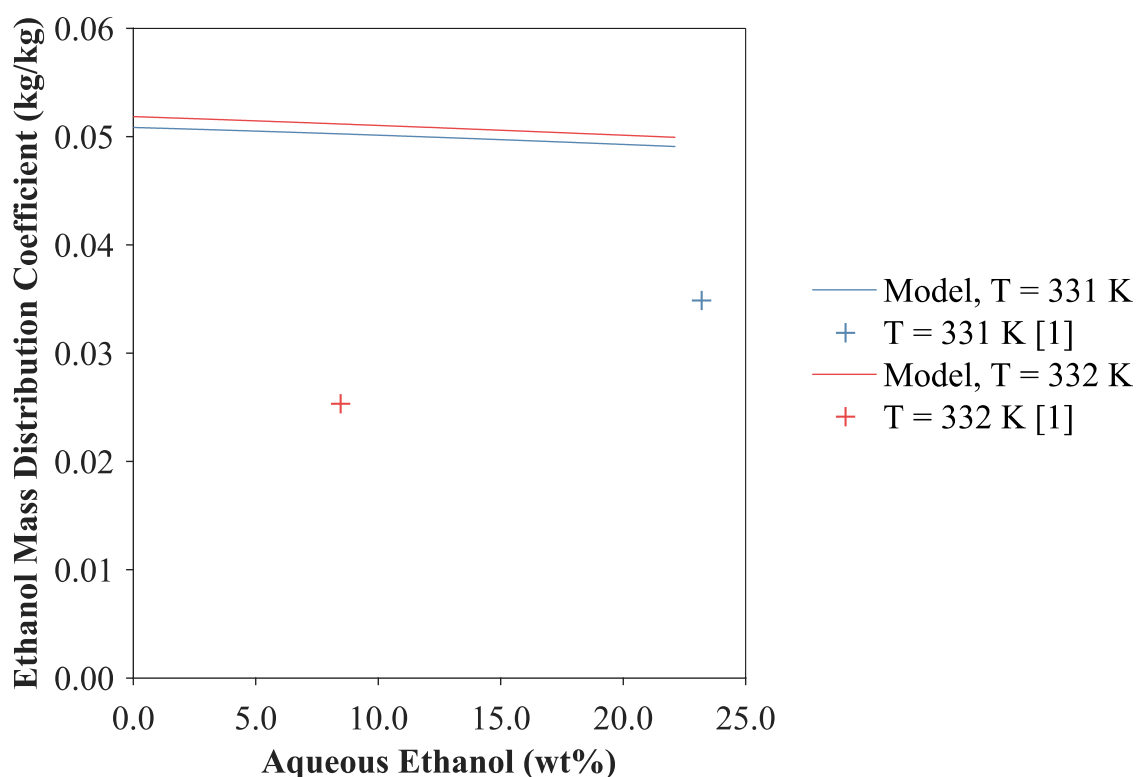


Figure 4-13: Comparison of predictions of mass distribution coefficient of ethanol in *n*-hexane *versus* water with measurements of ternary LLE by [1] Gomis *et al.* (2007)

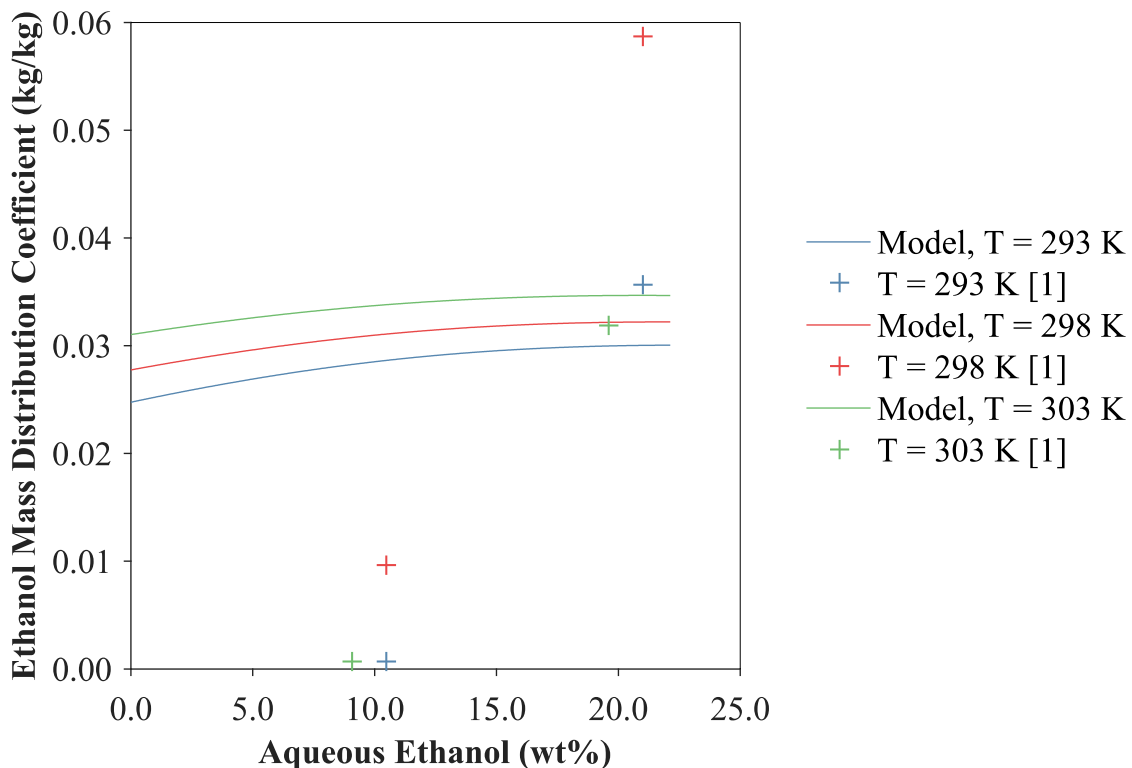


Figure 4-14: Comparison of predictions of mass distribution coefficient of ethanol in *n*-pentane *versus* water with measurements of ternary LLE by [1] Qasim *et al.* (2016)

4.5.4 Discussion

The predictions of the distribution coefficients of butanol, shown in Figure 4-7, produced a similar trend to those estimated (at infinite dilution) in Section 2.6. The estimates in Section 2.6 were calculated by considering the gradient of the bubble-point pressure at infinite dilution, relative to that of Raoult's Law (\mathcal{M}). Predicted values for the distribution coefficients at infinite dilution in C₆ hydrocarbons in Figure 4-7 were close to those estimated in Section 2.6. This was expected, since $\mathcal{M} \sim 0$ for these hydrocarbons, and the value of distribution coefficient is largely unaffected by the accuracy of \mathcal{M} for $\mathcal{M} \sim 0$. However, for C₄ hydrocarbons (for which $\mathcal{M} \sim 1$), the estimates produced in Section 2.6 significantly underestimated the value of distribution coefficient. Calculated distribution coefficients in 1-butene from Figure 4-7 were around twice those estimated in Section 2.6, whilst distribution coefficients in *n*-butane at low temperature were almost an order of magnitude higher than estimated in Section 2.6. The higher values predicted in Figure 4-7 meant that the C₄ alkanes were predicted to outperform *n*-hexane in terms of distribution coefficient by as much as a factor of 2, contrary to the conclusions based

on the estimates in Section 2.6. *N*-butane had the highest distribution coefficient for butanol at infinite dilution at fermentation temperatures (~1 kg/kg at 37°C).

Solvents with a high selectivity for butanol over acetone or ethanol would provide a highly selective extraction process, removing butanol with very little transfer of side-products. Solvents with a lower selectivity would mean a higher transfer of side-products, which would potentially allow side-products to be separated from the broth using the extraction process. Figure 4-11 suggests that the selectivity of butanol over ethanol in C₄ – C₆ hydrocarbons is very high, and hence transfer of ethanol into these solvents during extraction would probably be minimal. The selectivity of butanol over acetone varies with solvent: it was predicted to be lower (~1.5) for 1-butene at fermentation temperatures and low aqueous compositions (< 1 wt% aqueous butanol); conversely, it was predicted to be ~4 for pentane at high aqueous compositions (>3 wt% aqueous butanol). Therefore, with careful selection of the solvent and extraction temperature, it might be possible to remove substantial quantities of acetone side-products from the fermentation broth as part of an extraction using volatile hydrocarbons. Equally, it would be possible to remove butanol selectively. Acetone's high volatility would mean that even if high quantities were transferred to the extractant, a substantial proportion of the acetone in the extractant stream would be vaporised during distillation.

As shown in Figures 4-12 – 4-14, there was significant disagreement amongst different sources of LLE measurements, suggesting that the LLE at these low concentrations is difficult to measure accurately. LLE measurements suffer from similar experimental difficulties as those found in *Pxy* VLE measurements, because the concentration of two phases must be measured simultaneously, requiring recirculating equilibrium cells. Regardless, the model predicted distributions coefficients of a similar magnitude to those given by measurements of LLE. However, due to the variation in, and limited quantity of, measurements at dilute concentrations, it is difficult to draw any firm conclusions about the accuracy of the distribution coefficient model in comparison with empirical values.

4.5.5 Conclusion

Of the six solvents modelled, 1-butene shows the greatest potential as an extractant, especially for extraction at an elevated temperature or in broths of high butanol titre. The mass distribution coefficients of 1-hexene and *n*-butane were predicted to be similar to those of 1-butene at fermentation temperatures, and indeed slightly higher at 25°C at

infinite dilution. The lower volatility of 1-hexene means that it would require highly reduced pressures to perform distillation from butanol using low-grade heat. However, *n*-butane would be an excellent potential alternative to 1-butene, especially for extractions of dilute butanol at fermentation temperatures, with both solvents yielding a mass distribution coefficient at infinite dilution of ~1 kg/kg at 37°C.

As expected, a significant increase in butanol distribution coefficient with temperature was predicted, increasing by a factor of around 3 - 4 between 25°C and 100°C. However, some solvents showed a peak in distribution coefficient at the upper end of this temperature range for higher compositions of butanol. Predictions of the distribution coefficients of *iso*-butanol in *n*-hexane were slightly higher than those of *n*-butanol, by up to 25% at higher temperatures and at infinite dilution. This suggests that the energy requirements for the separation of *iso*-butanol would be lower than those of *n*-butanol in an extraction process employing volatile hydrocarbons as extractants. However, further equilibria measurements for *iso*-butanol systems are required to confirm this conclusion.

But-1-ene was also predicted to possess the highest distribution coefficients for acetone amongst the solvents modelled, with a mass distribution coefficient for acetone of ~0.6 kg/kg at 37°C. This is potentially advantageous if the extraction of acetone is desirable. Distribution coefficients for ethanol for all solvents were predicted to be very low (~0.1 kg/kg). The predictions of distribution coefficient loosely correlate with the limited quantity of measurements of LLE available at low solute concentrations. However, the accuracy and limited quantity of these measurements made verifying the model impossible.

4.6 Design and Efficiency of the Liquid-Liquid Extraction Unit

Thus far, the equilibria of the extraction of butanol from the aqueous broth into hydrocarbons has been investigated. However, in practice, the effects of mass transport might limit the transfer of butanol in the extraction. There are many designs of extraction units, but two simple design cases will be considered here:

- Direct extraction in the fermenter, *in situ*;
- Counter-current extraction ‘*in stream*’

4.6.1 Direct Extraction in the Fermenter, *in situ*

Direct extraction in the fermenter is attractive because it does not involve additional equipment. If sufficient contact time and area were provided between the two phases, it

would be possible to achieve near-equilibrium between the aqueous broth and a hydrocarbon extractant in the fermenter, thereby maximizing the concentration of butanol in the solvent phase.

One simple design to achieve high contact between the two phases would be to disperse the solvent in the broth at the bottom of the fermenter. Since the solvent is lighter than the aqueous phase, the bubbles of solvent would rise and coalesce at the surface, forming a layer of solvent containing extracted products. Butanol-rich solvent might be drawn off this top layer and sent to the distillation system for solvent recovery. The solvent flowrate could be used to control (and hence limit) the butanol titre in the broth to prevent product toxicity.

Whilst direct extraction in the fermenter is an attractive proposition, there are several design challenges and restrictions. Firstly, the extraction would be performed at the broth temperature; extraction at elevated temperature would not be possible. In addition, the fermenter would have to be operated at a total pressure above the solvent vapour pressure at the fermentation temperature in order to keep the solvent in the liquid phase. This could be problematic for the more volatile solvents, such as C₄ hydrocarbons, which would necessitate operating the fermenter at pressures in excess of 3 – 4 bara. This elevated pressure could impact on gas product (*e.g.* CO₂) concentrations in the liquid broth, and consequently affect the organism productivity. In addition, significant quantities of volatile solvent might be evaporated into the fermenter off-gas, potentially necessitating even higher pressures to minimise this loss, or requiring energy-intensive solvent recovery from the fermenter off-gas.

Solvent loss in the gas phase might be even more problematic in the fermentation of synthesis gases, where gas flowrates are high. However, such fermentation systems might benefit from operating at elevated pressure, since this improves mass transfer of CO and H₂ substrates into the broth. *In situ* extraction could also result in significant quantities of gaseous substrate being carried over into the solvent phase. Fermenter designs for the fermentation of synthesis gases are often relatively complex in order to assist with the poor mass transfer of CO and H₂ into the aqueous phase, and so the addition of another liquid phase might complicate this further. High levels of agitation in the fermenter could prevent the dispersed solvent phase from coalescing, leading to foaming or the formation of emulsions.

In situ extraction would also lead to an increased direct exposure of organisms to the solvent, thereby exacerbating the any effects of the toxicity of the solvent. Indirect toxicity issues (due to removal of key intermediates, for example) might also be exacerbated due to high mass transfer driving forces between the broth and the solvent.

Many of these issues cannot easily be accounted for theoretically, and vary with the fermenter type, fermentation process and organism. Key properties for the quantification of problems such as mass transfer and solvent coalescence include interfacial tensions, phase densities and viscosities, all of which vary significantly with the exact broth composition. Therefore, experimental work on the relevant organism, fermenter and broth would be required in order to examine these issues. However, extraction of butanol directly in the fermenter remains an attractive proposition due to its apparent simplicity and high driving force for mass transfer. It is probably feasible for some fermentation processes, given that it has been demonstrated for other solvents, *e.g.* for the extraction of butanol directly into biodiesel (Yen and Wang, 2013). Some researchers have taken the idea further still, and have proposed conducting ABE fermentation, extraction, and distillation separation of the solvent and butanol, all in a single unit (Jin *et al.*, 2017).

4.6.2 Counter-Current Extraction, '*in stream*'

Counter-current extraction in a separate unit to the fermenter would require an additional piece of equipment compared to direct extraction in the fermenter. However, this would allow more flexibility in the design. Employing a separate liquid-liquid extractor would de-couple the mass transfer processes in the fermenter from those in the extraction, allowing each of these to be optimised separately. The extraction could be performed at a different temperature from that of the fermentation; in the presence of organisms *in stream*; or following the filtration of the organisms, when thermal shock or toxicity issues are of concern. The extraction could also be performed at a different pressure to the fermentation, reducing issues surrounding gaseous fermentation substrates and products in the fermenter. Depending on the design of the extraction system, the system could be optimised to reduce the formation of emulsions and to separate the two phases efficiently.

Counter-current operation would allow the driving force for mass transfer to be maximised, although a large number of stages might be required to produce solute concentrations close to equilibrium with the fermentation broth. Many different types of counter-current equipment exist and are well-documented, the choice of which depends on the physical properties of the extraction and the scale of operation (Treybal, 1951).

These include: spray towers; packed towers; baffle towers; perforated plate-towers; mixer-settler systems; spinner columns.

The number of stages employed in a counter-current liquid extraction is a compromise between the number of equilibrium stages (which increases capital costs, and operation costs due to increased pressure drops) and the effective distribution coefficient achieved in the distillation column. This compromise has been briefly examined in the model depicted in Figure 4-15. In this simple model, the following simplifying assumptions were made:

- Only butanol and water were considered in the fermentation broth. This was considered to be a reasonable approximation for this simple model, given that the predictions of the selectivity of butanol over side-products were high, and that the concentration of other components in the broth would probably be very low.
- Water and the solvent were approximated as being completely immiscible and hence only butanol and the solvent were considered in the solvent phase. Given the low mutual solubilities of water with C₄ – C₅ hydrocarbons, this assumption was reasonable.
- Butanol was assumed to be dilute (*c.f.* typical broth titres of ~1 wt%)
- The solvent recycle was assumed to be pure (*i.e.* butanol-free). Due to the high volatility difference between C₄ – C₅ hydrocarbons and butanol, this was a reasonable approximation for the separation by distillation of butanol and the solvent.
- The mass distribution coefficient was assumed to be approximately constant for the range of butanol compositions in the extractor; the extractor was assumed to be isothermal to eliminate any variations due to temperature.

The distribution coefficient based on mass fractions, rather than the molar distribution coefficient, was employed. For butanol systems, molar distribution coefficients were found to vary slightly more with butanol composition in the relevant range (0 - ~3wt%) than their equivalent mass distribution coefficients, due to the difference in the molar masses of butanol and water.

The proportion of butanol drawn from the broth transferred into the solvent phase was defined in the parameter η ('transfer efficiency'):

$$\eta = \frac{\text{Butanol in solvent product}}{\text{Butanol in aqueous LLX feed}} \quad (4-20)$$

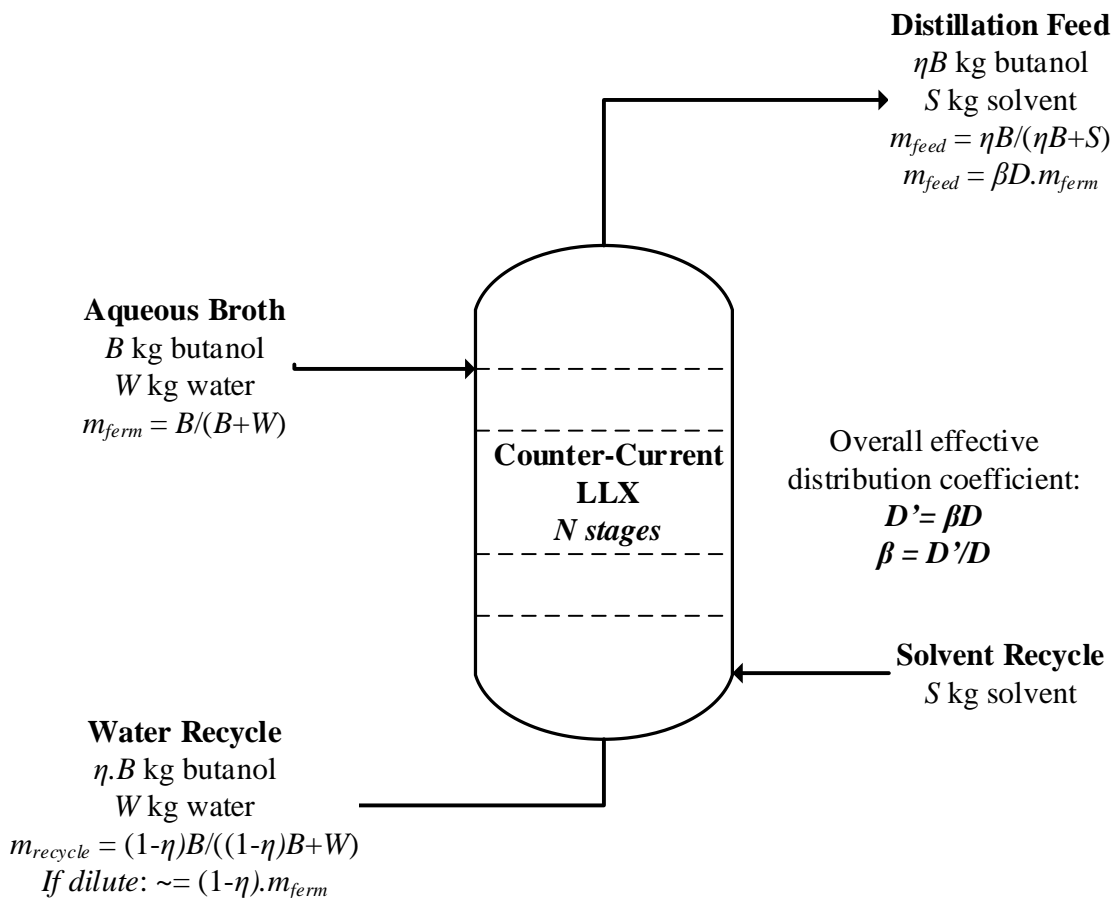


Figure 4-15: Simple model of counter-current extraction, *in stream*, of butanol from fermentation broths

m_x = mass fraction of butanol in stream x

Therefore, if B kg of butanol were present in the aqueous feed to the LLX, $\eta \cdot B$ kg of butanol would be transferred to the solvent, and $(1 - \eta)B$ kg of butanol would be recycled to the fermenter, as shown in Figure 4-15. By neglecting the mutual solubility of water and the solvent, and assuming the aqueous phase is dilute ($B \ll W$):

$$m_{ferm} = \frac{B}{B + W} \cong \frac{B}{W} \quad (4-21)$$

$$m_{recycle} = \frac{(1 - \eta)B}{(1 - \eta)B + W} \cong \frac{(1 - \eta)B}{W} = (1 - \eta)m_{ferm} \quad (4-22)$$

By assuming that the distribution coefficient was approximately constant with butanol composition, and the system was dilute and immiscible (*i.e.* solvent flowrates in both phases were constant in the extraction), the number of theoretical equilibrium stages was calculated from the Kremser equations (Green, 1997). Assuming that the solvent recycle was butanol-free, the number of theoretical equilibrium stages (N) was given by:

$$N = \begin{cases} \frac{\ln \left[\left(\frac{m_{ferm}}{m_{recycle}} \right) \left(1 - \frac{1}{\epsilon} \right) + \frac{1}{\epsilon} \right]}{\ln \epsilon}, & \epsilon \neq 1 \\ \frac{m_{ferm}}{m_{recycle}} - 1, & \epsilon = 0 \end{cases} \quad (4-23)$$

$$\epsilon = \frac{S \cdot D_{Bu}^{mass}}{W} \quad (4-24)$$

The ‘extraction efficiency’, β , was defined as the difference between the distribution coefficient at equilibrium (D_{Bu}^{mass}) and the *effective* distribution coefficient ($D_{Bu}'^{mass}$), *i.e.* the ratio between the mass fraction in aqueous butanol (the broth drawn from the fermenter, m_{ferm}) and the mass fraction of butanol in the solvent extract (the ‘feed’ to the distillation system, m_{feed}):

$$\beta = \frac{D_{Bu}'^{mass}}{D_{Bu}^{mass}}; D_{Bu}'^{mass} = \frac{m_{feed}}{m_{ferm}} \quad (4-25)$$

Hence, from the definitions of β and η , the number of theoretical stages is given by:

$$\epsilon = \frac{\eta}{\beta} \quad (4-26)$$

$$N = \begin{cases} \frac{\ln \left(\frac{1 - \eta}{1 - \beta} \right)}{\ln \left(\frac{\eta}{\beta} \right)}, & \eta \neq \beta \\ \frac{\eta}{1 - \eta}, & \eta = \beta \end{cases} \quad (4-27)$$

Hence, as η or β approach unity, the number of theoretical stages approaches infinity. The transfer efficiency, η , affects the aqueous flowrate to and from the fermenter. This can be shown by considering the quantity of butanol transferred (assuming the aqueous phase is dilute):

$$\eta B = (m_{recycle} - m_{ferm})W \quad (4-28)$$

Therefore, substituting eqs. (4-21) and (4-22) for m_{ferm} and $m_{recycle}$:

$$\therefore \left(\frac{W}{\eta B} \right) = \frac{1}{\eta \cdot m_{ferm}} \text{ kg/kg butanol transferred} \quad (4-29)$$

Hence, low values of transfer efficiency increase any operating costs associated with the aqueous side (*e.g.* pumping costs, any heating and cooling loads). Conversely, the extraction efficiency, β , affects the concentration of butanol produced on the solvent side,

and so lower values of β increase the cost of solvent distillation by reducing the concentration of butanol fed to the distillation system (m_{feed}):

$$m_{feed} = \beta \cdot m_{ferm} \cdot D_{Bu}^{mass}(T_{ext}) \quad (4-30)$$

Furthermore, higher values of extraction efficiency (β) reduce the quantity of solvent required (S), which was given by:

$$m_{feed} = \frac{\eta B}{S + \eta B} \cong \frac{\eta B}{S} \text{ (dilute butanol)} \quad (4-31)$$

$$\therefore \left(\frac{S}{\eta B} \right) \cong \frac{1}{m_{feed}} = \frac{1}{\beta \cdot m_{ferm} \cdot D_{Bu}^{mass}(T_{ext})} \text{ kg/kg butanol transferred} \quad (4-32)$$

Therefore, the solvent-to-aqueous ratio is given by:

$$\therefore \left(\frac{S}{W} \right) \cong \frac{\eta}{\beta \cdot D_{Bu}^{mass}(T_{ext})} \text{ kg/kg} \quad (4-33)$$

Hence, high values of extraction efficiency would probably be more advantageous than high values of transfer efficiency, since the operating costs on the aqueous side of the extraction would likely be relatively trivial compared to the operating costs on the solvent side of the extraction (which include distillation). However, a compromise for these two competing factors must be found since distillation costs might mostly be provided for by low-grade, waste heat. The optimisation of these two parameters was explored in a flowsheet model for the entire separation system in Chapter 5.

Figure 4-16 shows the relationship between the number of theoretical stages and the transfer and extraction efficiencies. As can be seen, relatively high extraction efficiencies can be achieved for a relatively low number of theoretical equilibrium stages; *e.g.* 90% extraction efficiency is achievable in 4 stages with a transfer efficiency of 70%. This equates to a solvent-to-aqueous ratio of ~0.8 kg/kg (for distribution coefficients ~1 kg/kg), which equates to ~1.3 m³/m³.

In practice, the number of stages required would be higher than that calculated for the number of equilibrium stages, due to mass transfer resistances. This is often accounted for in a ‘stage efficiency’ parameter, which is the ratio of theoretical to actual stages. This efficiency depends on the type and design of equipment used, operation parameters such as flowrates, and the physical properties of the two streams. Since mass transfer parameters are difficult to measure directly, this efficiency is often calculated from empirical correlations (Green, 1997; Treybal, 1951). Because the calculation of mass

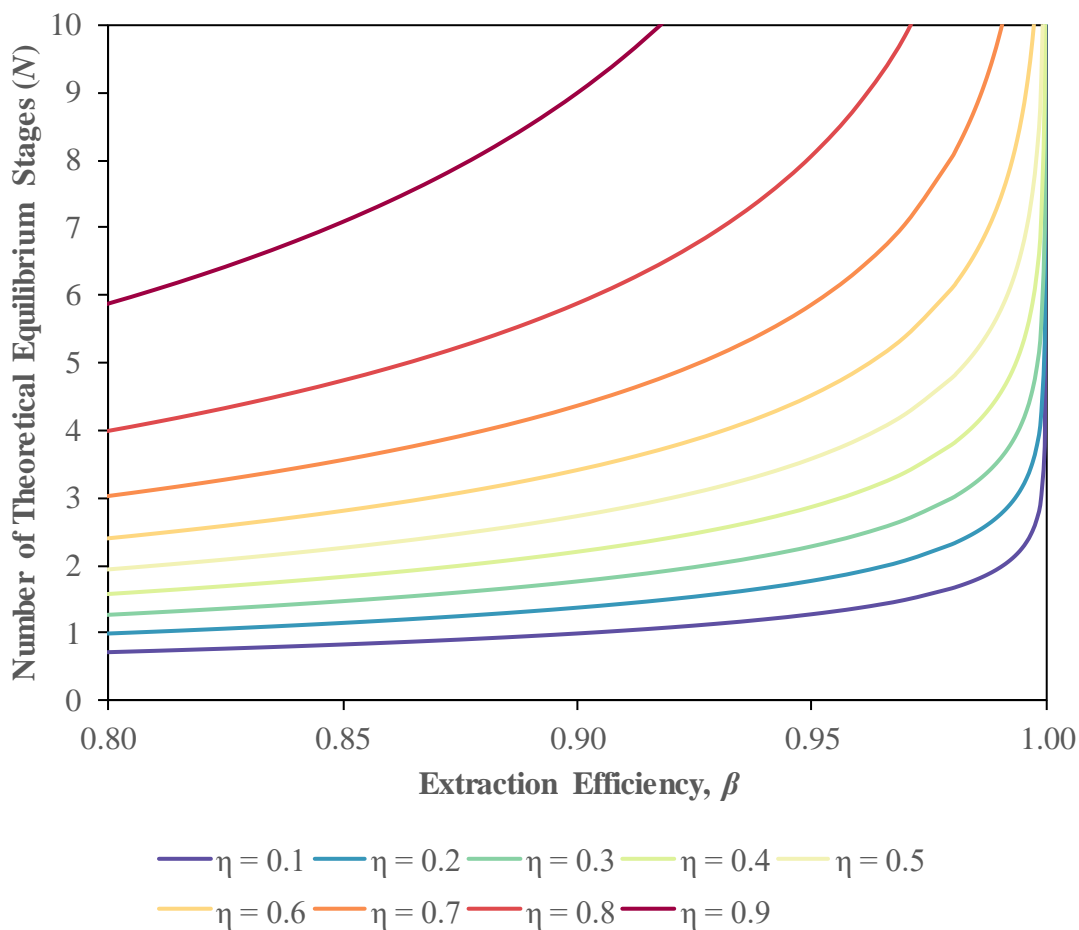


Figure 4-16: Number of theoretical equilibrium stages (N) in a liquid-liquid extraction as a function of extraction efficiency (β) and transfer efficiency (η)

transfer coefficients is complex and highly dependent on the properties of the broth and the precise design of extractor, the calculation of stage efficiency has not been examined in this work.

As an alternative to calculating stage efficiency, the efficiencies of column systems can be expressed in terms of the height of an equivalent theoretical stage or plate (HETS or HETP). Sinnott (2005) suggest that typical HETS values are 1 – 2.5 m for sieve plates and 0.5 – 1.5 m for packed columns. These values would suggest that a 10 m column would provide the equivalent of 4 – 20 theoretical equilibrium stages. A 10 m column would require around 1 bar additional pressure to overcome hydrostatic pressure (noting that the pressure at the top of the column must still be above the vapour pressure of the solvent), in addition to any other pressure losses in the extraction column, *e.g.* due to dispersion.

Figure 4-17 details the transfer efficiency as a function of extraction efficiency for a counter-current extraction with 5 equilibrium stages. As can be seen in Figure 4-17, high

extraction efficiencies could be achieved in such an extractor without reducing transfer efficiency dramatically.

4.6.3 Conclusion

Direct *in situ* extraction from fermentation broths is an attractive proposal due to its apparent simplicity and high efficiency. However, in practice, this approach might cause several issues for extractions employing volatile hydrocarbons as solvents, particularly in fermentations which produce significant quantities of off-gas. Issues of organism toxicity to solvents would also be exacerbated. Direct *in situ* extraction also limits the temperature of the extraction to that of the fermentation. Careful design of the fermenter would be required to achieve adequate mass transfer and phase separation, which could be difficult in complex fermentations where substrate mass transfer is also poor.

In stream extraction is more flexible and conventional, allowing operation with or without cells present, in addition to permitting operation at an elevated temperature. However, it would require additional unit operations, and reduces the driving force for mass transfer. For a counter-current extraction of butanol from water using volatile hydrocarbons, a simple model was developed to explore the relationship between the size of an extractor column, the ‘extraction efficiency’ (the proportion of equilibrium distribution coefficient achieved) and the ‘transfer efficiency’ (the proportion of butanol transferred in the

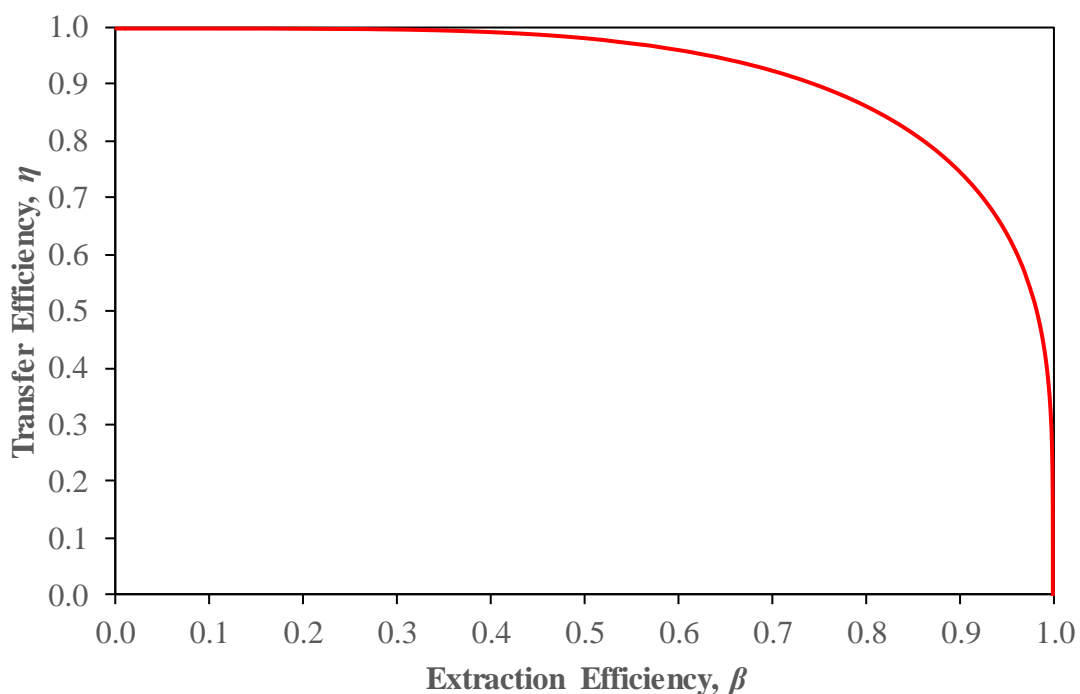


Figure 4-17: Transfer efficiency (η) as a function of extraction efficiency (β) for a counter-current liquid-liquid extraction with 5 theoretical equilibrium stages

extractor). The model predicted that, for this system, a column around 10 m high (5 theoretical equilibrium stages) could achieve an extraction efficiency of 90% (*i.e.* very close to the equilibrium), with a transfer efficiency of around 70%. It was postulated that high extraction efficiency was preferred over high transfer efficiency, since extraction efficiency impacts on the concentration of butanol and the solvent flowrate on the solvent side of the extraction.

5. A Flowsheet Model of Liquid-Liquid Extraction using Volatile Hydrocarbons

5.1 Introduction

In this chapter, a simple flowsheet model was built to estimate the energy consumption of a separation system for the extraction of aqueous butanol using volatile hydrocarbons. Many researchers have screened potential liquid extractants based on their distribution coefficient for aqueous butanol (*e.g.* Dadgar and Foutch, 1986; Groot *et al.*, 1990; Kim *et al.*, 1999). Whilst this is an important factor in the selection of a suitable extractant, it has merely been used as a rough proxy for the energy consumption of the system in these studies. This has meant that such studies have over-looked extractants such as volatile hydrocarbons. The results of the flowsheet model have allowed for a fairer comparison of potential extractants.

Here, the separation of a binary mixture of butanol and water was considered. This is equivalent to System 1 in simulations of distillation outlined in Appendix A. It was not possible to predict the solubility of water in the mixture of the solvent and butanol produced in the extraction, or the solubility of the hydrocarbon in the aqueous phase from the measurements of equilibria available. The mutual solubilities of pure water and the relevant hydrocarbons were shown to be very low in the investigation in Section 2.4 (*e.g.* the solubilities of C₄ – C₅ hydrocarbons in water were < 0.1 wt% at fermentation temperatures). Therefore, in the absence of ternary equilibria for the solubilities of water and the relevant hydrocarbons in butanol-water-hydrocarbon mixtures, the mutual solubility of water and the solvent was neglected for the purposes of the simple flowsheet model. In addition, side-products and other components in the broth were neglected.

The effects of mutual solubility and of multicomponent broths could be considered in a more detailed model, in order to investigate their impacts on the purity of the butanol product and on the requisite purge rates of the solvent and broth recycle. A more complex, multicomponent simulation of the separation system could readily be built in, for example, a Process simulation package such as UniSim Design. However, UniSim Design cannot employ flexible activity models such as the Legendre activity model. For the purposes of this chapter, a simple flowsheet model was found to be more illustrative

of the behaviour and limitations of the extraction scheme, and also allowed for rapid testing and comparison of different solvents and operating conditions simultaneously.

5.2 Assumptions and Methodology

5.2.1 Assumptions

A simple model was developed to estimate the energy required for the separation of *n*-butanol from water using C₄ – C₆ hydrocarbons as extractants. The following assumptions were made:

- Only binary separation of *n*-butanol and water was considered; other broth components were neglected.
- The mutual solubility of water and hydrocarbons was neglected and is justified on the basis that the mutual solubility of these components is minimal, as discussed in Section 2.4
- The distribution coefficients predicted in Chapter 4, based on binary activity models and neglecting the mutual solubility of water and hydrocarbons, were assumed to be valid. This was justified on the basis that butanol is dilute in fermentation broths (*c.f.* typical broth titres of ~0.25 mol% butanol) and so ternary interactions are negligible.
- Liquid-liquid extraction was modelled using the model developed in Chapter 4. The liquid-liquid extractor was assumed to be a column-type unit operated with counter-current contacting. The effect of hydrostatic pressure over the height of the column on the operating conditions was accounted for but the system was assumed to be isothermal meaning that enthalpy of mixing and external heat transfer were assumed to be negligible. The mass distribution coefficient of butanol was approximated as being constant with butanol concentration. The effect of butanol concentration on distribution coefficient was considered in Chapter 4, where it was shown to be reasonably constant over a range of dilute concentrations of butanol.
- Distillation columns and heat exchangers were assumed to be isobaric in order to simplify the model. No compressors were required in the design, and so negligible additional energy would be required for pumping to account for any pressure losses.

- Heat exchangers were assumed to be operated in counter-current to maximise heat recovery.
- Since C₄ – C₆ hydrocarbon solvents have high volatilities compared to butanol, separation *via* distillation is relatively simple. Therefore, the tops product composition for both columns were approximated as pure solvent.
- Distillation columns were designed using the Fenske-Underwood-Gilliland short-cut method (Green, 1997), which assumed constant molar overflow in the columns. For the purposes of calculating the minimum number of stages required using the Fenske equation, a purity of 99.99 mol% was assumed for the solvent in the distillates and for the butanol product. For all other purposes in the flowsheet model, the solvent was approximated as pure in the distillate and the butanol product was approximated as pure, due to their high purity specifications.
- Minimum boiling-point azeotropes were ignored. These were predicted to form for C₆ hydrocarbons with butanol above ~30°C (at a very low butanol concentration). Whilst this might be problematic for C₆ hydrocarbons in practice, C₆ hydrocarbons were merely included in this flowsheet model for comparison with C₄ – C₅ hydrocarbons. In any case, the very low total pressures required to perform the distillation of C₆ hydrocarbons and butanol using low-grade heat would likely make the use of C₆ hydrocarbons unfeasible.

5.2.2 Model of a Simple Distillation Column

Figure 5-1 shows a simple approach to calculating the heat required for the distillation of butanol and volatile hydrocarbon solvents. Consider what happens when B kg butanol and S kg solvent is fed to the column as a mixed feed in a given time. Taking a mass balance over the column yields a solvent mass (S) in each stream as:

$$S = \frac{(1 - m_{feed})}{m_{feed}} B; S_{bot} = \frac{(1 - m_{bot})}{m_{bot}} B \quad (5-1)$$

$$S_{top} = S - S_{bot} \quad (5-2)$$

where m_{feed} and m_{bot} are the mass fractions of butanol in the distillation column feed and bottoms respectively, and B is the mass of butanol in the feed.

An energy balance on the condenser yields the condenser duty (E_{cond}) as:

$$E_{cond} = (R + 1)S_{top}\Delta\hat{H}_{solv}^{vap}(T_{cond}) \quad (5-3)$$

where R is the reflux ratio and $\Delta\hat{H}_{solv}^{vap}(T_{cond})$ is the specific enthalpy of vaporisation of the solvent at the condenser temperature (T_{cond}).

An energy balance on the distillation column itself yields the reboiler duty (E_{reboil}) as:

$$\begin{aligned} E_{reboil} = & S_{top} [\hat{H}_{solv}^L(T_{cond}) + (R + 1)\Delta\hat{H}_{solv}^{vap}(T_{cond})] \\ & + [S_{bot} \hat{H}_{solv}^L(T_{reboil}) + B\hat{H}_{Bu}^L(T_{reboil}) + (S_{bot} + B)\Delta\hat{H}_{Bu,S}^E(m_{reboil}, T_{feed})] \\ & - [S \hat{H}_{solv}^L(T_{feed}) + B\hat{H}_{Bu}^L(T_{feed}) + (S + B)\Delta\hat{H}_{Bu,S}^E(m_{feed}, T_{feed})] \end{aligned} \quad (5-4)$$

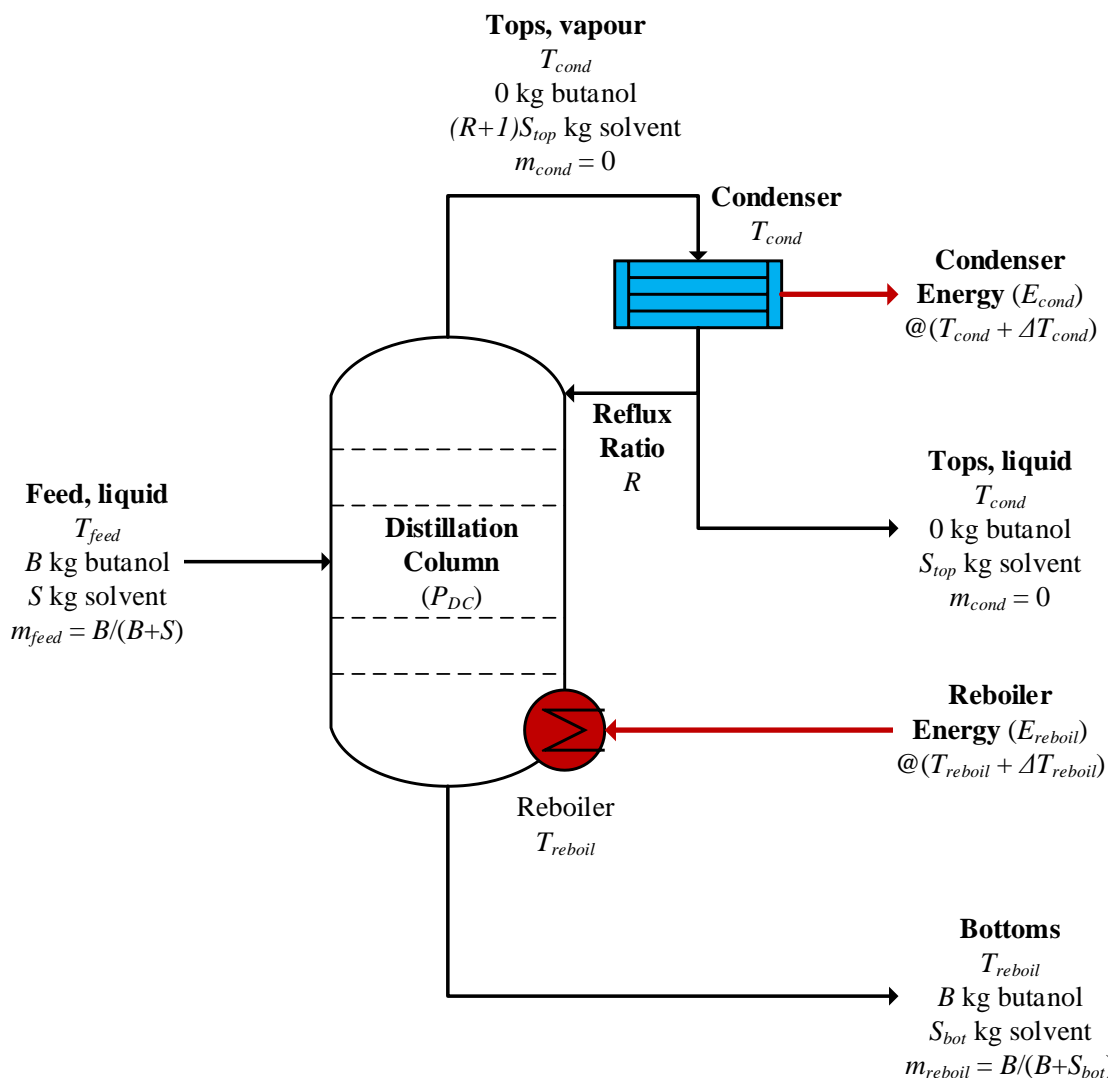


Figure 5-1: Simple model of a distillation column for the binary separation of butanol from volatile hydrocarbon solvents. Here, m_X = mass fraction of butanol in stream X . T_X = temperature of stream X

Specific liquid enthalpies ($\hat{H}^L(T)$) and enthalpies of vaporisation ($\Delta\hat{H}_{solv}^{vap}(T)$) were calculated as a function of temperature (T) from DIPPR correlations. The parameters and equations used for the calculation of pure component properties are given in the Supplementary Material included with this dissertation. Excess enthalpies of mixing ($\Delta H^{LE}(m, T)$) were neglected as they were found to be negligible in comparison to latent heats of vaporisation when calculated using the Legendre activity model for butanol-solvent pairs.

The minimum reflux ratio (R_{min} , for an infinite number of stages) was estimated using the Underwood equations (Green, 1997). For a binary mixture of hydrocarbon (HC) and butanol (Bu), assuming a saturated liquid feed ($q = 1$), the 1st Underwood equation collapses to:

$$R_{min} = \frac{1}{(\alpha_{HC,Bu} - 1)} \left[\frac{(1 - x_{cond})}{(1 - x_{feed})} - \left(\frac{x_{cond}}{x_{feed}} \right) \alpha_{HC,Bu} \right] \quad (5-5)$$

where x_i is the mole fraction of butanol at location i and $\alpha_{HC,Bu}$ is the average relative volatility of the solvent *versus* butanol, approximated as the geometric average at the conditions in the condenser and reboiler:

$$\alpha_{HC,Bu} = [\alpha_{HC,Bu}(T_{cond}, x_{cond}) \cdot \alpha_{HC,Bu}(T_{reboil}, x_{reboil})]^{0.5} \quad (5-6)$$

where relative volatility is defined as usual as the ratio of the vapour (y) and liquid (x) molar composition at equilibrium:

$$\alpha_{HC,Bu}(T, x_{Bu}) = \frac{K_{HC}}{K_{Bu}} = \frac{(y/x)_{HC}}{(y/x)_{Bu}} \quad (5-7)$$

The K values follow from the general condition for VLE for component i :

$$K_i = \frac{y_i}{x_i} = \frac{\gamma_i(x_i, T, P) \cdot (\phi_i^{sat} \cdot P_i^{sat}) \exp\left(\frac{V_i^L(P - P_i^{sat})}{RT}\right)}{\phi_i(y_i, T, P) \cdot P} \quad (5-8)$$

Thus K_i was calculated using the Leg-virial Model developed in Chapter 3 (comprising the Legendre activity model for the liquid phase and the virial equation of state for the vapour phase). Alternatively, where column temperatures exceeded the Leg-virial Model, $\alpha_{HC,Bu}$ was calculated by assuming Raoult's Law, which approximates $\alpha_{HC,Bu}$ as:

$$\alpha_{HC,Bu} = \left[\frac{P_{HC}^{sat}(T_{cond})}{P_{Bu}^{sat}(T_{cond})} \cdot \frac{P_{HC}^{sat}(T_{reboil})}{P_{Bu}^{sat}(T_{reboil})} \right]^{0.5} \quad (5-9)$$

where $P_{HC}^{sat}(T)$ and $P_{Bu}^{sat}(T)$ are the saturation pressures of the hydrocarbon solvent and butanol respectively at temperature T .

Noting that the butanol content in the condenser (x_{cond}) was negligible, the minimum reflux ratio simplified to:

$$R_{min} = \frac{1}{(\alpha_{HC,Bu} - 1)} \frac{1}{(1 - x_{feed})} \quad (5-10)$$

The minimum number of stages at total reflux (N_m) was approximated by the Fenske equation (Green, 1997), which for a binary mixture of hydrocarbon solvent and butanol is given by:

$$N_m = \frac{\ln\left(\frac{x_{reboil}(1 - x_{cond})}{x_{cond}(1 - x_{reboil})}\right)}{\ln \alpha_{HC,Bu}} \quad (5-11)$$

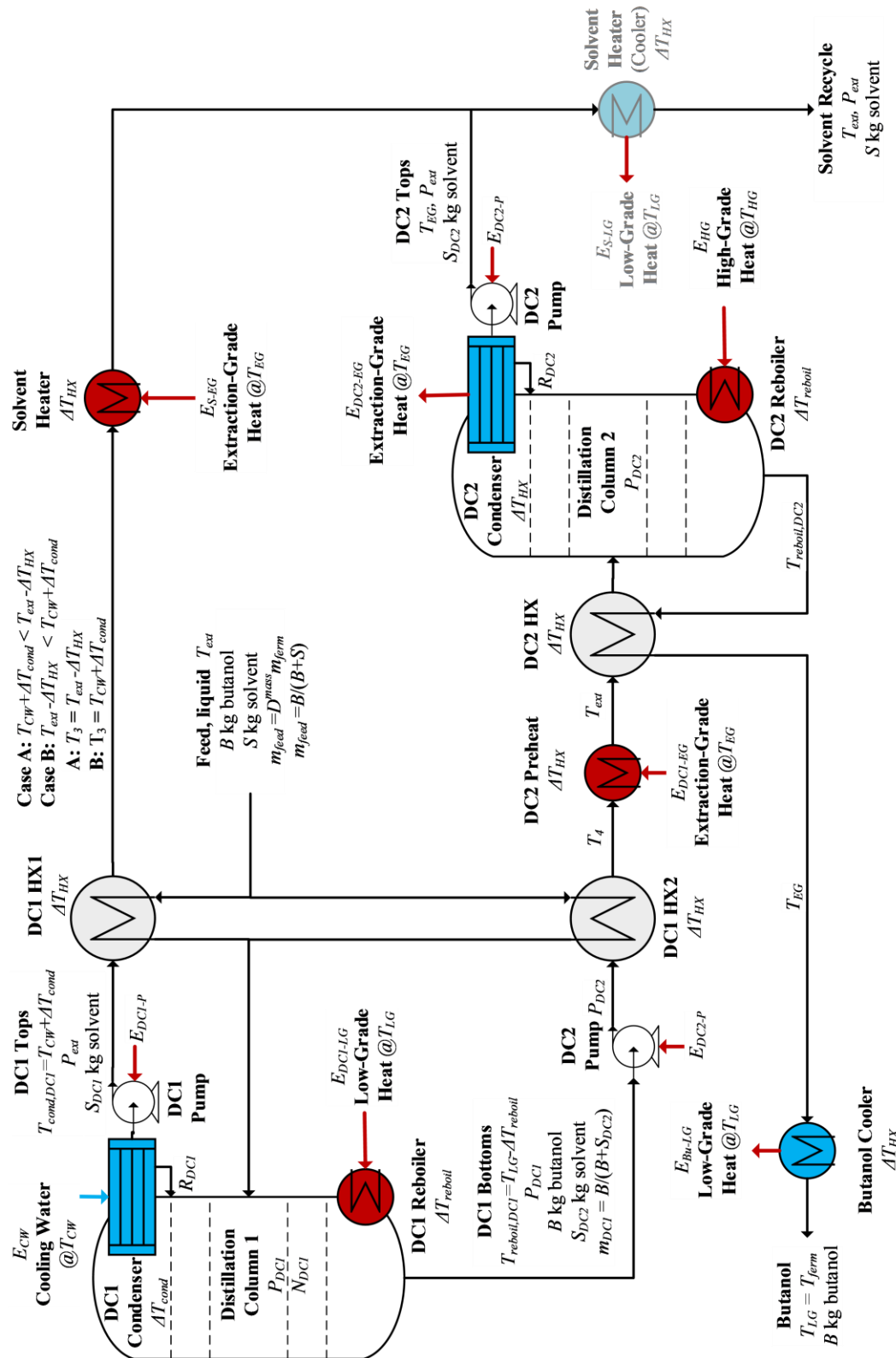
For the purpose of the Fenske equation, purities of 99.99 mol% were assumed for solvent in the distillate, and for the butanol product. The actual number of stages (N) and the actual reflux ratio (R) were related via the Gilliland correlation using values of R_{min} and N_m (Green, 1997):

$$\frac{N - N_m}{N + 1} = 1 - \exp\left[\left(\frac{1 + 54.4\Psi}{11 + 117.2\Psi}\right) \frac{(\Psi - 1)}{\Psi^{0.5}}\right] \quad (5-12)$$

$$\Psi = \frac{R - R_{min}}{R + 1} \quad (5-13)$$

5.2.3 Operating Conditions of the Flowsheet Distillation Columns

Figure 5-2 proposed a flowsheet for the separation of butanol and the volatile solvent using a scheme with two distillation columns in order to utilise low-grade heat.


 Figure 5-2- Simplified flowsheet model for the distillation of butanol and C₄ - C₆ hydrocarbons using low-grade heat

Four grades of heat were required in the flowsheet model: cooling water, low-grade heat, extraction-grade heat, and high-grade heat. The temperature of the cooling water (T_{CW}) available is dependent on plant location and climate. This temperature, plus some driving force ΔT_{cond} , determined the condenser temperature in distillation column 1 (DC1) and hence determined the pressure in DC1 (P_{DC1}). As the condenser was assumed to contain near-pure solvent:

$$T_{cond}^{DC1} = T_{CW} + \Delta T_{cond} \quad (5-14)$$

$$P_{DC1} = P_{solv}^{sat}(T_{cond}^{DC1}) \quad (5-15)$$

Pure vapour pressures were calculated using DIPPR correlations, the parameters and equations for which are given in the Supplementary Material included with this dissertation. Low-grade heat was assumed to be provided at least in part by the fermenter. Therefore the fermentation temperature (T_{ferm}) was used to determine the temperature of low-grade heat (T_{LG}):

$$T_{LG} = T_{ferm} \quad (5-16)$$

Low-grade heat was used in the reboiler of DC1, and so the temperature of the reboiler stage on DC1 (T_{reboil}^{DC1}) was determined by the temperature of the low-grade heat, minus a driving force (ΔT_{reboil}):

$$T_{reboil}^{DC1} = T_{LG} - \Delta T_{reboil} \quad (5-17)$$

Note that since the condenser temperature (T_{cond}^{DC1}) must be below the reboiler temperature (T_{reboil}^{DC1}) in DC1:

$$T_{reboil}^{DC1} > T_{cond}^{DC1} \quad (5-18)$$

$$\therefore (T_{LG} - \Delta T_{reboil}) > (T_{CW} + \Delta T_{cond}) \quad (5-19)$$

$$\therefore T_{CW} < T_{ferm} - (\Delta T_{reboil} + \Delta T_{cond}) \quad (5-20)$$

Equation (5-20) means that there is a limit to the magnitude of temperature driving forces on the condenser and reboiler. For example, if the temperature of cooling water was 20°C, and the fermenter temperature was 37°C, then the condenser and reboiler temperature driving forces must sum to less than 17 K (average 8.5 K per heat exchanger). These temperature driving forces are relatively low, and so would necessitate large transfer areas on the heat exchangers. However, heat transfer coefficients for boiling and condensation processes are very high, which would help to reduce the transfer area required.

The reboiler was at vapour-liquid equilibrium (VLE), and so the temperature and pressure in the reboiler determined the composition of butanol produced in the bottoms of DC1. This composition can be found using the general condition for VLE for each component, i :

$$\phi_i(y_i, T, P) \cdot y_i P = \gamma_i(x_i, T, P) \cdot x_i (\phi_i^{sat} \cdot P_i^{sat}) \cdot \exp\left(\frac{V_i^L(P - P_i^{sat})}{RT}\right) \quad (5-21)$$

where $T = T_{reboil}^{DC1}$, $P = P_{DC1}$. Activity coefficients (γ_i) were calculated from the Legendre activity model developed in Chapter 3 for binary mixtures of butanol and the relevant hydrocarbons (the ‘Leg-virial Model’). Fugacity coefficients (ϕ_i) were calculated using the virial equation (detailed in Appendix D). The VLE conditions (eq. (5-21)) were solved iteratively for butanol and the relevant hydrocarbon to find the liquid composition, x_i at VLE. This was converted into a mass fraction to give m_{DC1} , the mass fraction of butanol produced by DC1.

The aqueous broth and the solvent recycle required heating to the extraction temperature (T_{ext}) before entering the extraction column. This was performed in liquid-phase heat exchangers (with a temperature driving force ΔT_{HX}). The extraction temperature determined the temperature of extraction-grade heat (T_{EG}) required in these heat exchangers:

$$T_{EG} = T_{ext} + \Delta T_{HX} \quad (5-22)$$

The first distillation column could not completely separate the solvent from butanol due to the limited temperature gradient in DC1. The second distillation column (DC2) completed the separation. This was conducted at an elevated pressure that was selected to produce extraction-grade heat in the condenser of DC2, thereby maximising useful heat recovery in this column. Given that the condenser contained approximately pure solvent, the pressure of DC2 (P_{DC2}) was equal to the saturation pressure of the solvent at the temperature of extraction-grade heat:

$$P_{DC2} = P_{solv}^{sat}(T_{EG}) \quad (5-23)$$

The heat for the reboiler in DC2 was provided by high-grade heat. As DC2 was assumed to produce approximately pure butanol in the bottoms, the temperature of high-grade heat (T_{HG}) required was determined by the saturation temperature of butanol at the column pressure (P_{DC2}), plus a temperature driving force ΔT_{reboil} :

$$T_{HG} = T_{Bu}^{sat}(P_{DC2}) + \Delta T_{reboil} \quad (5-24)$$

5.2.4 Model of the Extraction

Figure 5-3 outlines the flowsheet for the extraction of butanol from an aqueous broth. *In stream* extraction, operated in counter-current, was assumed for the extraction. The simple model outlined in Section 4.6.2 was employed. The extraction efficiency (β) related the effective and equilibrium distribution coefficients in the LLX column:

$$m_{feed} = \beta \cdot m_{ferm} \cdot D_{Bu}^{mass}(m_{ferm}, T_{ext}) \quad (5-25)$$

The mass distribution coefficient at equilibrium, D_{Bu}^{mass} , was approximated as being constant with the composition of butanol in the extractor. The predictions of distribution coefficient of butanol made in Chapter 4 were used to calculate D_{Bu}^{mass} , evaluated at the extraction temperature (T_{ext}) and the mass fraction of butanol in the aqueous feed (m_{ferm}).

If B kg of butanol were transferred in the LLX column, then the butanol in the fermenter draw would therefore be B/η and thus the butanol in the fermenter recycle $B(1 - \eta)/\eta$. The transfer efficiency, η , therefore affects the flowrate of water to and from the fermenter (W):

$$W = \frac{B}{\eta} \frac{(1 - m_{ferm})}{m_{ferm}} \quad (5-26)$$

As derived in Section 4.6.2, the number of theoretical equilibrium LLX stages was related to the transfer and extraction efficiencies by:

$$N_{LLX} = \begin{cases} \frac{\ln\left(\frac{1-\beta}{1-\eta}\right)}{\ln\left(\frac{\eta}{\beta}\right)}, & \eta \neq \beta \\ \frac{\eta}{1-\eta}, & \eta = \beta \end{cases} \quad (5-27)$$

The number of equilibrium stages (N_{LLX}) was assumed to be 5. As discussed in Chapter 4 this allows for high extraction and transfer efficiencies to be achieved. This equates to a column height of ~10 m, assuming a height of an equivalent theoretical stage (HETS) of 2 m (Sinnott, 2005). As discussed in Chapter 4, a wide range of standard designs for the extraction system (including a series of mixers instead of a column system) could be employed depending on the properties of the broth and extractant. For the purposes of this model, the performance of the extractor is summarised by the extraction and transfer efficiency and the pressure drop (1 bara).

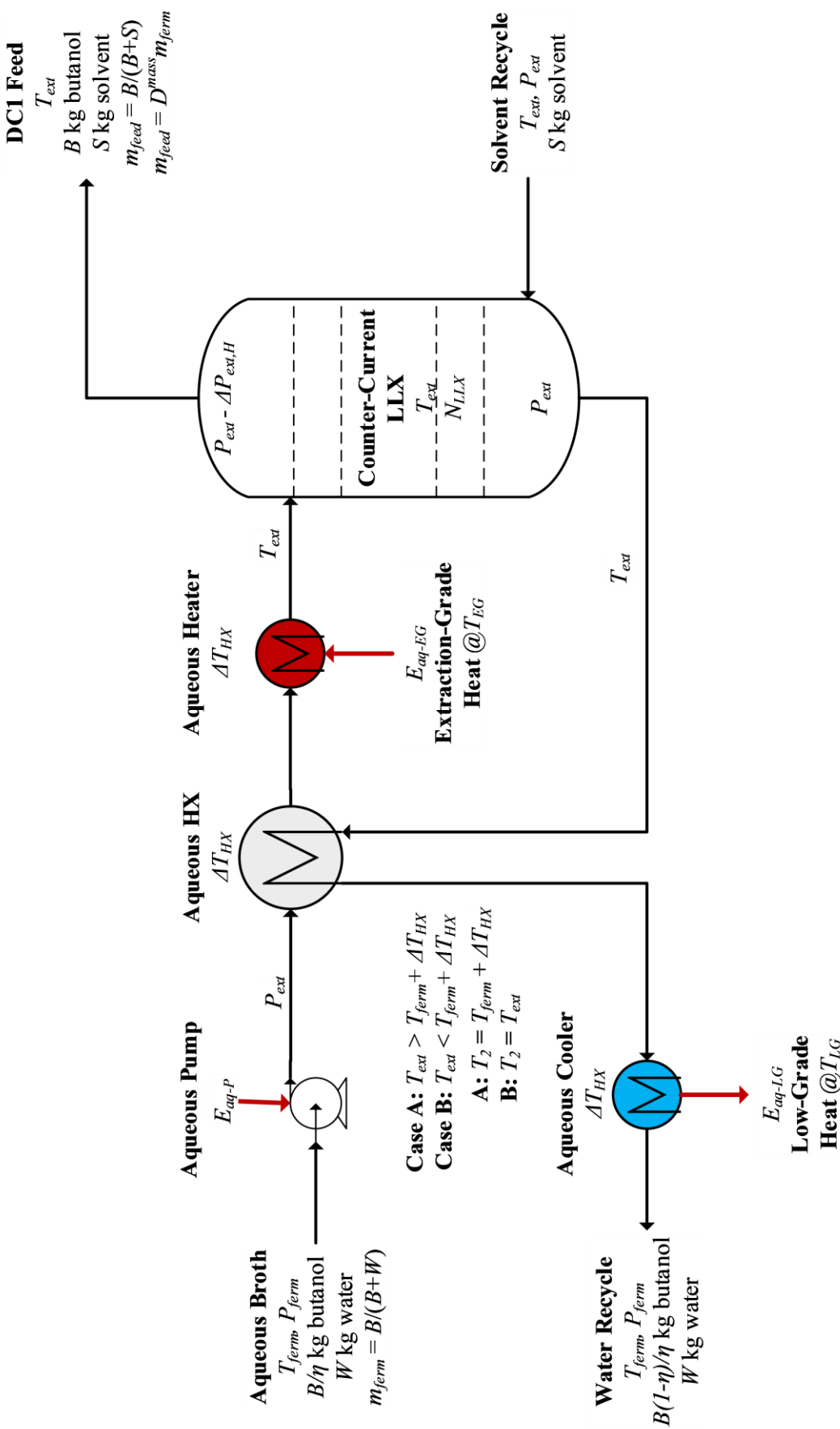


Figure 5-3 – Simplified flowsheet model for the extraction of butanol from aqueous fermentation broths

It was necessary to ensure that the solvent was in the liquid phase in the extraction column at T_{ext} . Therefore, the pressure of DC2 (P_{DC2}), equivalent to the vapour pressure of solvent at T_{EG} , was assumed at the top of the extraction column. However, the hydrostatic pressure gradient ($\Delta P_{ext,H}$) meant that the pressure was ~1 bara higher (height, $H_{LLX} \sim 10$ m; density $\rho \sim 1000$ kg/m³) at the bottom of the extraction column, *i.e.*:

$$P_{ext} = P_{DC2} + \Delta P_{ext,H} = P_{DC2} + \rho g H_{LLX} = P_{DC2} + 1 \text{ bara} \quad (5-28)$$

Therefore, the solvent was at least ΔT_{HX} below its saturation temperature throughout the extractor.

Initially, the extraction efficiency (β) of the LLX column was assumed to be 90%, yielding a transfer efficiency (η) of 75%. The impact of varying extraction and transfer efficiencies was also examined.

5.2.5 Heating Requirements for the Aqueous Phase

In order to perform extractions at a higher temperature than the fermentation, the aqueous broth would need heating before entering the extraction column. The butanol-lean water produced by the extraction would also need cooling back to the temperature of the fermentation before broth recycle. If the extraction temperature were more than ΔT_{HX} above the fermentation temperature, a portion of these heat loads could be heat integrated in ‘Aqueous HX’, as shown in Figure 5-3. Assuming counter-current operation, the temperature pinch occurs at the cold end of ‘Aqueous HX’ ($T_{ferm}, T_{ferm} + \Delta T_{HX}$). Neglecting the excess heat capacity of water and butanol, the heat recovered in ‘Aqueous HX’ was calculated as:

$$E_{Aq\ HX} = W [\hat{H}_{H2O}^L(T_{ext}) - \hat{H}_{H2O}^L(T_2)] + \frac{B(1-\eta)}{\eta} [\hat{H}_{Bu}^L(T_{ext}) - \hat{H}_{Bu}^L(T_2)] \quad (5-29)$$

where:

$$T_2 = \begin{cases} T_{ferm} + \Delta T_{HX}, & T_{ferm} + \Delta T_{HX} < T_{ext} \\ T_{ext}, & T_{ferm} + \Delta T_{HX} \geq T_{ext} \end{cases} \quad (5-30)$$

Similarly, the low-grade heat recovered by the water recycle in ‘Aqueous Cooler’ was given by:

$$E_{LG}^{aq} = W [\hat{H}_{H2O}^L(T_2) - \hat{H}_{H2O}^L(T_{ferm})] + \frac{B(1-\eta)}{\eta} [\hat{H}_{Bu}^L(T_2) - \hat{H}_{Bu}^L(T_{ferm})] \quad (5-31)$$

The extraction-grade heat required for heating the aqueous broth in ‘Aqueous Heater’ was calculated as:

$$E_{Aq\ HX} = W \left[\hat{H}_{H_2O}^L(T_{ext}) - \hat{H}_{H_2O}^L(T_1) \right] + \frac{B}{\eta} \left[\hat{H}_{Bu}^L(T_{ext}) - \hat{H}_{Bu}^L(T_1) \right] + E_{Aq\ HX} \quad (5-32)$$

5.2.6 Heating Requirements for the Organic Phase

The mass of solvent required (S) was calculated from the mass fraction of butanol produced by the extraction, m_{feed} :

$$S = \frac{(1 - m_{feed})}{m_{feed}} B \quad (5-33)$$

where B is the mass of butanol transferred in the extraction (kg). Similarly, the mass of solvent in the feed of DC2 (S_{DC2}) was calculated from the mass fraction of butanol produced in the bottoms of DC1 (m_{DC1}), assuming 100% recovery of butanol in the bottoms of DC1:

$$S_{DC2} = \frac{(1 - m_{DC1})}{m_{DC1}} B \quad (5-34)$$

The mass of solvent produced in the distillate of DC1 was calculated as the difference between S and S_{DC1} :

$$S_{DC1} = S - S_{DC2} = \left(\frac{(1 - m_{feed})}{m_{feed}} - \frac{(1 - m_{DC1})}{m_{DC1}} \right) B \quad (5-35)$$

Both DC1 and DC2 were assumed to be isobaric and were assumed to have 10 and 20 equilibrium stages respectively ($N_{DC1} = 10$, $N_{DC2} = 20$). The reflux ratio in each column (R_{DC1}, R_{DC2}) was calculated using the Fenske-Underwood-Gilliland method outlined in Section 5.2.2. Relative volatility ($\alpha_{HC,Bu}$) for DC1 was calculated by employing the Leg-virial Models developed in Chapter 3 at the condenser and reboiler conditions in eqs. (5-6) – (5-65-8). The temperature of DC2 exceeds 100°C, the upper limit of the measurements on which the Leg-virial Model was based. Therefore, for the purposes of estimating the relative volatility in order to estimate the minimum reflux ratio of DC2, Raoult's Law was assumed (eq. (5-9)). This was a reasonable approximation at these temperatures, since the activity coefficient of butanol at trace composition in hydrocarbons (as in the distillate) was found to be closer to unity at 100°C than at lower temperatures.

The condenser duty of DC1 (E_{CW}^{DC1}) was assumed to be provided by cooling water and was calculated using the model of a simple distillation column:

$$E_{CW}^{DC1} = (R_{DC1} + 1)S_{DC1}\Delta\hat{H}_{solv}^{vap}(T_{cond}^{DC1}) = (R_{DC1} + 1)S_{DC1}\Delta\hat{H}_{solv}^{vap}(T_{CW} + \Delta T_{cond}) \quad (5-36)$$

The condenser in DC1 produced liquid solvent at a temperature T_{cond}^{DC1} ($= T_{CW} + \Delta T_{cond}$), which, after being pumped back up to extraction pressure, was re-heated to the extraction temperature (T_{ext}) before solvent recycle. The reboiler in DC1 produced the bottoms product at a low temperature ($T_{LG} - \Delta T_{reboil}$), which also required re-heating before the distillation in DC2 at a higher temperature. Depending on the magnitude of the temperature driving forces of the reboiler and condenser, some of the heat required for both of these re-heating operations could be provided by the feed to DC1, which was at the extraction temperature (T_{ext}). This feed stream, by definition, has a similar heat capacity to the sum of the output streams of the fermenter (neglecting excess heat capacity and change in heat capacity over this small temperature range). This heat integration was performed in ‘DC1 HX1’ and ‘DC1 HX2’. Assuming counter-current operation, the pinch in temperature occurred at the hot end of both of these heat exchangers (T_{ext} , $T_{ext} - \Delta T_{HX}$). The heat transferred in DC1 HX1 ($E_{DC1,HX1}$) was calculated by:

$$E_{DC1,HX1} = S_{DC1} \left(\hat{H}_{solv}^L(T_3) - \hat{H}_{solv}^L(T_{CW} + \Delta T_{cond}) \right) \quad (5-37)$$

where T_3 depends on the viability of heat transfer (dependent on the magnitude of temperature driving forces):

$$T_3 = \begin{cases} T_{ext} - \Delta T_{HX}, & T_{CW} + \Delta T_{cond} < T_{ext} - \Delta T_{HX} \\ T_{CW} + \Delta T_{cond}, & T_{CW} + \Delta T_{cond} \geq T_{ext} - \Delta T_{HX} \end{cases} \quad (5-38)$$

Similarly, the heat transferred in DC1 HX2 ($E_{DC1,HX2}$) was calculated by:

$$\begin{aligned} E_{DC1,HX2} = S_{DC2} & \left(\hat{H}_{solv}^L(T_4) - \hat{H}_{solv}^L(T_{CW} + \Delta T_{cond}) \right) \\ & + B \left(\hat{H}_{Bu}^L(T_4) - \hat{H}_{Bu}^L(T_{CW} + \Delta T_{cond}) \right) \end{aligned} \quad (5-39)$$

where T_4 depends on the viability of heat transfer and was given by:

$$T_4 = \begin{cases} T_{ext} - \Delta T_{HX}, & T_{LG} + \Delta T_{reboil} < T_{ext} - \Delta T_{HX} \\ T_{LG} - \Delta T_{reboil}, & T_{LG} + \Delta T_{reboil} \geq T_{ext} - \Delta T_{HX} \end{cases} \quad (5-40)$$

The reboiler duty in DC1, provided by low-grade heat, was calculated using the model of a simple distillation column. The heat removed by DC1 HX1 ($E_{DC1,HX1}$) and DC1 HX2 ($E_{DC1,HX2}$) from the feed to DC1 at T_{ext} must be accounted for:

$$\begin{aligned} E_{LG}^{DC1} = E_{DC1,HX1} & + E_{DC1,HX2} + S_{DC1} \left[\hat{H}_{solv}^L(T_{cond}^{DC1}) + (R_{DC1} + 1)\Delta\hat{H}_{solv}^{vap}(T_{cond}^{DC1}) \right] \\ & + [S_{DC2} \hat{H}_{solv}^L(T_{reboil}^{DC1}) + B\hat{H}_{Bu}^L(T_{reboil}^{DC1})] \\ & - \left[S \hat{H}_{solv}^L(T_{ext}) + B\hat{H}_{Bu}^L(T_{ext}) + (S + B)\Delta\hat{H}_{Bu,S}^{LE}(m_{feed}, T_{ext}) \right] \end{aligned} \quad (5-41)$$

The condenser in DC2 provided extraction-grade heat. Its duty (E_{EG}^{DC2}) was also calculated using the simple distillation model:

$$E_{EG}^{DC2} = (R_{DC2} + 1)S_{DC2}\Delta\hat{H}_{solv}^{vap}(T_{EG}) \quad (5-42)$$

The final portion of heat required for re-heating the solvent recycle from DC1 to the extraction temperature (T_{ext}) was provided by a combination of direct heating *via* mixing with the solvent recycle from DC2 (which was at T_{EG} , *i.e.* ΔT_{HX} above T_{ext} required), and heating using extraction-grade heat in ‘Solvent Heater’, as shown in Figure 5-2. A heat balance yields the extraction-grade heat required by ‘Solvent Heater’ as:

$$E_{EG}^S = S\hat{H}_{solv}^L(T_{ext}) - S_{DC1}\hat{H}_{solv}^L(T_{*2}) - S_{DC2}\hat{H}_{solv}^L(T_{EG}) \quad (5-43)$$

However, if the amount of solvent distilled in DC2 exceeded that produced by DC1, it was possible that E_{EG}^S could become negative. In this circumstance, instead of requiring extraction grade heat, the heat exchanger ‘Solvent Heater’ produced low-grade heat $E_{S,LG}$:

$$\begin{aligned} E_{LG}^S &= -[S\hat{H}_{solv}^L(T_{ext}) - S_{DC1}\hat{H}_{solv}^L(T_{*2}) - S_{DC2}\hat{H}_{solv}^L(T_{EG})] \\ E_{EG}^S &= 0 \end{aligned} \quad (5-44)$$

The feed to DC2 could be pre-heated further after DC1 HX2 up to the extraction temperature using extraction-grade heat. This was performed in ‘DC2 Preheat’, as shown in Figure 5-2, and the extraction-grade heat required (E_{EG}^{DC1}) was calculated as:

$$\begin{aligned} E_{EG}^{DC1} &= S_{DC2}(\hat{H}_{solv}^L(T_{ext}) - \hat{H}_{solv}^L(T_4)) \\ &\quad + B(\hat{H}_{Bu}^L(T_{ext}) - \hat{H}_{Bu}^L(T_4)) \end{aligned} \quad (5-45)$$

The DC2 reboiler required high-grade heat and produced butanol product at temperature T_{reboil}^{DC2} . Some of this heat could be recovered and used to pre-heat the feed for DC2 further still in ‘DC2 HX’. Since the feed to DC2, by definition, has a higher heat capacity than the butanol product, the temperature pinch for this heat exchanger occurred at the cold end (T_{reboil}^{DC1} , $T_{reboil}^{DC1} + \Delta T_{HX}$), assuming counter-current operation. The heat transferred in ‘DC2 HX’ ($E_{DC2,HX}$) was calculated as:

$$E_{DC2,HX} = B(\hat{H}_{Bu}^L(T_{reboil}^{DC2}) - \hat{H}_{Bu}^L(T_{reboil}^{DC1} + \Delta T_{HX})) \quad (5-46)$$

The reboiler duty of DC2 was then calculated in a similar manner to that of DC1, by employing the simple distillation model. As for the calculation of the duty of DC1, the heat provided by DC2 HX ($E_{DC2,HX}$) to the feed to DC2 at T_{ext} must be accounted for:

$$E_{HG} = S_{DC2} [\widehat{H}_{solv}^L(T_{EG}) + (R_{DC2} + 1)\Delta\widehat{H}_{solv}^{vap}(T_{EG})] + B\widehat{H}_{Bu}^L(T_{reboil}) - [S_{DC2}\widehat{H}_{solv}^L(T_{ext}) + B\widehat{H}_{Bu}^L(T_{ext})] - E_{DC2\ HX} \quad (5-47)$$

Finally, a small amount of low-grade heat could be recovered from the butanol product stream (assuming that $\Delta T_{reboil} \leq \Delta T_{HX}$) in ‘Butanol Cooler’:

$$E_{LG}^{Bu} = B \left(\widehat{H}_{Bu}^L(T_{LG} + \Delta T_{HX} - \Delta T_{reboil}) - \widehat{H}_{Bu}^L(T_{LG}) \right) \quad (5-48)$$

This produced butanol at $T_{LG} = T_{ferm}$.

5.2.7 Total Heating Requirements

All streams (B, W) entered and left the model at the fermentation temperature (T_{ferm}), and hence the net heating minus the net cooling requirements summed to zero (since excess enthalpies of mixing were neglected).

The extraction-grade energies were summed to give the total extraction-grade heat required by the system:

$$E_{EG} = E_{EG}^S + E_{EG}^{aq} - E_{EG}^{DC2} \quad (5-49)$$

If the net extraction-grade heat, E_{EG} , was negative (*i.e.* surplus extraction-grade heat was produced), then this heat was employed as low-grade heat. Therefore, the total low-grade heat required was calculated as:

$$E_{LG} = \begin{cases} E_{LG}^{DC1} - E_{LG}^{Bu} - E_{LG}^{aq} - E_{LG}^S, & E_{EG} > 0 \\ E_{LG}^{DC1} - E_{LG}^{Bu} - E_{LG}^{aq} - E_{LG}^S + E_{EG}, & E_{EG} \leq 0 \end{cases} \quad (5-50)$$

Finally, if the net low-grade heat, E_{LG} , was negative (*i.e.* surplus low-grade heat produced), then in this scenario equated, further cooling was required. This cooling was performed by cooling water. Hence, the total demand for cooling water was given by:

$$E_{CW} = \begin{cases} E_{CW}^{DC1}, & E_{LG} > 0 \\ E_{CW}^{DC1} - E_{LG}, & E_{LG} \leq 0 \end{cases} \quad (5-51)$$

5.2.8 Pumping Requirements

Four pumps are shown in Figures 5-2 and 5-3:

- ‘Aqueous Pump’, which pumps fermenter draw from fermenter pressure to the extraction pressure
- ‘DC1 Pump’, which pumps condensate from DC1 to the extraction pressure
- ‘DC2 Pump’, which pumps condensate from DC2 to the extraction pressure
- ‘DC2 Feed Pump’, which pumps the bottoms from DC1 to the pressure in DC2

For the purposes of calculating the energy required for pumping, an isentropic efficiency of 85% was assumed. Due to the relatively small pressure changes involved in the system, any temperature rise in the liquid during pumping was neglected. The volume change on mixing of water or solvent and butanol was also neglected. The energy required for each of the four pumps was therefore given by:

Aqueous Pump:

$$E_{aq-P} = \left(\left(\frac{B}{\eta} \right) \hat{V}_{Bu}(T_{ferm}) + W \hat{V}_{H2O}(T_{ferm}) \right) \frac{(P_{ext} - P_{ferm})}{0.85} \quad (5-52)$$

DC1 Pump

$$E_{DC1-P} = \left(S_{DC1} \hat{V}_{solv}(T_{cond,DC1}) \right) \frac{(P_{ext} - P_{DC1})}{0.85} \quad (5-53)$$

DC2 Pump

$$E_{DC2-P} = \left(S_{DC2} \hat{V}_{solv}(T_{cond,DC2}) \right) \frac{(P_{ext} - P_{DC1})}{0.85} \quad (5-54)$$

DC2 Feed Pump

$$E_{DC2\ feed-P} = \left(B \hat{V}_{Bu}(T_{reboil,DC1}) + S_{DC2} \hat{V}_{solv}(T_{reboil,DC1}) \right) \frac{(P_{DC2} - P_{DC1})}{0.85} \quad (5-55)$$

It should be noted that, depending on the extraction and fermentation pressure, the ‘Aqueous Pump’ might be required on the recycle stream rather than on the broth draw as shown in Figure 5-3 (*e.g.* solvents with normal vapour pressures below 1 bara). However, in this simulation, a fermenter pressure of 1 bara was assumed, and a hydrostatic head in the extraction column ($\Delta P_{ext,H}$) of 1 bara was assumed. Therefore, the extraction pressure was always above the fermentation pressure.

The power requirement of the pumps was electrical which was assumed to be provided by electrical production from heat produced in the upstream process. A conservative efficiency of 25% was assumed for the conversion of heat produced upstream in the plant to electricity.

5.2.9 Simulation in Matlab

The flowsheet was simulated in MathWorks® MATLAB. Simulation in a software package such as Matlab was particularly advantageous over a flowsheet package, such as UniSim, because it allowed simultaneous simulation of the model at many different operating conditions in order to optimise energy consumption.

Table 5-1 – Summary of numerical assumptions for the flowsheet simulation of the extraction of aqueous butanol by volatile hydrocarbons

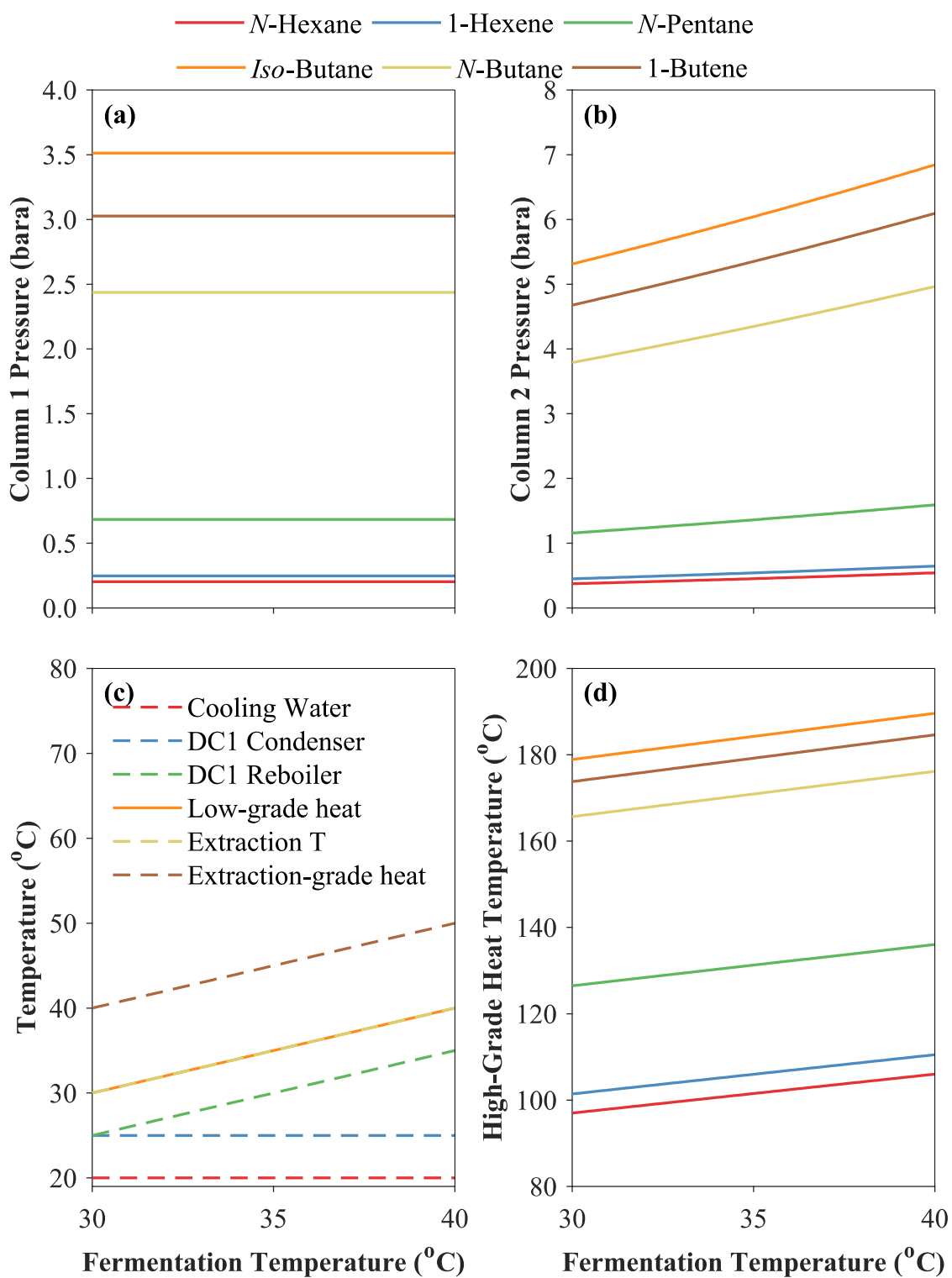
Parameter	Symbol	Value	Unit
Temperature Driving Force, DC1 and DC2 Reboiler	ΔT_{reboil}	5	°C
Temperature Driving Force, DC1 Condenser	ΔT_{cond}	5	°C
Temperature Driving Force, all other heat exchangers	ΔT_{HX}	10	°C
Cooling Water Temperature	T_{CW}	20	°C
Fermentation Temperatures	T_{ferm}	30 – 40	°C
Extraction Temperatures	T_{ext}	30 – 100	°C
Fermenter Pressure	P_{ferm}	1	bara
Isentropic Efficiency of Pumps		85	%
Efficiency of conversion of heat to electrical power		25	%
LLX Column, Hydrostatic Pressure	$\Delta P_{ext,H}$	1	bara
Number of Equilibrium Stages, LLX Column	N_{LLX}	5	
Number of Equilibrium Stages, Distillation Column 1	N_{DC1}	10	
Number of Equilibrium Stages, Distillation Column 2	N_{DC2}	20	

Table 5-1 summarises the numerical assumptions made in the flowsheet simulation. Physical properties (specific volumes, enthalpies of vaporisation, liquid enthalpies) were calculated as a function of temperature using DIPPR correlations (Rowley *et al.*, 2008), the parameters and equations for which are given in the Supplementary Material included with this dissertation.

5.3 Results of the Simple Flowsheet Model for Extractions Performed at Fermentation Temperatures

The flowsheet model was firstly run for cases in which the extraction was performed at the same temperature as the fermentation. This approach is simpler than extraction at elevated temperatures, because it could potentially be performed without cell removal, which might otherwise be required to prevent thermal shock. A cooling water temperature of 20°C was assumed. A temperature difference of 5°C was assumed in the condensers (ΔT_{cond}) and the DC1 reboiler (ΔT_{reboil}), and a temperature difference of 10°C was assumed for all other heat exchangers (ΔT_{HX}). These temperature driving forces of the reboiler and condenser in DC1 combined with the temperature of the cooling water necessitated a minimum fermentation temperature of 30°C *via* eq. (5-20) in order to utilise low-grade heat at the fermentation temperature in DC1. Fermentation temperatures in the range 30 – 40°C were therefore investigated.

Figure 5-4 shows the operating conditions (temperatures and pressures) for the system with fermentation temperatures in this range. As can be seen in Figure 5-4a-b, extractions employing C₅ and C₆ hydrocarbons as solvents required reduced pressures in DC1 and significantly so for C₆ solvents. Conversely, C₄ hydrocarbons required elevated pressures in both columns, up to 7 bara for the most volatile (*iso*-butane) in DC2. The operating temperatures determined by the fermentation temperature and the temperature driving forces are detailed in Figure 5-4c. As shown, the fermentation temperature is equal to the extraction temperature. The temperature gradient in DC1, *i.e.* the difference between the condenser and reboiler temperatures in DC1, thereby increased with fermentation temperature. As shown in Figure 5-4c, a fermentation temperature of at least 30°C was required to provide a temperature gradient in DC1; at 30°C, the temperature of the reboiler equals that of the condenser in DC1. The temperature of high-grade heat was a function of the extraction temperature (and hence, of the fermentation temperature in this case), as shown in Figure 5-4d for each solvent. It increased approximately linearly with fermentation temperature, up to a maximum of ~190°C for extraction by *iso*-butane from a broth at 40°C.



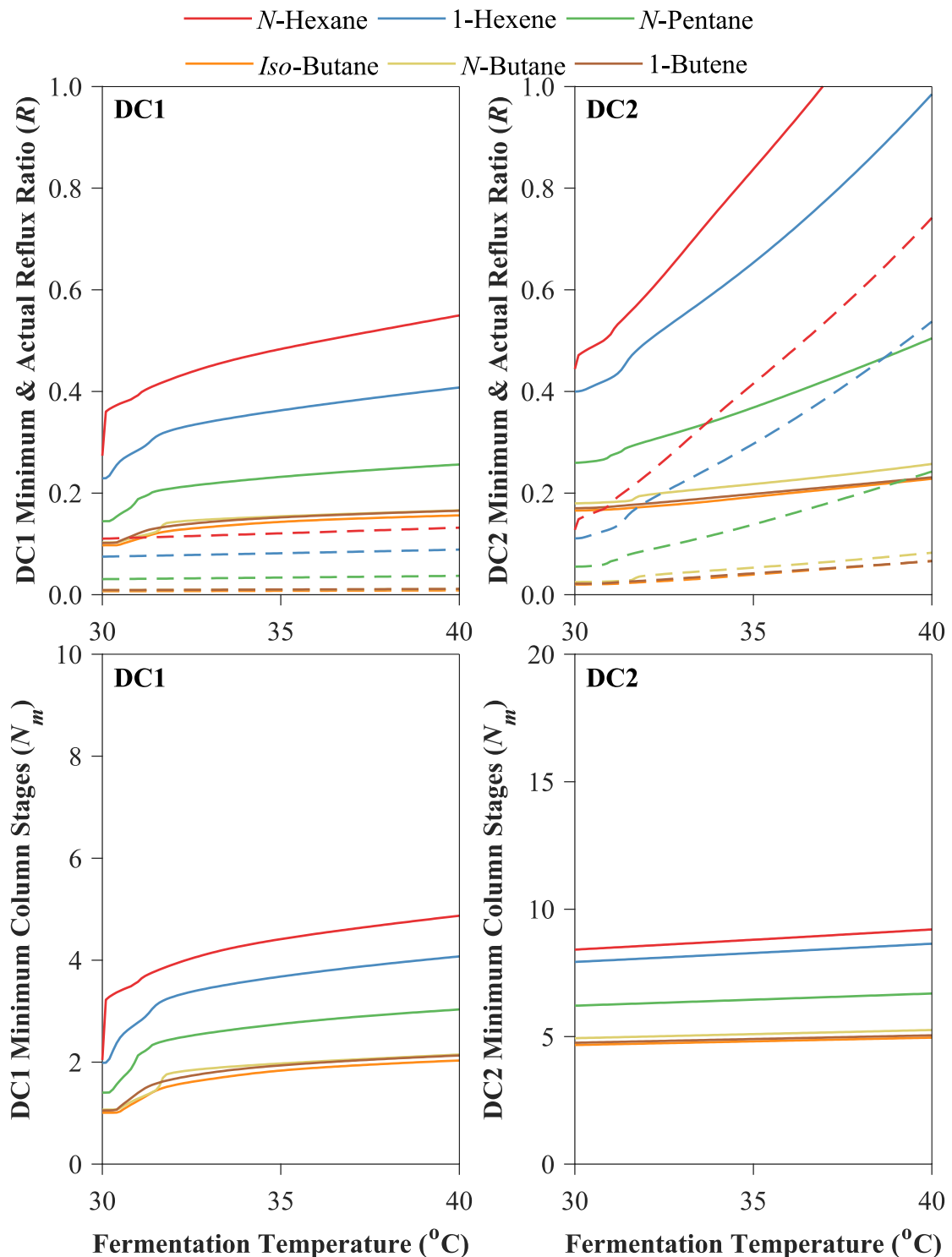
$$\Delta T_{cond} = 5^{\circ}\text{C}; \quad \Delta T_{cond} = 5^{\circ}\text{C}; \quad \Delta T_{HX} = 10^{\circ}\text{C}$$

$$T_{CW} = 20^{\circ}\text{C}; \quad T_{ext} = T_{ferm}$$

Figure 5-4a-d: Operating temperatures and pressures in the flowsheet model for extractions from aqueous butanol at fermentation temperatures

The actual and minimum reflux ratios, and the minimum number of stages for both DC1 and DC2, as calculated by the Fenske-Underwood-Gilliland method, is shown in Figure 5-5. As expected, the reflux ratio in DC1 was low (~0.1 for C₄ hydrocarbons) due to the large difference in volatility between the solvents and butanol. The reflux ratio was higher in DC2 because the relative volatility of the solvent *versus* butanol decreases with temperature, although it was still less than 0.2 for C₄ solvents. The reflux ratio of the less volatile C₆ solvents exceeded unity in DC2 at a fermentation temperature of 40°C, resulting in higher duties in DC2 for these solvents. In both columns, the ratio of minimum to actual number of equilibrium stages, N_m/N , was less than 0.5 for all solvents, and less than 0.25 for the C₄ solvents. This suggested that for the more volatile solvents, the number of stages in both columns could be halved without a significant impact on energy demand.

Figure 5-6 shows the concentration of butanol in the feed of each distillation column. The concentration of butanol in the feed to DC1 was determined by the distribution coefficient at equilibrium, the extraction efficiency and the butanol concentration in the aqueous broth. Figure 5-6 gives results for an extraction efficiency of 90% and an aqueous broth concentration of 2 wt% butanol. As shown in Figure 5-6a, the concentration in the feed to DC1, m_{feed} , increased slightly between 30°C and 40°C, due to an increase in distribution coefficient with temperature. The feed concentration in this example was around 1.5 – 3 wt% for the C₄ solvents. N-butane and 1-butene were predicted to have the highest distribution coefficients; extractions employing butane resulted in slightly higher butanol concentrations in the solvent at lower temperatures, whilst extractions employing 1-butene resulted in slightly higher butanol concentrations at higher temperatures. It was not possible to explore the effect of temperature on the distribution coefficient of butanol between *iso*-butane and water because the required VLE measurements for butanol-*iso*-butane mixtures were only available at 318 K. The distribution coefficient calculated at 318 K would probably be slightly higher than that at fermentation temperatures (< 313 K), based on the temperature dependence of the distribution coefficient in other C₄ hydrocarbons. As a result, the distribution coefficient was taken as constant with temperature and so the feed concentration of butanol to DC1 did not vary with fermentation temperature for extractions using *iso*-butane, as shown in Figure 5-6a.



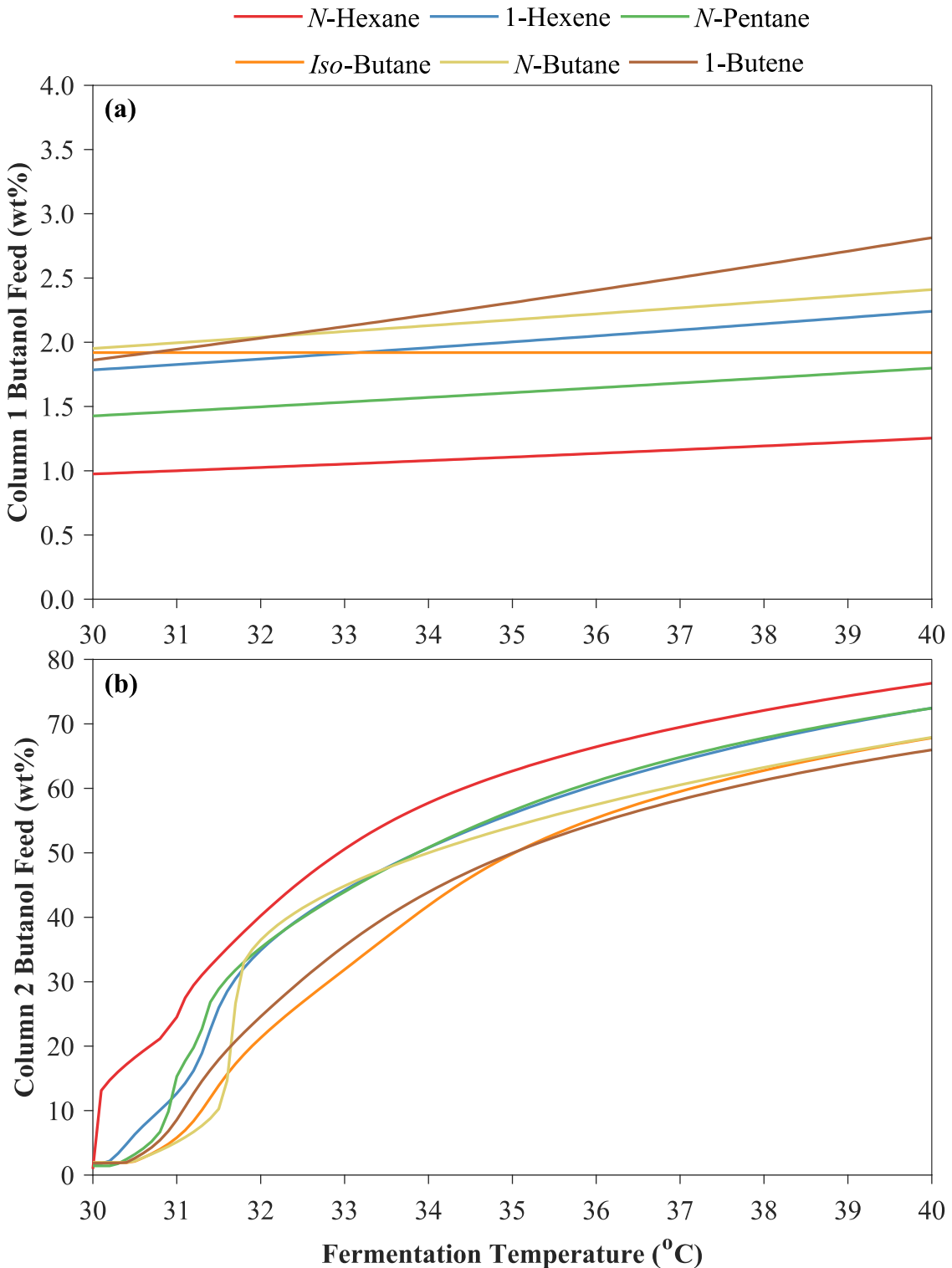
$$\Delta T_{cond} = 5^{\circ}\text{C}; \quad \Delta T_{cond} = 5^{\circ}\text{C}; \quad \Delta T_{HX} = 10^{\circ}\text{C}$$

$$T_{CW} = 20^{\circ}\text{C}; \quad T_{ext} = T_{ferm}$$

$$N_{LLX} = 5; \quad N_{DC1} = 10; \quad N_{DC2} = 20; \quad \beta = 90\%; \quad \eta = 75\%$$

Figure 5-5: Column stages and reflux ratios predicted by the flowsheet model for extractions from aqueous butanol at 2 wt% performed at fermentation temperatures

Minimum Reflux Ratios: dashed lines; Actual Reflux Ratios: solid lines



$$\Delta T_{cond} = 5^{\circ}\text{C}; \quad \Delta T_{cond} = 5^{\circ}\text{C}; \quad \Delta T_{HX} = 10^{\circ}\text{C}; \quad E_{LG}^{ferm} = 0 \text{ MJ/kg}$$

$$T_{CW} = 20^{\circ}\text{C}; \quad T_{ext} = T_{ferm}; \quad m_{Bu}^{aq} = 2.0 \text{ wt\%}; \quad m_{Bu,DC1} = m_{Bu,DC1}^{max}$$

$$N_{LLX} = 5; \quad N_{DC1} = 10; \quad N_{DC2} = 20; \quad \beta = 90\%; \quad \eta = 75\%$$

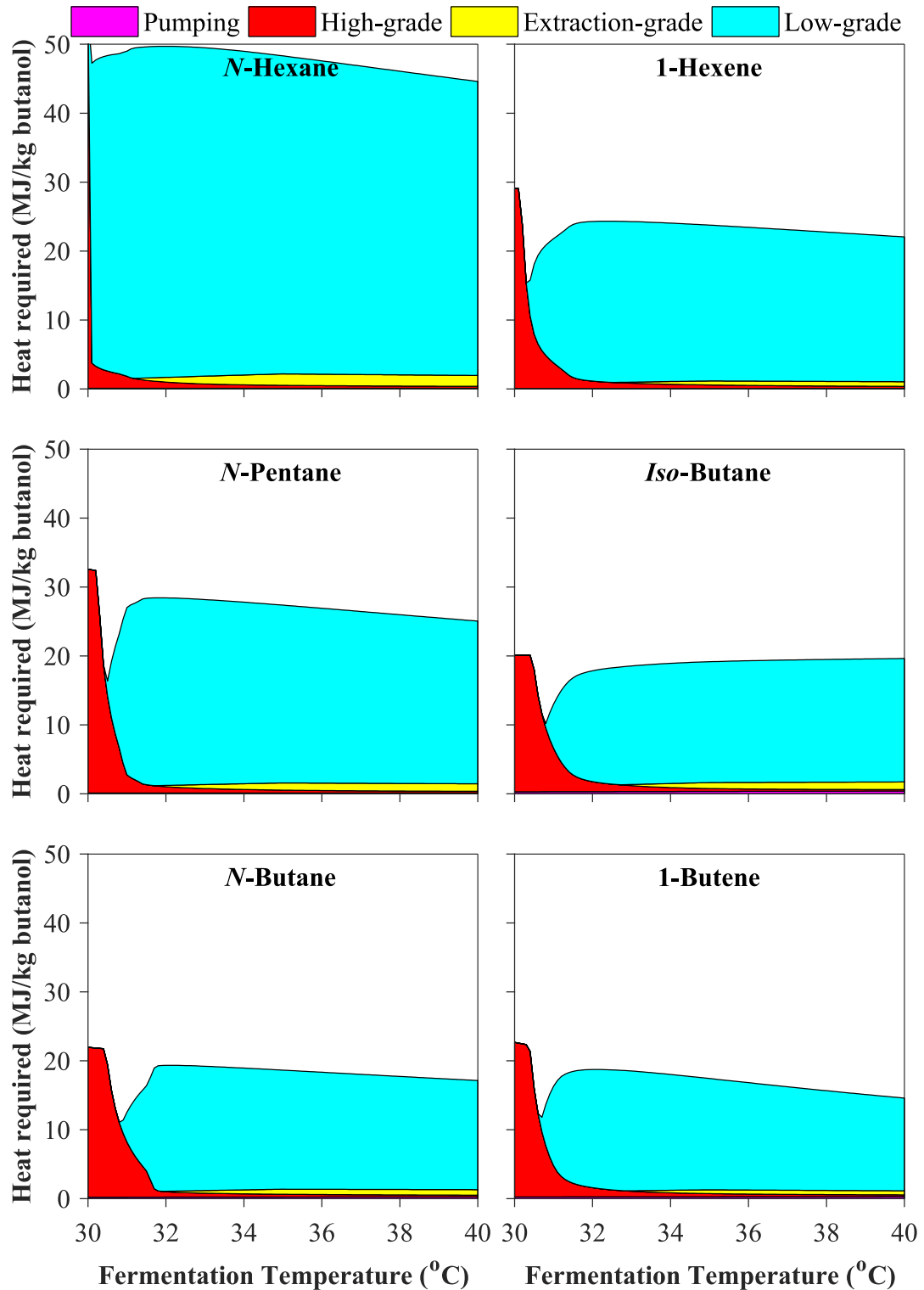
Figure 5-6a-b: Butanol composition of feeds to each distillation column (a: DC1, b: DC2) calculated by the flowsheet model for extractions from aqueous butanol at 2 wt% performed at fermentation temperature

The concentration of butanol in the feed to DC2 (from the bottoms of DC1) was a function of the VLE between the solvent and butanol, and the temperature gradient in DC1. When the temperature of the fermentation was very close to 30°C, the temperature of required low-grade heat was low and the temperature gradient in the first column was close to zero, as shown in Figure 5-4c. Thus, at fermentation temperatures close to 30°C, DC1 could not produce a concentration of butanol higher than that of its feed.

However, as shown in Figure 5-6b, the flowsheet model found that even a small temperature gradient (1 – 2°C) enabled DC1 to concentrate butanol significantly. The butanol composition in the bottoms of DC1 exceeded 20 wt% in all solvents for a fermentation temperature of 32°C (2°C gradient in DC1). At slightly higher fermentation temperatures the butanol composition produced by DC1 was significantly higher, exceeding 50 wt% in all solvents for a fermentation temperature of 37°C.

The heat requirements of the extraction and distillation system, categorised by grade of heat, are detailed in Figure 5-7 and 5-8 for fermentation broth concentrations of 2 wt% and 1 wt% butanol respectively. Beyond fermentation temperatures of 30 – 32°C, DC1 could produce butanol at a high concentration and performed most of the separation. Hence, as shown in both figures, the high-grade heat required for the reboiler on DC2 is trivial (< 0.5 MJ/kg butanol). The aqueous concentration did not affect the high-grade heat required. This was because the concentration of butanol in the feed to DC2 was unaffected by the aqueous concentration, provided that there was a small temperature gradient in DC1 to concentrate the butanol beyond that achieved by the extraction.

A small amount of extraction-grade heat was also required to re-heat the solvent produced in the distillate of DC1 to the extraction temperature before solvent recycle. Most of the solvent was separated by DC1; as a result, the duty of the condenser in DC2 was low and therefore very little extraction-grade heat could be provided by the condenser in DC2. Above broth temperatures of 30 – 32°C, the extraction-grade and high-grade heat requirements were less than 1 – 2 MJ/kg butanol for all solvents for an aqueous broth of 2 wt%. Simulations of distillation in Appendix A found that the separation of butanol and water by distillation requires approximately $28/m_{Bu}^{aq}$ (wt%) MJ/kg butanol. Therefore, the total extraction-grade and high-grade heat requirements predicted by the flowsheet model represented ~10% of the energy cost of distillation for the separation of aqueous butanol at 2 wt%.



$$\Delta T_{cond} = 5^{\circ}\text{C}; \Delta T_{cond} = 5^{\circ}\text{C}; \Delta T_{HX} = 10^{\circ}\text{C}; E_{LG}^{ferm} = 0 \text{ MJ/kg}$$

$$T_{CW} = 20^{\circ}\text{C}; T_{ext} = T_{ferm}; m_{Bu}^{aq} = 2.0 \text{ wt\%}; m_{Bu,DC1} = m_{Bu,DC1}^{\max}$$

$$N_{LLX} = 5; N_{DC1} = 10; N_{DC2} = 20; \beta = 90\%; \eta = 75\%$$

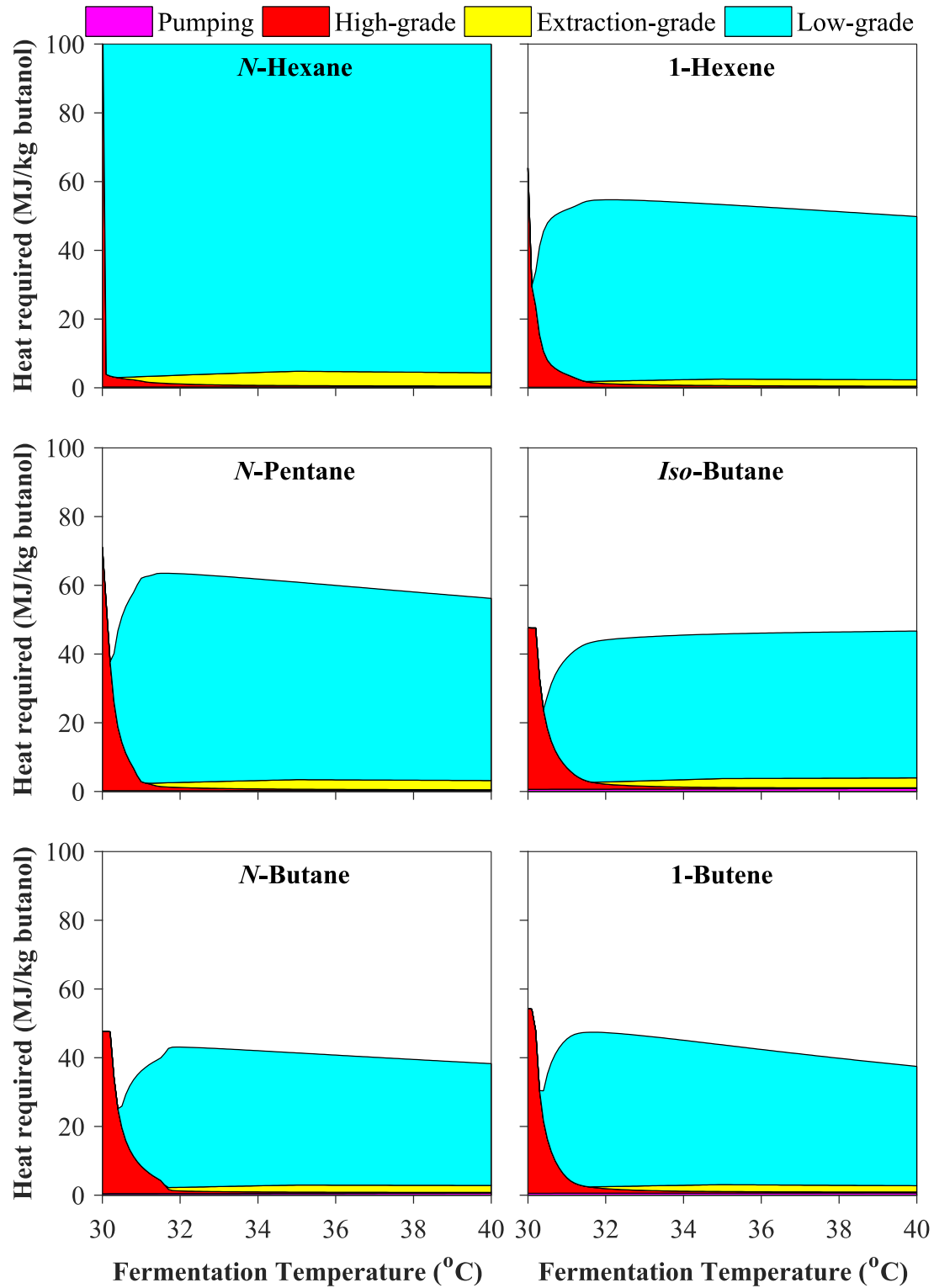
Figure 5-7: Net energy requirements predicted by the flowsheet model for extractions from aqueous butanol feeds of 2 wt% performed at fermentation temperatures using six hydrocarbon solvents

The extraction-grade heat requirements for the extraction of aqueous butanol at 1 wt% (Figure 5-8) were around double those of a 2 wt% broth, since the quantity of solvent produced in the distillate of DC1 was around double that at 2 wt%. Hence, since there was no additional extraction-grade heat provided by the condenser of DC2, the total high-grade and extraction-grade heat requirements increased to 3 – 5 MJ/kg butanol for all solvents, as shown in Figure 5-8.

The quantity of extraction-grade heat also increased slightly with fermentation temperature. The main reason for this was that the quantity of extraction-grade heat provided from the condenser of DC2 decreased as the extraction temperature (equal to the fermentation temperature) increased, because lower quantities of solvent were condensed in the distillate of DC2.

The low-grade heat required was clearly significant for all solvents, as shown in both Figures 5-7 and 5-8. For extractions from a 2 wt% broth (Figure 5-7), C₄ and 1-hexene solvents required 10 – 15 MJ/kg butanol of low-grade heat above broth temperatures of 32°C. Extraction using pentane required 15 – 20 MJ/kg butanol, whilst hexane required 25 – 30 MJ/kg butanol of low grade-heat. The low-grade heat requirements for extraction of butanol from a 1 wt% broth were roughly twice that from a 2 wt% broth, since the feed concentration to DC1 is reduced by around a factor of two.

The variation in the low-grade heat required between each solvent was due to the distribution coefficient of butanol in the solvent; higher distribution coefficients resulted in higher feed concentrations to DC1, and consequently lower low-grade heat requirements. This also resulted in lower extraction-grade heat requirements, due to the lower quantity of solvent that needed re-heating to extraction temperatures. Since distribution coefficient was predicted to increase with temperature, a reduction in low-grade heat requirements as the fermenter temperature increased was also predicted. This is most noticeable for 1-butene, as shown in both Figures 5-7 and 5-8. It should be remembered that the distribution coefficient in *iso*-butane was not temperature-dependent, because the required measurements of VLE were only available at 318 K.



$$\Delta T_{cond} = 5^{\circ}\text{C}; \Delta T_{cond} = 5^{\circ}\text{C}; \Delta T_{HX} = 10^{\circ}\text{C}; E_{LG}^{ferm} = 0 \text{ MJ/kg}$$

$$T_{CW} = 20^{\circ}\text{C}; T_{ext} = T_{ferm}; m_{Bu}^{aq} = 1.0 \text{ wt\%}; m_{Bu,DC1} = m_{Bu,DC1}^{max}$$

$$N_{LLX} = 5; N_{DC1} = 10; N_{DC2} = 20; \beta = 90\%; \eta = 75\%$$

Figure 5-8: Net energy requirements predicted by the flowsheet model for extractions from aqueous butanol feeds of 1 wt% performed at fermentation temperatures using six hydrocarbon solvents

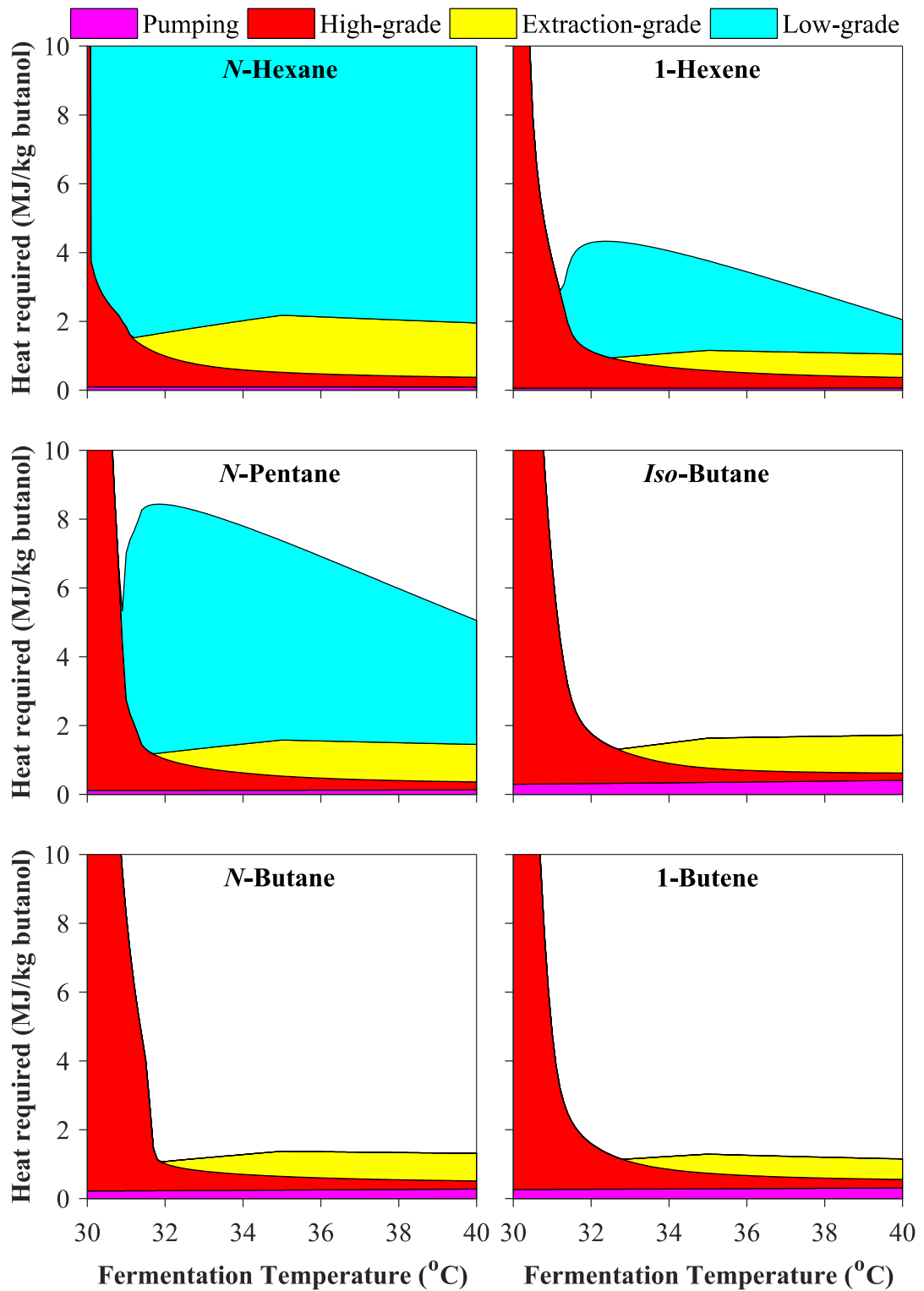
5.3.1 Accounting for the Supply of Low-Grade Heat

The low-grade heat requirement clearly dominated the heat requirements of the separation system. This heat could partly be provided by waste heat from the fermenter. The heat produced by the organisms during the fermentation of synthesis gases, as well as during ABE and *iso*-butanol fermentations, was estimated in Appendix G. The fermentation of synthesis gases was found to produce large quantities of low-grade heat; 20 MJ/kg butanol produced was estimated for the total heat evolved from both the organisms (~16 MJ/kg) and the stirrer (~4 MJ/kg at 2 kW/m³ and 1 kg butanol/m³/h). ABE and *iso*-butanol fermentations were found to have a significantly lower heats of reaction, and were estimated to produce around 1 – 2 MJ/kg butanol of low-grade heat.

However, the fermenter would not be the only source of low-grade, waste heat on such fermentation plants. Low-grade heat could be abundant on a fermentation plant from processes such as: seed train fermentation processes, upstream substrate preparation, such as acid and enzymatic hydrolysis of biomass, waste heat from sterilisation processes, high-rate wastewater treatment and any vapour streams from upstream flash separations to increase slurry concentration and remove volatile components. In the case of biochemical processes, the analysis in Appendix G did not consider heat sources (such as the temperature of liquid feeds) which might contribute to fermenter heat other than the heat generated by the organism and the stirrer. The quantity and temperature of low-grade heat which would be economically viable for use on different types of fermentation plants could vary significantly, and so was difficult to estimate.

As an example, Figure 5-9 shows the heat requirements of the separation system for extractions performed at fermentation temperatures from a 2 wt% aqueous broth with a low-grade heat supply of 20 MJ/kg butanol. Figure 5-10 shows the same for a 1 wt% broth. As shown in Figure 5-9, for extractions from a 2 wt% broth, 20 MJ/kg butanol was found to be sufficient to provide the low-grade heat requirements for most solvents. This led to total heat requirements of less than 2 MJ/kg butanol. This was mostly in the form of extraction-grade heat, which was at a relatively low temperature (< 50°C), as shown in Figure 5-9.

For a fermenter concentration of 1 wt% butanol, 20 MJ/kg butanol of waste heat from the fermenter was found to be insufficient to provide all the low-grade heat requirements for all solvents, as shown in Figure 5-10.

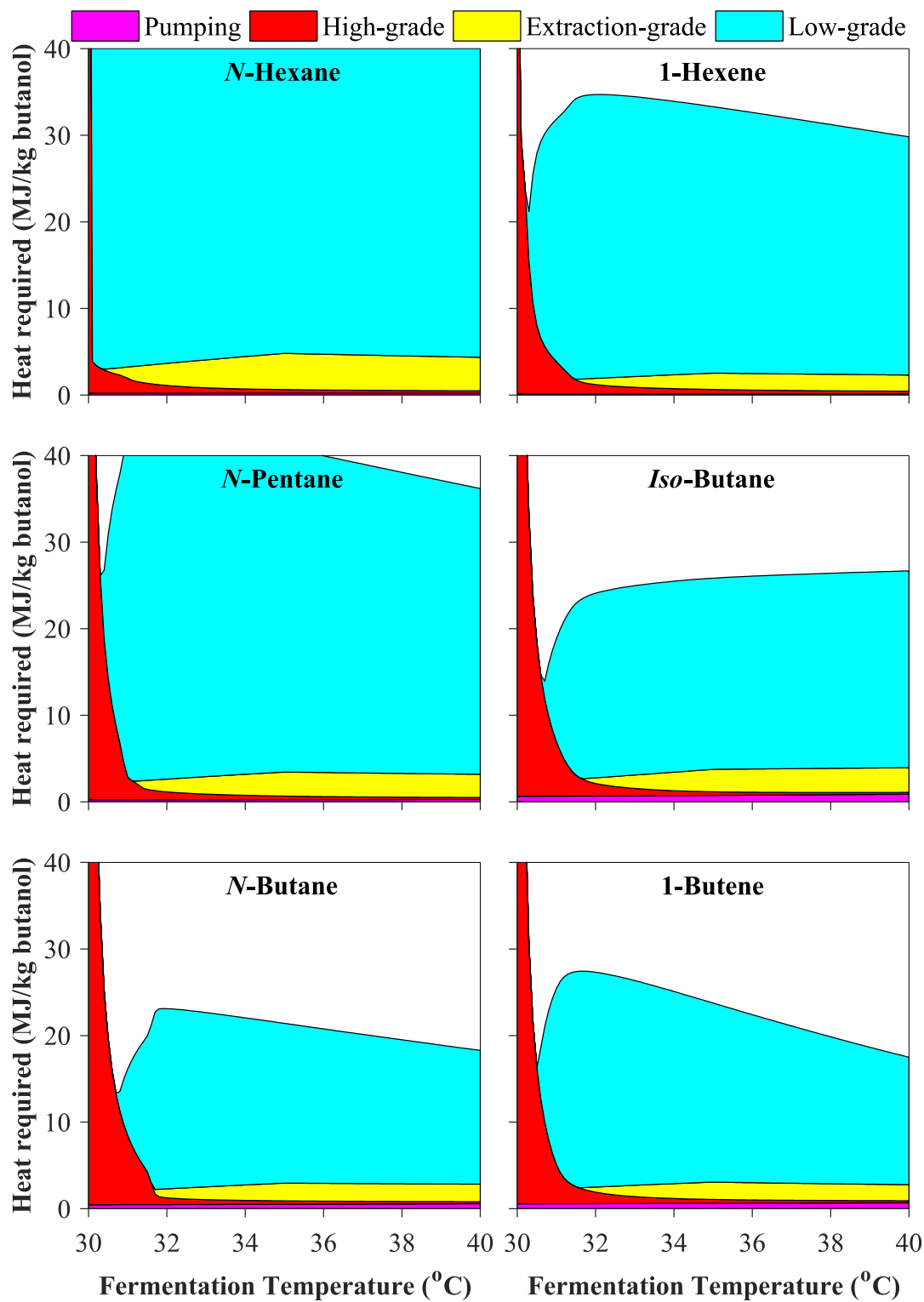


$$\Delta T_{cond} = 5^{\circ}\text{C}; \Delta T_{cond} = 5^{\circ}\text{C}; \Delta T_{HX} = 10^{\circ}\text{C}; E_{LG}^{ferm} = 20 \text{ MJ/kg}$$

$$T_{CW} = 20^{\circ}\text{C}; T_{ext} = T_{ferm}; m_{Bu}^{aq} = 2.0 \text{ wt\%}; m_{Bu,DC1} = m_{Bu,DC1}^{\max}$$

$$N_{LLX} = 5; N_{DC1} = 10; N_{DC2} = 20; \beta = 90\%; \eta = 75\%$$

Figure 5-9: Net energy requirements predicted by the flowsheet model for extractions from aqueous butanol feeds of 2 wt% performed at fermentation temperatures, with 20 MJ/kg low-grade heat provided by the fermenter



$$\Delta T_{cond} = 5^{\circ}\text{C}; \Delta T_{cond} = 5^{\circ}\text{C}; \Delta T_{HX} = 10^{\circ}\text{C}; E_{LG}^{ferm} = 20 \text{ MJ/kg}$$

$$T_{CW} = 20^{\circ}\text{C}; T_{ext} = T_{ferm}; m_{Bu}^{aq} = 1.0 \text{ wt\%}; m_{Bu,DC1} = m_{Bu,DC1}^{\max}$$

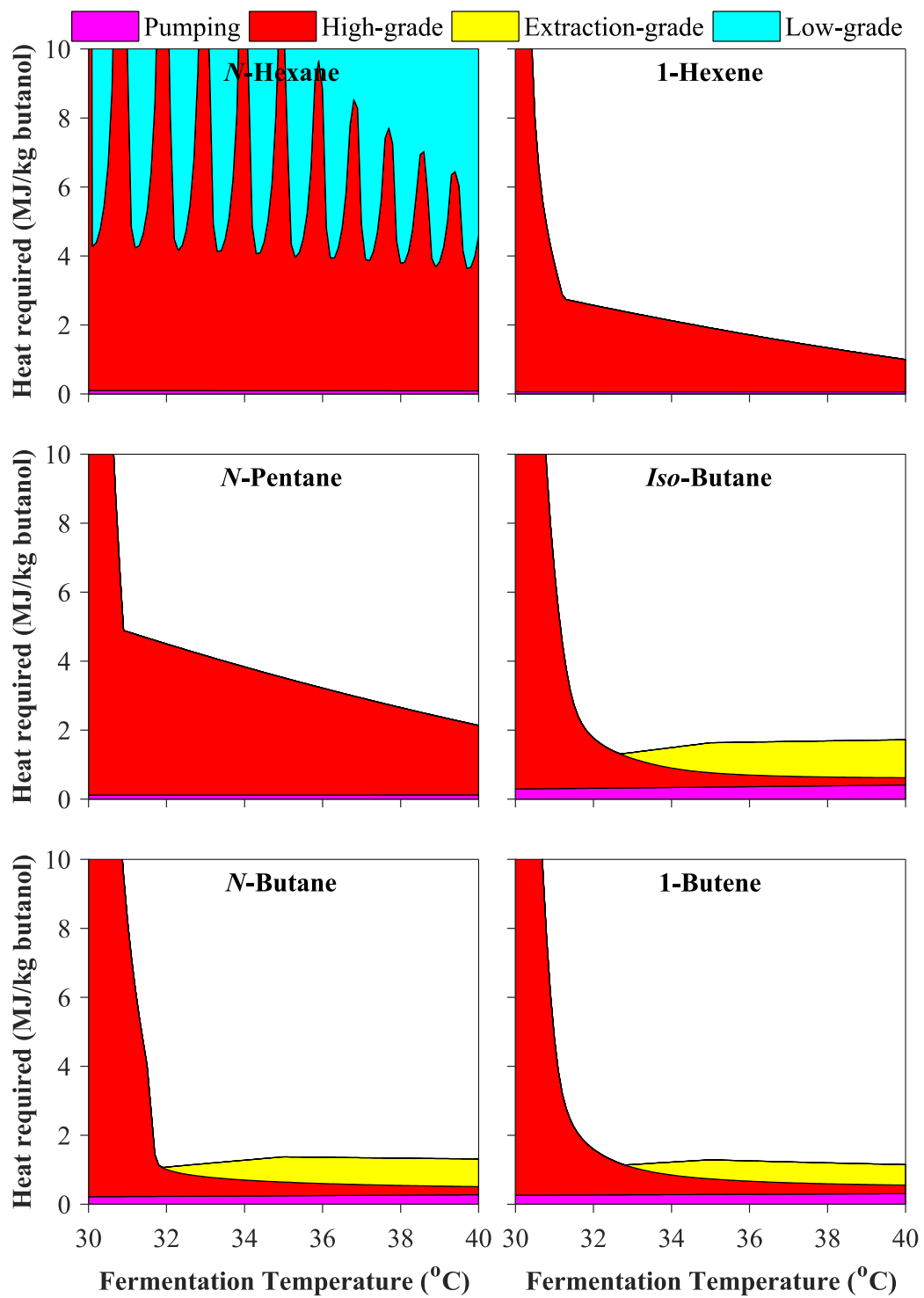
$$N_{LLX} = 5; N_{DC1} = 10; N_{DC2} = 20; \beta = 90\%; \eta = 75\%$$

Figure 5-10: Net energy requirements predicted by the flowsheet model for extractions from aqueous butanol feeds of 1 wt% performed at fermentation temperatures, with 20 MJ/kg low-grade heat provided by the fermenter

5.3.2 Optimising the Temperature Gradient of DC1

If 20 MJ/kg butanol were the total quantity of low-grade heat available on the fermentation plant, the remaining low-grade heat requirements would have to be supplied by heat of a higher grade. One method to reduce the heat requirement would be to increase the condenser temperature in DC1, thereby reducing the temperature gradient in the column. Consequently, this would reduce the low-grade heat required in DC1 and thus the composition of butanol produced by DC1. Whilst this would increase the heat required by DC2, the heat supplied to DC2 can be used to displace other heat requirements: heat generated in the condenser of DC2 could be used to supply extraction-grade heat elsewhere in the system. Or, if the supply of extraction-grade heat exceeded demand, then it could be used to supply low-grade heat. Conversely, heat supplied to DC1 is merely lost in cooling water utility. Therefore, supplying higher grade heat to DC1 would be less efficient than shifting demand onto DC2 and supplying more high-grade heat to DC2. This modification was simulated in the flowsheet model by increasing ΔT_{cond} , thereby raising the temperature of the condenser in DC1 ($T_{cond}^{DC1} = T_{CW} + \Delta T_{cond}$). Figure 5-11 details the heat requirements predicted by a flowsheet simulation of the extraction of 2 wt% aqueous butanol, in which ΔT_{cond} was varied in order to match the low-grade heat requirement to that available as waste heat and from heat integration. The simulation was repeated for extraction from a 1 wt% aqueous broth, shown in Figure 5-12. In both simulations, it was assumed that 20 MJ/kg butanol of low-grade heat was available from the fermenter.

Alternatively, the reboiler temperature in DC1 could be decreased. This would have a similar effect to increasing the condenser temperature, since the temperature gradient would be decreased. However, it was found to be more energy efficient to increase the condenser temperature, because this strategy reduces the heat required to re-heat the solvent produced from the condenser of DC1. Reducing the condenser temperature also increased the pressure of the lowest pressure in the system (DC1), thereby reducing the energy required for pumping.

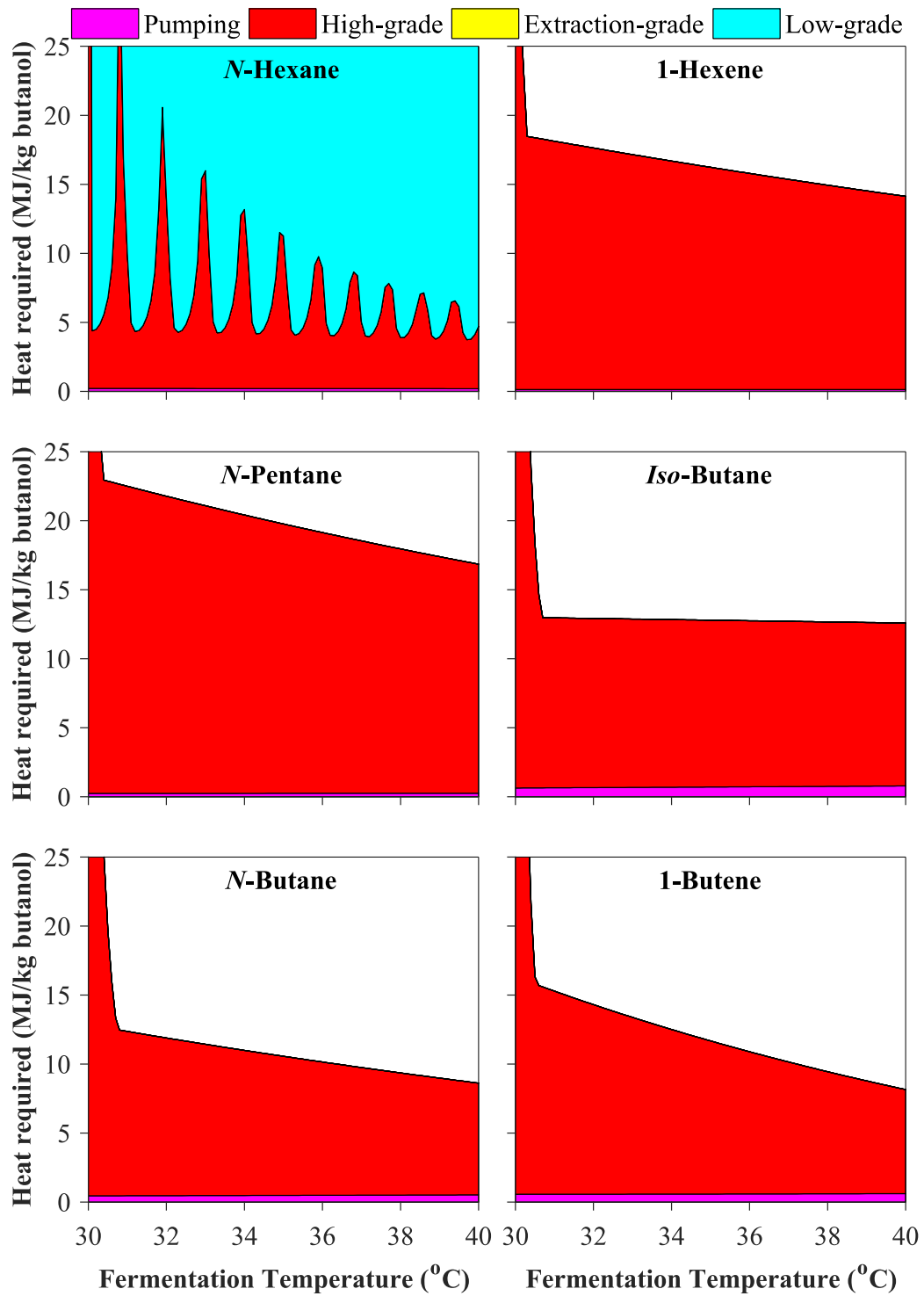


$$\Delta T_{cond} = 5^{\circ}\text{C}; \Delta T_{cond} = 5^{\circ}\text{C}; \Delta T_{HX} = 10^{\circ}\text{C}; E_{LG}^{ferm} = 20 \text{ MJ/kg}$$

$$T_{CW} = 20^{\circ}\text{C}; T_{ext} = T_{ferm}; m_{Bu}^{aq} = 2.0 \text{ wt\%}; m_{Bu,DC1} = m_{Bu,DC1}^{optim}$$

$$N_{LLX} = 5; N_{DC1} = 10; N_{DC2} = 20; \beta = 90\%; \eta = 75\%$$

Figure 5-11: Heat requirements predicted by the flowsheet model for the extraction of aqueous butanol at 2 wt% using six hydrocarbons solvents at fermentation temperatures, with 20 MJ/kg low-grade heat available. The temperature gradient of DC1 was optimised to minimise the total heat demand.



$$\Delta T_{cond} = 5^\circ\text{C}; \Delta T_{ext} = 5^\circ\text{C}; \Delta T_{HX} = 10^\circ\text{C}; E_{LG}^{ferm} = 20 \text{ MJ/kg}$$

$$T_{CW} = 20^\circ\text{C}; T_{ext} = T_{ferm}; m_{Bu}^{aq} = 1.0 \text{ wt\%}; m_{Bu,DC1} = m_{Bu,DC1}^{\text{optim}}$$

$$N_{LLX} = 5; N_{DC1} = 10; N_{DC2} = 20; \beta = 90\%; \eta = 75\%$$

Figure 5-12: Heat requirements predicted by the flowsheet model for the extraction of aqueous butanol at 1 wt% using six hydrocarbons solvents at fermentation temperatures, with 20 MJ/kg low-grade heat available. The temperature gradient of DC1 was optimised to minimise the total heat demand.

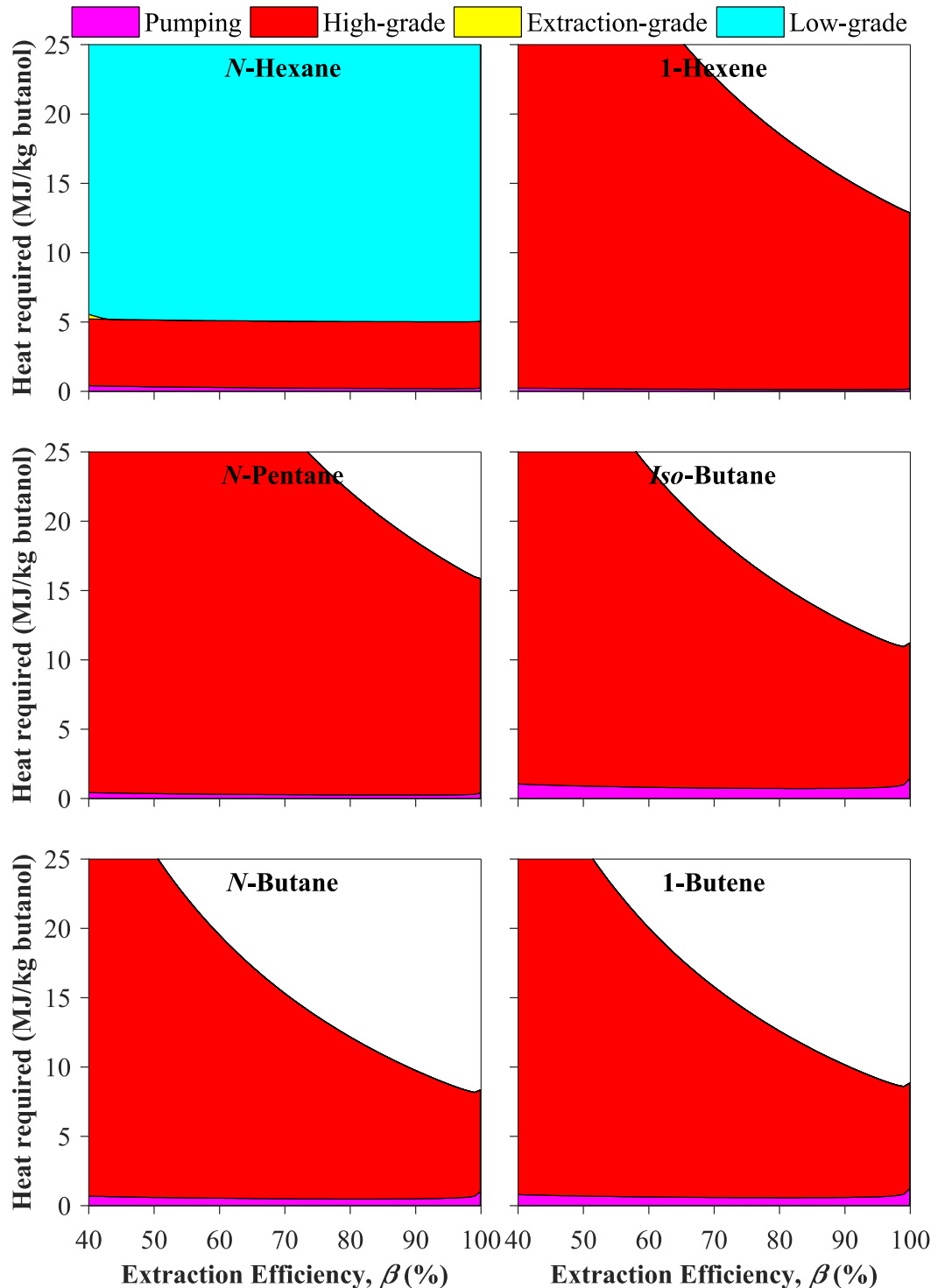
As can be seen in Figure 5-11, in contrast to Figure 5-9 for pentane, optimising the composition of butanol produced in DC1 led to reductions in the total heat demand. However, it necessitated more heat in the form of high-grade heat. The effect of reduced overall heat demand is more pronounced in Figure 5-12, which shows the optimised system for a 1 wt% aqueous broth. For *n*-butane, total heat demand was under 10 MJ/kg butanol above fermentation temperatures of ~32°C.

Simulations of extractions employing hexane required very small temperatures gradients in DC1 because of the large requirement for low-grade heat for extractions with this solvent. This led to instabilities in the simulation results, as seen in both Figures 5-11 and 5-12. The VLE of hexane and butanol included an azeotrope at a low butanol composition, which was ignored for the purposes of the simulation. However, this prevented the simulation from being able to produce a butanol composition in the bottoms of DC1 lower than that of the azeotrope composition. This caused instability in the calculation of the composition of butanol produced by DC1.

5.3.3 Optimisation of Extraction Efficiency

The optimisation of one other parameter was considered: extraction efficiency (β). As discussed in Section 4.6, there is a trade-off between extraction efficiency and transfer efficiency, being inversely proportional to each other for a fixed number of extraction stages. Higher extraction efficiency results in higher butanol concentrations in the solvent, and hence lowers the heating and pumping requirements in the solvent phase. Higher transfer efficiency results in lower water flowrates, and hence higher energy penalties on the aqueous side of the extraction. The heat requirements of the system for extraction at a fermentation temperature of 37°C of aqueous butanol at 1 wt%, with a low-grade heat supply of 20 MJ/kg butanol, are shown in Figure 5-13 as a function of extraction efficiency. The temperature gradient of DC1 was also optimised to minimise net heat consumption.

As can be seen in Figure 5-13, optimal extraction efficiencies are above 95% for all solvents; indeed, for less volatile solvents requiring near-ambient pressures of extraction, the minima are scarcely visible. The effect of decreased extraction efficiency on the net heat requirement was found to be large: ~4 MJ/kg butanol for every 10% decrease in extraction efficiency.



$$\Delta T_{cond} = 5^{\circ}\text{C}; \Delta T_{cond} = 5^{\circ}\text{C}; \Delta T_{HX} = 10^{\circ}\text{C}; E_{LG}^{ferm} = 20 \text{ MJ/kg}$$

$$T_{CW} = 20^{\circ}\text{C}; T_{ext} = T_{ferm}; m_{Bu}^{aq} = 1.0 \text{ wt\%}; m_{Bu,DC1} = m_{Bu,DC1}^{optim}$$

$$N_{LLX} = 5; N_{DC1} = 10; N_{DC2} = 20; \beta = \text{Various}; \eta = \text{Various}$$

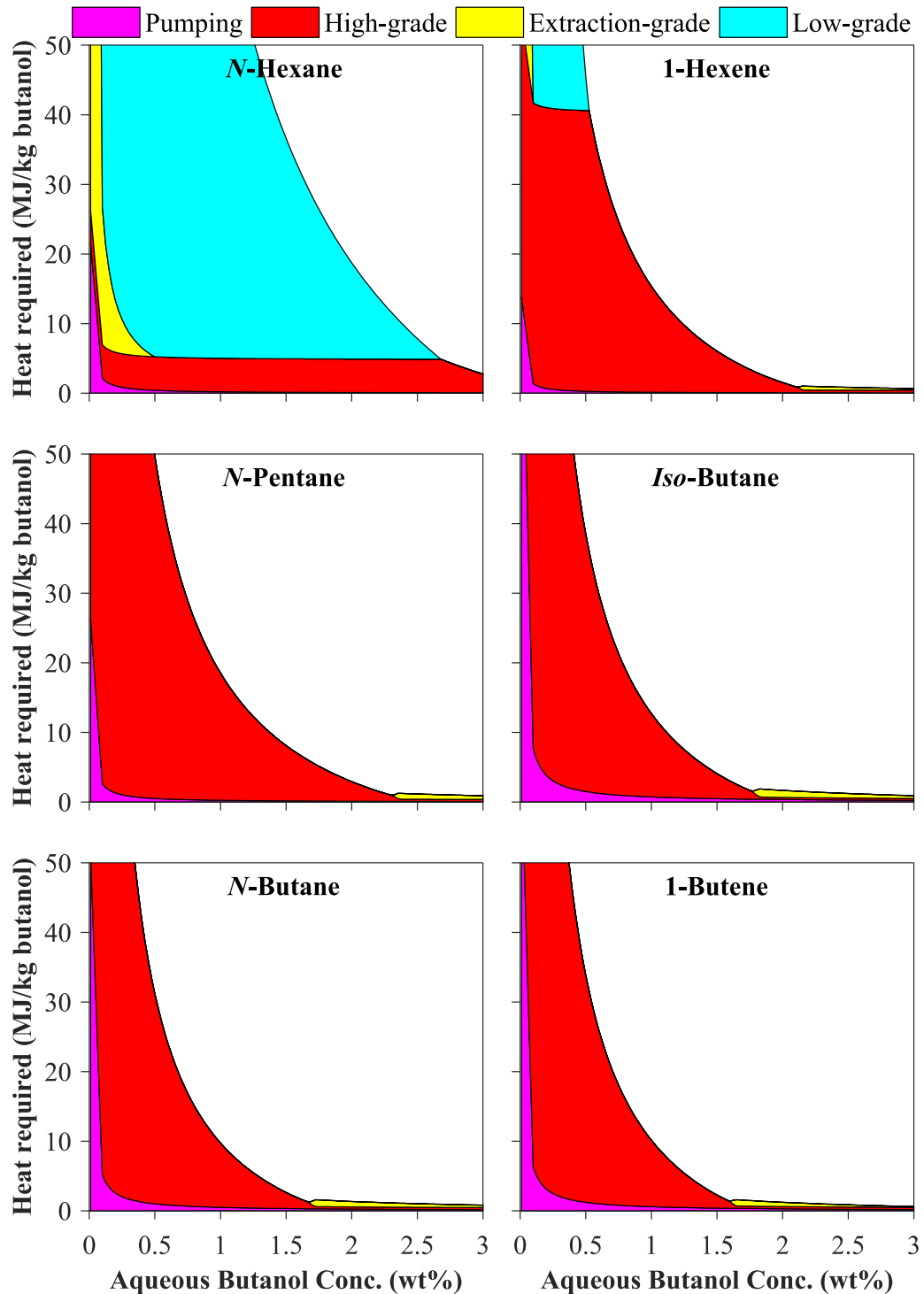
Figure 5-13: Heat requirements predicted by the flowsheet model for the extraction of aqueous butanol at 1 wt% using six hydrocarbons solvents as a function of extraction efficiency, with 20 MJ/kg low-grade heat available. The temperature gradient of DC1 was optimised to minimise the total heat demand.

5.3.4 Effect of the Composition of Aqueous Butanol

Finally, the effect of the composition of aqueous butanol on the energy requirements of the separation system is detailed in Figure 5-14. The simulation given in this figure was for a fermentation temperature of 37°C, an extraction efficiency of 90%, and a supply of low-grade heat of 20 MJ/kg butanol; the temperature gradient of DC1 was optimised to minimise total heat consumption. As shown, the low-grade heat supply was insufficient at low concentrations, requiring large quantities of high-grade heat in DC1. Therefore, if supply of low-grade heat is limited and the titre of butanol is very low, another approach is required.

5.4 Discussion: Extraction at Fermentation Temperatures

Large, positive deviations from Raoult's Law were predicted for the VLE of butanol and volatile hydrocarbons by the Leg-virial Model in Chapter 3, especially above dilute butanol concentrations. The VLE behaviour of butanol with C₄ hydrocarbons was found to be optimal for the extraction of butanol. Despite having bubble-point pressure gradients close to that of Raoult's Law at infinite dilution which resulted in large distribution coefficients for the extraction of dilute butanol, above these dilute butanol concentrations, C₄ hydrocarbons exhibited large positive deviations from Raoult's Law. The shallow bubble-point pressure gradient at moderate butanol concentration for the VLE of butanol with C₄ – C₅ solvents causes rapid changes in the bubble-point composition with temperature. This behaviour is demonstrated in Figure 5-6b, which shows the butanol composition produced by DC1 increasing dramatically above fermentation temperatures of 31 – 32°C (temperature gradient of 1 – 2°C in DC1). At a fermentation temperature of 37°C, DC1 was predicted to produce butanol at 50 – 70 wt% using low-grade heat from the fermenter (7°C temperature gradient in DC1). These results, based on the VLE models devised in Chapter 3, were far higher than the predictions of around 20 - 25 wt% butanol made using Raoult's Law in Section 2.5 for the same temperature gradients in DC1. This high composition of butanol is significant as it means that the vast majority of the separation of butanol and the solvent could be performed in DC1 using only low-grade heat, even with temperature differences between the cooling water and the low-grade heat as low as 12 – 17°C. As a result, the requirements for high-grade heat (in DC2) were predicted to be insignificant, as shown in Figures 5-7 and 5-8.



$$\Delta T_{cond} = 5^{\circ}\text{C}; \Delta T_{cond} = 5^{\circ}\text{C}; \Delta T_{HX} = 10^{\circ}\text{C}; E_{LG}^{ferm} = 20 \text{ MJ/kg}$$

$$T_{CW} = 20^{\circ}\text{C}; T_{ext} = T_{ferm}; m_{Bu}^{aq} = \text{Various}; m_{Bu,DC1} = m_{Bu,DC1}^{optim}$$

$$N_{LLX} = 5; N_{DC1} = 10; N_{DC2} = 20; \beta = 90\%; \eta = 75\%$$

Figure 5-14: Heat requirements predicted by the flowsheet model for the extraction of aqueous butanol using six hydrocarbons solvents as a function of aqueous butanol composition, with 20 MJ/kg low-grade heat available. The temperature gradient of DC1 was optimised to minimise the total heat demand.

The total heat requirements of the separation system, excluding low-grade heat requirements, increased with fermentation temperature above $\sim 32^{\circ}\text{C}$. This was perhaps counter-intuitive, because the distribution coefficient increased with temperature. Whilst an increased fermentation temperature resulted in a decrease in low-grade heat requirements (*e.g.* Figure 5-7), it also led to an increase in extraction-grade heat requirements. The increased fermentation temperature resulted in an increase in the temperature of low-grade heat thereby increasing the concentration of butanol in the feed of DC2, and hence reducing the duty of DC2. This reduced the high-grade heat requirement. However, this reduction in high-grade heat was merely exchanged for an increase of the same magnitude in requirement for extraction-grade heat, as the reduction in duty of DC2 also reduced the extraction-grade heat provided by the condenser of DC2.

In addition, the increase in the fermenter temperature increased the temperature of the extraction, which thereby increased the quantity of heat required to re-heat the solvent from the temperature of the condenser in DC1 (determined by the temperature of the cooling water). This increase in extraction-grade heat requirement outweighed the effect of the slight reduction in solvent flowrate which resulted from the increased distribution coefficient at a higher extraction temperature.

As predicted, the energy requirements of the extraction scheme were found to be minimised at very high extraction efficiencies, as shown in Figure 5-13. This was because for extractions performed at the fermentation temperature, energy was only required in the aqueous phase for the aqueous pump. Therefore, the optimum system was approximately an *in situ* extraction system, where extraction would be performed directly in the fermenter (where effectively $\beta = 100\%, \eta = 0\%$). In practice, the transfer efficiency (η) would have a lower limit in an *in stream* extraction, as there are limitations on the ratio of solvent-to-aqueous flowrates (eq. 4-33) in the design of the extractor. There would likely be other costs and problems associated with very high broth flowrates as $\eta \rightarrow 0$. Therefore, for the purposes of these simulations, an extraction efficiency of 90% (equating to a transfer efficiency of 75% with 5 equilibrium stages) was a reasonable compromise between β and η , that does not significantly impact on the energy requirements compared to that of the optima operating points.

The high-grade and extraction-grade heat requirements of the system were small, especially compared to distillation. As expected, low-grade heat requirements were predicted to be substantial, depending on the concentration of butanol in the broth. Whilst

20 MJ/kg butanol of waste heat was sufficient to supply all the low-grade heat requirements at 2 wt% butanol (Figure 5-9), it was found to be insufficient in many cases at 1 wt% (Figure 5-10).

As shown in Figure 5-12, the total heat requirements of the separation system demonstrated the expected behaviour with fermentation temperature (which results in an increase in the distribution coefficient) when the temperature gradient of DC1 was optimised. The flowsheet model predicting modest decreases in total heat requirements with an increase in fermentation temperature. This is contrary to the system when the temperature gradient of DC1 was not optimised system; *e.g.* Figure 5-10 details minima in total heat demand at fermentation temperatures of around 32°C. This minima occurred because at around this fermentation temperature, the temperature gradient in DC1 resulted in the low-grade heat requirements being met by the waste heat supply and heat integration. Above this fermentation temperature, the temperature gradient of the first column increases, allowing a greater degree of separation in the first column. This results in shift in duty from DC2 to DC1, thus increasing the low-grade heat demand beyond that which is available as waste heat. However, this resulted in an increase in the overall heat requirements, as high-grade heat used in DC2 was effectively recycled in the form of extraction-grade heat in the condenser of DC2. Overall, this led to a rise in the total heat requirements (although a reduction in high-grade heat). Therefore, if a limited quantity of low-grade heat were available, the temperature gradient in DC1 should be optimised to limit the low-grade heat requirements to that supplied by waste heat and heat integration.

5.5 Results of the Simple Flowsheet Model for Extractions Performed at Elevated Temperatures

If the availability of low-grade heat were limited, and the aqueous butanol concentration relatively low, an alternative method to reduce the overall heat requirements of the separation scheme would be to perform the extraction at an elevated temperature. This would increase the distribution coefficient in the extraction and hence increase the butanol concentration in the feed to DC1.

Figure 5-15 details operating temperatures and pressures for the extraction of butanol performed at 37°C – 100°C, assuming a fermentation temperature of 37°C. Whilst the operating conditions in DC1 were unchanged from simulations of extractions performed at fermentation temperatures, the reboiler temperature and column pressure in DC2 rose

with the extraction temperature in order to produce extraction-grade heat in the condenser of DC2. Pressures became particularly significant at the higher extraction temperatures for the more volatile C₄ solvents, exceeding 20 bara above 90°C extractions.

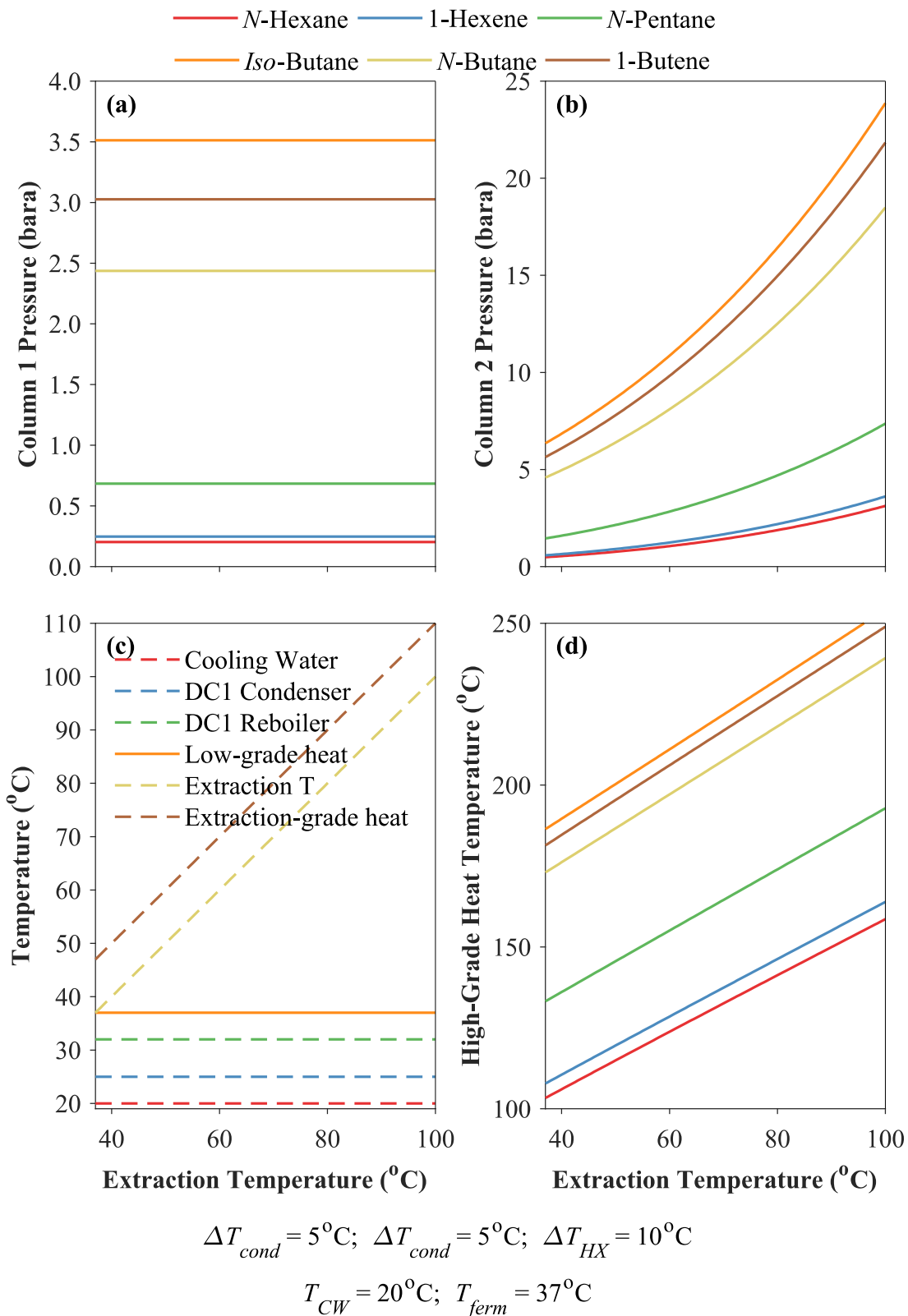
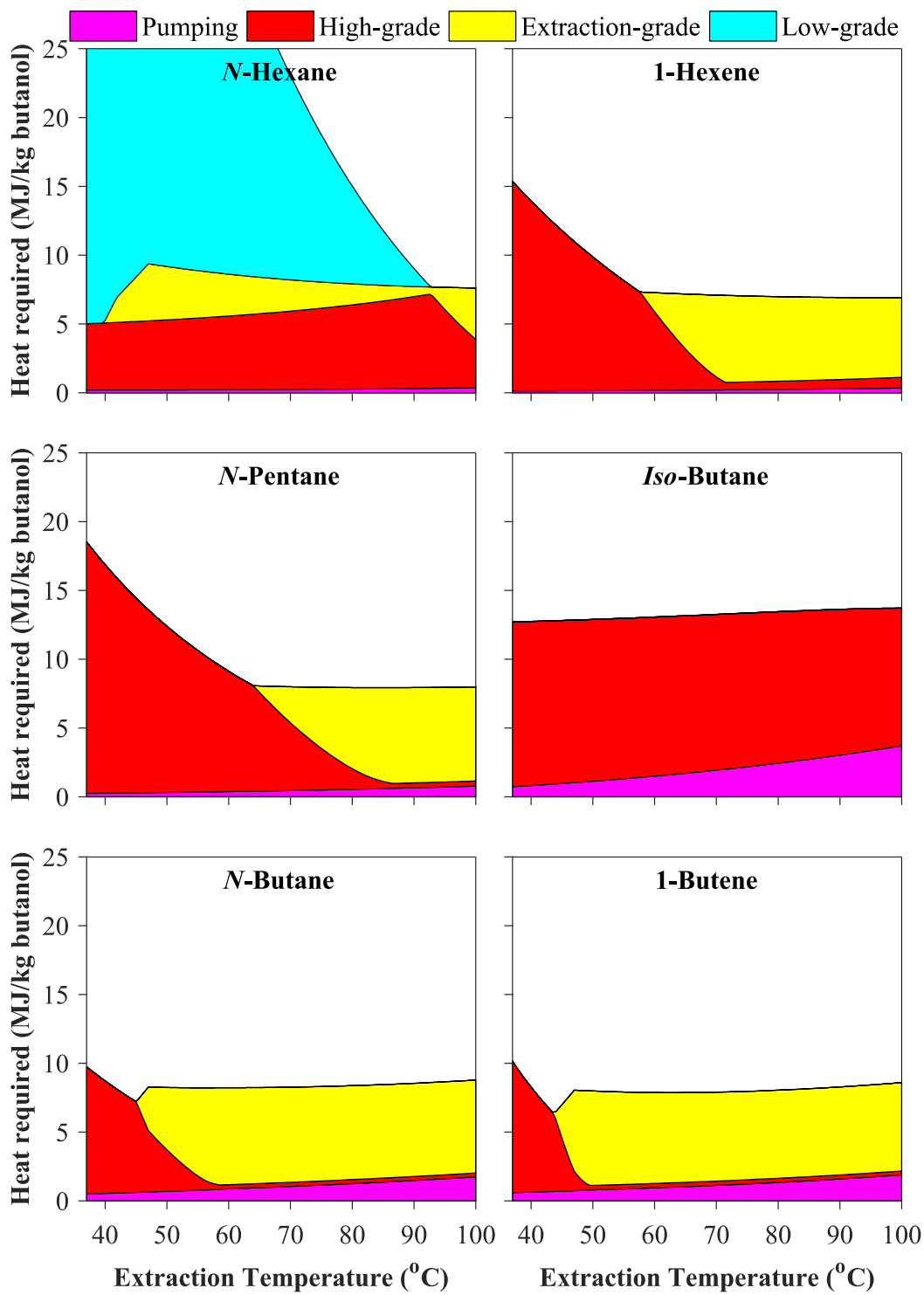


Figure 5-15: Operating temperatures and pressures in the flowsheet model for extractions from aqueous butanol at elevated temperatures

Like extraction at fermentation temperatures, the temperature profile in DC1 could be optimised to match the low-grade heat available to the separation system. This is shown in Figure 5-16 for the extraction of 1 wt% aqueous butanol at 37°C – 100°C, with a low-grade heat supply of 20 MJ/kg butanol. Unlike operation at fermentation temperatures, significant extraction-grade heat was required, which increased as the extraction temperature increased. The extraction-grade heat demand could not be completely supplied by the recycling of high-grade heat as extraction-grade heat in the condenser of DC2. Since some extraction-grade heat was recycled as low-grade heat in the ‘Aqueous Cooler’ on the broth recycle, the additional extraction-grade heat requirements resulted in larger quantities of low-grade heat being available by heat integration; this increased the separation achieved in DC1. This increased separation was compounded by the effect of the increased distribution coefficient at higher extraction temperatures, which reduced the demand for low-grade heat in DC1.

This resulted in a shift in duty from DC2 to DC1 when the temperature gradient of DC1 was optimised, which reduced the quantity of extraction-grade heat supplied by the condenser in DC2. Above extraction temperatures of 47°C, the decrease in requirements for high-grade heat in DC2 was merely replaced with requirements for extraction-grade heat due to the decrease in extraction-grade heat supplied by the condenser of DC2, as shown in Figure 5-16. Hence the total extraction- and high-grade heat required did not decrease significantly above 47°C. Extraction temperatures above 47°C (fermentation temperature plus 10°C) did not increase the duty required in the feeds to the extractor due to the heat integration with the streams leaving the fermenter.

For butane and 1-butene, a minimum energy consumption at an extraction temperature of ~42°C is visible in Figure 5-16. At this point, no extraction-grade heat was required, as sufficient extraction-grade heat was available from recycle of high-grade heat in the condenser of DC2. Above this point, the demand for extraction-grade heat increased (to a maximum at 47°C), and demand for high-grade heat decreased. However, the increased pumping requirements caused an overall rise in energy requirements. Energy requirements for pumping was more significant in the more volatile, C₄ solvents because the pressure of the extractor increased with extraction temperature. This pumping requirement increased with extraction temperature.



$$\Delta T_{cond} = 5^\circ\text{C}; \quad \Delta T_{cond} = 5^\circ\text{C}; \quad \Delta T_{HX} = 10^\circ\text{C}; \quad E_{LG}^{ferm} = 20 \text{ MJ/kg}$$

$$T_{CW} = 20^\circ\text{C}; \quad T_{ferm} = 37^\circ\text{C}; \quad m_{Bu}^{aq} = 1.0 \text{ wt\%}; \quad m_{Bu,DC1} = m_{Bu,DC1}^{optim}$$

$$N_{LLX} = 5; \quad N_{DC1} = 10; \quad N_{DC2} = 20; \quad \beta = 90\%; \quad \eta = 75\%$$

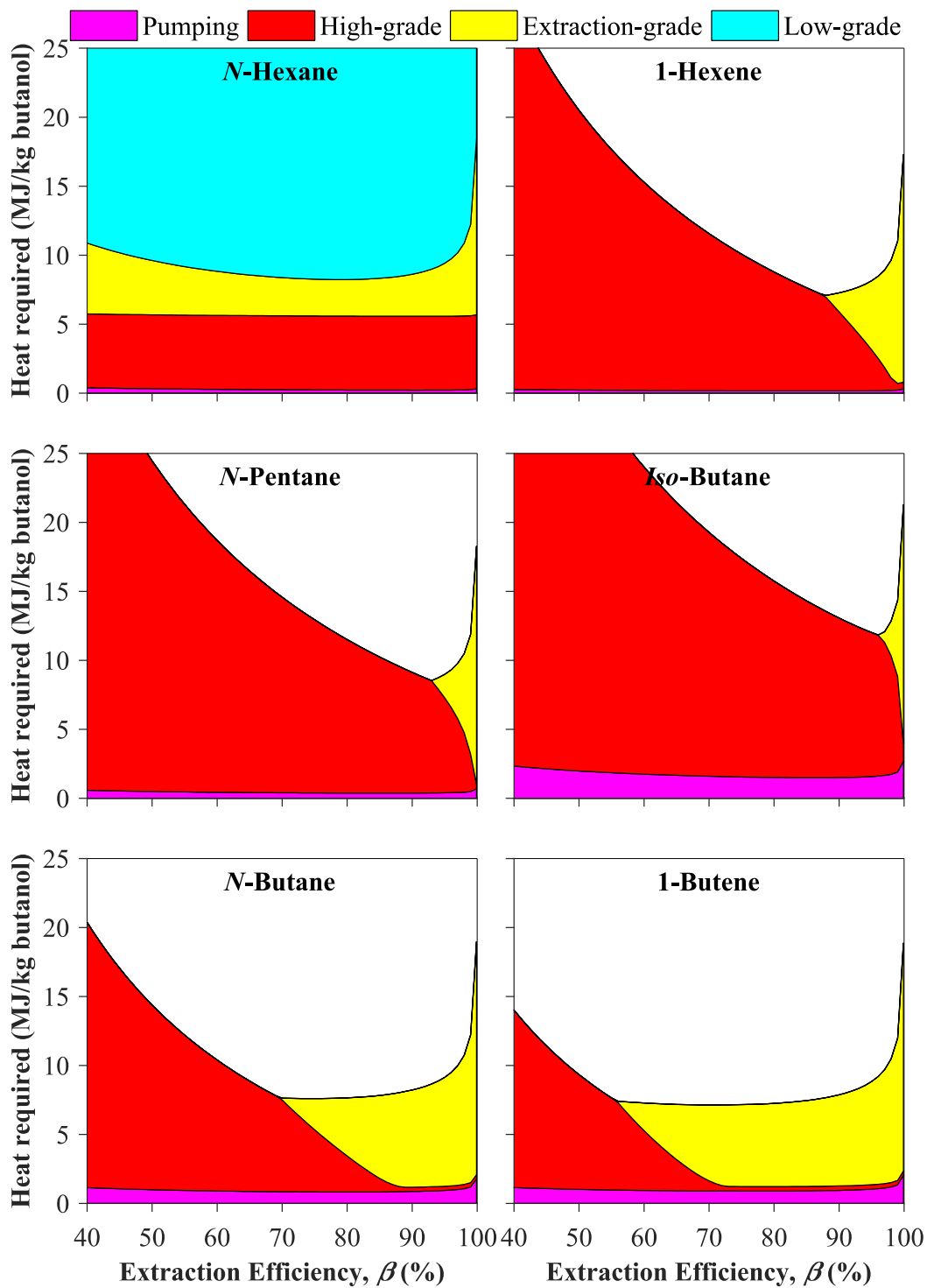
Figure 5-16: Heat requirements predicted by the flowsheet model for the extraction of aqueous butanol at 1 wt% using six hydrocarbons solvents at elevated temperatures, with 20 MJ/kg low-grade heat available. The temperature gradient of DC1 was optimised to minimise the total heat demand.

5.5.1 Optimisation of the Extraction Efficiency

The increased use of extraction-grade heat on the aqueous side of the extraction rebalanced the compromise between extraction efficiency and transfer efficiency. Figure 5-17 details the energy requirements of the system at an extraction temperature of 60°C as a function of extraction efficiency (the temperature gradient of DC1 was optimised, assuming 20 MJ/kg butanol waste heat was supplied to the system). As can be seen, the minima total heat requirements at this extraction temperature were around 70% for 1-butene and *n*-butane. These equated to transfer efficiencies of around 90%.

At extraction efficiencies lower than this optimum point, the composition of butanol in the feed of DC1 decreased. As a result, there was insufficient low-grade heat available to produce the maximum butanol concentration possible in the reboiler of DC1, as shown in Figure 5-17. Therefore, the temperature gradient in DC1 was reduced in order to compensate, thus shifting demand to DC2.

Conversely, at extraction efficiencies higher than ~70%, the quantity of low-grade heat supplied to the system was sufficient that the temperature gradient in DC1 was at its upper limit. Thus, increasing the extraction efficiency further, which increased the effective distribution coefficient in the extraction, did not have a significant impact on the heat demand on the solvent-side of the extraction. However, due to a lower transfer efficiency, this did increase aqueous flowrates and increased the extraction-grade heat requirements. For extractions at elevated temperature, the optimisation of extraction efficiency was a more complex function of extraction temperature and the quantity of waste low-grade heat available, as shown in Figure 5-17.



$$\Delta T_{cond} = 5^{\circ}\text{C}; \Delta T_{cond} = 5^{\circ}\text{C}; \Delta T_{HX} = 10^{\circ}\text{C}; E_{LG}^{ferm} = 20 \text{ MJ/kg}$$

$$T_{CW} = 20^{\circ}\text{C}; T_{ferm} = 37^{\circ}\text{C}; m_{Bu}^{aq} = 1.0 \text{ wt\%}; m_{Bu,DC1} = m_{Bu,DC1}^{optim}$$

$$N_{LLX} = 5; N_{DC1} = 10; N_{DC2} = 20; \beta = \text{Various}; \eta = \text{Various}$$

Figure 5-17: Heat requirements predicted by the flowsheet model for the extraction of aqueous butanol at 1 wt% using six hydrocarbons solvents at 60°C as a function of extraction efficiency, with 20 MJ/kg low-grade heat available. The temperature gradient of DC1 was optimised to minimise the total heat demand.

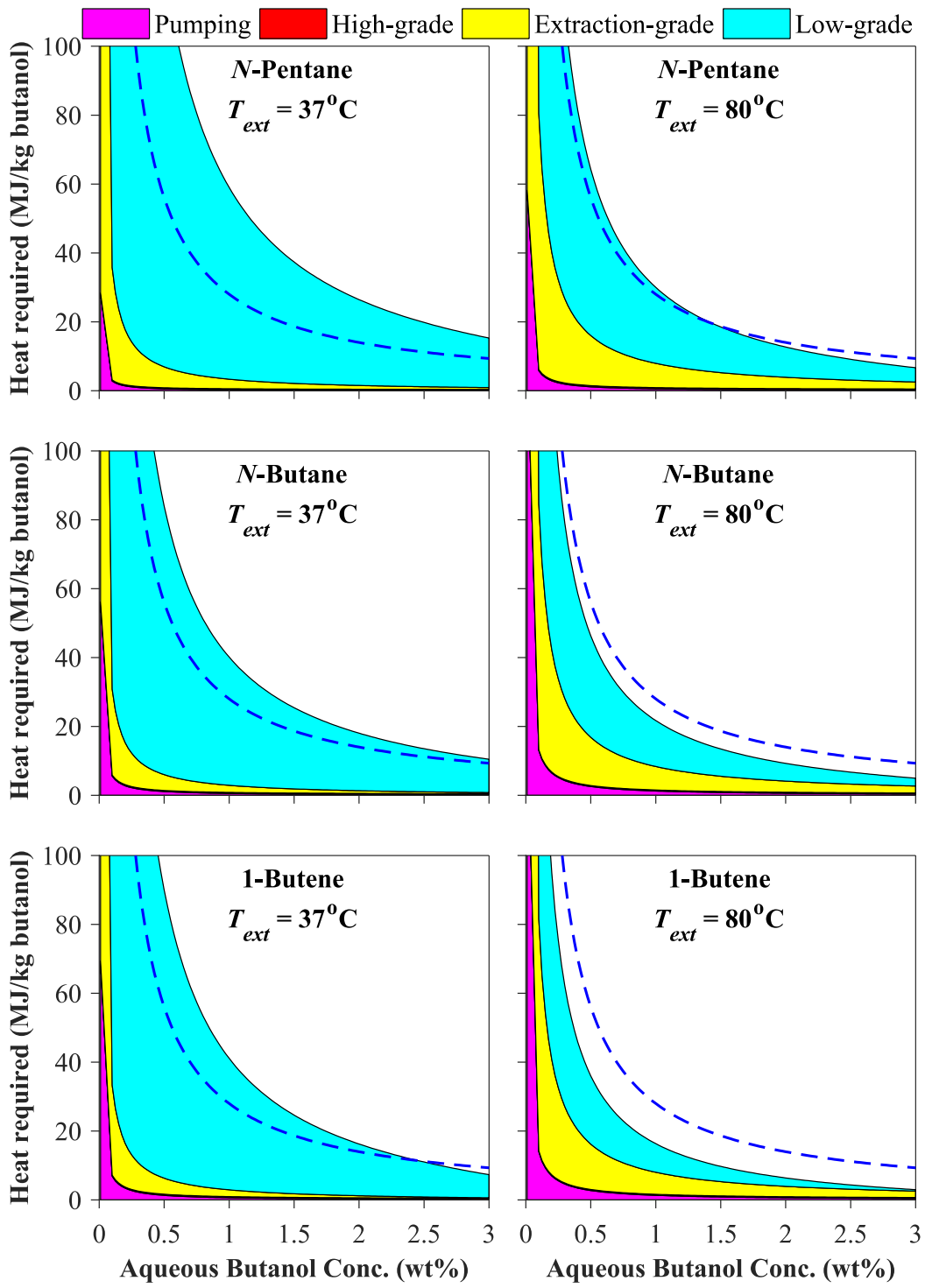
5.5.2 Comparison of Extraction at Fermentation Temperatures with Extraction at Elevated Temperatures

Figure 5-18 details the heat requirements of the separation system for extraction of aqueous butanol at both 80°C and 37°C (the fermentation temperature) as a function of aqueous butanol composition. The energy requirements predicted by the flowsheet model are shown for extractions employing pentane, *n*-butane and 1-butene, without optimisation of the temperature gradient of DC1, and without accounting for the quantity of waste heat supplied to the system. The figure also shows the heat requirements of separation of aqueous butanol by distillation for comparison, employing the approximate rule of thumb of $28/x_{Bu}$ (wt%)MJ/kg found by simulations of distillation in Appendix A.

As can be seen in Figure 5-18, the use of elevated temperature for the extraction reduced both the overall and the low-grade heat requirements, but at the penalty of increased extraction-grade heat and higher pumping demand. The use of elevated temperature for the extraction would be favourable in circumstances in which low-grade heat availability was limited. However, when sufficient low-grade heat is available, extraction at fermentation temperatures would be preferable.

Operation at fermentation temperatures led to very low energy consumption. The heat required was mostly in the form of extraction-grade heat, which is also relatively low-temperature – in this case 47°C. The heat demand compared very favourably with the distillation model. As expected, the more volatile C₄ solvents produced the lowest energy consumption, as they possess the highest distribution coefficients and were also the easiest to separate from butanol by distillation due to their high relative volatility. Of the C₄ solvents investigated, 1-butene performed best, since it has the highest distribution coefficients. It is also less volatile than the C₄ alkanes, thereby reducing pumping demand.

At very low butanol concentrations (*e.g.* 0.1 wt%), pumping demand became very high in C₄ solvents. At this point, operation at fermentation temperatures would be preferable in order to keep extraction-grade heat requirements low, and to keep the pressure difference between the two distillation columns to a minimum.



$$\Delta T_{cond} = 5^{\circ}\text{C}; \Delta T_{cond} = 5^{\circ}\text{C}; \Delta T_{HX} = 10^{\circ}\text{C}; E_{LG}^{ferm} = 0 \text{ MJ/kg}$$

$$T_{CW} = 20^{\circ}\text{C}; T_{ferm} = 37^{\circ}\text{C}; m_{Bu}^{aq} = \text{Various}; m_{Bu,DC1} = m_{Bu,DC1}^{\max}$$

$$N_{LLX} = 5; N_{DC1} = 10; N_{DC2} = 20; \beta = 90\%; \eta = 75\%$$

Figure 5-18: Heat requirements predicted by the flowsheet model for the extraction of aqueous butanol using three hydrocarbons solvents at 37°C and 80°C (not accounting for the low-grade heat available).

Dashed line: heat requirements of separation by distillation of aqueous butanol

5.6 Discussion: Extraction at Elevated Temperatures

Performing the extraction at elevated temperatures led to high pressures in DC2 for the more volatile C₄ solvents, as detailed in Figure 5-15d. Not only would this lead to very high pumping demands (as shown in Figure 5-16), but it would also add significantly to capital costs. Hence, operation at these pressures might be economically unfeasible. If this were the case, it would be possible to operate DC2 at much lower pressures. The temperature required for high-grade heat would also then be reduced. At these high extraction temperatures, the high-grade heat requirements in DC2 when employing C₄ solvents are very low and so the impact on the energy balance would minimal.

The increased requirements and recycle of extraction-grade heat meant that if sufficient low-grade heat was available, increasing the extraction temperature had minimal impact on total energy demand. This is illustrated in Figure 5-16.

5.7 Conclusion

A flowsheet for the extraction and subsequent distillation of butanol from aqueous broths using volatile hydrocarbons was successfully simulated. A two-column distillation system was used, which allows low-grade waste heat to be utilized in the first column, followed by a second column operated at a higher temperature.

Two major operating regimes were identified: operation at fermentation temperature and operation at an elevated temperature. Performing the extraction at fermentation temperatures was simpler and was found to be optimal when sufficient low-grade heat was available. Total separation of the solvent and butanol was not possible in the first column (DC1) since the temperature gradient was limited. Using models of VLE devised from VLE measurements in Chapter 3, the maximum butanol concentration produced in DC1 was calculated. The solvents showed positive deviation from Raoult's Law and so very high butanol concentrations could be produced in the low-grade distillation column at minimal temperature gradients; temperature gradients of 2°C in DC1 resulted in butanol compositions exceeding 25 wt%.

In scenarios in which the availability of waste, low-grade heat was more limited, the remaining overall heat requirements of the system could be reduced by optimising the temperature gradient in DC1. Reducing the temperature gradient reduced the concentration of butanol produced by DC1 and hence increased the heat demand in the second column (DC2). The temperature gradient of DC1 was optimised to match the

availability of low-grade heat. The high-grade heat supplied to DC2 was recycled *via* the condenser as extraction-grade heat. Therefore, reducing the temperature gradient of the DC1 shifted heat demand onto DC2, leading to a reduced overall demand for heat.

In scenarios in which the availability of low-grade heat was limited, an alternative strategy was to perform the extraction at an elevated temperature. This increased the distribution coefficient of butanol and hence decreased the demand for low-grade heat in DC1. However, this came at the penalty of increased extraction-grade heat demand. It was found that there was no benefit in increasing extraction temperature beyond the point where the low-grade heat demand was met by waste heat, since this merely continued to increase pumping demand. In most circumstances, extraction temperatures above 80°C would be excessive.

As expected, C₄ solvents were found to be the most energy-efficient solvents, with 1-butene performing best, since they had the highest distribution coefficients and were easiest to separate from butanol *via* distillation. However, they require higher operating pressures, which could become problematic at high extraction temperatures. It is unlikely that extraction at these temperatures would be necessary for these solvents.

Throughout the flowsheet simulations, it was assumed that the low-grade heat provided to DC1 was at the same temperature as the fermenter, because this was assumed to be the source of low-grade heat. In processes in which other sources of waste heat are available, extraction-grade heat might also be obtainable from waste heat sources slightly above the fermentation temperature, thereby reducing the net energy consumption further. This would alter the optimal operating conditions found in the simulations outlined, which were specific to the fermenter temperature, the solvent employed, and the availability and temperature of waste heat.

6. Conclusions

Butanol production by fermentation is a potentially important technology; in particular fermentation of biomass would allow renewable butanol to be produced. *In situ* product removal can significantly improve the productivity of butanol fermentations; however, separation (at the end of a fermentation, or *in situ*) of dilute butanol from aqueous broths is challenging and energy-intensive. In this dissertation, a novel method of *in situ* product removal has been devised and investigated, in which butanol would be extracted from the broth by C₄ or C₅ hydrocarbons. The extracted butanol would then be separated from the extractant by distillation. Owing to the high volatility of C₄ and C₅ hydrocarbons, most of the separation could be performed by distillation at moderate pressures using low-grade, waste heat from the fermenter or from other low-grade heat sources. The remainder of the separation of concentrated butanol in the volatile hydrocarbon could be performed in a second distillation column, operated at a higher pressure to increase heat integration. Hence, the overall, high-grade heat requirements of such a separation scheme would be small.

Aside from a low distribution of butanol in hydrocarbons *versus* water, the properties of volatile hydrocarbons for the extraction of butanol from aqueous broths are optimal. The mutual solubility of C₄ and C₅ hydrocarbons with water is very low. Whilst the measurements available for C₄ and C₅ hydrocarbons were limited, some rules of thumb were developed. The solubility of C₅ alkanes in water was ~50 mg/kg at 25°C – 50°C. This solubility approximately quadrupled for either a reduction in chain length (*e.g.* to a C₄ alkane), or an increase in the number of π bonds (*e.g.* C₅ alkane to C₅ alkene). Solubility of hydrocarbons in water approximately doubled between 25 – 50°C and 100°C. Conversely, the solubilities of water in C₄ alkanes was found to be lowest of the hydrocarbons investigated, with a solubility of approximately 200 mg/kg (~600 ppm) at typical fermentation temperatures. The solubilities in C₅ alkanes were predicted to be slightly higher (~250 mg/kg, ~1000 ppm), and the solubility in C₄ – C₅ alkenes was around 2 – 4 times higher than the equivalent alkanes (approximately 500 – 800 mg/kg, 1500 – 3000 ppm) at typical fermentation temperatures. The solubility of water in C₄ – C₅ hydrocarbons was predicted to increase by a factor of ~10 between typical fermentation temperatures and 100°C.

The low solubility of water in volatile hydrocarbons would result in extractions with very high selectivities of butanol over water, thereby eliminating the need for aqueous separation downstream. The low solubility of hydrocarbons in water reduces the loss of solvent into the aqueous broth. In addition, some C₄ hydrocarbons (*e.g.* 1-butene) could even be obtained from the product butanol, thereby potentially providing an inexpensive source of make-up solvent. The low solubility of hydrocarbons in water could minimise contact of the organism with the solvent hence reducing any toxicity problems. The toxicity of C₄ – C₅ hydrocarbons in butanol fermentations has not been examined, but results for hexane and other longer hydrocarbons suggests that the toxicity of hydrocarbons is very low (González-Peñas *et al.*, 2014; Groot *et al.*, 1990). The physical properties of short hydrocarbons also make them optimal extractants, *e.g.* a large difference in density with water, allowing for simple phase separation. Indeed, some authors have even proposed blending alkanes with high-performing solvents in order to improve their physical properties for extraction of butanol (González-Peñas *et al.*, 2014). Hydrocarbons are also compatible in a fuel blend in the product, inexpensive, relatively safe and stable.

In Chapter 2, the performance of such a separation scheme was estimated, and several modifications were explored. Distribution coefficients at equilibrium of butanol were predicted for C₄ – C₅ hydrocarbons. The highest coefficients were predicted for C₄ alkenes, and distribution coefficients were predicted to rise by a factor of 4 between typical fermentation temperatures and 100°C in all C₄ – C₅ solvents. The increased distribution coefficient of butanol in hydrocarbons at elevated temperatures can be exploited in the design of the separation scheme. If suitable heat integration is used, the extraction can be performed at elevated temperatures with a small energy penalty in increasing the temperature of the aqueous and organic feed streams to the extractor.

The design of the extraction system could also be modified to produce blends of gasoline with butanol *via* a four step process: (i) extraction of butanol from the aqueous broth by a volatile hydrocarbon; (ii) distillation of the butanol-hydrocarbon mixture employing low-grade heat in order to produce a higher concentration of butanol; (iii) extraction of butanol from the concentrated butanol-hydrocarbon mixture into water; (iv) extraction of butanol from the concentrated aqueous mixture directly into gasoline. The process could produce gasoline blends with high butanol content, as the distillation process can produce high concentration butanol. This process is an attractive method to produce butanol-

gasoline blends, as the entire process could be performed at fermentation or ambient temperatures, and thus does not involve the use of any high-grade heat.

The vapour-liquid equilibria of butanol, acetone and ethanol with six volatile C₄ – C₆ hydrocarbons (*n*-hexane, 1-hexene, *iso*-butane, *n*-butane and 1-butene) were investigated in Chapter 3. The flexible Legendre activity model was used to fit measurements of VLE and excess enthalpy as a function of temperature. This allowed accurate fitting of the activity coefficient at dilute product compositions, where activity models with only 2 – 3 parameters were unable to represent the rapidly changing behaviour. The virial equation of state was used to model the vapour phase. The VLE behaviour of C₄ hydrocarbons was found to be close to that hypothesised for an optimum extractant for the process:

- the behaviour at dilute butanol concentrations was closer to Raoult's Law than the other hydrocarbons, resulting in higher distribution coefficients of dilute butanol
- the binary demonstrated large positive deviations from Raoult's Law at above dilute butanol concentrations, which would allow significant separation by distillation with only a small temperature gradient
- no azeotropes were predicted which would complicate separation by distillation
- the high relative volatility of C₄ hydrocarbons *versus* butanol would minimise reflux ratio in distillation

Total separation of the solvent and butanol would not be possible in a distillation column in which the reboiler duty was supplied by waste heat from the fermenter and other similar waste heat sources, assuming that the condenser was cooled by, for example, cooling water (*i.e.* without refrigeration). The temperature of the low-grade heat and the cooling water creates a limited temperature gradient in this distillation column. Using models of VLE devised in Chapter 3, the maximum composition of butanol produced in a distillation column with a limited temperature gradient was calculated. Since the solvents demonstrate a large positive deviation from Raoult's Law, very high butanol concentrations could be produced in the distillation column at minimal temperature gradients; temperature gradients of 2°C and 7°C in the distillation column resulted in butanol compositions exceeding 25 wt% and 50 wt% respectively. These were far higher than estimates of the maximum composition of butanol produced in such a column estimated by assuming Raoult's Law in Chapter 2. This meant that the duty required to separate the resulting high concentration butanol from the solvent would be very low in a subsequent, higher temperature distillation column.

The binary activity models developed in Chapter 3 were used to predict the distribution coefficient at equilibrium of butanol, acetone and ethanol in the six C₄ – C₆ hydrocarbons *versus* water in Chapter 4. Distribution coefficients of *n*-butanol in *n*-butane and 1-butene were found to be highest (~1 kg/kg at 37°C). As expected, distribution coefficients of butanol in all solvents increased significantly with temperature, increasing by a factor of around 3 – 4 between 25°C and 100°C. However, some solvents showed a peak in distribution coefficient at the upper end of this temperature range for higher compositions of butanol. Distribution coefficients of ethanol in the six hydrocarbons were very low. This would make simultaneous extraction of ethanol very energy intensive. Distribution coefficients of acetone were a little higher (~0.6 kg/kg in 1-butene at 37°C), which means that simultaneous extraction of acetone might be feasible.

Distribution coefficients of *iso*-butanol were predicted in *n*-hexane and were compared to those of *n*-butanol. The higher volatility of *iso*-butanol increased the distribution coefficient of butanol by up to 25%. This conclusion concurred with the estimates based on the coexistence equation made in Chapter 2 of the distribution coefficients at infinite dilution of *iso*-butanol in relevant hydrocarbons compared with those of *n*-butanol. Whilst measurements of VLE equilibria for *iso*-butanol were not available with any C₄ – C₅ hydrocarbon, it was hypothesised that it was likely that distribution coefficients of dilute *iso*-butanol were slightly higher than those of dilute *n*-butanol.

In Chapter 5, the extraction of butanol from aqueous mixtures using volatile hydrocarbons was simulated using a simple flowsheet model in order to investigate the energy requirements of the separation scheme and to find optimal operation conditions. Performing the extraction at the same temperature as the fermentation is simpler than operation at elevated temperatures. This strategy was found to be optimal when sufficient low-grade, waste heat from the fermenter and other waste heat sources was available to meet the duty of the first of two distillation columns, in which butanol and the solvent were separated using low-grade heat.

In scenarios in which the availability of low-grade, waste heat was limited, the remaining overall heat requirements of the system could be reduced by optimising the temperature gradient in the low temperature column. Reducing the temperature gradient reduced the concentration of butanol produced by the first column and hence increased the heat demand in the second column. The temperature gradient of the first column could be optimised to match the availability of low-grade heat. The high-grade heat supplied to the second column was recycled *via* the condenser in the second column, which was used

to re-heat the solvent in the distillate of the first column before recycle back to the extraction. Therefore, reducing the temperature gradient of the first column shifted heat demand onto the second column, leading to a reduced overall demand for heat.

In scenarios in which the availability of low-grade, waste heat was limited, an alternative strategy was to perform the extraction at an elevated temperature. This did not impact on the system downstream of the first distillation column, but did increase the distribution coefficient of butanol and hence decreased the demand for low-grade heat in the first column. However, this came at the penalty of increased ‘extraction-grade’ heat, required to heat the feeds to the extraction column. This strategy was useful for reducing the demand for low-grade heat where supply of waste heat was limited. It was found that there was no benefit in increasing extraction temperature beyond the point where the low-grade heat demand was met by waste heat, since this merely continued to increase pumping demand as higher extraction temperatures required higher pressures to keep the solvent in the liquid phase. In most circumstances, extraction temperatures above 80°C would be excessive.

The operation of the liquid-liquid extractor was also investigated. For extractions at fermentation temperatures, there were negligible energy penalties in operating at very high aqueous flowrates in order to generate distribution coefficients close to those at equilibrium. Hence extraction directly from the fermenter would be optimal from the position of energy efficiency. Conversely, the compromise between aqueous flowrate and obtaining distribution coefficients close to equilibrium was more complex for extraction at elevated temperatures, where the energy was required to heat the aqueous feed to the extraction temperature. This prioritised lowering the aqueous flowrate, provided sufficient low-grade waste heat was available to perform the majority of the distillation in the low temperature column.

As expected, C₄ solvents were found to be the most energy-efficient solvents, with 1-butene performing best, since they had the highest distribution coefficients and were easiest to separate from butanol *via* distillation. Extractions performed at a typical fermentation temperature of 37°C required less than 2 MJ/kg butanol of high-grade heat (the majority of which would only be required at under 50°C), provided that the low-grade heat demand was met by waste heat. The low-grade heat requirements vary with butanol titre – under 20 MJ/kg and 40 MJ/kg butanol for 2 wt% and 1 wt% respectively.

However, one potential draw-back to using C₄ hydrocarbons (over C₅) is that they require operation at higher pressures, which could become potentially problematic if high extraction temperatures were used. However, it is unlikely that operation at these temperatures would be necessary and with minor alterations to the heat recovery strategy, these high pressures could be avoided for distillation, although not for the extraction.

This dissertation has demonstrated the advantages of employing volatile hydrocarbons in the extraction of butanol from aqueous fermentation broths, in particular its potential as a selective, separation technique with very low energy requirements. This contrasts with existing techniques for the separation of butanol from aqueous broths, which are energy-intensive and often require significant further separation (*e.g.* by distillation) as their selectivity towards butanol over water is comparatively poor. 1-butene was found to be the best performing of the C₄ – C₆ solvents investigated for the extraction of *n*-butanol. *N*-butane was found to perform very similarly in extractions of *n*-butanol at fermentation temperatures, particularly at lower titres, and should be highly selective over water, with solubilities of water in C₄ alkanes being the lowest of C₄₊ hydrocarbons. *N*-butane and 1-butene can also be regenerated from the *n*-butanol product (by dehydration to 1-butene and subsequent dehydrogenation to *n*-butane).

The high performance for the extraction of *n*-butanol by 1-butene could perhaps have been expected due to its similarity in structure and size to *n*-butanol: 1-butene comprises a C₄ hydrocarbon group, with a π bond at one end creating a slight dipole moment (as the hydroxyl group does in *n*-butanol). This similarity in structure allows mixtures of dilute *n*-butanol in 1-butene to exhibit more ideal behaviour, and hence exhibit low activity coefficients of butanol which result in higher distribution coefficients, whilst maintaining a very low mutual solubility with water. Its relative apolarity also increases its volatility and reduces its enthalpy of vaporisation compared to butanol, increasing the ease of separation by distillation. Based on this evaluation, 1-pentene might also be a good extractant for *n*-butanol, and *iso*-butene, *iso*-pentene and *iso*-butane might be good extractants for *iso*-butanol.

7. Future Work

The investigations into the extraction of dilute butanol from aqueous broths conducted in this dissertation were based on simulations and theoretical models. It is therefore imperative that the separation schemes investigated are verified experimentally.

In Chapter 2, the mutual solubilities of C₄ – C₅ hydrocarbons and water were investigated. There was a limited quantity of measurements available, especially for alkenes, and due to their sparing solubility, agreement between measurements was poor. The solubility of hydrocarbons in water is an important factor in the extraction of butanol from aqueous broths; low solubility in water reduces the loss of solvent into the aqueous phase. The effect of other components in the broth might influence the solubility of hydrocarbons in the broth. Therefore, the solubility of relevant hydrocarbons in aqueous fermentation broths should be investigated further.

Low solubility of hydrocarbons in water reduces the likelihood of toxicity in the aqueous broth. Hexane and other C₆₊ alkanes have been found to be non-toxic in butanol fermentations (Groot *et al.*, 1990). The toxicity of C₄ – C₅ hydrocarbons to organisms in the fermentation broth must be thoroughly examined. Solvents can interact with the organism in the broth *via* the solvent contained in the broth recycle from the extraction. Alternatively, solvents can interact with organisms directly if organisms are not removed from the broth prior to extraction in a separate unit, or if the extraction is performed in the fermenter itself. In addition, solvents can extract key intermediates and nutrients from the broth during the extraction, thus preventing organism growth or product synthesis. These problems must be examined experimentally, as the factors involved vary with the relevant organism, the method of extraction, and the composition of the broth.

In Chapter 3, the vapour-liquid equilibria (VLE) of six C₄ – C₆ hydrocarbons with *n*-butanol, acetone and ethanol were investigated. Flexible models predicting activity coefficients were built based on scarce measurements of VLE and excess enthalpy available in the literature. Further VLE measurements would allow the VLE of other hydrocarbons with fermentation products, and the VLE of *iso*-butanol with volatile hydrocarbons, to be investigated. In particular, the behaviour of C₄ alkenes, such as

iso-butene, would be of interest due to the performance of *n*-butanol in 1-butene. Measurements should be focussed on dilute compositions of butanol.

The regression procedure employed in Chapter 3 to fit VLE and excess enthalpy measurements to the flexible Legendre activity model could be refined. The over-fitting criterion employed was crude; a more sophisticated method could be devised. Inclusion of the number of stationary points of g^E and H^E and their derivatives was investigated and found to reduce over-fitting. The objective function employed in the regression could also be improved to account for errors in VLE and excess enthalpy measurements, if estimates of these could be produced. This would reduce over-fitting of scatter in the measurements. Finally, the Legendre activity model was not ideally suited to modelling the excess enthalpy measurements. A different model could be devised to represent more accurately the shape of excess enthalpy measurements with fewer coefficients.

The distribution coefficients at equilibrium of dilute butanol, ethanol and acetone in volatile hydrocarbons *versus* water were predicted in Chapter 4 from binary activity coefficients. No ternary liquid-liquid equilibria measurements for butanol in volatile hydrocarbons and water could be found. In addition, the presence of other components in the broth could have an impact on the equilibria. Measurements of the LLE of dilute butanol in relevant hydrocarbons from aqueous fermentation broths could provide accurate distribution coefficients of butanol and other fermentation products. Such measurements could also provide the mutual solubility of water and hydrocarbons as a function of butanol composition in aqueous broths. Distribution coefficients of butanol in relevant hydrocarbons *versus* water could also be measured for larger proportions of butanol than has hitherto been done. Such distribution coefficients would be important during the production of a gasoline-butanol blend by extraction, in which concentrated butanol in a volatile hydrocarbon could be extracted into pure water, before extraction from the water directly into gasoline.

The liquid-liquid equilibrium of butanol is not the only important factor during extraction. The mass transfer of butanol in extractions from aqueous fermentation broths should also be investigated. In addition, the formation of emulsion has been found to be problematic during some extraction processes. This must be investigated experimentally in fermentation broths, since the presence of salts and any surfactants, as well as the design of the extractor, can impact on this significantly. Demonstrations of the entire process - fermentation, extraction and distillation - would be extremely powerful for proof-of-concept, and in verifying the models of the separation process devised in this dissertation.

APPENDIX A. MODELLING THE DISTILLATION OF AQUEOUS BUTANOL FROM FERMENTATION BROTHS

A.1 Introduction

Several authors (Luyben, 2008; Mariano *et al.*, 2011; Outram *et al.*, 2016; Tao *et al.*, 2013a) have examined the energy requirements for distillation of butanol in ABE fermentation systems. The results provided energy consumption targets for comparison with improved separation schemes.

Three distillation schemes were investigated:

1. Separation of *n*-butanol and water
2. Separation of *n*-butanol, ethanol, acetic acid, butyric acid and water
3. Separation of *n*-butanol, ethanol, acetone, acetic acid, butyric acid and water

The first scheme (System 1) is the simplest case, in which only butanol is separated. This system represents the separation process for *iso*-butanol production, in which there are minimal side-products. However, *n*-butanol rather than *iso*-butanol was used in the simulation. Whilst *n*- and *iso*-butanol are not thermodynamically identical, they yield similar results in terms of the energy required for separation. In addition, significantly more equilibria measurements are available in the literature for *n*-butanol mixtures than for *iso*-butanol.

Use of *n*-butanol rather than *iso*-butanol in the binary mixture of System 1 also allows comparison to the multicomponent mixtures in the second and third schemes (System 2 and System 3). The multicomponent mixture of System 2 represents the typical products formed in the fermentation of synthesis gas, whereas System 3 represents the products formed in an ABE fermentation.

A.2 Assumptions

The principal numerical assumptions used for the simulation are summarised in Table A-1.

System 1 was based on a conventional two column system (Luyben, 2008), shown in Figure A-1. The fermenter broth was fed to a ‘water’ column, which removes most of the water in the bottoms and is sent for recycle. The distillate of butanol and water is an azeotrope, which was condensed and sent to a decanter for liquid-liquid phase separation. The decanter temperature can be varied, although simulations found that the temperature

of the decanter had a relatively small impact on overall energy use and identified an optimal temperature of 80°C to minimise energy use. This decanter temperature was used for the simulations presented in this work. The butanol-rich portion was sent to the ‘butanol’ column, which produced the product butanol in the bottoms (<0.01 wt% water) and recycled the butanol azeotrope produced in the distillate back to the decanter. The aqueous phase from the decanter was recycled to the beer column. Butanol recovery was set to 99.9%.

Table A-1 – Principle numerical assumptions used in the simulation of distillation of aqueous butanol separations

Assumption	System	Value
Feed temperature	1 – 3	30°C
Feed pressure	1 – 3	1 bara
Feed flowrate	1 – 3	1000 kg/h
Product temperatures	1 – 3	30°C
Product pressures	1 – 3	1 bara
‘Beer’ column pressure	1 – 3	1 bara
‘Beer’ column stages	1 – 3	40
‘Beer’ column, combined butanol and ethanol recovery (per pass)	2 – 3	99.75%
‘Beer’ column decanter temperature	2 – 3	90°C
Acetone column pressure	3	0.7 bara
Acetone column stages	3	50
Acetone column, acetone recovery	3	99.9%
Acetone product purity	3	99.9 wt%
Ethanol column pressure	2 – 3	0.3 bara
Ethanol column stages	2 – 3	40
Ethanol column, ethanol recovery	2 – 3	99.9%
Ethanol molecular sieve adsorption temperature	2 – 3	112°C

Assumption	System	Value
Ethanol molecular sieve water adsorption fraction	2 – 3	95%
Ethanol molecule sieve butanol & carboxylic acid adsorption	2 – 3	100%
Ethanol concentration, desorption of molecular sieve	2 – 3	70 wt%
Butanol column pressure	1	1 bara
	2 – 3	2 bara
Butanol column reflux ratio	2 – 3	0.01
Butanol product, water content	1 – 3	0.1 wt%
Butanol recovery	1	99.9

Systems 2 and 3, depicted in Figures A-2 and A-3 respectively, were based on the schemes developed by the NREL (Tao *et al.*, 2013a). In both, first, butanol, ethanol and any acetone were concentrated in a ‘beer’ column. This column removed the heavy broth components, including the carboxylic acids. The stillage (including the acids and other heavy broth components) was recycled *via* water treatment. The tops of the beer column phase were separated in a decanter. The organic phase, rich in acetone, ethanol and butanol was siphoned off, and the heavier aqueous phase was refluxed in the beer column. Combined butanol and ethanol recovery in the beer column was set to 99.75% per pass.

In System 3, the organic phase was fed to a low pressure (0.7 bara) column, the ‘acetone’ column. In System 2, the acetone column was omitted, since acetone is not a 'product of synthesis gas fermentation. In System 3, the acetone column was assumed to recover 99.9% of acetone input in the distillate at a purity of 99.9 wt%. The lower pressure of the acetone column was set in order to allow heat from the condenser in the beer column to provide heat for the reboiler heat in the acetone column.

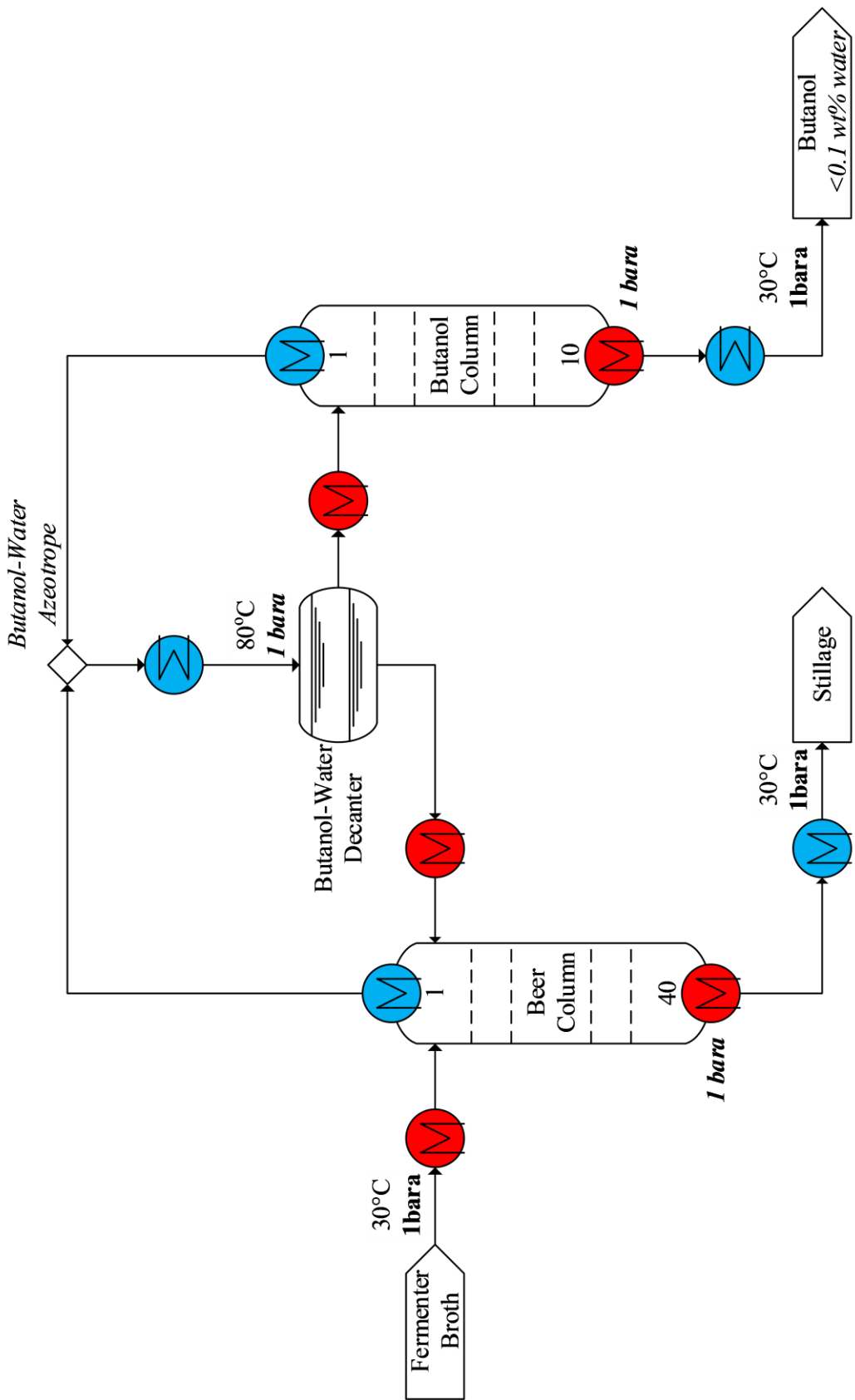


Figure A-1 – Distillation model to separate *n*-butanol and water

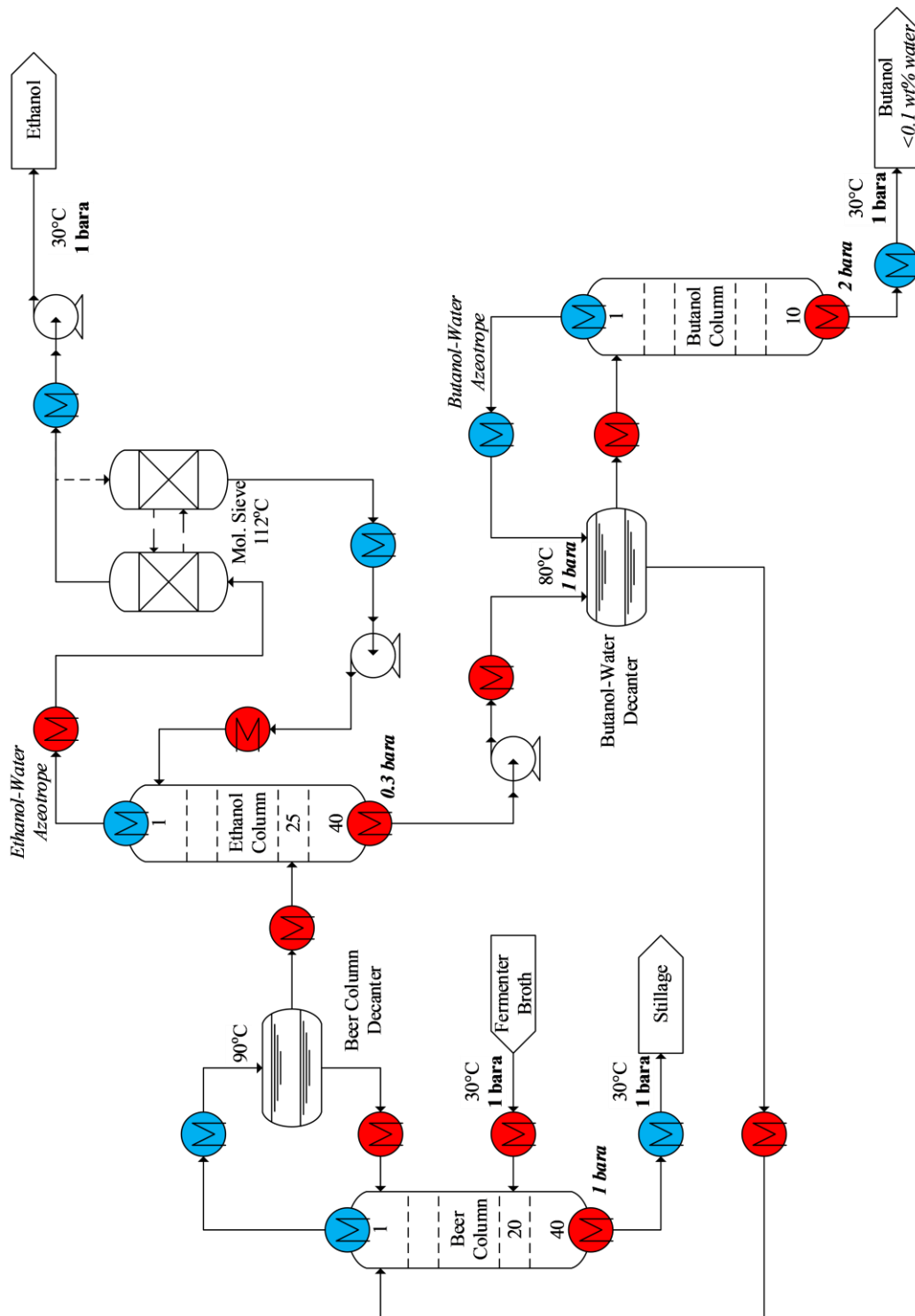


Figure A-2 – Distillation model to separate *n*-butanol, ethanol, acetic and butyric acids from water

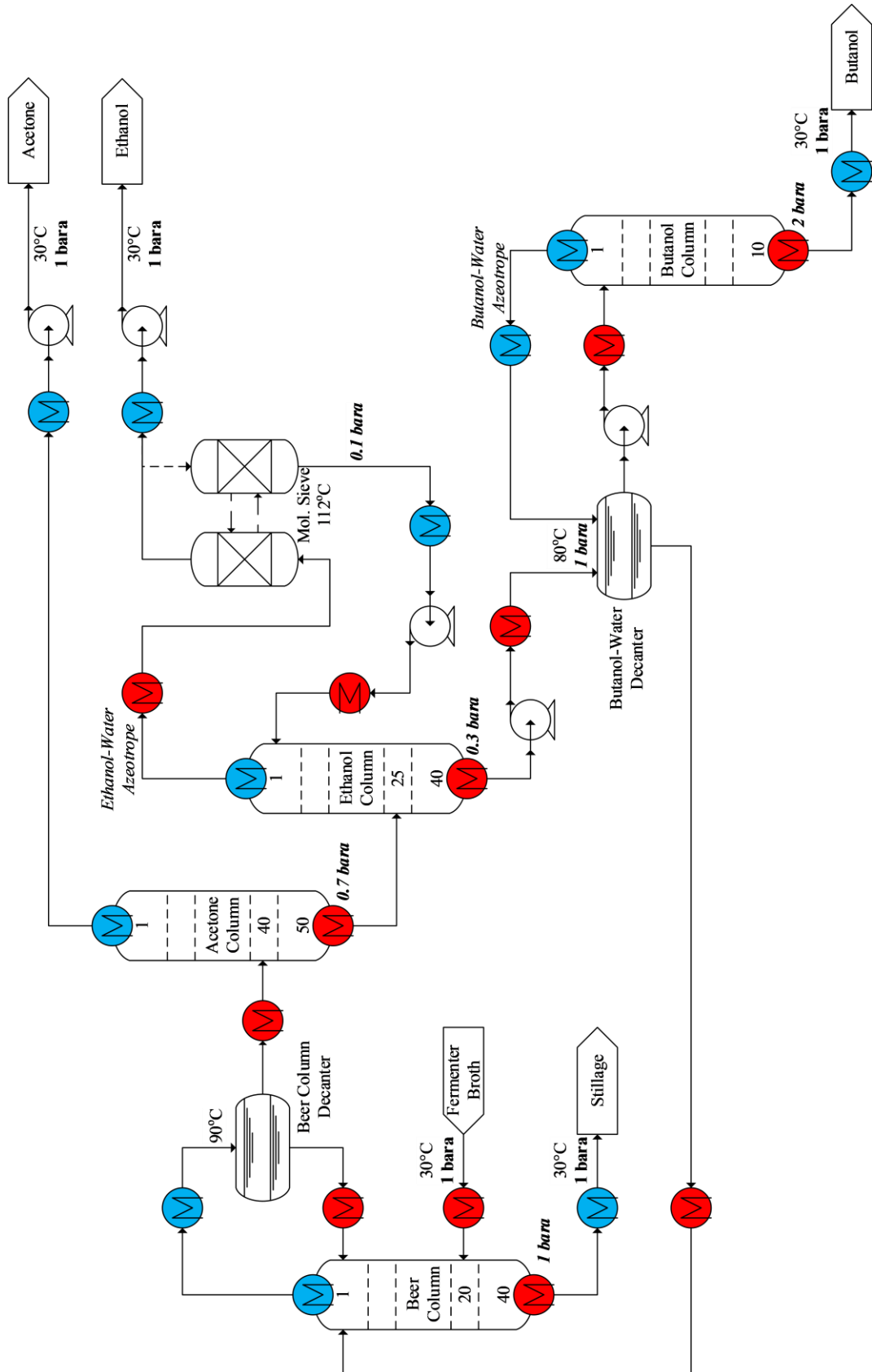


Figure A-3 – Distillation model to separate *n*-butanol, ethanol, acetone, acetic and butyric acids from water

In both System 2 and 3, the mixture was then fed to the ‘ethanol’ column at 0.3 bara, which formed an azeotropic mixture of ethanol and water in the vapour phase in the distillate, and liquid aqueous butanol in the bottoms. The ethanol column was assumed to recover 99.9% of the ethanol input. The ethanol column pressure was set to allow heat from the condenser in the beer column to provide heat for the reboiler in the ethanol column.

The azeotrope of ethanol and water produced in the distillate of the ethanol column was fed to a two-column system containing molecular sieves. This system was based on that proposed by NREL (Humbird *et al.*, 2011). One bed selectively adsorbed water whilst the azeotrope vapour flowed through it. The molecular sieve was assumed to adsorb 95% of the water, leaving most of the ethanol to pass through in the vapour phase, after which it was condensed to produce ethanol at ~99.7 wt% (depending on the impurities). Meanwhile, the other adsorption column was regenerated by stripping the water from the saturated adsorbent using pure ethanol vapour at low-pressure. The resulting vapour stream of ethanol and water was condensed and pumped back into the ethanol column. This stream was assumed to contain a mixture of 70 wt% ethanol in water. Trace butanol and acetic acid were also assumed to be completely adsorbed and subsequently completely desorbed by the molecular sieve because details of adsorption isotherms with these materials were not available.

In both Systems 2 and 3, the aqueous butanol from the bottom of the ethanol column was fed to a decanter and the organic phase from this was then fed to a butanol column in the same way as in System 1. However, the aqueous phase from this decanter was recycled back to the beer column, instead of the water column used in System 1. This prevents the build-up of acetone, ethanol and acetic acid in the decanter from previous columns that would otherwise occur. Since butanol is less volatile than water, significant vacuum would be required in the butanol column in order to reduce the reboiler temperature of the butanol column sufficiently to allow heat from the beer column condenser to be useable, in the same manner as for the acetone and ethanol columns. Instead, an elevated pressure of 2 bara was assumed for the butanol column in System 2 and 3. Whilst this slightly raised the temperature of the reboiler in this column, it allowed the condenser of the butanol column to provide some of the reboiler heat requirements of the beer column.

This meant that heat provided to the butanol column was not an additional load on the overall system. Figure A-4 summarises the heat integration strategy of the beer, acetone, ethanol and butanol reboilers and condensers in Systems 2 and 3.

In simulations for System 2 and 3, a reflux ratio of 0.01 was assumed for the butanol column (set as close to zero as possible in the simulation since reflux effectively occurs *via* the decanter, as in the beer column), and a mass fraction of water of 0.1 wt% was assumed in the product butanol. Butanol purity varied slightly throughout these simulations (*circa* 99 wt%) depending on the amount of acetic acid carried over from the decanter into the butanol column. A further separation stage could be added to remove excess carboxylic acids. However, the accuracy of the butanol purity in this simulation is not likely to be high enough to warrant modelling the additional stage. The requirement for an additional stage depends on the liquid-liquid equilibrium of trace acetic acid in the decanters, for which high quality thermodynamic equilibrium models were not available for this simulation.

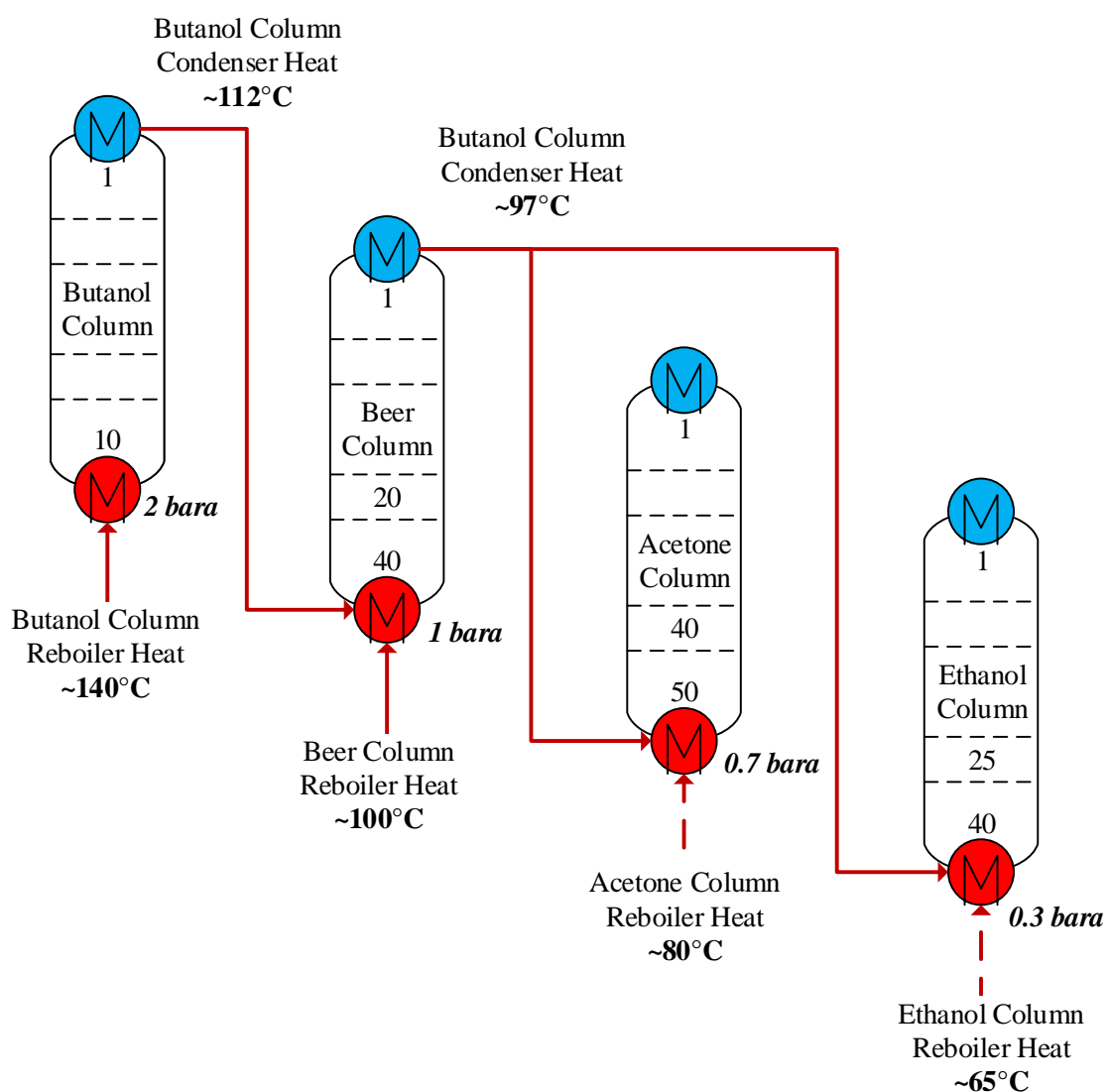


Figure A-4 – Distillation column heat integration strategy for Systems 2 and 3

A.3 Feed Composition

In all simulations, the feed to the distillation system was taken to flow at 1000 kg/h, and at 30°C, 1 bara. All products were cooled to 30°C at 1 bara.

In all three systems, dissolved gases (*e.g.* CO₂) were neglected. These non-condensable gases would be relatively trivial to remove as part of the distillation process, as they would be produced as off-gas in each condenser, mostly in the first decanter in each system. The quantity and composition of dissolved gases in the feed depend on the type of fermentation, and the exact operation of the fermentation system. If the quantity of dissolved gases were large, the non-condensable gas removed during the distillation process might contain significant quantities of products as vapour. In this scenario, refrigeration of the off-gas might be warranted in order to recover these products; however, this would present an additional energy load. Refrigeration systems might already be present in the fermentation system, in order to recover products from fermenter off-gas for example.

Only water, acetone, ethanol, *n*-butanol, acetic and butyric acid were considered in the simulation. Cells and other broth medium components were neglected. It was assumed that such components would either be filtered before distillation, or pass out the bottoms of the beer column in the stillage.

The relative quantity of each side product present in the feed is dependent on the fermentation stoichiometry. Table A-2 details the assumed relative molar ratios of products in the feed for each system

Table A-2 – Relative molar ratios of fermentation products assumed for distillation simulation feeds in each System

Component	System 1	System 2	System 3
Acetone	0	0	0.5
<i>n</i> -Butanol	1	1	1
Ethanol	0	0.33	0.1667
Butyric Acid	0	0.30	0.0463
Acetic Acid	0	0.75	0.0926
Source	(Butanol only)	Datta and Reeves (2014); Grethlein <i>et al.</i> (1990)	Tao <i>et al.</i> (2013a)

As detailed in Table A-2, the fermentation stoichiometries for System 2 were based on the product ratios calculated from the pilot plant measurements of Datta and Reeves (2014) and bench-scale measurements of Grethlein *et al.* (1990) for fermentation of synthesis gases to butanol. The product ratio of ethanol was estimated from measurements of electron efficiency for the conversion of synthesis gases to ethanol and butanol by Datta and Reeves (2014). The product ratios of carboxylic acids for System 2 was calculated based on the ratio of these products measured by Grethlein *et al.* (1990) and the assumption that the remainder of the balance of products based on the electron efficiencies of Datta and Reeves (2014) were acetic and butyric acids. System 3 was designed to represent ABE fermentation, for which significant information exists on fermentation stoichiometry for a range of organisms and scales. For the purpose of this simulation, the stoichiometry used by the NREL (Tao *et al.*, 2013a) was assumed for System 3, as detailed in Table A-2. The assumed product ratio is also in the typical ABE product ratio of 3 : 6 : 1 for acetone : butanol : ethanol (Green, 2011). A typical commercial ABE solvent titre is around 20 g/l (Green, 2011), which equates to a butanol titre of ~13 g/l for production in the typical ABE product ratio, the balance being ethanol and acetone.

A.4 Simulation in UniSim

The three models were investigated using the flowsheeting software UniSim Design 440. The Modified Inside-Out solver method was used to solve the distillation columns. This solver method was found to converge faster and was more stable than other solver methods, which was important due to the high number of recycle operations in the multicomponent systems. As in Outram *et al.* (2016), the Extended-NRTL model was used for calculation of multicomponent equilibria. This model is suited to this type of simulation, which contained a wide range of temperatures and concentrations, as well as azeotropes. UniSim's library of binary NRTL coefficients were used for the Extended-NRTL model. These have been shown to agree with experimental butanol-water equilibria by Outram *et al.* (2016). For binary pairs for which UniSim did not have NRTL coefficients available, coefficients were estimated using the UNIQUAC model. Liquid-liquid equilibria in decanters was predicted using coefficients estimated using the UNIQUAC liquid-liquid equilibrium model; vapour-liquid equilibria in distillation columns (and equilibria anywhere else) was calculated using the UNIQUAC vapour-liquid equilibrium model. It was found that using different binary coefficients did not impact significantly on the predicted energy consumption, but rather slightly altered the

balance of trace impurities (co-products, acetic acid, water) in the three product streams. The Soave-Redlich-Kwong equation of state was used to model the thermodynamics of the vapour phase. The choice of equation of state was found to have negligible impact on the predicted energy consumption.

Problems arose within UniSim when simulating the beer column when butyric acid was present; either the column solution would not converge, or the simulator erroneously predicted that all butyric acid, the heaviest component, would be recovered in the distillate. This suggested that the binary coefficients estimated for this carboxylic acid were incorrect. As a heavy component, it was therefore assumed that this component passed entirely to the bottom of the beer column and was therefore excluded from the beer column model in the simulation. The heat required for the reboiler in the simulation was adjusted to account for the additional heat required to heat butyric acid to the reboiler temperature.

Heat integration was performed using IChemE's Pinch Analysis spreadsheet tool (Kemp, 2006). A minimum temperature difference of 10 K was assumed for heat integration, on the basis that most heat integration was between condensers and reboilers, which have large heat transfer coefficients. Heat capacity was also assumed to be constant for sensible heat changes, and latent heat changes were assumed to be linear across the small temperature ranges over which phase changes occurred in any mixtures. The energy required for pumps was insignificant and was ignored.

A.5 Results of the Distillation Simulations

The UniSim simulations produced are given in the Supplementary Material included with this dissertation. Figure A-5 shows the net heat required, following heat integration, for each distillation System as a function of butanol concentration in the feed. As would be expected, for all three systems, the heat input required rises significantly as the concentration of butanol in the feed is lowered. Net heat inputs of *circa* 25 MJ/kg butanol are required to separate feeds at a butanol concentration of 1 wt% for all three systems. Figure A-6 shows the break-down of heat required in each distillation System in more detail, showing the heat demand of each column reboiler in each of the three systems (with heat consumption on a log scale).

The overall net heat consumption largely follows the trend of the falling heat demand for the beer column as the feed concentration of butanol increases, which largely dominates the heat demand. However, the heat demands of the reboilers of the ethanol, acetone and

butanol columns are constant with the feed concentration of butanol. At high concentrations of butanol feed, the heat demand of the ethanol column dominates.

A.6 Discussion of the Distillation Simulations

In all three Systems, the net heat required for distillation is a strong function of the butanol concentration in the feed. Indeed, for the binary case, System 1, the heat required is roughly inversely proportional to butanol concentration. The following relationship, a rough ‘rule of thumb’, was found (0.1 wt% - 5 wt%, maximum error 11%):

$$\text{Net heat demand} \cong \frac{28}{m_{Bu} (\text{wt \%})} \text{ MJ/kg butanol} \quad (\text{A-1})$$

Where m_{Bu} is the mass fraction of butanol in the feed (wt%).

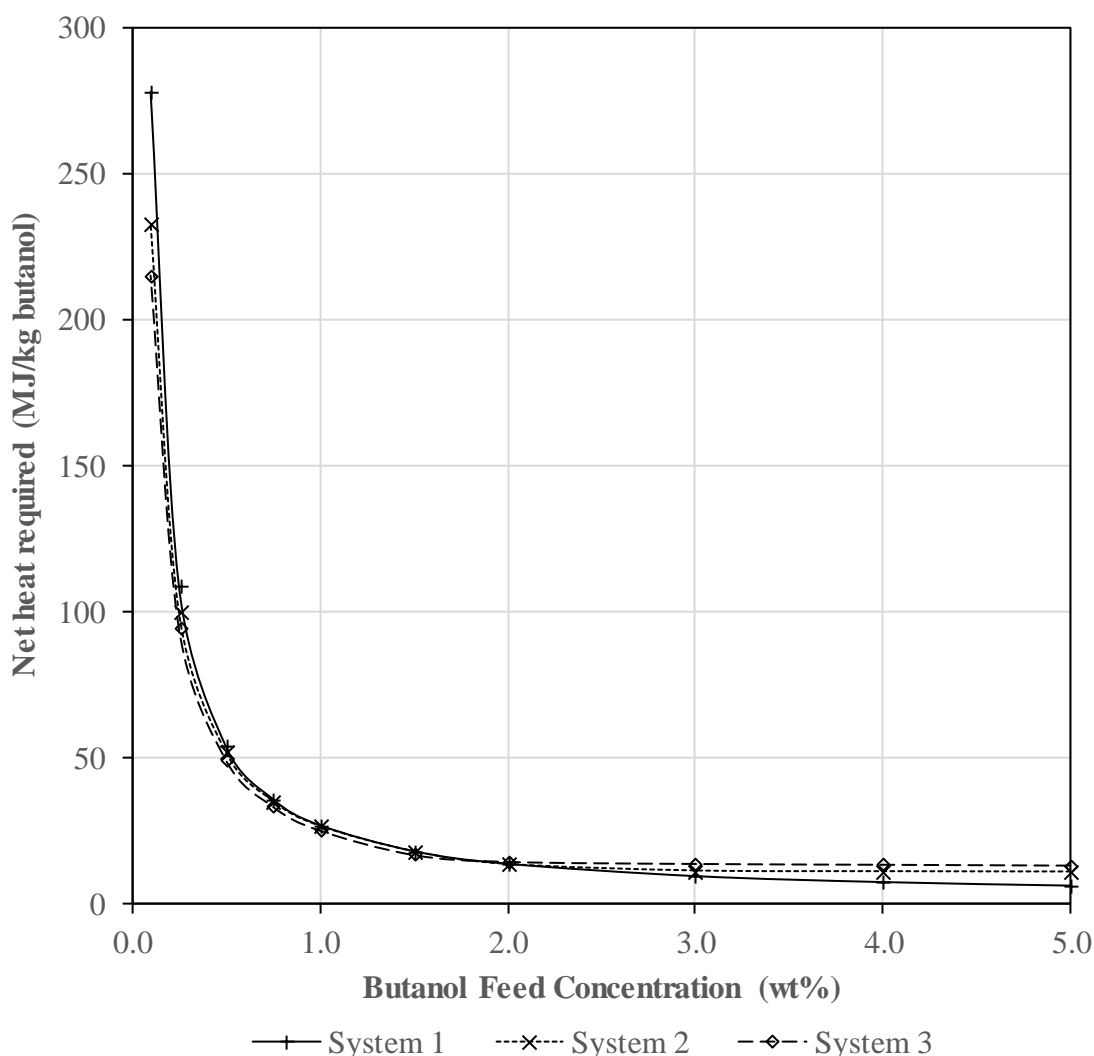


Figure A-5 – Net heat required for distillation per kg of separated butanol for Systems 1-3 as a function of butanol concentration

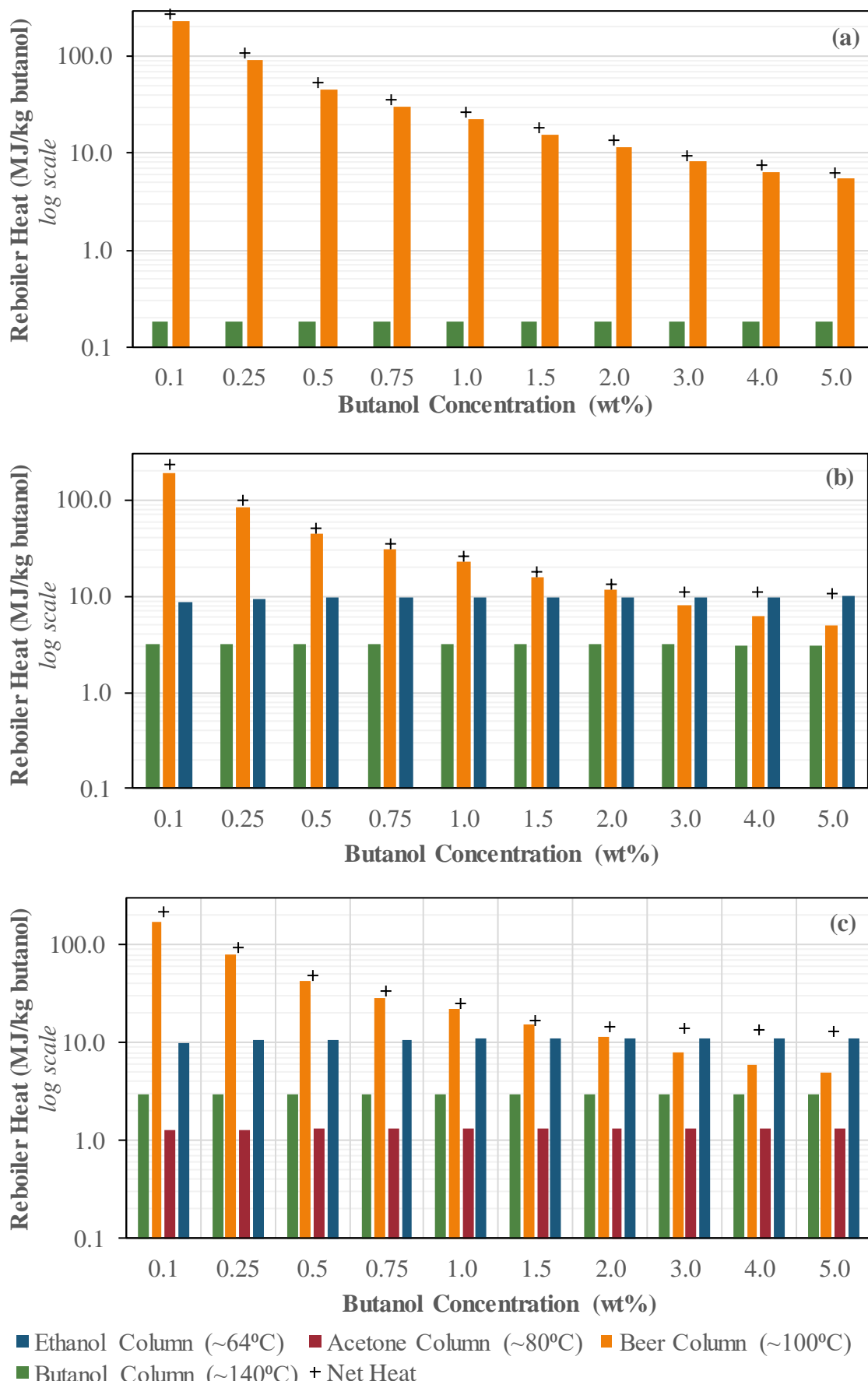


Figure A-6 – Reboiler heat demand (per kg butanol separated) of each distillation column for (a) System 1; (b) System 2; (c) System 3

For System 1, as would be expected, most of the heat is required for:

- i. pre-heating the feed to $\sim 100^{\circ}\text{C}$, as the final 10°C cannot be heat integrated
- ii. providing the reboiled vapour for the water column at $\sim 100^{\circ}\text{C}$

The reboiler load for the butanol column is relatively trivial, as seen in Figure A-6a. The heat required per unit of butanol for (i) is proportional to the mass flowrate of the aqueous feed. The heat required per unit of butanol for (ii) is also proportional to the quantity of aqueous feed, although it is less clear why this is the case. Theoretically, the water column can produce the butanol-water azeotrope in the distillate. This means that the heat required for the reboiler of the water column per unit butanol would be a function of the azeotrope composition. In practice, however, the number of stages in the column is finite (40 in this simulation) and in this simulation the butanol recovery is fixed. This results in the butanol in the distillate becoming less concentrated than the butanol-water azeotrope. Thus, the more dilute the feed concentration of butanol, the more dilute the resulting distillate concentration is. This results in a proportional relationship between the heat required for the reboiler of the water column (ii) and the quantity of aqueous feed. Hence, the heat required for System 1 per kg butanol is roughly proportional to the weight of the aqueous feed (per kg butanol), *i.e.* $1/m_{Bu}$, resulting in eq. (A-1).

As can be seen in Figure A-6a, the beer column dominates heat demand in System 1. This is also true for Systems 2 and 3 for butanol concentrations below 2 wt% in the feed, as shown in Figure A-6b-c. Since the heat required for the reboiler in the beer column drops as butanol concentration increases, the overall net heat required for the whole distillation system also decreases with increasing butanol concentration. The pressures of each distillation column in Systems 2 and 3 were designed to maximise heat recovery, as detailed in Figure A-4. The heat required for the acetone and ethanol columns can be supplied using heat from the beer column condenser. Therefore, the heat required for the separation of these side-products does not contribute to the net heat demand, provided there is suitable heat integration.

The compositions of flows downstream of the beer column do not vary significantly with the butanol concentration in the aqueous broth. Therefore, the heat requirement of the columns downstream of the beer column are approximately constant with butanol concentration in the aqueous broth. The beer column dominates heat demand below 2 wt% butanol concentration in the aqueous feed. Therefore, all heat consumed by the butanol column (at $\sim 140^{\circ}\text{C}$) can be recycled to supplement the heat demand of the

reboiler in the beer column (at $\sim 100^{\circ}\text{C}$). Further heat is then also required for the reboiler in the beer column, and all heat input to the beer reboiler can then be recycled to supply the entire heat requirements of the ethanol and acetone columns.

Above a feed concentration of 2 wt% butanol, the heat demand of the beer column reboiler is smaller than at more dilute butanol concentrations. This results in the ethanol column, rather than the beer column, dominating the heat demand in Systems 2 and 3, as shown in Figure A-6. This means that the heat recycled from the beer column will no longer be able to supply the heat required by the ethanol column. Hence, additional heat will be required to supplement the heat demand of the ethanol column. The net heat required by the distillation system no longer decreases with increased butanol concentration, as the system is dominated by the heat requirement of the ethanol column which does not depend on the butanol concentration in the aqueous feed.

There is therefore a critical butanol concentration in the feed, at which point the condenser of the beer column is no longer able to provide the heat requirements of the downstream columns. This critical concentration will depend on the relative molar composition of side-products in the feed. The higher the relative concentration of ethanol, the larger the heat requirement of the ethanol column. Since the heat requirement of the beer column decreases with increasing concentration of butanol in the feed, an increased concentration of ethanol in the feed results in a lower critical concentration of butanol. However, it should be noted that despite the relative molar ratio of ethanol in the feed differing by a factor of two between System 2 and System 3 (Table A-2), there was no difference in this critical butanol concentration in simulations of System 2 *versus* that of System 3. However, simulations were only run at discrete intervals: 1.5 wt%, 2 wt% and 3 wt% in the region of the critical butanol concentration.

Slightly unexpectedly, despite the additional solvents present in Systems 2 and 3, the net heat energy required for distillation is slightly lower in Systems 2 and 3 than in System 1 for feed concentrations under 2 wt% butanol. This is in part because the additional separations performed in the ethanol column and acetone column do not contribute to the net heat demand at butanol feed concentrations under 2 wt%. In addition, the presence of the more volatile ethanol and acetone components slightly lowers the heat requirement of the reboiler in the beer column. Because this reboiler dominates net energy consumption at low feed concentrations, the increased amounts of ethanol and acetone cause a slight reduction in net energy consumption. Of course, capital and maintenance

costs would still be significantly larger in Systems 2 and 3 because of the additional columns required.

The standard enthalpy of combustion of butanol is 36 MJ/kg. As shown in Figure A-5, large quantities of heat would need to be supplied to operate these distillation schemes, especially at low butanol concentrations. This heat demand often exceeds the combustion enthalpy of the butanol product, and due to the quantity would most likely have to come from combustion of additional feedstock.

At titres above 2 wt%, net heat demand drops to around 10 MJ/kg butanol or less, as seen in Figure A-5. This explains the benefits of increasing the butanol concentration fed to the distillation system where possible using *in situ* product recovery (*e.g.* gas and vacuum stripping). If the butanol concentration could be increased to 3 – 5 wt% with minimal energy requirement, conventional distillation could then complete the separation at a more reasonable energy cost. Distillation is also unsuitable for *in situ* product removal itself due to the high temperatures required by the beer column.

APPENDIX B. DERIVATION OF THE CO-EXISTENCE EQUATION AT CONSTANT TEMPERATURE, AND ESTIMATING DISTRIBUTION COEFFICIENTS FOR BUTANOL

B.1 Derivation of the Co-existence equation at constant temperature

Starting from the Gibbs-Duhem equation for the liquid and vapour phases at constant temperature for a closed binary mixture:

$$x_1 d\mu_1^L + x_2 d\mu_2^L = \underline{V}^L dP \quad (\text{B-1})$$

$$y_1 d\mu_1^V + y_2 d\mu_2^V = \underline{V}^V dP \quad (\text{B-2})$$

Noting that at equilibrium, $\mu_1^L = \mu_1^V (= \mu_1)$ and therefore $d\mu_1^L = d\mu_1^V (= d\mu_1)$, and also noting that $(y_1 - x_1) = -(y_2 - x_2)$, subtracting the liquid equation from the vapour equation yields:

$$(y_1 - x_1)(d\mu_1 - d\mu_2) = (\underline{V}^V - \underline{V}^L)dP \quad (\text{B-3})$$

Generally, the chemical potential of species i in the vapour phase can be found by considering the deviation from that of a pure ideal gas ($(\partial\mu_i^{RM}/\partial P)_{T,n} = \bar{V}_i$):

$$\mu_i^V = \mu_i^{o,pure,IG} + RT \ln \left(\frac{P}{P_o} \right) + RT \ln y_i + \int_0^P \left(\bar{V}_i^V - \frac{RT}{P} \right) dP \quad (\text{B-4})$$

$$\mu_i^V = \mu_i^{o,pure,IG} + RT \ln \left(\frac{y_i \phi P}{P_o} \right) \quad (\text{B-5})$$

$$\therefore d\mu_i^V = d\mu_i = RT \left[\frac{dP}{P} + \frac{dy_i}{y_i} + d\ln \phi_i \right] \quad (\text{B-6})$$

Hence, for the binary mixture of components 1 and 2, substituting into Eq. (B-3):

$$RT(y_1 - x_1) \left(\frac{dy_1}{y_1} + d\ln \phi_1 - \frac{dy_2}{y_2} - d\ln \phi_2 \right) = (\underline{V}^V - \underline{V}^L)dP \quad (\text{B-7})$$

and since $y_2 = (1 - y_1)$ and $dy_2 = -dy_1$:

$$RT(y_1 - x_1) \left(\frac{dy_1}{y_1(1 - y_1)} + d\ln \left(\frac{\phi_1}{\phi_2} \right) \right) = (\underline{V}^V - \underline{V}^L)dP \quad (\text{B-8})$$

Re-arrangement yields the co-existence equation at constant temperature:

$$\frac{dy_1}{dP} = y_1(1 - y_1) \left(\frac{\underline{V}^V - \underline{V}^L}{RT(y_1 - x_1)} - \frac{d\ln(\phi_1/\phi_2)}{dP} \right) \quad (\text{B-9})$$

B.2 Applying the Virial Equation to the Co-existence Equation

The virial equation for a binary mixture is given by (Appendix D):

$$\underline{V}^V = \frac{RT}{P} + y_1 B_{11} + y_2 B_{22} + y_1 y_2 \delta_{12} \quad (\text{B-10})$$

where B_{11} and B_{22} are the second virial coefficients for pure species 1 and 2 respectively, and $\delta_{12} = (2B_{12} - B_{11} - B_{22})$.

$$\ln \phi_1 = \frac{P}{RT} (B_{11} + y_2^2 \delta_{12}) = \frac{P}{RT} (B_{11} + (1 - y_1)^2 \delta_{12}) \quad (\text{B-11})$$

$$\ln \phi_2 = \frac{P}{RT} (B_{22} + y_1^2 \delta_{12}) \quad (\text{B-12})$$

Hence:

$$\frac{d \ln \left(\frac{\phi_1}{\phi_2} \right)}{dP} = \frac{d}{dP} \left(\frac{P}{RT} (B_{11} - B_{22} + ((1 - y_1)^2 - y_1^2) \delta_{12}) \right) \quad (\text{B-13})$$

$$\frac{d \ln \left(\frac{\phi_1}{\phi_2} \right)}{dP} = \frac{d}{dP} \left(\frac{P}{RT} (B_{11} - B_{22} + (1 - 2y_1) \delta_{12}) \right) \quad (\text{B-14})$$

$$\frac{d \ln \left(\frac{\phi_1}{\phi_2} \right)}{dP} = \frac{1}{RT} \left((B_{11} - B_{22} + (1 - 2y_1) \delta_{12}) + P(-2\delta_{12}) \frac{dy_1}{dP} \right) \quad (\text{B-15})$$

Substitution into the co-existence equation (B-9) gives:

$$\frac{dy_1}{dP} = \frac{y_1(1 - y_1)}{RT} \left(\frac{\underline{V}^V - \underline{V}^L}{(y_1 - x_1)} - (B_{11} - B_{22} + (1 - 2y_1)\delta_{12}) + 2P\delta_{12} \frac{dy_1}{dP} \right) \quad (\text{B-16})$$

$$\frac{dy_1}{dP} = \frac{y_1 y_2 (\underline{V}^V - \underline{V}^L - (y_1 - x_1)(B_{11} - B_{22} + (1 - 2y_1)\delta_{12}))}{(RT - 2Py_1 y_2 \delta_{12})(y_1 - x_1)} \quad (\text{B-17})$$

$$\frac{dy_1}{dP} = \frac{\underline{V}^V - y_1 B_{11} + y_1 B_{22} + x_1 B_{22} - x_1 B_{22} - \underline{V}^L - (y_1 - x_1)(1 - 2y_1)\delta_{12}}{(y_1 - x_1) \left(\frac{RT}{y_1 y_2} - 2\delta_{12} P \right)} \quad (\text{B-18})$$

From the virial equation definition for a binary mixture, eq. (B-10):

$$\frac{dy_1}{dP} = \frac{\frac{RT}{P} + x_1 B_{11} + x_2 B_{22} - \underline{V}^L - (y_1 - x_1)(1 - 2y_1)\delta_{12}}{(y_1 - x_1) \left(\frac{RT}{y_1 y_2} - 2\delta_{12} P \right)} \quad (\text{B-19})$$

B.3 Virial Co-existence Equation at $x_1 \rightarrow 0$

At $x_1 = y_1 \rightarrow 0$, $P = P_2^{sat}$:

$$\left(\frac{dy_1}{dP}\right)_{y_1 \rightarrow 0} = \lim_{y_1 \rightarrow 0} \left(\frac{\frac{RT}{P_2^{sat}} + B_{22} - \underline{V}_2^L}{(y_1 - x_1) \left(\frac{RT}{y_1} - 2\delta_{12}P \right)} \right) = \lim_{y_1 \rightarrow 0} \left(\frac{\underline{V}_2^V - \underline{V}_2^L}{(y_1 - x_1) \frac{RT}{y_1}} \right) \quad (\text{B-20})$$

$$\left(\frac{dy_1}{dP}\right)_{y_1 \rightarrow 0} = \lim_{y_1 \rightarrow 0} \left(\frac{\underline{V}_2^V - \underline{V}_2^L}{RT \left(1 - \frac{x_1}{y_1} \right)} \right) \quad (\text{B-21})$$

Applying L'Hôpital's Rule, this collapses to:

$$\left(\frac{dy_1}{dP}\right)_{y_1 \rightarrow 0} = \frac{\underline{V}_2^V - \underline{V}_2^L}{RT \left(1 - \left(\frac{dx_1}{dy_1} \right)_{y_1 \rightarrow 0} \right)} \quad (\text{B-22})$$

$$\left(1 - \left(\frac{dx_1}{dP} \right)_{y_1 \rightarrow 0} \left(\frac{dP}{dy_1} \right)_{y_1 \rightarrow 0} \right) \left(\frac{dy_1}{dP} \right)_{y_1 \rightarrow 0} = \frac{(\overline{V}_2^V - \overline{V}_2^L)}{RT} \quad (\text{B-23})$$

$$\left(\frac{dy_1}{dP} \right)_{y_1 \rightarrow 0} = \frac{(\underline{V}_2^V - \underline{V}_2^L)}{RT} + \frac{1}{\left(\frac{dP}{dx_1} \right)_{y_1 \rightarrow 0}} \quad (\text{B-24})$$

$$\left(\frac{dy_1}{dx_1} \right)_{y_1 \rightarrow 0} = \frac{(\underline{V}_2^V - \underline{V}_2^L)}{RT} \cdot \left(\frac{dP}{dx_1} \right)_{y_1 \rightarrow 0} + 1 \quad (\text{B-25})$$

B.4 Derivations of the Limiting Activity Co-efficient from the virial Co-existence Equation

The general statements for vapour-liquid equilibrium is:

$$\phi_i(y_i, T, P) \cdot y_i P = \gamma_i(x_i, T, P) \cdot x_i \cdot \phi_i^{sat} \cdot P_i^{sat} \cdot \exp\left(\frac{\underline{V}_i^L(P - P_i^{sat})}{RT}\right) \quad (\text{B-26})$$

which can be rearranged to give:

$$\gamma_i(x_i, T, P) = \frac{\phi_i(y_i, T, P) \cdot y_i P}{x_i \cdot \phi_i^{sat} \cdot P_i^{sat}} \cdot \exp\left(\frac{-\underline{V}_i^L(P - P_i^{sat})}{RT}\right) \quad (\text{B-27})$$

The limiting activity coefficient can be found the limit at $x_1 = y_1 \rightarrow 0$, where $P = P_2^{sat}$, $\phi_1 = \phi_1^\infty$, $\gamma_1 = \gamma_1^\infty$, by applying L'Hôpital's Rule

$$\gamma_1^\infty(T, P_2^{sat}) = \left(\frac{dy_1}{dx_1}\right)_{y_1 \rightarrow 0} \cdot \frac{\phi_1^\infty P_2^{sat}}{\phi_1^{sat} P_1^{sat}} \cdot \exp\left(\frac{-\underline{V}_1^L(P_2^{sat} - P_1^{sat})}{RT}\right) \quad (\text{B-28})$$

From expressions for ϕ_i using the virial equation (eqs. D-13 and D-14, Appendix D):

$$\frac{\phi_1^\infty P_2^{sat}}{\phi_1^{sat} P_1^{sat}} = \alpha_{2,1} \cdot \frac{\exp\left(\frac{P_2^{sat}(B_{11} + \delta_{12})}{RT}\right)}{\exp\left(\frac{P_1^{sat} B_{11}}{RT}\right)} \quad (\text{B-29})$$

$$\gamma_1^\infty(T, P_2^{sat}) = \left(\frac{dy}{dx_1}\right)_{y_1=0} \alpha_{2,1} \cdot \exp\left(\frac{(P_2^{sat} - P_1^{sat})(B_{11} - \underline{V}_1^L) + P_2^{sat} \delta_{12}}{RT}\right) \quad (\text{B-30})$$

where $\alpha_{2,1}$ is the relative volatility of component 2 *versus* component 1, *i.e.*:

$$\alpha_{2,1} = \frac{P_2^{sat}}{P_1^{sat}} \quad (\text{B-31})$$

Substituting the coexistence equation at $y_1 \rightarrow 0$ (eq. B-25) with the virial EoS (eq. (B-25)) and expressions for ϕ_i (eqs. D-13 and D-14, Appendix D) for the virial equation yields:

$$\begin{aligned} \gamma_1^\infty(T, P_2^{sat}) &= \left(\frac{(\underline{V}_2^V - \underline{V}_2^L)}{RT} \cdot \left(\frac{dP}{dx_1}\right)_{x_1=0} + 1 \right) \cdot \alpha_{2,1} \cdot \epsilon \\ \epsilon &= \exp\left(\frac{P_1^{sat}}{RT} \left((\alpha_{2,1} - 1)(B_{11} - \underline{V}_1^L) + \alpha_{2,1} \delta_{12} \right)\right) \end{aligned} \quad (\text{B-32})$$

For Raoult's Law (ideal case), the gradient dP/dx_1 is given by:

$$P = x_1 P_1^{sat} + (1 - x_1) P_2^{sat} \rightarrow \frac{dP}{dx_1} = (P_1^{sat} - P_2^{sat}) \quad (\text{B-33})$$

Appendix B - Derivation of the Co-Existence Equation at Constant Temperature, and Estimating Distribution Coefficients for Butanol

The bubble-point curve is a straight line for Raoult's Law. Writing the gradient dP/dx_1 relative to its gradient for the ideal mixture case (Raoult's Law):

$$\gamma_1^\infty(T, P_2^{sat}) = \left(\frac{(V_2^V - V_2^L)}{RT} \cdot \mathcal{M}(P_1^{sat} - P_2^{sat}) + 1 \right) \cdot \alpha_{2,1} \cdot \epsilon \quad (\text{B-34})$$

$$\gamma_1^\infty(T, P_2^{sat}) = \left(1 - \frac{P_2^{sat}(V_2^V - V_2^L)}{RT} \cdot \mathcal{M} \left(1 - \frac{1}{\alpha_{2,1}} \right) \right) \cdot \alpha_{2,1} \cdot \epsilon \quad (\text{B-35})$$

$$\gamma_1^\infty(T, P_2^{sat}) = \left(\alpha_{2,1} - (\alpha_{2,1} - 1) \mathcal{M} \frac{P_2^{sat}(V_2^V - V_2^L)}{RT} \right) \epsilon \quad (\text{B-36})$$

$$\begin{aligned} \gamma_1^\infty(T, P_2^{sat}) &= \left(\alpha_{2,1} - (\alpha_{2,1} - 1) \mathcal{M} \frac{P_2^{sat}(V_2^V - V_2^L)}{RT} \right) \epsilon \\ \epsilon &= \exp \left(\frac{P_1^{sat}}{RT} \left((\alpha_{2,1} - 1)(B_{11} - V_1^L) + \alpha_{2,1} \delta_{12} \right) \right) \end{aligned} \quad (\text{B-37})$$

Here \mathcal{M} is the gradient relative to Raoult's Law:

$$\left(\frac{dP}{dx_1} \right)_{y_1=0} = \mathcal{M}(P_1^{sat} - P_2^{sat}) \quad (\text{B-38})$$

When $\mathcal{M} = 1$ and the vapour phase assumed to be ideal (and Poynting correction is ignored by assuming V_1^L is negligible), $\gamma_1^\infty = 1$.

For systems with $P_2^{sat} > P_1^{sat}$, if $\mathcal{M} < 1$, $\gamma_1^\infty > 1$, the system will show positive deviation from Raoult's Law; in these cases, the species show a net repulsive force.

At $\mathcal{M} = 0$, the gradient of the bubble-point curve is zero at $x_1 = 0$

For $\mathcal{M} < 0$, the gradient of the bubble-point curve is positive for systems with $P_2^{sat} > P_1^{sat}$; in these systems, the vapour pressure initially increases with addition of the more volatile species 2, and hence the system forms a minimum boiling point azeotrope at some composition (by Rolle's Theorem (Munroe, 2018)). Conversely, if $\mathcal{M} < 1$, $\gamma_1^\infty < 1$ and the system will show negative deviation from Raoult's Law.

If $P_1^{sat} > P_2^{sat}$, these conclusions are reversed: if $\mathcal{M} < 1$, the system shows negative deviation from Raoult's Law and if $\mathcal{M} < 0$, the system forms a maximum boiling point azeotrope at some composition. $\mathcal{M} > 1$ would indicate positive deviation from Raoult's Law.

B.5 The Limiting Distribution Coefficient for Dilute Butanol in Hydrocarbons vs. Water

The limiting distribution coefficient for butanol is given by:

$$D_i^{\infty,molar} = \frac{\gamma_i^{\infty,aq}(P, T)}{\gamma_i^{\infty,org}(P, T)} \quad (\text{B-39})$$

As shown in Appendix E, the effect of pressure on activity coefficient can be neglected. Since water and the hydrocarbons explored have very low mutual solubilities, the concentration of water in the organic phase and the concentration of the hydrocarbon in the aqueous phase can be neglected, and binary activity coefficients for butanol in hydrocarbons and butanol in water can be used (*i.e.* the trace concentration of water in the hydrocarbon phase is assumed to have no impact on the activity coefficient of butanol in the organic phase *etc.*).

For the butanol (1) - hydrocarbon (2) binary system, for C₄ – C₆ hydrocarbons $P_2^{sat} > P_1^{sat}$. VLE data indicates that these systems show a positive deviation from Raoult's Law, but that most do not form an azeotrope. Therefore, for these systems, $0 < \mathcal{M} < 1$. The only exception is *n*-hexane, which shows a minimum boiling point azeotrope at a dilute butanol concentration; this means that for *n*-hexane, \mathcal{M} is slightly negative. Hence, using equation (B-37):

$$D_{Bu}^{\infty,molar}(T) = \frac{\gamma_{Bu}^{\infty,aq}(T)}{\left(\alpha_{2,1} - (\alpha_{2,1} - 1)\mathcal{M} \frac{P_2^{sat}(V_2^V - V_2^L)}{RT} \right) \epsilon} \\ \epsilon = \exp\left(\frac{P_1^{sat}}{RT} \left((\alpha_{2,1} - 1)(B_{11} - V_1^L) + \alpha_{2,1}\delta_{12} \right)\right) \quad (\text{B-40})$$

A thorough analyses of the limiting activity coefficient of butanol ($\gamma_{Bu}^{\infty,aq}(T)$) was conducted by Dohnal *et al*, (2006) (*n*-butanol) and Fenclova *et al*. (2007) (*iso*-butanol) over the temperature range 273 - 373 K. Their correlations for $\gamma_{Bu}^{\infty,aq}(T)$ are given in Appendix F.

APPENDIX C. MASS BALANCE OF THE EQUILIBRIUM CELL

The liquid composition at equilibrium (x_1) can be determined from the overall composition (z_1); the vapour composition at equilibrium (y_1); and the molar volume of the equilibrium cell (\underline{V}^{cell}). These compositions can be linked by a mass balance of the equilibrium cell. The cell volume is the sum of the liquid volume and the vapour volume:

$$\underline{V}^{cell} = \underline{V}^{cell}N^{cell} = (\psi N^{cell})\underline{V}^V + ((1 - \psi)N^{cell})\underline{V}^L \quad (C-1)$$

Where ψ is the mole fraction of the total cell contents in the vapour phase.

The moles of species 1 in the cell is the sum of the moles of species 1 in the liquid and vapour phases:

$$z_1N^{cell} = y_1(\psi N^{cell}) + x_1((1 - \psi)N^{cell}) \quad (C-2)$$

Rearranging both of these expressions for ψ yields:

$$\psi = \frac{z_1 - x_1}{y_1 - x_1} = \frac{\underline{V}^{cell} - \underline{V}^L}{\underline{V}^V - \underline{V}^L} \quad (C-3)$$

$$\therefore x_1 = \frac{z_1\underline{V}^V - y_1\underline{V}^{cell} + (y_1 - z_1)\underline{V}^L}{\underline{V}^V - \underline{V}^{cell}} \quad (C-4)$$

However, \underline{V}^L is a function of x_1 ; for a binary mixture:

$$\underline{V}^L = x_1\underline{V}_1^L + (1 - x_1)\underline{V}_2^L + \underline{V}_E^L = \underline{V}_2^L + x_1(\underline{V}_1^L - \underline{V}_2^L) + \underline{V}^{LE} \quad (C-5)$$

Where \underline{V}^{LE} is the molar excess volume on mixing (which is a function of x_1). Hence:

$$x_1 = \frac{z_1\underline{V}^V - y_1\underline{V}^{cell} + (y_1 - z_1)(\underline{V}_2^L + \underline{V}^{LE}(x_1))}{\underline{V}^V - \underline{V}^{cell} - (y_1 - z_1)(\underline{V}_1^L - \underline{V}_2^L)} \quad (C-6)$$

This is a problem as \underline{V}^{LE} is a complex function of x_1 , and so numerical techniques would be required to solve this equation. However, \underline{V}^{LE} can be neglected since $\underline{V}^{LE} \ll \underline{V}_2^L$. Note that the entire term containing \underline{V}^{LE} , $(y_1 - z_1)(\underline{V}_2^L + \underline{V}^{LE}(x_1))$, is usually negligible anyway, because $(y_1 - z_1) \sim O(z_1, y_1)$, and $\underline{V}_2^L \ll \underline{V}^V$. Hence, neglecting \underline{V}^{LE} :

$$\therefore x_1 = \frac{z_1\underline{V}^V - y_1\underline{V}^{cell} + (y_1 - z_1)\underline{V}_2^L}{\underline{V}^V - \underline{V}^{cell} - (y_1 - z_1)(\underline{V}_1^L - \underline{V}_2^L)} \quad (C-7)$$

APPENDIX D. VAPOUR PHASE EQUATIONS OF STATE

Calculation of molar volume in the vapor phase (\underline{V}_V) is essential for correcting overall cell mole fractions into liquid mole fractions. Calculation of vapor phase fugacity coefficients (ϕ_i) are essential for the calculation of activity coefficients. Both are calculable from equations of state.

Fugacity coefficients can be derived from equations of state by considering the residual Gibbs energy, *i.e.* the difference between the Gibbs energy of the real gas phase and that of the ideal gas phase (Raal and Muhlbauer, 1997):

$$\ln \phi_i = \int_0^P (\bar{Z} - 1) \frac{dP}{P} \quad (\text{D-1})$$

Where Z is compressibility factor ($P\underline{V}^V/RT$)

D.1 Ideal Gas Law

The molar volume and fugacity coefficients for an ideal gas are independent of composition and are given by:

$$\underline{V}^V = \frac{RT}{P} \quad (\text{D-2})$$

$$\phi_i = 1 \quad (\text{D-3})$$

The ideal gas law is a reasonable approximation at low pressures when intermolecular forces are negligible.

D.2 Soave-Redlich-Kwong Equation of State

The Soave-Redlich-Kwong (SRK) equation of state (Soave, 1972) is given by the solution of the following cubic in Z :

$$Z^3 - Z^2 + Z(A - B - B^2) - AB = 0 \quad (\text{D-4})$$

A (representing intermolecular forces) and B (representing finite molecular size) for a binary mixture are calculated from A_{ii} and B_i for the pure components:

$$A_{ii} = 0.42747 \frac{P_{r,i}}{T_{r,i}^2} \left(1 + (0.480 + 1.574\omega_i - 0.176\omega_i^2)(1 - T_{r,i}^{0.5}) \right)^2 \quad (\text{D-5})$$

$$B_i = 0.08664 \frac{P_{r,i}}{T_{r,i}} \quad (\text{D-6})$$

Where $T_{r,i}$ is reduced temperature ($T/T_{c,i}$) and $P_{r,i}$ is reduced pressure ($P/P_{c,i}$). Taking A_{12} (the interactions between species 1 and species 2) to be the geometric mean of A_{11} and A_{22} (*i.e.* neglecting the binary interaction parameter):

$$A_{12} = (A_1 A_2)^{0.5} \quad (\text{D-7})$$

$$A = y_1^2 A_{11} + y_1 y_2 A_{12} + y_2^2 A_{22} \quad (\text{D-8})$$

$$B = y_1 B_1 + y_2 B_2 \quad (\text{D-9})$$

Hence:

$$\underline{V}^V = Z \frac{RT}{P} \quad (\text{D-10})$$

$$\ln \phi_i = (Z - 1) \frac{B_i}{B} - \ln(Z - B) - \frac{A}{B} \left(2 \left(\frac{A_{ii}}{A} \right)^{0.5} - \frac{B_i}{B} \right) \ln \left(1 + \frac{B}{Z} \right) \quad (\text{D-11})$$

Equations of state such as Redlich-Kwong are cubic equations which allow modelling of the vapour phase based on the principle of corresponding states. Soave's modification optimised the equation for hydrocarbons.

D.3 Virial Equation of State

The molar volume of the vapor phase and fugacity coefficients for the virial equation of state for a binary mixture are given by:

$$\underline{V}^V = \frac{RT}{P} + y_1 B_{11} + y_2 B_{22} + y_1 y_2 \delta_{12} \quad (\text{D-12})$$

Where B_{11} and B_{22} are the second virial coefficients for pure species 1 and 2 respectively, and $\delta_{12} = (2B_{12} - B_{11} - B_{22})$. Therefore:

$$\ln \phi_1 = \frac{P}{RT} (B_{11} + y_2^2 \delta_{12}) \quad (\text{D-13})$$

$$\ln \phi_2 = \frac{P}{RT} (B_{22} + y_1^2 \delta_{12}) \quad (\text{D-14})$$

The virial equation of state is a truncated expansion of compressibility factor. Because it is truncated at the second term, it is valid at low to moderate pressures. The second virial coefficient (B_{ii}) accounts for intermolecular interactions between molecules, and many correlations and models exist for the purposes of calculating B_{ii} . In this work, the method of Tsonopoulos has been used (Tsonopoulos, 1974).

D.4 Tsonopoulos' Method for Calculation of Second Virial Coefficients

In Tsonopoulos' method (Tsonopoulos, 1974), the second virial coefficient for a binary mixture of species i and j is given by:

$$B_{ij} = \frac{RT_{c,ij}}{P_{c,ij}} \left(f^{(0)}(T_r) + \omega_{ij} f^{(1)}(T_r) + f^{(2)}(T_r) \right) \quad (\text{D-15})$$

$$f^{(0)}(T_r) = 0.1445 - \frac{0.330}{T_r} - \frac{0.1385}{T_r^2} - \frac{0.0121}{T_r^3} - \frac{0.000607}{T_r^8} \quad (\text{D-16})$$

$$f^{(1)}(T_r) = 0.0637 + \frac{0.331}{T_r^2} - \frac{0.423}{T_r^3} - \frac{0.008}{T_r^8} \quad (\text{D-17})$$

$$f^{(2)}(T_r) = \frac{a_{ij}}{T_r^6} - \frac{b_{ij}}{T_r^8} \quad (\text{D-18})$$

Where T_r is the reduced temperature of the mixture ($T/T_{c,ij}$). The parameters a_{ij} and b_{ij} are Tsonopoulos parameters for polar and associating species. These parameters are calculated from those of pure species, which depend on the dipole moment of the species. The reduced dipole moment ($\mu_{r,i}$) for a species, i , can be calculated from its dipole moment (μ_i), and is given by:

$$\mu_{r,i} = \frac{\mu_i^2 \left(\frac{P_c}{1.01325} \right)}{T_{c,i}^2} \quad (\text{D-19})$$

Where P_c is in Pa, T_c is in K and μ is in Debye. For non-polar molecules (e.g. alkanes), $a_{ii} = b_{ii} = 0$. For water, $a_{ii} = -0.0109$, $b_{ii} = 0$ (Poling *et al.*, 2001). For ketones, aldehydes and carboxylic acids, a_{ii} and b_{ii} are given by (Poling *et al.*, 2001):

$$a_{ii} = -0.000214\mu_{r,i} - (4.308 \times 10^{-21})\mu_{r,i}^8; \quad b_{ii} = 0 \quad (\text{D-20})$$

The values of a_{ii} and b_{ii} for slightly polar hydrocarbons (alkenes) were assumed to follow the same formula as ketones. For 1-alcohols except methanol (Poling *et al.*, 2001):

$$a_{ii} = 0.0878; \quad b_{ii} = 0.00908 + 0.0006957\mu_{r,i} \quad (\text{D-21})$$

This formula for 1-alcohols was assumed to be valid for *iso*-butanol.

The Tsonopoulos parameters (a_{ij}, b_{ij}) of the mixture for two polar species (*i.e.* a_{ii} and a_{jj} are both non-zero) are given by:

$$a_{ij} = 0.5(a_{ii} + a_{jj}), \quad b_{ij} = 0.5(b_{ii} + b_{jj}) \quad (\text{D-22})$$

For mixtures of polar with non-polar species (*i.e.* either or both molecules have $a_{ii} = 0$), the polar contribution to B_{ij} is neglected (*i.e.* $a_{ij} = b_{ij} = 0$).

Finally, critical temperature, pressure and acentricity of the mixture are calculated from the critical properties of pure components using the following mixing rules:

$$T_{c,ij} = (1 - k_{ij})(T_{c,i}T_{c,j})^{0.5} \quad (\text{D-23})$$

$$P_{c,ij} = 4T_{c,ij} \frac{\left(\frac{P_{c,i}V_{c,i}}{T_{c,i}} + \frac{P_{c,j}V_{c,j}}{T_{c,j}}\right)}{\left(V_{c,i}^{1/3} + V_{c,j}^{1/3}\right)^3} \quad (\text{D-24})$$

$$\omega_{ij} = 0.5(\omega_i + \omega_j) \quad (\text{D-25})$$

Where k_{ij} is the binary interaction parameter, a characteristic constant for each binary. For binaries containing species of similar size and chemical nature, k_{ij} is zero (and thus $T_{c,ij}$ is the geometric mean of $T_{c,i}$ and $T_{c,j}$). Tsonopoulos provided some average values for pairs of compounds of different types (Tsonopoulos, 1974). These have been assumed in this work, and are given in Table D-1.

Table D-1 – Binary Interaction Parameters for pairs of different types of compounds

$k_{ij} = k_{ji}$	Hydrocarbons	Ketones	Alcohols & Carboxylic Acids	Water
Hydrocarbons	0	0.13	0.15	0.40
Ketones	0.13	0	0.05	0.15
Alcohols & Carboxylic Acids ¹	0.15	0.05	0	0.10
Water	0.40	0.15	0.10	0

¹ Carboxylic acids not included in Tsonopoulos (1974); they were assumed to have binary interactions similar to those of alcohols.

D.5 Comparison of Second virial Coefficients of Pure Pentane and Butanol Calculated by Different Methods

To evaluate predictions of second virial coefficients obtained from different methods, a comparison was conducted. Three methods for the calculation of second virial coefficients of pure *n*-pentane and *n*-butanol were compared: the Tsonopoulos method (as detailed above); a DIPPR correlation (Rowley *et al.*, 2008); and the method of O'Connell and Prausnitz (1967) (used in the reduction of VLE measurements of pentane and butanol by Ronc and Ratcliff (1976)). Second virial coefficients predicted by each of these three methods for butanol and pentane at 30°C and 60°C are shown in Table D-2.

Figure D-1 plots the DIPPR correlation against empirical values of the second virial coefficient contained in the DIPPR database (Rowley *et al.*, 2008). This figure demonstrates that the values of the second virial coefficient predicted for butanol by the DIPPR correlation at 30°C and 60°C ($1000/T = 3.3$ and 3.0) are significantly lower than the empirical values in the DIPPR database at these temperatures. Predictions of the second virial coefficient of butanol by the Tsonopoulos method were closest to the empirical measurements. The values detailed in Table D-2 for this method are close to the experimental values in Figure D-1. Conversely, the method of O'Connell and Prausnitz predicted implausible values for the second virial coefficient of butanol that were far higher than the empirical values in Figure D-1. For pentane, all three methods produced good predictions of second virial coefficient compared to the empirical values. This was expected, as pentane is a simple, non-polar molecule.

Due to its accuracy in predicting both pentane and butanol coefficients, the Tsonopoulos method was selected for the calculation of second virial coefficients in this work.

Table D-2 – Second virial coefficients of butanol and pentane at 30°C and 60°C, calculated using the DIPPR correlation; the Tsonopoulos method; and the method of O’Connell & Prausnitz. Approximate empirical values from the DIPPR database are also detailed, obtained from Figure D-1

B_{ii} (m ³ /kmol)	Pentane		Butanol	
	30°C	60°C	30°C	60°C
DIPPR correlation	-1.31	-0.97	-8.84	-4.46
Tsonopoulos method	-1.07	-0.84	-4.37	-2.30
O’Connell and Prausnitz	-1.16	-0.92	0.37	0.23
Empirical values from DIPPR database (approximate)	-1.3	-1.0	-4.5	-2.5

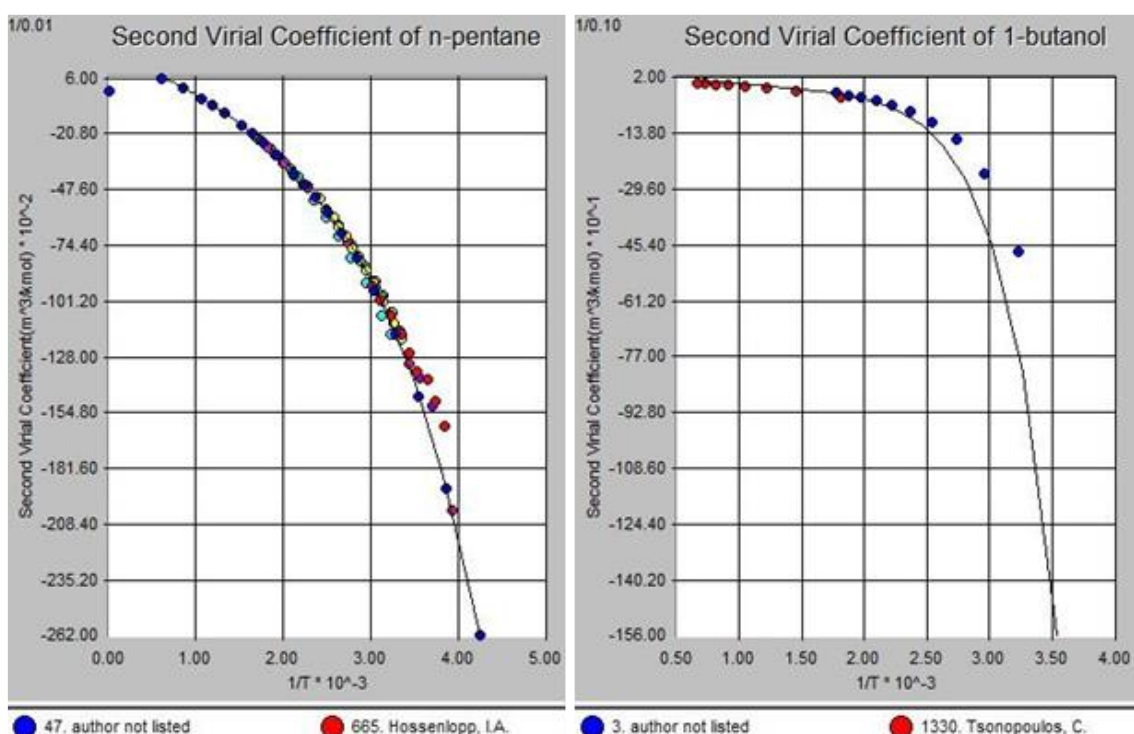


Figure D-1 – Second virial coefficients of pentane and butanol calculated by DIPPR correlations (line, -) and empirical measurements listed in DIPPR database (points). Not all data points could be shown for butanol. This figure was produced by the DIPPR database as export of empirical measurements in the DIPPR database was not possible.

APPENDIX E. VARIATION OF ACTIVITY COEFFICIENTS WITH TEMPERATURE AND PRESSURE

E.1 Theoretical dependence of activity coefficient on temperature and pressure

Starting from the total differential of Gibbs free energy:

$$dG = \left(\frac{\partial G}{\partial P}\right)_{T,n} dP + \left(\frac{\partial G}{\partial T}\right)_{P,n} dT + \sum_i \left(\frac{\partial G}{\partial n_i}\right)_{T,P,n_j} dn_i \quad (\text{E-1})$$

From the definition of Gibbs free energy ($G = H - TS$), combining the first and second law yields the fundamental thermodynamic relationship for Gibbs energy:

$$dG = VdP - SdT + \sum_i \left(\frac{\partial G}{\partial n_i}\right)_{T,P,n_j} dn_i \quad (\text{E-2})$$

Rearranging the definition of Gibbs free energy ($G = H - TS$) for S :

$$dG = VdP + \frac{G}{T}dT - \frac{H}{T}dT + \sum_i \left(\frac{\partial G}{\partial n_i}\right)_{T,P,n_j} dn_i \quad (\text{E-3})$$

Writing G , V and H as $G^{ideal} + G^E$ etc. yields the same equation for excess properties:

$$dG^E = V^EdP + \frac{G^E}{T}dT - \frac{H^E}{T}dT + \sum_i \left(\frac{\partial G^E}{\partial n_i}\right)_{T,P,n_j} dn_i \quad (\text{E-4})$$

Dividing by nRT and rearranging:

$$\frac{d\bar{G}^E}{RT} - \frac{\bar{G}^E}{RT^2}dT = \frac{V^E}{RT}dP - \frac{H^E}{RT^2}dT + \sum_i \frac{1}{RT} \left(\frac{\partial G^E}{\partial n_i}\right)_{T,P} dx_i \quad (\text{E-5})$$

$$d\left(\frac{\bar{G}^E}{RT}\right) = \frac{V^E}{RT}dP - \frac{H^E}{RT^2}dT + \sum_i \frac{\bar{G}_i^E}{RT} dx_i \quad (\text{E-6})$$

From the definition of activity coefficient, $RT \ln \gamma_i = \bar{G}_i^E$:

$$d\left(\frac{\bar{G}^E}{RT}\right) = \frac{V^E}{RT}dP - \frac{H^E}{RT^2}dT + \sum_i \ln \gamma_i dx_i \quad (\text{E-7})$$

Hence:

$$\frac{\partial \left(\frac{\bar{G}^E}{RT}\right)}{\partial P} \frac{\partial}{\partial P} \left(\frac{\partial \ln \gamma_i}{\partial P}\right)_{T,x} = \frac{\bar{V}_i^E}{RT} \quad (\text{E-8})$$

$$\left(\frac{\partial \ln \gamma_i}{\partial T}\right)_{P,x} = -\frac{\bar{H}_i^E}{RT^2} \quad (\text{E-9})$$

E.2 Practical variation of activity coefficient with pressure

Excess volume data can be used to calculate the variation of activity coefficient with pressure, since:

$$\left(\frac{\partial \ln \gamma_i}{\partial P}\right)_{T,x} = \frac{\bar{V}_i^E}{RT} \quad (\text{E-10})$$

$$\therefore \frac{\gamma_i(P_B)}{\gamma_i(P_A)} = \exp \left[\frac{\bar{V}_i^E}{RT} (P_B - P_A) \right] \quad (\text{E-11})$$

The following empirical fit of excess volume data for *n*-butanol (1) and pentane (2) at 298.15 K was used to demonstrate the effect of pressure on activity coefficient (Sastry and Valand, 1998):

$$\underline{V}^E = x_1(1-x_1) \sum_{n=0}^3 a_n (2x_1 - 1)^n \quad (\text{E-12})$$

Where: $a_0 = -0.6179 \times 10^{-3} \text{ m}^3/\text{kmol}$; $a_1 = -0.1979 \times 10^{-3} \text{ m}^3/\text{kmol}$;

$a_2 = 1.525 \times 10^{-3} \text{ m}^3/\text{kmol}$; $a_3 = -1.7139 \times 10^{-3} \text{ m}^3/\text{kmol}$.

Partial molar excess volume for the binary mixture is therefore given by:

$$\bar{V}_1^E = \underline{V}^E + (1-x_1) \left(\frac{\partial \underline{V}^E}{\partial x_1} \right)_{T,P} \quad (\text{E-13})$$

$$\left(\frac{\partial \underline{V}^E}{\partial x_1} \right)_{T,P} = (1-2x_1) \sum_{n=0} a_n (2x_1 - 1)^n + x_1(1-x_1) \sum_{n=1} 2n \cdot a_n (2x_1 - 1)^{n-1} \quad (\text{E-14})$$

$$\therefore \bar{V}_1^E = (1-x_1) \left[(1-x_1) \sum_{n=0} a_n (2x_1 - 1)^n + 2x_1 \sum_{n=1} n \cdot a_n (2x_1 - 1)^{n-1} \right] \quad (\text{E-15})$$

Figure E-1 shows the difference between activity coefficients at one pressure versus another as a function of butanol composition for the butanol/pentane system at 25°C. As can be seen, even for a pressure change of 100 bar, the maximum error is only ~1%. Hence, the effect of pressure on activity coefficient has been ignored in this work.

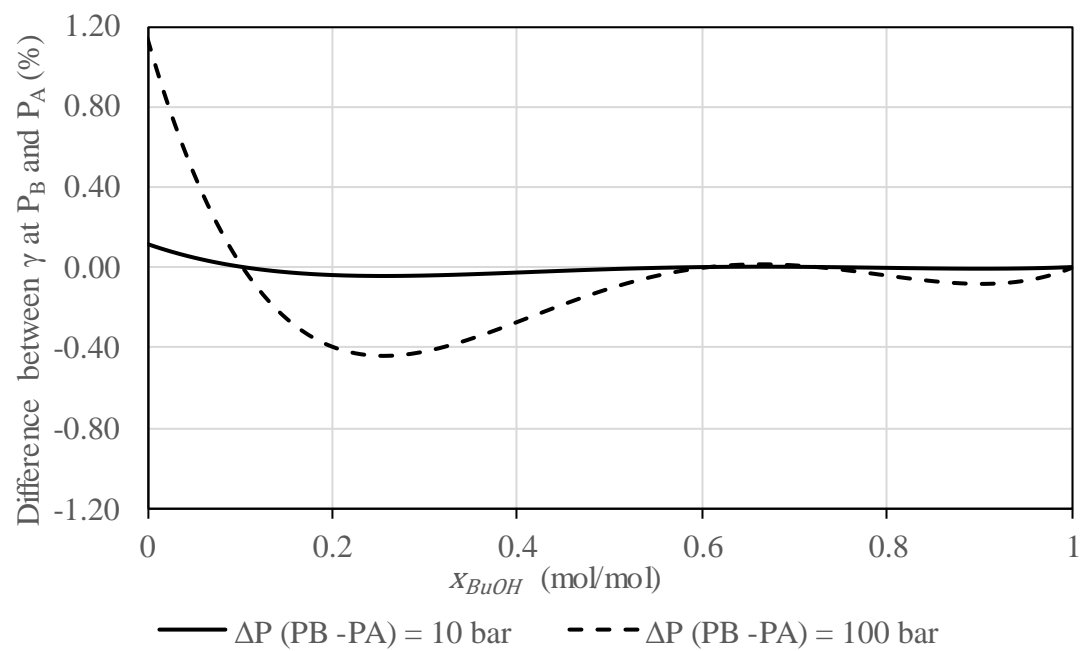


Figure E-1 – The negligible effect of pressure on activity co-efficient (butanol-pentane at 25°C)

APPENDIX F. LIMITING ACTIVITY COEFFICIENTS OF WATER AND ALCOHOLS AT INFINITE DILUTION

F.1 The Limiting Activity Coefficient of Alcohols at Infinite Dilution in Water

A thorough analysis of the limiting activity coefficients of alcohols at infinite dilution in water has been conducted by Dohnal *et al.* (2006) (*n*-butanol) and Fenclova *et al.* (2007) (*iso*-butanol) over the temperature range 273 - 373 K. The researchers compiled infinite dilution measurements of relevant alcohols in water available in the literature (activity coefficients γ_i^∞ , excess enthalpies $\bar{H}_i^{E,\infty}$, and excess heat capacities $\bar{C}_{p,i}^{E,\infty}$), and also recorded some experimental measurements of their own. An estimate of the standard error in each measurement was made and hence used to regress the available measurements into correlations for each alcohol in the form:

$$\ln \gamma_i^\infty = A + B \cdot \left(\frac{T_{ref}}{T} \right) + C \cdot \left(\frac{T_{ref}}{T} \right) \exp \left(D \frac{T}{T_{ref}} \right) \quad (\text{F-1})$$

$$\bar{H}_i^{E,\infty} = RT_{ref} \left[B - C \left(D \frac{T_{ref}}{T} - 1 \right) \exp \left(D \frac{T}{T_{ref}} \right) \right] \quad (\text{F-2})$$

$$\bar{C}_{p,i}^{E,\infty} = -RCD^2 \frac{T}{T_{ref}} \exp \left(D \frac{T}{T_{ref}} \right) \quad (\text{F-3})$$

where T is the temperature in Kelvin, in comparison to a reference temperature, T_{ref} , set at 298.15 K. The coefficients A, B, C and D are correlation parameters. The correlation assumed that excess heat capacity was an exponential function of temperature.

The objective function minimised during the regressions of Dohnal, Fenclova *et al.* was:

$$OF = \sum_{k=1}^{n_G} \frac{[\ln \gamma_{i,k}^\infty(\text{exp}) - \ln \gamma_{i,k}^\infty(\text{calc})]^2}{s^2(\ln \gamma_{i,k}^\infty(\text{exp}))} + \sum_{k=1}^{n_H} \frac{[\bar{H}_{i,k}^{E,\infty}(\text{exp}) - \bar{H}_{i,k}^{E,\infty}(\text{calc})]^2}{s^2(\bar{H}_{i,k}^{E,\infty}(\text{exp}))} + \sum_{k=1}^{n_C} \frac{[\bar{C}_{p,i,k}^{E,\infty}(\text{exp}) - \bar{C}_{p,i,k}^{E,\infty}(\text{calc})]^2}{s^2(\bar{C}_{p,i,k}^{E,\infty}(\text{exp}))} \quad (\text{F-4})$$

where n_G , n_H and n_C are the number of activity coefficient, partial excess enthalpy, and partial excess heat capacity measurements employed in the regression respectively, and s is the standard error in each individual measurement. The values of coefficients $A - D$ found by Dohnal, Fenclova *et al.* are given in Table F-1. In addition, Table F-1 details

the temperature for which the correlations predict a maximum value in γ_i^∞ . This is around 65°C for butanol isomers, and ~110°C for ethanol.

Table F-1 – Model parameters for the limiting activity coefficient of alcohols in water, and the temperature of the maximum limiting activity coefficient predicted by the correlations of Dohnal, Fenclova *et al.*

Alcohol	A	B	C	D	T _{max} (K)	Reference
Ethanol	-2.2437	-6.9054	-34.0965	2.3357	380.1	[1]
N-butanol	-3.7993	11.8850	-66.0410	-2.7677	337.6	[1]
Iso-butanol	-3.3156	11.0223	-65.1637	-2.8295	338.9	[2]

[1] = Dohnal *et al.* (2006); [2] = Fenclova *et al.* (2007)

F.2 The Limiting Activity Coefficient of Water at Infinite Dilution in Butanol Isomers

An analogous correlation to those of Dohnal, Fenclova *et al.* for the activity of water in butanols at infinite dilution was not available. Instead, a correlation was produced using a similar methodology to Dohnal *et al.* (2006).

Table F-2 contains the values of activity coefficients of water at infinite dilution in *n*- and *iso*-butanol found in the literature, along with estimates of the standard error in each value. Where values were obtained from sources listed in the compilation of Dohnal, Fenclova *et al.* for butanol in water, estimates of the standard error given in this compilation were used for these values. For other values, estimates of standard error were based on the type of measurement.

The range of values available for the activity coefficient of water in *n*-butanol were much less comprehensive than the compilation of activity coefficients by Dohnal, Fenclova *et al.* for water in *n*-butanol. Therefore, excess heat capacity was neglected. The following temperature dependence of the activity coefficient of water at infinite dilution in *n*-butanol was assumed:

$$\ln(\gamma_{H_2O}^\infty(T)) = \ln(\gamma_{H_2O}^\infty(T_{ref})) + \left(\frac{1}{T} - \frac{1}{T_{ref}}\right) \frac{\bar{H}_{H_2O}^\infty(T_{ref})}{R} \quad (\text{F-5})$$

where T is the temperature in Kelvin, in comparison to a reference temperature, T_{ref} (298.15 K). The partial molar excess enthalpy of water at infinite dilution in *n*-butanol at the reference temperature, $\bar{H}_{H_2O}^\infty(T_{ref})$, is determined by the regression.

Table F-2 – Limiting activity coefficients of water in butanol isomers at infinite dilution obtained in the literature, and corresponding estimates of standard error for a) *n*-butanol; b) *iso*-butanol

[1] = Fischer and Gmehling (1994); [2] = Lobien and Prausnitz (1982); [3] = Pierotti *et al.*, (1959); [4] = Tochigi and Kojima (1976); [5] = Wang *et al.* (1993). All values were also available from the compilation of Gmehling (2014b), from which erroneous sources (incorrect mixtures) were removed.

a) Water in *n*-butanol

Temperature <i>K</i>	$\ln(\gamma_{H_2O}^\infty)$	Measurement Method	$s(\ln(\gamma_{H_2O}^\infty))$	Ref.
298.15	1.34	Calculated from phase equilibria	0.2	[3]
308.20	1.69	GLC (with gas phase correction)	0.2	[5]
323.23	1.65	Static method	0.2	[1]
333.15	1.26	Calculated from phase equilibria	0.2	[3]
343.15	1.18	Ebulliometry	0.1	[1]
353.15	1.14	Ebulliometry	0.2	[2]
363.15	1.12	Ebulliometry	0.35	[2]
363.15	1.39	Ebulliometry	0.1	[4]
372.15	1.09	Ebulliometry	0.5	[2]
373.15	1.17	Calculated from phase equilibria	0.2	[3]
373.15	1.39	Ebulliometry	0.1	[4]
383.15	1.06	Ebulliometry	0.5	[2]

b) Water in *iso*-butanol

Temperature	$\ln(\gamma_{H_2O}^\infty)$	Measurement Method	$s(\ln(\gamma_{H_2O}^\infty))$	Ref.
<i>K</i>				
323.23	1.65	Static method	0.2	[1]

The literature values for the activity coefficient of water in *n*-butanol at infinite dilution, detailed in Table F-2, were regressed to produce a correlation in the form of eq. (F-5). The same objective function as in Dohnal, Fenclova *et al.* (eq. (F-4)) was employed:

$$OF = \sum_{k=1}^{n_G} \frac{[\ln \gamma_{i,k}^{\infty}(\text{exp}) - \ln \gamma_{i,k}^{\infty}(\text{calc})]^2}{s^2(\ln \gamma_{i,k}^{\infty}(\text{exp}))} \quad (\text{F-6})$$

Figure F-1 shows the resultant correlation predictions for the limiting activity coefficient of water in *n*-butanol at infinite dilution as a function of temperature, in comparison to values found in the literature (detailed in Table F-2). As shown, the activity coefficient decreases slightly with temperature and the model predicts most of the values in Table F-2 within standard error.

Table F-3 details the parameters resulting from the regression for the limiting activity coefficient of water in butanols. Only one value of the activity coefficient of water at infinite dilution in *iso*-butanol was identified, and so no temperature dependence could be established for the activity coefficient of water in *iso*-butanol. Therefore, in the absence of further measurements, a constant value was employed.

Table F-3 – Model parameters for limiting activity coefficient of water in butanols in water, and the temperature of the minimum limiting activity coefficient predicted by the correlation

Alcohol	$\ln(\gamma_{H2O}^{\infty}(T_{ref}))$	$\frac{\bar{H}_{H2O}^{\infty}(T_{ref})}{RT_{ref}}$	T_{ref} (K)	T_{max} (K)
<i>N</i> -butanol	1.4458	0.7944	298.15	347.8
<i>Iso</i> -butanol	1.6500	0	298.15	-

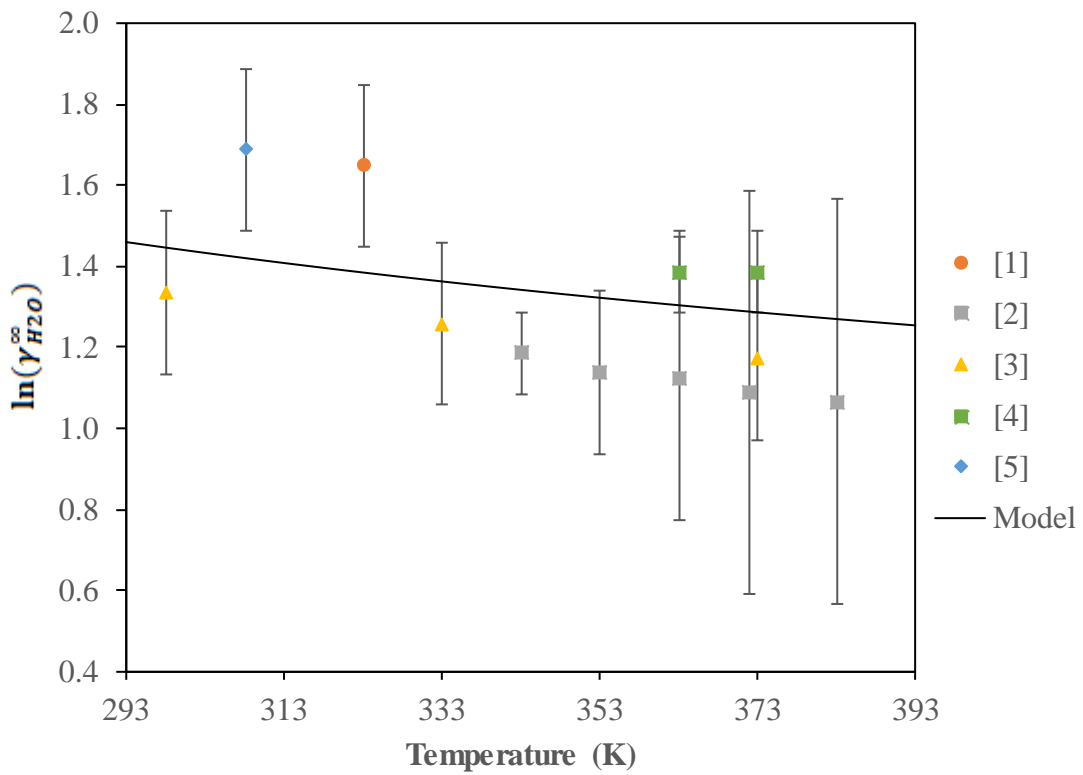


Figure F-1: Limiting activity coefficients of water in *n*-butanol at infinite dilution predicted by the correlation *versus* values used in the regression of the correlation

[1] = Fischer and Gmehling (1994); [2] = Lobien and Prausnitz (1982); [3] = Pierotti *et al.*, (1959); [4] = Tochigi and Kojima (1976); [5] = Wang *et al.* (1993).

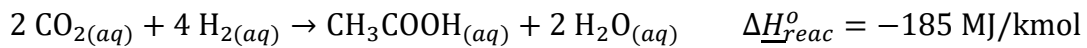
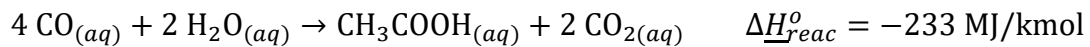
APPENDIX G. LOW-GRADE HEAT PRODUCED BY FERMENTATION

As heats of fermentation were not readily available for butanol production by fermentation, they were estimated by an analysis of the processes occurring in the fermenter.

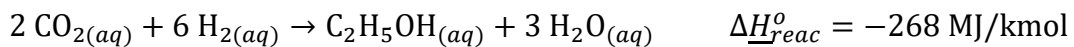
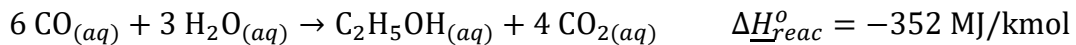
G.1 Fermentation of Synthesis Gases

Fermentation of CO, or CO₂ and H₂, by acetogenic organisms comprises the following reactions and corresponding reaction enthalpies (calculated by employing enthalpies of formation obtained from Poling *et al.* (2001)):

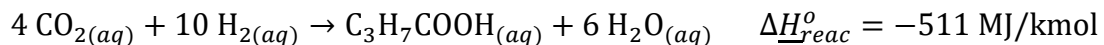
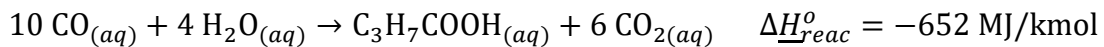
Acetic Acid



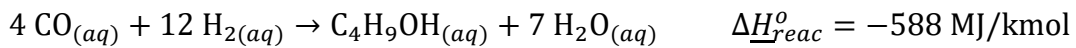
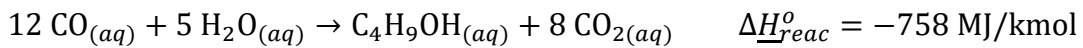
Ethanol



Butyric Acid

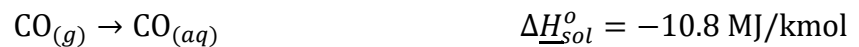


Butanol



The substrates, CO, and H₂ and CO₂, were assumed to be supplied to the fermenter in gaseous form. Any CO₂ produced was also assumed to be removed from the fermenter in gaseous form. In practice, depending on the system, some CO₂ would be removed from the fermenter in aqueous form, along with some inert gases in the feed (*e.g.* N₂). Conversely, some water and other products would be removed in the off-gas from the fermenter. These effects were ignored.

The enthalpy of solution from the gaseous to aqueous phase for CO, CO₂ and H₂ was obtained from Sander (2015) by relating the enthalpy of solution to the gradient of Henry's Constant with respect to temperature:



Assuming a molar ratio of products of 1 : 0.333 : 0.3 : 0.75 for butanol : ethanol : butyric acid : acetic acid (Section A.3), the product reactions were combined to yield an enthalpy of reaction of 17 and 13 MJ/kg butanol using CO and H₂ as substrates respectively. Similarly, -0.5 and 3 MJ/kg butanol of heat released by the dissolution and evaporation of gaseous reactants and products was calculated using the same product ratios. Therefore, the fermentation of synthesis gases yielded around 16 MJ/kg butanol *via* either substrate.

The organism uses the energy released by the oxidation of CO and H₂ to generate ATP for use in other processes. Bertsch and Müller (2015) conducted a thorough analysis of the Wood-Ljungdahl pathway for the biochemical conversion of CO and H₂ into acids and alcohols, and determined the theoretical ATP production for each of these products *via* each substrate. Using the same molar product ratio as above, the ATP production outlined by Bertsch and Müller (2015) equated to 6 – 7.4 moles of ATP generated per mole of butanol *via* fermentation of CO, and -0.1 – 1.2 moles of ATP per mole of butanol *via* fermentation of H₂. There was a range of values for ATP generation as the ATP generated by the production of butanol and butyric acid depends on the energy-conservation mechanisms of some steps in the pathway. These mechanisms vary with the specific organism. The enthalpy of reaction for conversion of ADP to ATP is around 31 MJ/kmol, depending on the conditions (Hammes and Hammes-Schiffer, 2015). Therefore, up to 3 or 0.5 MJ/kg butanol of the enthalpy of reaction is effectively adsorbed by the organism into the carrier ATP during the synthesis of products from CO and H₂ respectively. This reduces the heat released during product formation, resulting in a release of 13 or 16 MJ/kg butanol of heat during product synthesis from CO or H₂ respectively.

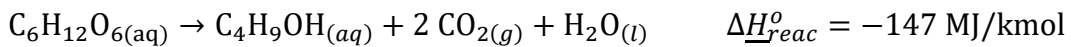
The ATP production during fermentation equates to an energy efficiency of 15 - 20% for CO routes, and up to 5% for H₂ routes. The ATP produced would be utilised by the cell for cell growth or maintenance. These processes would probably release much of the

energy stored in the ATP as heat, especially given the low energy efficiencies highlighted. However, working on a conservative basis, the effect of this heat release was ignored.

Finally, in a stirred tank reactor, a significant amount of power would be required to dissolve the relatively insoluble CO and H₂ substrates. Working with a rule-of-thumb of 2 kW/m³ of stirrer power, and a productivity of butanol of 1 kg/m³/h, this would result in around 7 MJ/kg butanol of heat being dissipated by the stirrer. Productivities of up to 1.8 kg/m³/h have been recorded for continuous ABE fermentations (Green, 2011), although this is far higher than typical productivities which are usually less than around 1 kg ABE/m³/h (Outram *et al.*, 2017). Given that such productivities are for a mature, liquid-substrate based process, it is unlikely that butanol production from the fermentation of synthesis gases (a relatively immature process) would exceed productivities of 1 kg/m³/h. Lower productivities would require larger fermenter volumes, resulting in higher stirrer powers. Equally, large fermenter volumes would increase the motivation to design fermenters with lower power requirements. Using this rough estimate of stirrer power, it is probable that the fermenter for the fermentation of synthesis gases to butanol would produce in excess of **20 MJ/kg butanol of heat**.

G.2 *Iso*-Butanol Fermentation

Iso-butanol is produced by fermentation from glucose *via* following reaction (Feldman *et al.*, 2013):



In order to calculate the enthalpy of reaction, a value of -1271.1 MJ/kmol was obtained for the enthalpy of formation of solid α -glucose from NIST (2016). An enthalpy of solution for glucose of + 11 MJ/kmol was assumed (Taylor and Rowlinson, 1955). The remaining enthalpies of formation were taken from Poling *et al.* (2001). These values yielded a heat of fermentation of ~2 MJ/kg butanol. Two moles of ATP are generated in the synthesis of *iso*-butanol from glucose (Feldman *et al.*, 2013). Using the same analysis as for the fermentation of synthesis gases, the generation of ATP would require ~0.8 MJ/kg butanol of the enthalpy of reaction; this equates to an efficiency of ~40%. Some stirring would be required in the fermenter, although the power demand of the stirrer would be small given that the substrates would be in aqueous form.

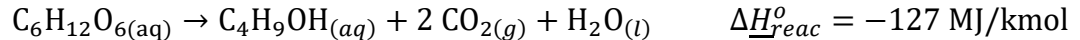
G.3 ABE Fermentation

ABE fermentations comprise the following reactions for the synthesis of products from glucose (Tao et al., 2014a):

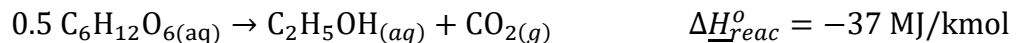
Acetone



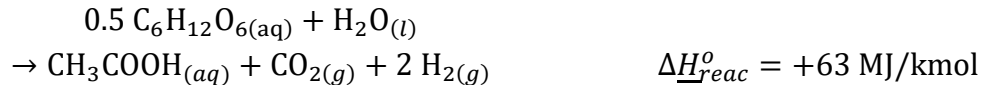
N-Butanol



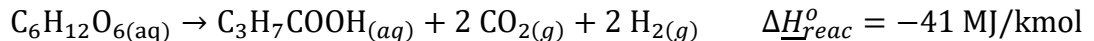
Ethanol



Acetic Acid



Butyric Acid



In order to calculate the enthalpies of reaction, the same values for the enthalpy of formation, and of solution for glucose, were employed as for the analysis of *iso*-butanol fermentation. Assuming a molar product ratio of 0.5 : 1 : 0.1667 : 0.0463 : 0.0926 for acetone : butanol : ethanol : butyric acid : acetic acid (Section A.3), combining the above reactions yielded a heat of fermentation of ~1.0 MJ/kg butanol produced.

Nomenclature: Symbols, Abbreviations and Acronyms

Symbol	Units	Description
Latin		
A_k, B_k, C_k	-	Legendre Activity model coefficients (k -th)
B	kg	Mass of butanol
B_{ij}, B_{i-j}	m^3/kmol	Second virial Coefficient of species i and j
C_p	$\text{J}/\text{kmol}/\text{K}$	Heat capacity at constant pressure $\left(= \left(\frac{\partial H}{\partial T} \right)_P \right)$
C_v	$\text{J}/\text{kmol}/\text{K}$	Heat capacity at constant volume $\left(= \left(\frac{\partial U}{\partial T} \right)_V \right)$
c	kmol/m^3	Concentration
D_i^{molar}	mol/mol	Molar distribution coefficient of species i
$D_i^{\infty,molar}$	mol/mol	Molar distribution coefficient at infinite dilution of species i
D_i^{mass}	kg/kg	Mass distribution coefficient of species i
$D_i^{\infty, mass}$	mol/mol	Mass distribution coefficient at infinite dilution of species i
$E_{(X)}$	MJ/kg	Energy required for (X)
G	J	Gibbs Free Energy
g	m/s^2	Acceleration due to gravity
g^E	$\text{J}/\text{kmol}/\text{K}$	Specific excess Gibbs free energy $\left(= G^E / RT \right)$
H	J	Enthalpy
ΔH_i^{vap}	J	Enthalpy change of vaporization of species i
Mr	kg/kmol	Molar Mass

Symbol	Units	Description
m_i	kg/kg	Mass fraction of species i
N	kmol	Total number of moles ($= \Sigma N_i$)
N_i	kmol	Number of moles of species i
n	kmol/s	Total molar flowrate ($= \Sigma n_i$)
n_i	kmol/s	Molar flowrate of species i
OF	-	Objective Function
P	Pa	Pressure
P_i^{sat}	Pa	Pure vapour Pressure of species i
p_i	Pa	Partial pressure of species i
R	J/kmol/K	Universal Gas Constant ($= 8314.5 \text{ J/kmol/K}$)
R_{DC}	-	Reflux Ratio of distillation column DC
R_{min}^{DC}	-	Minimum Reflux Ratio (of distillation column DC)
S	kg	Mass of solvent
$S_{i,j}$	-	Selectivity of species i over species j (in LLX)
T	K	Temperature
U	J	Internal energy
V	m^3	Volume
W	kg	Mass of water
x_i	mol/mol	Liquid mole fraction of species i
y_i	mol/mol	Vapour mole fraction of species i
z_i	mol/mol	Overall (vapour + liquid) mole fraction of species i

Symbol	Units	Description
Greek		
$\alpha_{i,j}$	-	Relative volatility of species i <i>versus</i> species j
β	-	Extraction efficiency (in LLX)
γ_i	-	Activity co-efficient of species i
γ_i^∞	-	Limiting activity co-efficient at infinite dilution of species i
Δx	-	Change in quantity x
ϵ	-	Short-hand parameter (defined during use)
η	-	Transfer efficiency (in LLX)
μ_i	-	Chemical Potential of species i ($= \overline{G}_i$)
ρ	kg/m ³	Mass density
ρ_m	kg/kmol	Molar density
ϕ_i	-	Fugacity coefficient of species i
ϕ_i^{sat}	-	Fugacity coefficient of pure species i at saturation
ψ	-	Gilliland correlation parameter
ψ	-	Vapour fraction (mole basis)
ψ_i	-	Fraction of moles of species i in vapour phase
ω	-	Acentricity factor
Scripts		
\mathcal{H}_i^I	kmol/m ³ /Pa	Henry's Law Constant of species i in phase I
\mathcal{M}	-	Ratio of gradient dP/dx at $x = 0$ relative to gradient for Raoult's Law

Symbol	Units	Description
Accents		
\underline{a}	/kmol	Molar quantity
\hat{a}	/kg	Specific quantity
\overline{a}	/kmol	Partial molar quantity
Subscripts		
$a_i, a_j \dots$		Species i , species j ...
a_{Ace}		Species = acetone
a_{Bu}, a_{BuOH}		Species = <i>n</i> -butanol
a_{bot}		In bottoms product of distillation column
a_c		Critical quantity (<i>e.g.</i> critical temperature T_c)
a_{calc}		Calculated value (from model)
a_{cond}		In the condenser
a_{Et}, a_{EtOH}		Species = ethanol
a_{exp}		Experimental (measured) value
a_{ferm}		In the fermenter
a_{HC}		Species = hydrocarbon
a_{iBu}, a_{iBuOH}		Species = <i>iso</i> -butanol
a_{reboil}		In the reboiler
a_{top}		In tops product (distillate) of distillation column

Symbol	Units	Description
Superscripts		
a^{aq}		In the aqueous phase
a^{cell}		Quantity of the equilibrium cell
a^E		Excess quantity
a^L		Quantity of the liquid phase
a^{max}		Maximum quantity
a^{min}		Minimum quantity
a^{org}		In the organic phase
a^{sat}		Saturated (at VLE)
a^{sol}		At the solubility limit
a^V		Quantity of the vapour phase
a^{vap}		Of vaporisation
a_i^∞		At infinite dilution of species i
Abbreviations		
AA		Acetic Acid
ABE		Acetone-Butanol-Ethanol (fermentation)
Ace		Acetone
BA		Butyric Acid
Bu, BuOH		(<i>N</i>)-Butanol
DC		Distillation Column System
DC1		Distillation Column 1
DC2		Distillation Column 2
EoS		Equation of State (of the vapour phase)
Et, EtOH		Ethanol

Symbol	Units	Description
HC		Hydrocarbon
i, i-		<i>Iso-</i>
iBu, iBuOH		<i>Iso</i> -Butanol
IBE		<i>Iso</i> -propanol-Butanol-Ethanol (fermentation)
IGL		Ideal Gas Law
LLE		Liquid-Liquid Equilibrium
LLX		Liquid-Liquid Extraction
NRTL		Non-Random Two-Liquid activity model
SRK		Soave-Redlich-Kwong (equation of state)
VLE		Vapour-Liquid Equilibrium
VLLE		Vapour-Liquid-Liquid Equilibrium

References

- 110th United States Congress, 2007. Energy Independence and Security Act of 2007. Washington, WA, USA.
- Aguilar, F., Alaoui, F.E.M., Segovia, J.J., Villamanan, M.A., Montero, E.A., 2012. Ether + alcohol + hydrocarbon mixtures in fuels and bio-fuels: Excess enthalpies of binary mixtures containing dibutyl ether (DBE) or 1-butanol and 1-hexene or methylcyclohexane or toluene or cyclohexane or 2 , 2 , 4-trimethylpentane at 298.15 K and 313.1. *Fluid Phase Equilib.* 315, 1–8. <https://doi.org/10.1016/j.fluid.2011.11.005>
- Atsumi, S., Hanai, T., Liao, J.C., 2008. Non-fermentative pathways for synthesis of branched-chain higher alcohols as biofuels. *Nature* 451, 86–89. <https://doi.org/10.1038/nature06450>
- Baez, A., Cho, K.M., Liao, J.C., 2011. High-flux isobutanol production using engineered *Escherichia coli*: A bioreactor study with in situ product removal. *Appl. Microbiol. Biotechnol.* 90, 1681–1690. <https://doi.org/10.1007/s00253-011-3173-y>
- Belousov, V.P., Sokolova, E.P., 1966. Mischungswärme der Flüssigkeiten. IV. Mischungswärme in binären Systemen Aceton-Wasser, Methylethylketon-Wasser und Cyclohexan-Wasser. *Vestn.Leningr.Univ.Fiz.Khim.* 16, 90–93.
- Berro, C., Rogalski, M., Peneloux, A., 1982. Excess Gibbs Energies and Excess Volumes of 1-Butano-n-Hexane and 2-Methyl-1-propanol-n-Hexane Binary Systems. *J. Chem. Eng. Data* 27, 352–355.
- Bertsch, J., Müller, V., 2015. Bioenergetic constraints for conversion of syngas to biofuels in acetogenic bacteria. *Biotechnol. Biofuels* 8, 1–12. <https://doi.org/10.1186/s13068-015-0393-x>
- Black, C., Joris, G.G., Taylor, H.S., 1948. The solubility of water in hydrocarbons. *J. Chem. Phys.* 16, 537–543. <https://doi.org/10.1063/1.1746932>
- Blahušiak, M., Marták, J., Miranda, F., Schlosser, Š., Teixeira, J., 2013. Effect of viscosity of a liquid membrane containing oleyl alcohol on the pertraction of butyric acid. *Chem. Pap.* 67, 1560–1568. <https://doi.org/10.2478/s11696-013-0370-4>

- Brown, I., Fock, W., Smith, F., 1964. Heats of Mixing. V. Systems of n-Alcohols with n-Hexane. *Aust. J. Chem.* 17, 1106–1118.
- Brown, T.F., 1948. Distribution in Hydrocarbon Solvent Systems. *Ind. Eng. Chem.* 40, 103–106. <https://doi.org/10.1021/ie50457a030>
- Butamax Advanced Biofuels LLC, 2014. Butamax and Highwater Ethanol Complete Phase 1 of Biobutanol Retrofit Project Including Installation of Novel Corn Oil Separation Technology [WWW Document]. URL http://www.butamax.com/Portals/0/pdf/2_ButamaxandHighwaterEthanolCompletePhase1ofBiobutanolRetrofitProject.pdf (accessed 5.26.15).
- Campbell, S.W., Wilsak, R.A., Thodos, G., 1987. (Vapor + liquid) equilibrium behavior of (n-pentane + ethanol) at 372.7, 397.7, and 422.6 K. *J. Chem. Thermodyn.* 19, 449–460. [https://doi.org/10.1016/0021-9614\(87\)90142-X](https://doi.org/10.1016/0021-9614(87)90142-X)
- Cárdenas, H., Cartes, M., Mejía, A., 2015. Atmospheric densities and interfacial tensions for 1-alkanol (1-butanol to 1-octanol)+water and ether (MTBE, ETBE, DIPE, TAME and THP)+water demixed mixtures. *Fluid Phase Equilib.* 396, 88–97. <https://doi.org/10.1016/j.fluid.2015.03.040>
- Chaudhry, M.M., Van Ness, H.C., Abbott, M.M., 1980. Excess Thermodynamic Functions for Ternary Systems. 6. Total-Pressure Data and GE for Acetone-Ethanol-Water at 50°C. *J. Chem. Eng. Data* 25, 254–257.
- Collins, S.G., Christensen, J.J., Izatt, R.M., Hanks, R.W., 1980. The excess enthalpies of 10 (n-pentane + an n-alkanol) mixtures at 298.15 K. *J. Chem. Thermodyn.* 12, 609–614.
- Dadgar, A.M., Foutch, G.L., 1986. Dadgar & Foutch PDF.pdf, in: Scott, C.D. (Ed.), Proceedings of the Seventh Symposium on Biotechnology for Fuels and Chemicals. pp. 611–620.
- Daniell, J., Köpke, M., Simpson, S., 2012. Commercial Biomass Syngas Fermentation, Energies. <https://doi.org/10.3390/en5125372>
- Datta, R., Reeves, A., 2014. Syntrophic Co-culture of Anaerobic Microorganism for Production of n-Butanol from Syngas. US 2014/0206066. <https://doi.org/US2010/0311130 A1>
- Deak, A., Victorov, A.I., de Loos, T.W., 1995. High pressure VLE in alkanol + alkane mixtures. Experimental results for n-butane + ethanol, + 1-propanol, + 1-butanol

- systems and calculations with three EOS methods. *Fluid Phase Equilib.* 107, 277–301.
- Dell'Era, C., Zaytseva, A., Uusi-kyyny, P., Pokki, J., Pakkanen, M., Aittamaa, J., 2007. Vapour–liquid equilibrium for the systems butane + methanol, + 2-propanol, +1-butanol, +2-butanol, +2-methyl-2-propanol at 364.5 K. *Fluid Phase Equilib.* 254, 49–59. <https://doi.org/10.1016/j.fluid.2007.02.028>
- Dohnal, V., Fenclová, D., Vrbka, P., 2006. Temperature Dependences of Limiting Activity Coefficients, Henry's Law Constants, and Derivative Infinite Dilution Properties of Lower (C1–C5) 1-Alkanols in Water. Critical Compilation, Correlation, and Recommended Data. *J. Phys. Chem. Ref. Data* 35, 1621–1651. <https://doi.org/10.1063/1.2203355>
- Dürre, P., 2016. Butanol formation from gaseous substrates. *FEMS Microbiol. Lett.* 363, 1–7. <https://doi.org/10.1093/femsle/fnw040>
- Dürre, P., 2011a. Fermentative production of butanol—the academic perspective. *Curr. Opin. Biotechnol.* 22, 331–336. <https://doi.org/10.1016/j.copbio.2011.04.010>
- Dürre, P., 2011b. Fermentative production of butanol—the academic perspective. *Curr. Opin. Biotechnol.* 22, 331–336. <https://doi.org/10.1016/j.copbio.2011.04.010>
- Ellis, S.R.M., Garbett, R.D., 1960. A New Equilibrium Still for the Study of Partially Miscible Systems. *Ind. Eng. Chem.* 52, 385–388.
- European Biofuels Technology Platform, 2014. Biobutanol [WWW Document]. URL <http://www.biofuelstp.eu/butanol.html> (accessed 1.9.15).
- Evanko, W.A., Eyal, A.M., Glassner, D.A., Maio, F., Aristidou, A.A., Evans, K., Gruber, P.R., Hawkins, A.C., Meinhold, P., Feldman, R.M.R., Gunawardena, U., Urano, J., 2013. Recovery of higher alcohols from dilute aqueous solutions. US 8,614,077 B2.
- Ezeji, T.C., Qureshi, N., Blaschek, H.P., 2007. Bioproduction of butanol from biomass: from genes to bioreactors. *Curr. Opin. Biotechnol.* 18, 220–7. <https://doi.org/10.1016/j.copbio.2007.04.002>
- Feldman, R.M.R., Gunawardena, U., Urano, J., Meinhold, P., Aristidou, A., Dundon, C.A., Smtih, C., 2013. US 8,455,239 B2 Yeast Organism Producing Isobutanol at a high yield. US 8,455,239 B2.
- Fenclova, D., Dohnal, P., Vrbka, P., Lastovka, V., 2007. Temperature Dependence of

- Limiting Activity Coefficients, Henry's Law Constants, and Related Infinite Dilution Properties of Branched (C3 and C4) Alkanols in Water. Measurement, Critical Compilation, Correlation, and Recommended Data. *J. Chem. Eng. Data* 52, 989–1002. <https://doi.org/10.1021/je600567z>
- Fischer, K., Gmehling, J., 1994. P-x and Infinite Dilution Activity Coefficient Data for the Different Binary Butanol-Water Systems at 50°C. *J. Chem. Eng. Data* 39, 309–315.
- Gaddy, J.L., Arora, D.K., Ko, C.-W., Phillips, J.R., Basu, R., Wikstrom, C. V., Clausen, E.C., 2007. United States Patent Date of Patent : US 7,285,402 B2.
- Ghellai, S., Belabbaci, A., Villamanan, R.M., Carmen Martin, M., Villamanan, M.A., Negadi, L., 2013. Vapour – liquid equilibria of binary and ternary mixtures containing 1-butanol, 2,2,4-trimethylpentane and 1-hexene at T = 313.15 K. *J. Chem. Thermodyn.* 63, 164–168. <https://doi.org/10.1016/j.jct.2013.04.003>
- Gmehling, J. (Ed.), 2014a. 1-Butanol-Water Azeotropic Data: Datasheet from “Dortmund Data Bank (DDB) – Thermophysical Properties Edition 2014” in SpringerMaterials (http://materials.springer.com/thermophysical/docs/azd_c39c174).
- Gmehling, J., 2014b. Water-1-Butanol Activity Coefficients at Infinite Dilution: Datasheet from “Dortmund Data Bank (DDB) – Thermophysical Properties Edition 2014” in SpringerMaterials (https://materials.springer.com/thermophysical/docs/act_c174c39).
- Gomis, V., Font, A., Pedraza, R., Saquete, M.D., 2007. Isobaric vapor-liquid and vapor-liquid-liquid equilibrium data for the water-ethanol-hexane system. *Fluid Phase Equilib.* 259, 66–70. <https://doi.org/10.1016/j.fluid.2007.04.011>
- Gomis, V., Font, A., Saquete, M.D., García-Cano, J., 2012. LLE, VLE and VLLE data for the water-n-butanol-n-hexane system at atmospheric pressure. *Fluid Phase Equilib.* 316, 135–140. <https://doi.org/10.1016/j.fluid.2011.11.025>
- González-Peñas, H., Lu-Chau, T.A., Moreira, M.T., Lema, J.M., 2014. Solvent screening methodology for in situ ABE extractive fermentation. *Appl. Microbiol. Biotechnol.* 98, 5915–5924. <https://doi.org/10.1007/s00253-014-5634-6>
- Góral, M., Mączyński, A., Wiśniewska-Gocłowska, B., 2004. Recommended liquid-liquid equilibrium data. Part 2. Unsaturated hydrocarbon-water systems. *J. Phys. Chem. Ref. Data* 33, 579–591. <https://doi.org/10.1063/1.1647146>

References

- Gracia, M., Sanchez, F., Perez, P., Valero, J., Gutierrez Losa, C., 1992. Vapour pressures of (butan-1-ol + hexane) at temperatures between 283.10 K and 323.12 K. *J. Chem. Thermodyn.* 24, 463–471.
- Green, D.W., 1997. Perry's Chemical Engineers' Handbook, 7th ed. McGraw-Hill, New York.
- Green, E.M., 2011. Fermentative production of butanol--the industrial perspective. *Curr. Opin. Biotechnol.* 22, 337–43. <https://doi.org/10.1016/j.copbio.2011.02.004>
- Grethlein, A.J., Worden, R.M., Jain, M.K., Datta, R., 1990. Continuous production of mixed alcohols and acids from carbon monoxide. *Appl. Biochem. Biotechnol.* 24–25, 875–884. <https://doi.org/10.1007/BF02920301>
- Grethlein, A.J., Worden, R.M., Jain, M.K., Datta, R., 1991. Evidence for production of n-butanol from carbon monoxide by *Butyribacterium methylotrophicum*. *J. Ferment. Bioeng.* 72, 58–60. [https://doi.org/10.1016/0922-338X\(91\)90147-9](https://doi.org/10.1016/0922-338X(91)90147-9)
- Griswold, J., Wong, S.Y., 1952. No Title. *Chem. Eng. Progr. Symp. Ser.* 48, 18–34.
- Groot, W.J., Soedjak, H.S., Donck, P.B., van der Lans, R.G.J.M., Luyben, K.C.A.M., Timmer, J.M.K., 1990. Butanol recovery from fermentations by liquid-liquid extraction and membrane solvent extraction. *Bioprocess Eng.* 5, 203–216. <https://doi.org/10.1007/BF00376227>
- Guerrero, H., Giner, I., Artigas, H., Lafuente, C., Gascon, I., 2010. Isothermal Vapor-Liquid Equilibrium of Ternary Mixtures Containing 2-Methyl-1-propanol or 2-Methyl-2-propanol, n-Hexane, and 1-Chlorobutane at 298.15 K. *J. Chem. Eng. Data* 55, 739–744. <https://doi.org/10.1021/je900436f>
- Ha, S.H., Mai, N.L., Koo, Y.M., 2010. Butanol recovery from aqueous solution into ionic liquids by liquid-liquid extraction. *Process Biochem.* 45, 1899–1903. <https://doi.org/10.1016/j.procbio.2010.03.030>
- Hahn, H.-D., Dämbkes, G., Rupprich, N., Bahl, H., Frey, G.D., 2013. Butanols, in: Ullmann's Encyclopedia of Industrial Chemistry. American Cancer Society. https://doi.org/10.1002/14356007.a04_463.pub3
- Hammes, G.G., Hammes-Schiffer, S., 2015. Physical Chemistry for the Biological Sciences, 2nd ed. Wiley, Hoboken, New Jersey.
- Hibbard, R.R., Schalla, R.L., 1952. Research memorandum - Solubility of Water in

Hydrocarbons, National Advisory Committee For Aeronautics. Washington, WA, USA.

Hodgson, P.J., Dennis, J.S., 2017. No Title. PCT/GB2018/000057.

Holderbaum, T., Utzig, A., Gmehling, J., 1991. Vapour-liquid equilibria for the system butane/ethanol at 25.3, 50.6 and 72.5°C. *Fluid Phase Equilib.* 63, 219–226. [https://doi.org/10.1016/0378-3812\(91\)80032-Q](https://doi.org/10.1016/0378-3812(91)80032-Q)

Huang, H.J., Ramaswamy, S., Liu, Y., 2014. Separation and purification of biobutanol during bioconversion of biomass. *Sep. Purif. Technol.* 132, 513–540. <https://doi.org/10.1016/j.seppur.2014.06.013>

Humbird, D., Davis, R.E., Tao, L., Kinchin, C.M., Hsu, D.D., Aden, A., Schoen, P., Lukas, J., Olthof, B., Worley, M., Sexton, D., Dudgeon, D., 2011. Process Design and Economics for Biochemical Conversion of Lignocellulosic Biomass to Ethanol, NREL Technical Report. <https://doi.org/10.2172/1013269>

Ishii, N., 1935. Studies on Volatility of Fuels Containing Ethyl Alcohol V-VI. *J. Soc. Chem. Ind. Jap.* 38, 659.

Islam, A., Kabadi, V., 2011. Universal liquid mixture model for vapor-liquid and liquid-liquid equilibria in hexane-butanol-water system over the temperature range 10 - 100 °C. *Chem. Process Eng.* 32, 101–115. <https://doi.org/10.2478/v10176-011-0009-3>

Islam, A.W., Javvadi, A., Kabadi, V.N., 2011. Universal Liquid Mixture Models for Vapor-Liquid and Liquid-Liquid Equilibria in the Hexane-Butanol-Water System. *Ind. Eng. Chem. Res.* 50, 1034–1045.

Islam, A.W., Kabadi, V., 2009. Models for Infinite Dilution Activity Coefficients in Ternary Liquid Systems, in: Nzewi, E., Reddy, G., Luster-Teasley, S., Kabadi, V., Chang, S.-Y., Schimmel, K., Uzochukwu, G. (Eds.), *Proceedings of the 2007 National Conference on Environmental Science and Technology*. Springer, New York, pp. 311–317. <https://doi.org/10.1007/978-0-387-88483-7>

Islam, A.W., Rahman, M.H., 2012. A review of Barker's activity coefficient method and VLE data reduction. *J. Chem. Thermodyn.* 44, 31–37. <https://doi.org/10.1016/j.jct.2011.08.013>

Jin, F., Zhang, X., Hua, D., Xu, H., Li, Y., Mu, H., 2017. Study on the in-situ coupling process of fermentation, extraction and distillation for biobutanol production: process analysis, in: IOP Conference Series: Earth and Environmental Science.

<https://doi.org/10.1088/1755-1315/5>

Kantzow, C., Mayer, A., Weuster-Botz, D., 2015. Continuous gas fermentation by Acetobacterium woodii in a submerged membrane reactor with full cell retention. *J. Biotechnol.* 212, 11–18. <https://doi.org/10.1016/j.jbiotec.2015.07.020>

Kemp, I.C., 2006. Pinch Analysis and Process Integration: A User Guide on Process Integration for the Efficient Use of Energy, 2nd Editio. ed. Butterworth-Heinemann. <https://doi.org/10.1016/B978-0-7506-8260-2.X5001-9>

Kim, J.K., Iannotti, E.L., Bajpai, R., 1999. Extractive recovery of products from fermentation broths. *Biotechnol. Bioprocess Eng.* 4, 1–11. <https://doi.org/10.1007/BF02931905>

Köpke, M., Mihalcea, C., Liew, F., Tizard, J.H., Ali, M.S., Conolly, J.J., Al-Sinawi, B., Simpson, S.D., 2011a. 2,3-Butanediol Production By Acetogenic Bacteria, an Alternative Route To Chemical Synthesis, Using Industrial Waste Gas. *Appl. Environ. Microbiol.* 77, 5467–75. <https://doi.org/10.1128/AEM.00355-11>

Köpke, M., Noack, S., Dürre, P., 2011b. The Past, Present, and Future of Biofuels – Biobutanol as Promising Alternative, in: Bernardes, M.A.D.S. (Ed.), *Biofuel Production - Recent Developments and Prospects*. InTech, Rijeka, pp. 451–486. <https://doi.org/10.5772/20113>

Kraemer, K., Harwardt, A., Bronneberg, R., Marquardt, W., 2010. Separation of butanol from acetone-butanol- ethanol fermentation by a hybrid extraction- distillation process. *Comput. Chem. Eng.* 35, 949–963. <https://doi.org/10.1016/j.compchemeng.2011.01.028>

Kuitunen, S., Uusi-kyyny, P., Pokki, J., Pakkanen, M., Alopaeus, V., 2008. Vapor-Liquid Equilibrium for 1-Butanol + 1-Butene at (318.4 and 364.5) K and Vapor-Liquid Equilibrium of 1-Butanol + 2-Methylpropane, + n-Butane and 1-Butene + 2-Methylpropane at 318.4 K. *J. Chem. Eng. Data* 53, 2454–2461. <https://doi.org/10.1021/je8004672>

Kurkijärvi, A.J., Lehtonen, J., 2014. Dual extraction process for the utilization of an acetone-butanol-ethanol mixture in gasoline. *Ind. Eng. Chem. Res.* 53, 12379–12386. <https://doi.org/10.1021/ie500131x>

Kuschel, F., Kraetsch, H., Kehlen, H., Sackmann, H., 1977. Vapor-Liquid Equilibria. *AIChE J.* 23, 205–207.

- Lane, J., 2018. From the Dump to the Pump: Fulcrum BioEnergy breaks ground on landmark trash-to-jet fuel project [WWW Document]. Biofuels Dig. URL <http://www.biofuelsdigest.com/bdigest/2018/05/16/from-the-dump-to-the-pump-fulcrum-bioenergy-breaks-ground-on-landmark-trash-to-jet-fuel-technology/>
- LanzaTech, 2015. LanzaTech Facilities [WWW Document]. URL <http://www.lanzatech.com/facilities/> (accessed 5.27.15).
- Leeper, S.A., Wankat, P.C., 1982. Gasohol Production by Extraction of Ethanol from Water Using Gasoline as Solvent. *Ind. Eng. Chem. Process Des. Dev.* 21, 331–334.
- Leland, T.W., Mcketta, J.J., 1955. Phase Equilibrium in 1-Butene — Water System and Correlation of Hydrocarbon Water Solubility Data. <https://doi.org/10.1021/ie50546a058>
- Letcher, T.M., Heyward, C., Wootton, S., Letcher, T.M., Shuttleworth, B., 1986. Ternary phase diagrams for gasoline-water-alcohol mixtures. *Fuel* 65, 891–894. [https://doi.org/10.1016/0016-2361\(86\)90192-4](https://doi.org/10.1016/0016-2361(86)90192-4)
- Lobien, G.M., Prausnitz, J.M., 1982. Infinite-Dilution Activity Coefficients from Differential Ebulliometry. *Ind. Eng. Chem. Fundam.* 21, 109–113. <https://doi.org/10.1021/i100006a002>
- Luyben, W.L., 2008. Control of the Heterogeneous Azeotropic n -Butanol/Water Distillation System. *Energy & Fuels* 22, 4249–4258. <https://doi.org/10.1021/ef8004064>
- Lyzlova, R. V, Zaiko, L.N., Susarev, M.P., 1979. Experimental Study and Calculation of Equilibrium Between Liquid and Vapor in the n-Butyl alcohol-Isobutyl alcohol-Water Ternary System at 35 °C. *Zhurnal Prikl. Khimii* 52, 551–555.
- Maczynski, A., Shaw, D.G., Goral, M., Wisniewska-goclowska, B., 2007. Alcohols with Water IUPAC-NIST Solubility Data Series. 82. Alcohols with Water—Revised and Updated: Part 1. C4 Alcohols with Water. *J. Phys. Chem. Ref. Data* 36, 59–132. <https://doi.org/10.1063/1.2366707>
- Mariano, A.P., Keshtkar, M.J., Atala, D.I.P., Maugeri Filho, F., Wolf Maciel, M.R., Maciel Filho, R., Stuart, P., 2011. Energy Requirements for Butanol Recovery Using the Flash Fermentation Technology. *Energy & Fuels* 25, 2347–2355. <https://doi.org/10.1021/ef200279v>
- Mascal, M., 2012. Chemicals from biobutanol: technologies and markets. *Biofuels*,

References

- Bioprod. Biorefining 6, 483–493. <https://doi.org/10.1002/bbb>
- McDougal, R.J., Jasperson, L. V, Wilson, G.M., 2014. Vapor–Liquid Equilibrium for Several Compounds Relevant to the Biofuels Industry Modeled with the Wilson Equation. *J. Chem. Eng. Data* 59, 1069–1085.
- McFall, T.A., Post, M.E., Collins, S.G., 1981. The excess enthalpies of 10 (n-butane + alcohol) mixtures at 298.15 K. *J. Chem. Thermodyn.* 13, 41–46.
- Mixon, F.O., Gumowski, B., Carpenter, B., 1965. Computation of vapor-liquid equilibrium data from solution vapor pressure measurements. *Ind. Eng. Chem. Fundam.* 4, 455–459. <https://doi.org/10.1021/i160016a017>
- Mokraoui, S., Coquelet, C., Valtz, A., Hegel, P.E., Richon, D., 2007. New Solubility Data of Hydrocarbons in Water and Modeling Concerning Vapor - Liquid - Liquid Binary Systems 9257–9262. <https://doi.org/10.1021/ie070858y>
- Munroe, R., 2018. Rolle's Theorem [WWW Document]. xkcd. URL <https://xkcd.com/2042/> (accessed 9.6.18).
- NIST, 2016. The National Institute of Standards and Technology (NIST) Chemistry Webbook [WWW Document]. URL <http://webbook.nist.gov/> (accessed 2.1.16).
- O'Connell, J.P., Prausnitz, J.M., 1967. Empirical Correclation of Second Virial Coefficients for Vapor-Liquid Equilibrium Calculations. *I&EC Process Des. Dev.* 6, 245–250.
- Ogorodnikov, S.K., Kogan, V.B., Nemtsov, M.S., 1961. Liquid-Vapor Equilibrium in Binary Systems of Hydrocarbons with Acetone. III. *J.Appl.Chem.USSR* 34, 313–319.
- Oudshoorn, A., Van Der Wielen, L.A.M., Straathof, A.J.J., 2009. Assessment of options for selective 1-butanol recovery from aqueous solution. *Ind. Eng. Chem. Res.* 48, 7325–7336. <https://doi.org/10.1021/ie900537w>
- Outram, V., Lalander, C.A., Lee, J.G.M., Davies, E.T., Harvey, A.P., 2017. Applied in situ product recovery in ABE fermentation. *Biotechnol. Prog.* 33, 563–579. <https://doi.org/10.1002/btpr.2446>
- Outram, V., Lalander, C.A., Lee, J.G.M., Davis, E.T., Harvey, A.P., 2016. A comparison of the energy use of in situ product recovery techniques for the Acetone Butanol Ethanol fermentation. *Bioresour. Technol.* 220, 590–600.

<https://doi.org/10.1016/j.biortech.2016.09.002>

Phillips, J.R., Atiyeh, H.K., Tanner, R.S., Torres, J.R., Saxena, J., Wilkins, M.R., Huhnke, R.L., 2015. Butanol and hexanol production in *Clostridium carboxidivorans* syngas fermentation: Medium development and culture techniques. *Bioresour. Technol.* 190, 114–121. <https://doi.org/10.1016/j.biortech.2015.04.043>

Pierotti, G.J., Deal, C.H., Derr, E.L., 1959. Activity Coefficients and Molecular Structure. *Ind. Eng. Chem.* 51, 95–102. <https://doi.org/10.1021/ie50589a048>

Plank, C.A., Olson, J.D., Null, H.R., Muthu, O., Smith, B.D., 1981. Reduction of total-pressure vapor-liquid equilibrium data. Common pitfalls encountered. *Fluid Phase Equilib.* 6, 39–59.

Pokki, J.-P., 2004. Development of Vapour Liquid Equilibrium Calculation Methods for Chemical Engineering Design. *Chem. Eng. Rep. Ser.* Helsinki University of Technology Department.

Polak, J., Lu, C., 1973. Mutual Solubilities of Hydrocarbons and Water at 0 and 25.

Poling, B.E., Prausnitz, J.M., O'Connell, J.P., 2001. *The Properties of Gases and Liquids*, 5th ed. McGraw-Hill, New York. <https://doi.org/10.1036/0070116822>

Qasim, F., Choi, H.C., Shin, J.S., Park, S.J., 2016. Liquid-liquid equilibrium data for water-ethanol-entrainer ternary system with entrainers: Cyclohexane, n-pentane, DEE (diethyl ether), DIPE (di-isopropyl ether), ETBE (ethyl tert-butyl ether). *Korean J. Chem. Eng.* 33, 2179–2185. <https://doi.org/10.1007/s11814-016-0066-x>

Qureshi, N., Hughes, S., Maddox, I.S., Cotta, M.A., 2005. Energy-efficient recovery of butanol from model solutions and fermentation broth by adsorption. *Bioprocess Biosyst. Eng.* 27, 215–222. <https://doi.org/10.1007/s00449-005-0402-8>

Raal, J.D., Muhlbauer, A.L., 1997. *Phase Equilibria - Measurement and Computation*. CRC Press.

Reimers, J.L., Bhethanabotla, V.R., Campbell, S.W., 1992. Total Pressure Measurements for Pentane + Methanol + Ethanol at 303.15 K. *J. Chem. Eng. Data* 37, 127–130. <https://doi.org/10.1021/je00005a033>

Renewable Fuel Association, 2018. *2018 Ethanol Industry Outlook*.

Rhim, J.N., Park, S.S., Lee, H.O., 1974. Isothermal Vapor-Liquid Equilibrium for the Binary System Acetone-Water by the Total Pressure Method. *J. KICHE* 12, 179–

187.

- Rodriguez, V., Pardo, J., Lbpez, M.C., Royo, F.M., Urieta, J.S., 1993. Vapor Pressures of Binary Mixtures of Hexane + 1-Butanol,+ 2-Butanol,+ 2-Methyl-1-propanol,or + 2-Methyl-2-propanolat 298.15 K. *J. Chem. Eng. Data* 38, 350–352.
- Roffler, S., Blanch, H.W., Wilke, C.R., 1987. Fermentation of Acetone and Extractive Design and Economic : Process Butanol Evaluation. *Biotechnol. Prog.* 131–140. <https://doi.org/10.1002/btpr.5420030304>
- Rohan, 2018. n-Butanol Market worth 5.58 Billion USD by 2022 [WWW Document]. MarketandMarkets. URL <https://www.marketsandmarkets.com/PressReleases/n-butanol.asp>
- Ronc, M., Ratcliff, G.R., 1976. Measurement of Vapor-Liquid Equilibria Using a SemiContinuous Total Pressure Static Equilibrium Still. *Can. J. Chem. Eng.* 54, 326–332.
- Rowley, R., Wilding, W., Oscarson, J., Yang, Y., Zundel, N., 2008. DIPPR Data Compilation of Pure Chemical Properties. AIChE, New York.
- Sander, R., 2015. Compilation of Henry's law constants (version 4.0) for water as solvent. *Atmos. Chem. Phys.* 15, 4399–4981. <https://doi.org/10.5194/acp-15-4399-2015>
- Sastray, N. V, Valand, M.K., 1998. Densities, Viscosities, and Relative Permittivities for Pentane + 1-Alcohols (C1 to C12) at 298.15 K. *J. Chem. Eng. Data* 43, 152–157.
- Schiel-Bengelsdorf, B., Dürre, P., 2012. Pathway engineering and synthetic biology using acetogens. *FEBS Lett.* 586, 2191–2198. <https://doi.org/10.1016/j.febslet.2012.04.043>
- Serra, M.C.C., Palavra, A.M.F., 2003. Solubility of 1-Butene in Water and in a Medium for Cultivation of a Bacterial Strain 32.
- Sinnott, R.K., 2005. Coulson & Richardson's Chemical Engineering, Volume 6, 4th ed. Elsevier, Oxford.
- Sipowska, J.T., Lemon, L.R., Ott, J.B., Brown, P.R., Marchant, B.G., 1994. Excess enthalpies and excess volumes for (butane + butan-1-ol) at the temperatures (298.15, 323.15, and 348.15) K and pressures (5, 10, and 15) MPa. *J. Chem. Thermodyn.* 26, 1275–1286.
- Smallwood, I.M., 1996. Handbook of organic solvent properties. Arnold, London.

[https://doi.org/10.1016/S0143-7496\(97\)88687-3](https://doi.org/10.1016/S0143-7496(97)88687-3)

Soave, G., 1972. Equilibrium constants from a modified Redlich-Kwong equation of state. *Chem. Eng. Sci.* 27, 1197–1203. [https://doi.org/10.1016/0009-2509\(72\)80096-4](https://doi.org/10.1016/0009-2509(72)80096-4)

Stern, N., 2007. *The Economics of Climate Change: The Stern Review*. Cambridge University Press, New Yorks, NY, USA.

Stockhardt, S., Hull, C.M., 1931. Vapor-Liquid Equilibria and Boiling-Point Composition Relations for Systems n-Butanol-Water and Isobutanol-Water. *Ind. Eng. Chem.* 23, 1438–1440.

Sugi, H., Katayama, T., 1977. Liquid-Liquid Equilibrium data for three ternary systems of aqueous alcohol solutions and applicatbility of the analytical solutions of groups. *J. Chem. Eng. Japan* 10, 400–402.

Talley, P.K., Sangster, J., Bale, C.W., Pelton, A.D., 1993. Prediction of vapor-liquid and liquid-liquid equilibria and thermodynamic properties of multicomponent organic systems from optimized binary data using the Kohler method. *Fluid Phase Equilib.* 85, 101–128. [https://doi.org/10.1016/0378-3812\(93\)80007-A](https://doi.org/10.1016/0378-3812(93)80007-A)

Tao, L., He, X., Tan, E.C.D., Zhang, M., Aden, A., 2013a. Comparative techno-economic analysis and reviews of n-butanol production from corn grain and corn stover. *Biofuels, Bioprod. Biorefining* 8, 342–361. <https://doi.org/10.1002/bbb>

Tao, L., He, X., Tan, E.C.D., Zhang, M., Aden, A., Renewable, N., 2014a. Comparative techno-economic analysis and reviews of n-butanol production from corn grain and corn stover. <https://doi.org/10.1002/bbb>

Tao, L., Tan, E.C.D., McCormick, R., Zhang, M., Aden, A., He, X., Zigler, B.T., 2014b. Techno-economic analysis and life-cycle assessment of cellulosic isobutanol and comparison with cellulosic ethanol and n-butanol. *Biofuels, Bioprod. Biorefining* 8, 30–48. <https://doi.org/10.1002/bbb>

Tao, L., Tan, E.C.D., McCormick, R., Zhang, M., Aden, A., He, X., Zigler, B.T., 2013b. Techno-economic analysis and life-cycle assessment of cellulosic isobutanol and comparison with cellulosic ethanol and n-butanol. *Biofuels, Bioprod. Biorefining* 8, 30–48. <https://doi.org/10.1002/bbb>

Taylor, J.B., Rowlinson, J.S., 1955. The thermodynamic properties of aqueous solutions of glucose. *Trans. Faraday Soc.* 51, 1183–1192.

- The European Union, 2009. European Union Directive 2009/28/EC. Off. J. Eur. Union 52.
- Tochigi, K., Kojima, K., 1976. The Determination of Group Wilson Parameters to Activity Coefficients by Ebulliometer. *J. Chem. Eng. Japan* 9, 267–273.
- Treybal, R.E., 1951. Liquid Extraction, 1st ed. McGraw-Hill, New York, NY, USA.
- Tsonopoulos, C., 1999. Thermodynamic analysis of the mutual solubilities of normal alkanes and water. *Fluid Phase Equilib.* 156, 21–33. [https://doi.org/10.1016/S0378-3812\(99\)00021-7](https://doi.org/10.1016/S0378-3812(99)00021-7)
- Tsonopoulos, C., 1974. An Empirical Correlation of Second Virial Coefficients. *AIChE J.* 20, 263–272.
- Usui-Kyyny, P., Pokki, J.P., Laakkonen, M., Aittamaa, J., Liukkonen, S., 2002. Vapor liquid equilibrium for the binary systems 2-methylpentane + 2-butanol at 329.2 K and n-hexane + 2-butanol at 329.2 and 363.2 K with a static apparatus. *Fluid Phase Equilib.* 201, 343–358. [https://doi.org/10.1016/S0378-3812\(02\)00080-8](https://doi.org/10.1016/S0378-3812(02)00080-8)
- Varteressian, K.A., Fenske, M.R., 1937. The System Methylcyclohexane– Aniline–n-Heptane. *Ind. Eng. Chem.* 29, 270–277. <https://doi.org/10.1021/ie50327a005>
- Voutsas, E.C., Pamouktsis, C., Argyris, D., Pappa, G.D., 2011. Measurements and thermodynamic modeling of the ethanol-water system with emphasis to the azeotropic region. *Fluid Phase Equilib.* 308, 135–141. <https://doi.org/10.1016/j.fluid.2011.06.009>
- Wang, S., Wang, W., Feng, X., Wu, Y., 1993. Measurement of the Activity Coefficients at Infinite Dilution and Their Relations with Temperature. *Gaoxiao-huaxue-gongcheng-xuebao* 7, 14–21.
- Yen, H.W., Wang, Y.C., 2013. The enhancement of butanol production by in situ butanol removal using biodiesel extraction in the fermentation of ABE (acetone-butanol-ethanol). *Bioresour. Technol.* 145, 224–228. <https://doi.org/10.1016/j.biortech.2012.11.039>
- Zaher, J.J., 2015. Method for production of butanol using extractive fermentation. US 9,156,760 B2.
- Zeppieri, S., Rodríguez, J., López De Ramos, A.L., 2001. Interfacial tension of alkane + water systems. *J. Chem. Eng. Data* 46, 1086–1088.